AD

USAAVLABS TECHNICAL REPORT 67-75

XV-5A AERODYNAMIC-PROPULSION DATA CORRELATION AND CHARACTERISTICS DEVELOPMENT BASED ON WIND TUNNEL CHARACTERISTICS

By

W. C. PARKS
R. L. SWINGLE
W. A. SWOPE

JULY 1968

U. S. ARMY AVIATION MATERIEL LABORATORIES
FORT EUSTIS, VIRGINIA

CONTRACT DA 44-177-AMC-456 (T)
RYAN AERONAUTICAL COMPANY
SAN DIEGO, CALIFORNIA

DEPARTMENT OF THE ARMY
U. S. ARMY AVIATION MATERIEL LABORATORIES
FORT EUSTIS, VIRGINIA 23604

This report has been reviewed by the U. S. Army Aviation Materiel Laboratories and the Air Force Flight Dynamics Laboratory and is considered to be technically sound. The work was performed under Contract DA 44-177-AMC-456(T) in an attempt to collect, catalogue, evaluate, and correlate wind tunnel and thrust stand data for the XV-5A aircraft configuration.

The purpose of this contract was to establish how accurate (or reasonable) current wind tunnel test procedures and data correction techniques are with respect to valid and meaningful V/STOL aircraft model testing.

Disclaimers

The findings in this report are not to be construed as an official Department of the Army position unless so designated by other authorized documents.

When Government drawings, specifications, or other data are used for any purpose other than in connection with a definitely related Government procurement operation, the United States Government thereby incurs no responsibility nor any obligation whatsoever; and the fact that the Government may have formulated, furnished, or in any way supplied the said drawings, specifications, or other data is not to be regarded by implication or otherwise as in any manner licensing the holder or any other person or corporation, or conveying any rights or permission, to manufacture, use, or sell any patented invention that may in any way be related thereto.

Trade names cited in this report do not constitute an official endorsement or approval of the use of such commercial hardware or software.

Disposition Instructions

Destroy this report when no longer needed. Do not return it to originator.

Task 1F125901A14233
Contract DA 44-177-AMC-456(T)
USAAVLABS Technical Report 67-75
July 1968

XV-5A AERODYNAMIC-PROPULSION DATA CORRELATION AND CHARACTERISTICS DEVELOPMENT BASED ON WIND TUNNEL CHARACTERISTICS

Final Report

By

W. C. Parks
R. L. Swingle
W. A. Swope

Prepared by

Ryan Aeronautical Company
San Diego, California

for

U. S. ARMY AVIATION MATERIEL LABORATORIES
FORT EUSTIS, VIRGINIA

SUMMARY

This report contains the results of a wind tunnel and thrust stand data correlation and characteristics generation program using data from tests of the U.S. Army XV-5A Lift Fan Research Aircraft. The program efforts were limited to the lift fan mode of operation and were restricted to correlation of longitudinal test results and to de elopment of longitudinal stability characteristics for calculated flight conditions.

Data from five wind tunnel programs provided the primary basis for the work; flight test data were excluded from the effort.

The majority of the data correlation work was performed utilizing results from the Ryan 1/6-scale and NASA full-scale model tests which had been conducted during the period of aircraft development. Correlation was limited primarily to wing-body characteristics. Where possible, corrections for configuration differences were developed, and the effects of dynamic dissimilarity of the fan systems were evaluated in the data comparison effort. Finally, wind tunnel wall corrections were applied to the full-scale data.

Correction factors, although not complete and often questionable, almost exclusively reduced differences in the characteristics from the two models, but generally accounted for less than half the difference exhibited by the uncorrected data. In general, disparity between the two sets of data increased with increase in flight speed. Good correlation of incremental effects of louver vector and stagger resulted from comparison of louver effectiveness. Correlation of angle-of-attack derivatives was good except for pitching moment below approximately 55 knots.

Application of tunnel wall corrections did not yield clearly defined results; the correlation study did not yield conclusive results concerning scale effects.

Expressions for the longitudinal stability derivatives for the XV-5A were developed, and numerical values of the derivatives were calculated for various determined equilibrium flight conditions in the fan mode. Fair quantitative agreement was obtained from comparison of calculated stability derivatives and those obtained during static and dynamic testing of the NASA-Langley 0.18-scale model.

The scope of the correlation effort was adjusted from that originally planned as several unexpected problems developed during the program. Comparative investigation of results from the two NASA-Ames full-scale model test programs eventually removed from further consideration the test with the ground board installed. Further, expected data from force tests of the NASA-Langley 0.18-scale XV-5A model were not made available to the program. The 0.18-scale model tests had been conducted in three different wind tunnel test sections for the specific purpose of evaluation of tunnel wall effects, but a low level of confidence developed during reevaluation of the data prior to release to Ryan. Additionally, wing-body correlation efforts using the NASA full-scale and Ryan 1/6-scale model data were not as successful as originally anticipated,

thereby justifying no similar attempt to correlate complete model results.

Despite the limiting of the correlation effort, it is felt that the work reported herein is contributory to solutions of the problem of acquiring accurate development test data. The complexities of the aerodynamic-propulsion test programs investigated typify those encountered in V/STOL aircraft. It is felt that the material given here will be instructive to the research engineer or scientist who is working to develop improved testing techniques as well as the aerodynamicist desirous of obtaining reliable design data.

FOREWORD

This report presents the result of efforts to correlate data for the XV-5A VTOL aircraft configuration, including small-scale and full-scale wind tunnel investigations and wind tunnel and thrust stand tests of the actual aircraft. The work was performed for the U.S. Army Aviation Materiel Laboratories, under Contract Number DA 44-177-AMC-456(T).

Mr. Richard L. Scharpf was the Contracting Officer's Representative at the start of the program, with these responsibilities being taken over later in the program by Mr. Robert P. Smith. Mr. C. T. Turner, Jr., was the Project Engineer for the Contractor.

The Ryan Aeronautical Company wishes to express its gratitude to the NASA personnel at Ames Research Center and Langley Research Center who assisted in providing a significant portion of the data assembled in this effort.

The authors wish to acknowledge the specialized program efforts of Messrs. W. B. Davis, D. G. Schattschneider, and E. G. Sevigny, who are also contributors to this report.

TABLE OF CONTENTS

TABLE OF CONTENTS (Continued)

TABLE OF CONTENTS (Continued)

TABLE OF CONTENTS (Continued)

LIST OF ILLUSTRATIONS

LIST OF ILLUSTRATIONS (Continued)

LIST OF ILLUSTRATIONS (Continued)

LIST OF ILLUSTRATIONS (Continued)

LIST OF TABLES

LIST OF SYMBOLS

A	Gross area of rotor or propeller, $\pi D^2/_2$, sq ft
A_F	Gross area of wing fans, $\pi D_F{}^2/_2$, sq ft
A_m	Momentum area of lifting system, sq ft
A_T	Wind tunnel test section area, sq ft
a.c.	Aerodynamic center
B	Semiwidth of wind tunnel test section, ft
b	Wing span, ft
b'	Lateral distance from center of model to right-hand side of wind tunnel (viewed from behind), ft
C_D	Drag coefficient, D/qS
$C_D{}^s$	Slipstream drag coefficient, D/q^sA_F
C_L	Lift coefficient, L/qS
$C_L{}^s$	Slipstream lift coefficient, L/q^sA_F
$C_{\ell_{2d}}$	Two-dimensional lift coefficient
C_m	Pitching moment coefficient, $M/qS\bar{c}$
$C_m{}^s$	Slipstream pitching moment coefficient, $M/q^sA_FD_F$
CM	Complete model
C_N	Normal force coefficient, N/qS
$C_N{}^s$	Slipstream normal force coefficient, N/q^sA_F
$C_p{}^s$	Fan power coefficient, $P\rho^{1/2}/(T_{ooo}/A_F)^{3/2}A_F$
$C_{p_o}{}^s$	Fan power coefficient at $V=\beta_v=\beta_s=0^o$
C_X	Longitudinal force coefficient, X/qS

C_X^s	Slipstream longitudinal force coefficient, $X/q^s A_F$
$\bar{c}$	Mean aerodynamic chord, ft
D	Drag force, lb; or fan diameter, ft
H	Semiheight of wind tunnel, ft
h	Height of center of model above wind tunnel floor, ft
i_t	Horizontal stabilizer incidence angle, deg
K	A constant
K_i	Horizontal tail induced drag factor
K_{NF}	Nose fan lift ratio, L_{NF}/T_o
L	Lift force, lb
L_o	Equilibrium lift, lb
ℓ_t	Distance along the body X-axis from the model c.g. to the a.c. of the horizontal tail, ft
M	Pitching moment, ft-lb
$\dot{m}$	Mass flow rate, slugs/sec
N	Normal force along body Z-axis, lb; fan rotational speed, RPM; or model geometric scale factor
n	Stream tube contraction ratio; the ratio of final induced velocities in far wake to initial induced velocities at model. Assumed to be unity.
P	Hypothetical power delivered to the fans from both engines, ft-lb/sec
q	Freestream dynamic pressure, $1/2\rho V^2$, lb/sq ft; or pitch rate, rad/sec
q^s	Slipstream dynamic pressure, $q + \frac{T_{ooo}}{A_F}$, lb/sq ft
R	Fan Radius, ft
S	Reference area, sq ft. Unsubscripted symbol refers to wing area
T	Gross fan thrust, rotor or propeller thrust, lb

T_c^s	Wing fan thrust coefficient, T_{ooc}/q^sA_F
$T_{c_{NF}}^s$	Nose fan thrust coefficient, $(T_o/q^sA)_{NF}$
T_o	Nose fan static gross thrust, lb
T_{ooo}	Wing fan static gross thrust with $\beta_v=0$ and $\beta_s=0$, lb
t	Time, sec
U	Total velocity in direction of body X-axis, ft/sec
u	Longitudinal perturbation velocity, ft/sec
V	Total velocity along the flight path, ft/sec or kn
W	Total velocity in direction of body Z-axis, ft/sec; or weight, lb
W_a	Engine airflow, lb/sec
w	Vertical perturbation velocity along body Z-axis, ft/sec
w_h	Reference velocity, $-(L/n\rho A_F)^{1/2}$, ft/sec
X	Longitudinal force with respect to body axes, lb
x	Longitudinal distance from the c.g. to the line of action of normal force N, ft
$\bar{x}$	Longitudinal distance between the wing fan hub centerline and the line of action of normal force N, ft
$(x_{cg}-x_{WF})$	Longitudinal distance between the c.g. and the centerline of the wing fans, ft
x_{cg}	Fuselage station of model c.g., ft
x_{NF}	Longitudinal distance from the c.g. to the centerline of the nose fan, ft
x_{WF}	Fuselage station of wing fan centerline, ft
Z	Vertical force with respect to body axes, lb
z	Distance along the body Z-axis from the model c.g. to the line of action of longitudinal force X, ft

z_t	Distance along the body Z-axis from the c.g. to the a.c. of the horizontal tail, ft
α	Angle of attack, deg or rad
$\Delta\alpha$	Interference angle due to wind tunnel boundaries, deg or rad
β	Wing fan exit louver angle, deg
β_s	Exit louver stagger angle, deg
β_v	Exit louver vector angle, deg
γ	Ratio of wind tunnel width to wind tunnel height, B/H
Δ	Increment
δ	Control deflection measured in deg or in.; general interference factor; or ambient pressure ratio
δ_{pfd}	Nose fan thrust reverser door deflection, measured from the closed position, deg
ε	Average downwash angle at the horizontal tail, deg
ζ	Ratio of wind tunnel semiheight to height of model above the wind tunnel floor, H/h
η	Ratio of lateral distance between model center and right-hand side of wall (viewed from behind) to semiwidth of wind tunnel, b'/B
η_t	Dynamic pressure ratio at the horizontal tail, q_t/q
θ	Pitch angle, rad or deg; or ambient atmosphere absolute temperature ratio
ρ	Mass density of air, slugs/cu ft
σ	Ambient atmosphere density ratio
χ	Wake skew angle, measured between the positive Z-axis and the wake centerline, deg
χ_{eff}	Effective wake skew angle, $45^\circ + \frac{\chi}{2}$, deg

ω	Angular velocity of model oscillatory drive system, rad/sec; or fan rotational velocity, rad/sec

NOTE: A dot above a symbol denotes the differentiation of the symbol with respect to time.

SUBSCRIPTS

avg	Average
c or corr	Corrected
c.g. or cg	Center of gravity
D	Drag
d	Aileron droop
E	Equivalent
e	Elevator
F	Wing fans
FS	Full-scale
f	Wing trailing edge flap
g	Gas generator
i	Induced
INT	Interference
j	Fan exit
L	Lift
m	Model
max	Maximum
NF	Nose fan
o	Initial, zero, or reference condition
ooo	Zero speed, zero vector, zero stagger
P	Constant power
pfd	Pitch fan door

R	Ram drag
s	Stagger
sc	Collective lift stick position
se	Longitudinal control stick position
T	Total; or tunnel
t or ht	Horizontal tail
u	Longitudinal induced velocity
unt	Untrimmed
u, D	Longitudinal interference velocity due to drag
u, L	Longitudinal interference velocity due to lift
v	Vector; or vertical stabilizer
W or w	Wing
WB	Wing-body combination alone
WF	Wing fan
v	Vertical induced velocity
w, D	Vertical interference velocity due to drag
w, L	Vertical interference velocity due to lift

ABBREVIATIONS

a.c.	Aerodynamic center
B.L.	Buttline
c.g. or cg	Center of gravity
cl	Chord line
CVAL	Convair Aeronautical Laboratory
EAFB	Edwards Air Force Base
eff	Effective

F.S.	Fuselage station
KN or KTS	Knots
L.E.	Leading edge
MAC	Mean aerodynamic chord
max	Maximum
ref	Reference
RPM	Revolutions per minute
S.L.	Sea level
STA.	Station
Std.	Standard
T.E.	Trailing edge
Var.	Variable
WB	Wing-body
W.L.	Waterline

1.0 INTRODUCTION

Aerodynamic-propulsion characteristics obtained by means of wind tunnel testing for V/STOL aircraft, or aircraft which depend on power for the generation of lift, may require fairly large corrections to represent the flight vehicle. The nature of these corrections is not clearly established. The large turning angles, the wake of the propulsion-lift system, and the large differences in the flow field across various parts of the model render the normal wind tunnel corrections inadequate for this type of testing. Various research programs have been undertaken by such people as Messrs. H. Heyson of NASA-Langley Research Center and William Rae of the University of Washington in an effort to develop suitable corrections or to establish the limitations of present corrections. These efforts, though, have dealt almost exclusively with small-scale model data. To date, there has been very little opportunity to compare small-scale wind tunnel model data for a V/STOL configuration with comparable full-scale data. One notable exception to this has been afforded by the development program of the XV-5A aircraft.

The XV-5A is a lift fan-type aircraft. It is supported in hovering and low-speed flight by two tip-turbine lift fans, one of which is buried in each wing. A third fan is located in the nose for low-speed trim and pitch control. Low-speed control about the other two axes is accomplished by modulating the magnitude or direction of the thrust vectors of the wing fans.

In the course of development of the XV-5A aircraft, three small-scale models and one full-scale model underwent wind tunnel investigations. In addition, the actual aircraft was tested in a full-scale tunnel and on a static thrust stand as well as with an exhaustive flight test program.

With this quantity of data available, it was felt that significant insight could be gained into the problems and limitations of wind tunnel testing for the development of V/STOL-type aircraft. Accordingly, Ryan was awarded a contract by the U.S. Army to assemble this data and to correlate the data from the various sources, utilizing configuration, tunnel wall, and power corrections as deemed advisable. This effort was limited to correlation of wind tunnel results, therefore excluding flight test data. An additional objective of this program was to establish the performance characteristics and the longitudinal stability and control derivatives suitable for a three-degree-of-freedom simulation of the XV-5A aircraft based on the results of the data correlation effort. The specific objectives of this study are itemized below.

1. Examine the adequacy of wind tunnel and thrust stand testing techniques used in previous XV-5A fan mode tests and the accuracy of the data derived therefrom.

vestigate the effect of model geometric and lift fan flow differences on data correlation and investigate methods for correction.

3. Evaluate existing wind tunnel wall correction techniques for applicability and suitability in aiding correlation of data.

4. Develop aircraft speed-power trim characteristics and static longitudinal stability and control derivatives.

5. Identify need for additional wind tunnel tests to fill in data gaps, if required.

6. Collect and catalog available XV-5A fan mode wind tunnel and thrust stand data.

7. Identify and examine all test conditions and testing techniques used, such as model and tunnel test section geometric relationships, test section flow distortion and turbulence levels, method of model support, data point stabilization time, and static test procedure.

8. Identify and examine data acquisition system accuracies such as force balance accuracies in terms of repeatability and resolution, power measurement accuracy, recording or display instrument accuracies, and stability of reference voltages.

9. Identify and examine all correction factors used, such as standard wind tunnel wall and tare and interference corrections.

2.0 DATA AVAILABLE

2.1 TEST PROGRAMS

The development of the U.S. Army XV-5A V/STOL aircraft was supported by powered and unpowered small-scale model wind tunnel tests, wind tunnel tests of a full-scale model, wind tunnel tests of the actual aircraft, and thrust stand tests of the actual aircraft. In addition, a 0.18-scale model of the XV-5A was built by NASA-Langley for use in several NASA investigations. This model was free-flight tested in the full-scale tunnel and was force tested in three different test sections, including the 30-x-60-foot full-scale test section. Data were obtained for the XV-5A configuration through a total of 12 separate test programs, exclusive of actual flight test.

Since the models were designed and built at various times during the development of the actual aircraft, each of them differed from the final aircraft configuration to some degree. The initial intent was to use the 0.18-scale Langley data as the basic data for correlation, since it most nearly represented the XV-5A aircraft configuration and since it was the only powered model data where one model had been tested in more than one test section. Data from other programs would require more configuration corrections, but would supplement the basic data.

2.2 ORGANIZATION OF CORRELATION EFFORT

With the numerous data sources, the many corrections to be made, and considering the primary and secondary objectives of the program, there were more than the usual number of ramifications to be considered in organizing, scheduling, and coordinating the work flow. This work flow and the breakdown of major tasks can best be described diagrammatically, as in Figure 1.

As collection and cataloging of data were started, work was also started on the study of wind tunnel wall corrections, and on the development of the equations for the longitudinal dimensional stability derivatives. As may be seen from Figure 1, the results of each area of effort directly supported a subsequent step. Following the collection and cataloging of the data, they were screened for accuracy and general suitability for use in actual correlation effort. These data then had to be reduced to a common coefficient system and plotted in a comparable manner before final selection of data to be correlated could be made. As the data collection and cataloging was proceeding, a list of parameters was established for which data correlation would be attempted. A list of the longitudinal stability and control derivatives that would be required for a longitudinal three-degree-of-freedom small perturbation study was also drawn up. The list of parameters for correlation is shown in Table I along with the data sources thought to be available for each parameter. The list of stability and control derivatives was the same as that which is presented in Appendix II of this report. The status of the 0.18-scale model data was not known at the time the table was prepared.

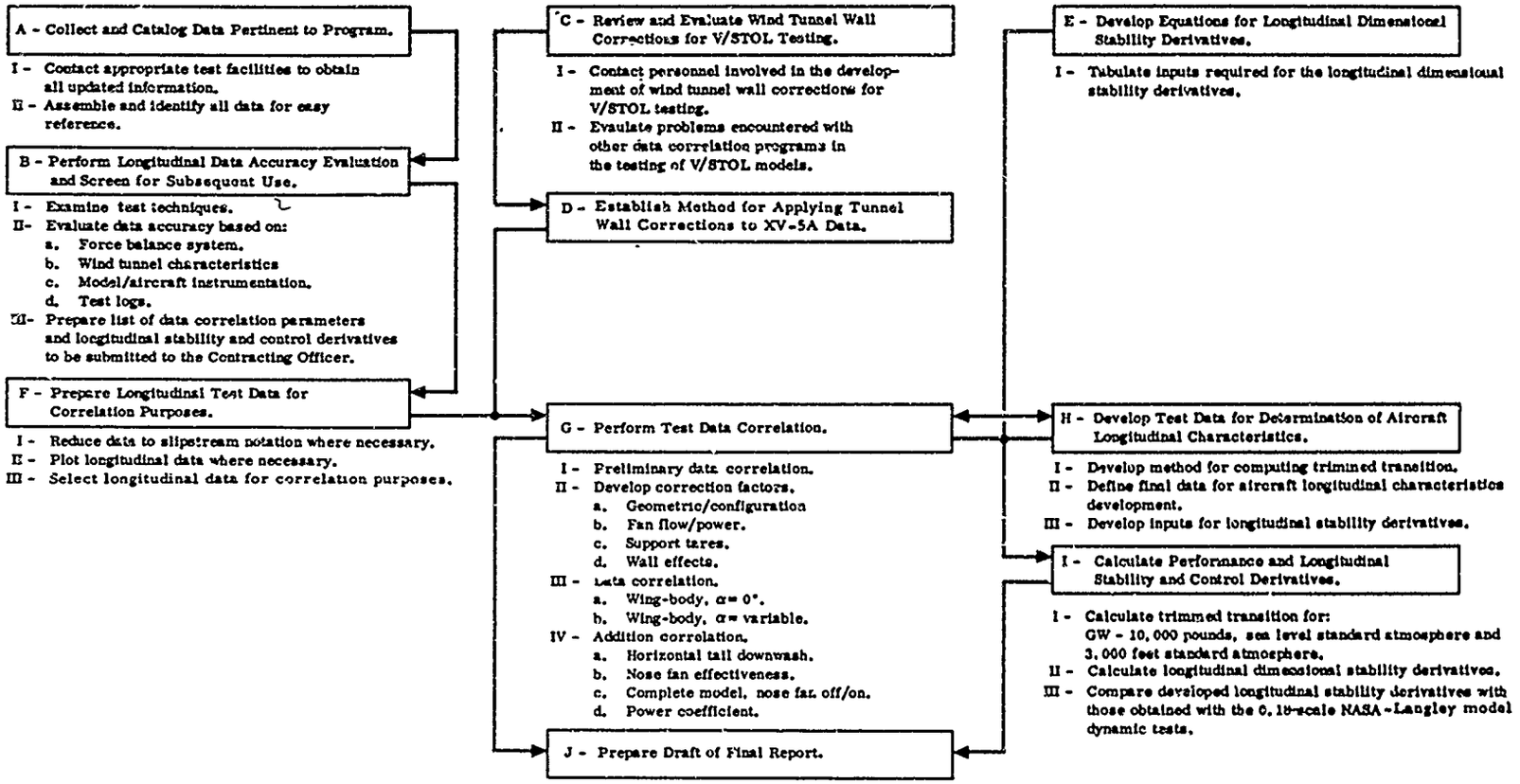

Figure 1. Organization of Data Correlation Effort.

TABLE I. STABILITY AXES LONGITUDINAL DATA CORRELATION PARAMETERS

PARAMETER	1/6-SCALE MODEL WIND TUNNEL TEST	FULL-SCALE MODEL WIND TUNNEL TEST	AIRCRAFT WIND TUNNEL TEST	AIRCRAFT EAFB TEST STAND
$C_{m_{WB(\alpha=0^\circ)}}^{s}$ Vs. T_c^s, f (β_v, β_s)	X	X		
$C_{m_{CM(\alpha=0^\circ)}}^{s}$ Vs. T_c^s, f (β_v, β_s)	X	X	X	T_c^s=1.00 only
$C_{m_{WB}}^{s}$ Vs. α, f (T_c^s, β_v)	X	X		
$C_{m_{CM}}^{s}$ Vs. α, f (T_c^s, β_v)	X	X	X	
$C_{L_{WB(\alpha=0^\circ)}}^{s}$ Vs. T_c^s, f (β_v, β_s)	X	X		
$C_{L_{CM(\alpha=0^\circ)}}^{s}$ Vs. T_c^s, f (β_v, β_s)	X	X	X	T_c^s=1.00 only
$C_{L_{WB}}^{s}$ Vs. α, f (T_c^s, β_v)	X	X		
$C_{L_{CM}}^{s}$ Vs. α, f (T_c^s, β_v)	X	X	X	

TABLE I. - Continued

PARAMETER	1/6-SCALE MODEL WIND TUNNEL TEST	FULL-SCALE MODEL WIND TUNNEL TEST	AIRCRAFT WIND TUNNEL TEST	AIRCRAFT EAFB TEST STAND
$C_{D_{WB(\alpha=0^\circ)}}^{s}$ Vs. T_c^s, f (β_v, β_s)	X	X		
$C_{D_{CM(\alpha=0^\circ)}}^{s}$ Vs. T_c^s, f (β_v, β_s)	X	X	X	T_c^s=1.00 only
$C_{D_{WB}}^{s}$ Vs. α, f (T_c^s, β_v)	X	X		
$C_{D_{CM}}^{s}$ Vs. α, f (T_c^s, β_v)	X	X	X	
$\varepsilon_{ht(\alpha=0^\circ)}$ Vs. T_c^s, f (β_v)	X	X		
ε_{ht} Vs. α, f (T_c^s, β_v)	X	X		
$C_{p_{WF(\alpha=0^\circ)}}^{s}$ Vs. T_c^s, f (β_v, β_s)	X			T_c^s=1.00 only
$\left(C_p^s/C_{p_o}^s\right)_{wf(\alpha=0^\circ)}$ Vs. T_c^s, f (β_v, β_s)	X			
$\left(\Delta C_m^s\right)_{\delta_{pfd}(\alpha=0^\circ)}$ Vs. T_c^s	X	X	X	
$\left(\Delta C_m^s\right)_{\delta_{pfd}}$ Vs. δ_{pfd}, f (T_c^s, α)	X	X	X	T_c^s=1.00 only

The review of tunnel wall correction methods led to the establishment of the actual tunnel wall correction factors to be used for each test program to be included in the correlation effort.

The trimmed transition was to be analyzed using the correlated data. Based on this trimmed transition, the correlated data, and the equations that had been developed, the XV-5A performance and longitudinal stability derivatives were to be calculated.

As the work progressed, it became necessary to deviate from this approach in some respects due to the unavailability of some data and unexpected problems encountered during the correlation effort. The actual procedures followed are discussed in Sections 4.0, 5.0 and 6.0.

2.3 MODEL DESCRIPTIONS

The characteristics of the XV-5A aircraft and the models whose data were used in this study are described below. The geometric variations of the models and the XV-5A aircraft are listed in Table II.

2.3.1 RYAN 1/8-SCALE CONVENTIONAL MODEL (NO FANS)

General Dynamics Convair (CVAL) Test 343, 6-19 June 1962.

General Dynamics Convair (CVAL) Test 343A, 21-27 August 1962.

Wing Span = 3.729 feet.

The model consisted of a wing equipped with single-slotted-type flaps, ailerons and removable inserts for wing-fan-inlet cover and wing-fan-exit louver surface simulation, fuselage with intake duct internal simulation for two General Electric J-85 gas generators, a "Tee"-type empennage with rudder and elevators, and a tricycle landing gear with simulated doors. The model was constructed so that the wing and fuselage could be tested separately and interference effects obtained for component buildup.

The right-hand wing and fuselage were equipped with pressure orifices to obtain pressure profile data. The right aileron, right elevator, and the rudder balance cavities were equipped with pressure orifices. Only the aileron and elevator balance cavities had pressure seals. Pressures were read directly through scanivalves with pressure transducers installed inside the fuselage.

Number 150 Carborundum grit was used on the model in a predetermined pattern to fix transition of the boundary layer during the test except for a few runs involving a grit study.

All control surfaces were adjusted manually prior to a given run.

TABLE II. XV-5A AND MODEL GEOMETRY

Physical Characteristics	Units	Model or Source							
		XV-5A (Refs.14, 36)		1/6-Scale* (Ref.10)		0.18-Scale* (Refs.1, 37)		Full-Scale (Ref.12)	
Wing									
Projected area	sq ft		260.321		260.5		261.5		285.6
Aspect ratio	-		3.419		3.42		3.44		3.11
Taper ratio Inboard panel	-		0.752		0.752		0.756		0.698
Outboard panel	-		0.394		0.395		0.396		0.458
Span	ft		29.833		29.85		30.0		29 80
Chord at									
(B.L.) root	(in.)in.	(0.00)	145.000	(0.00)	144.9	(0.00)	144.8	(0.00)	154.56
(B.L.) break of .25 chord line	(in.)in.	(100.75)	109.005	(100.8)	100.9		109.2		107.88
(B.L.) tip	(in.)in.	(179.00)	43.000	(179.0)	43.0		43.3	(178.80)	49.44
MAC	(in.)		112.919		113.0		111.9		121.68
F.S. of L.E. MAC	in.		211.140		-		-		-
Airfoil section at (B.L.)	(in.)	(170.05) NACA 0012-64(mod)			-	NACA 0012-64(mod)		NACA 65-210(mod)	
Airfoil maximum thickness at									
(B.L.) root	(in.)%	(24.00)	10.55		11.96		-	(24.00)	10.00
(B.L.) fan centerline	(in.)%	(61.00)	11.84		-		-		-
(B.L.) break of .25 chord line	(in.)%	(100.75)	13.64		-		-		-
(B.L.) wing max. thickness	(in.)%		-		-		-	(91.19)	12
(B.L.) tip	(in.)%	(170.05)	12.00		-		-	(178.80)	10
Geometric twist at									
root	(in.)deg	(0)	- 0.30		-		-		-
wing-body junction	(in.)deg	(24)	- 0.10	Inboard panel	0.00	Inboard panel	0		-
fan centerline	(in.)deg	(61)	+ 0.20		-		-		-
inboard-outboard junction	(in.)deg	(100.75)	+ 0.65		-		-		-
tip	(in.)deg	(170.05)	- 3.00	Outboard panel	- 3.00	Outboard panel	-3		-
Dihedral inboard panel	deg		0.000		0.00		0		-
outboard panel (B.L.)	(in.)deg		4.000	(106.4)	6.00		-6		-

TABLE II. - Continued

Physical Characteristics	Units	XV-5A	1/6-Scale	0.18-Scale	Full-Scale
Wing - continued					
Sweep					
L.E. - Inboard panel	deg	19.660	19.66	-	20.8
L.E. - Outboard panel	deg	36.881	36.88	-	38.2
.25 Chord line - Inboard panel	deg	15.000	15.00	15	16
.25 Chord line - Outboard panel	deg	28.343	28.34	28	28
T.E. - Inboard panel	deg	0.00	0.00	-	0.00
T.E. - Outboard panel	deg	-5.399	-5.36	-	-14.1
F.S. of root chord L.E. (B.L.)	(in.)in. (0.00)	180.050	(0.00) 180.00	-	(0.00) 176.53
F.S. of .25 MAC	in.	239.380	-	-	238.47
B.L. of semispan MAC	in.	75.353	-	-	76.96
Ailerons					
Area (aft of hinge line, per side)	sq ft	10.057	10.15	11.71	None
Aspect ratio	-	4.041	4.190	-	"
Spanwise location	-	0.573 to 1.000 b/2	0.563 to 1.000 b/2	-	"
Span (per side)	ft	6.375	6.51	-	"
Chord length (aft of hinge line)					
(B.L.)	(in.)in. (102.50)	20.622	(100.8) 20.5	25% wing chord	"
(B.L.)	(in.)in. (179.00)	17.239	(179.0) 17.1	-	"
MAC	in.	18.981	-	-	"
F.S. of hinge line (B.L.)	(in.)in. (103.61)	304.370	(100.8)304.2	-	"
	(in.)in. (168.43)	301.060	(159.8)301.5	-	"
B.L. of panel MAC	in.	139.610	-	-	"
Taper ratio	-	0.836	0.833	-	"
Type of balance	-	Internal sealed Pressure balance	Radius nose unsealed	-	"
F.S. of .25 MAC	in.	307.249	-	-	"

TABLE II. - Continued

Physical Characteristics	Units	XV-5A	1/6-Scale	0.18-Scale	Full-Scale
Balance Tab					
Area (aft of hinge line, per side)	sq ft	1.375	None	None	None
Aspect ratio	-	8.026	"	"	"
Taper ratio	-	0.927	"	"	"
Span (per side)	ft	3.322	"	"	"
Spanwise location	-	0.573 to 0.795 b/2	"	"	"
Chord length (aft of hinge line)					
(B.L.)	(in.)in.	(102.50) 5.156	"	"	"
(B.L.)	(in.)in.	(142.36) 4.777	"	"	"
MAC	in.	4.969	"	"	"
F.S. of hinge line					
(B.L.)	(in.)in.	(102.50) 319.894	"	"	"
(B.L.)	(in.)in.	(142.36) 316.506	"	"	"
F.S. of .25 MAC	in.	319.470	"	"	"
B.L. of panel MAC	in.	122.176	"	"	"
Type of balance	-	Radius nose unsealed	"	"	"
Flap					
Type, Airfoil section	-	Single slotted, NACA 63$_4$021 (mod)	Single slotted	Single slotted	Single slotted
Area (per side)	sq ft	12.684	12.5	14.21	12.56
Aspect ratio	-	3.246	3.274	-	2.837
Taper ratio	-	1.00	1.00	1.00	1.00
Span (per side)	ft	6.417	6.39	-	5.97
Spanwise location	-	0.138 to 0.568 b/2	0.138 to 0.563 b/2	-	0.134 to 0.535 b/2
Chord length					
(B.L.)	(in.)in.	(24.75) 23.721	(24.7) 23.7	-	25.25
(B.L.)	(in.)in.	(101.75) 23.721	(100.8) 23.7	-	-
MAC	in.	23.721	23.7	25.35	-
F.S. of hinge line	in.	308.150	309.0	-	318.84

TABLE II. - Continued

Physical Characteristics	Units	XV-5A	1/6-Scale	0.18-Scale	Full-Scale
Flap - continued					
W.L. of hinge line	in.	92.580	92.4	-	-6.5
F.S. of .25 MAC	in.	307.259	-	-	-
B.L. of panel MAC	in.	63.250	-	-	-
Horizontal Tail					
Area	sq ft	52.864	50.6	50.6	56.7
Aspect ratio	-	3.288	3.01	3.00	2.82
Taper ratio	-	0.466	0.500	0.50	1.00
Span	ft	13.183	12.32	12.32	12.66
Chord length at					
(B.L.) root	(in.)in.	(0.00) 65.640	(0.00) 65.6	65.9	53.76
(B.L.) tip	(in.)in.	(79.10) 30.600	(74.1) 32.8	32.65	53.76
MAC	in.	50.24	51.1	-	53.76
Airfoil section	-	NACA 64 A 012	NACA 64 A 012	NACA 64$_1$A 012	NACA 63- 009
Dihedral	deg	0.000	0.00	-	0.00
Sweep					
L.E.	deg	19.519	14.5	-	0.00
.25 chord line	deg	13.697	8.44	13.70	0.00
T.E.	deg	-5.058	-10.4	-	0.00
F.S. of .25 MAC (W.L.)	(in.)in.	(206.00) 493.439	-	-	(206.20) 493.81
F.S. root chord L.E. (W.L.)	(in.)in.	(206.00) 468.560	(206)468	-	(206.20) 480.37
B.L. of panel MAC	in.	34.749	-	-	-
F.S. of horiz tail pivot point (W.L.)	(in.)in.	(201.25) 496.700	(201)496	-	(206.20) 493.81
Tail length coefficient	-	2.250	-	-	-
Elevator					
Area (aft of hinge line, per side)	sq ft	5.985	None	None	No dimensions
Aspect ratio	-	5.001	"	"	" "
Taper ratio	-	0.638	"	"	" "
Span (per side)	ft	5.471	"	"	" "

TABLE II. - Continued

Physical Characteristics	Units	XV-5A		1/6-Scale	0.18-Scale	Full-Scale	
Elevator - continued							
Spanwise location	-	0.054 to 0.884		None	None	No Dimensions	
Chord length (aft of hinge line)							
(B.L.)	(in.)in.	(4.26)	16.033	"	"	"	"
(B.L.)	(in.)in.	(69.91)	10.224	"	"	"	"
MAC	in.		13.343	"	"	"	"
F.S. of elevator hinge line (W.L.)	(in.)in.	(206.00)	517.790	"	"	"	"
F.S. of .25 MAC (W.L.)	(in.)in.	(206.00)	521.126	"	"	"	"
B.L. of panel MAC	in.		34.664	"	"	"	"
Type of balance	-	Internal sealed Pressure balance		"	"	"	"
Vertical Tail							
Area (excluding dorsal)	sq ft		50.995	51.00	50.90	"	"
Aspect ratio	-		1.178	1.18	1.18	"	"
Taper ratio	-		0.520	0.520	0.52	"	"
Span	ft		7.75	7.75	7.77	"	"
Chord length							
root (W.L.)	(in.)in.	(113.00)	103.920	(113)104.00	100.80	"	"
tip (W.L.)	(in.)in.	(206.00)	54.000	(206) 54.00	54.00	"	"
MAC	in.		81.590	81.60	-	"	"
Airfoil section at root (W.L.)	(in.)	(113.00) NACA 64A012-016.5		(113) NACA 64A012-016.5	NACA 64_1A-012	"	"
at tip (W.L.)	(in.)	(206.00) NACA 64A012-013		(206) NACA 64A012	-	"	"
Sweep							
L.E.	deg		35.435	35	-	"	"
.25 chord line	deg		30.000	29.51	30	"	"
T.E.	deg		9.918	9.3	-	"	"

TABLE II - Continued

Physical Characteristics	Units	XV-5A	1/6-Scale	0.18-Scale	Full-Scale
Vertical Tail - continued					
F.S. of root chord L.E. (W.L.)	(in.)in.	(113.00) 408.450	(113)408.00	-	No Dimensions
F.S. of .25 MAC	in.	458.451	-	-	" "
W.L. of MAC	in.	154.600	-	-	" "
Tail length coefficient	-	1.940	-	-	" "
Rudder					
Area (aft of hinge line)	sq ft	6.395	5.58	6.18	None
Aspect ratio	-	4.228	3.621	-	"
Taper ratio	-	0.674	0.520	-	"
Span	ft	5.20	4.49	-	"
Chord length (aft of hinge line)					
root	in.	(18% of vertical tail chord) 17.634	(18% of vertical tail chord) 17.45	17.32	"
tip	in.	(18% of vertical tail chord) 11.882	(18% of vertical tail chord) 12.42	12.0	"
MAC	in.	14.945	12.42	-	"
Sweep rudder hinge line	deg	15.184	14.56	-	"
F.S. of root chord at hinge line	in.	496.132	497.00	-	"
W.L. of root chord at hinge line	in.	122.072	125.80	-	"
F.S. of tip chord at hinge line	in.	512.475	511.00	-	"
W.L. of tip chord at hinge line	in.	182.293	178.00	-	"
F.S. of .25 MAC	in.	507.378	-	-	"
W.L. of .25 MAC	in.	149.248	-	-	"
Spanwise location of hinge line	-	-	.139 to .101 b_v	-	"
Type of balance	-	Internal sealed Pressure balance	-	-	"

TABLE II. - continued

Physical Characteristics	Units	XV-5A	1/6-Scale	0.18-Scale	Full-Scale
Rudder Trim Tab					
Area (aft of hinge line)	sq ft	0.714	None	None	None
Aspect ratio	-	6.057	"	"	"
Taper ratio	-	0.870	"	"	"
Span	ft	2.080	"	"	"
Chord (aft of hinge line)					
root (25% of local rudder chord)	in.	4.408	"	"	"
tip (25% of local rudder chord)	in.	3.833	"	"	"
MAC	in.	4.128	"	"	"
Sweep of hinge line	deg	11.451	"	"	"
F.S. of root chord at hinge line	in.	508.896	"	"	"
W.L. of root chord at hinge line	in.	118.608	"	"	"
F.S. of tip chord at hinge line	in.	513.768	"	"	"
W.L. of tip chord at hinge line	in.	143.147	"	"	"
F.S. of .25 MAC	in.	512.271	"	"	"
W.L. of .25 MAC	in.	130.322	"	"	"
Type of balance	-	Radius nose unsealed	"	"	
Wing Fan					
Diameter	ft	5.208	5.20	5.22	5.20
Area (per fan)	sq ft	21.305	21.250	21.400	21.226
F.S. of fan center line	in.	256.000	256.000	256.000	256.69
B.L. of fan center line	in.	61.000	61.32	60.90	59.47
Direction of rotation - right-hand	-	C.W.**	C.W.	-	C.C.W.
left-hand	-	C.C.W.***	C.C.W.	-	C.C.W.

TABLE II. - Continued

Physical Characteristics	Units	XV-5A	1/6-Scale	0.18-Scale	Full-Scale
Nose Fan					
Diameter	ft	3.00	3.125	3.00	3.00
Area	sq ft	7.07	7.67	7.07	7.07
F.S. of fan centerline	in.	59.00	59.0	58.9	59.22
B.L. of fan centerline	in.	0.00	0.00	0.00	0.00
Direction of rotation*	-	C.W.	C.C.W.	-	C.C.W.

* All dimensions are for equivalent full-scale aircraft.
** C.W. - Clockwise
*** C.C.W. - Counterclockwise

2.3.2 RYAN 1/6-SCALE FAN-POWERED MODEL

General Dynamics Convair (CVAL) Test 344, 5-10 July 1962.

General Dynamics Convair (CVAL) Test 344A, 7 September-16 October 1962.

Wing span = 4.972 feet.

The model consisted of a wing equipped with single-slotted-type flaps, ailerons, and a lift fan unit mounted in the inboard section of each wing; a fuselage with a pitch control fan mounted in the nose; a "Tee"-type empennage with movable rudder and horizontal stabilizer; and a main landing gear with simulated doors, but no nose gear.

Each wing fan unit consisted of a 36-blade rotor, a 55-blade exit stator, a bellmouth inlet, and a gearbox centered by three supporting struts 90 degrees apart. Each wing fan unit was driven by a 32-horsepower electric motor attached to a gearbox and mounted within the fuselage. The motor-to-fan gear ratio was 1.46:1.0. The exit louver assembly consisted of 13 movable louvers attached to the lower frame of the fan unit. The odd-numbered louvers were remotely controlled by a screw-type actuator mounted within the fuselage. The even-numbered louvers were connected to the driven louvers by calibrated links to provide exit louver stagger. Butterfly-type closure doors were attached to the wing upper surfaces by means of chordwise struts on the wing fan centerlines. The doors were set manually. The right-hand wing fan, motor, and gearbox assembly were mounted to a five-component strain gage balance and isolated from surrounding structure. No simulation of fan turbine exhausts was provided.

The nose fan consisted of a 10-blade rotor, a 9-blade exit stator, and a gearbox. It was driven by a 15-horsepower electric motor attached to a gearbox and mounted within the fuselage. The motor-to-fan gear ratio was 0.741:1.0. The nose fan inlet consisted of 7 fixed-position louvers and a hub fairing mounted on the bellmouth inlet. These louvers were removed and replaced with a faired cover to simulate the closed configuration. Pitch fan thrust modulator doors were hinged below the fan unit. In the closed position, they closed the lower fan opening and faired into the fuselage. The doors were adjustable manually to five positions, which included fully closed.

The left wing, fuselage, left wing fan bellmouth, and pitch fan bellmouth were equipped with pressure orifices to obtain pressure profile data. In addition, Kiel tubes and static pressure taps were installed at the exits of these two fans. Pressures were read directly through scanivalves connected to pressure transducers installed inside the fuselage. A 16-tube static pressure inlet rake connected to a manometer board was used during a number of runs on the left wing fan.

The right wing fan inlet door hinge moments were measured with strain gages.

Landing gear and doors, wing fan inlet doors, pitch fan inlet louvers and modulator doors, and the horizontal and vertical tail were removable so that interference effects could be obtained for the model buildup. Data could not be obtained for the wing alone, because the fuselage housed the electric motors and gearboxes required to drive the wing fans. Control surfaces were adjusted manually except for the wing-fan-exit louvers.

Internal ducting of the gas generators was not simulated. The engine air inlet was not simulated and was closed by a faired plug during the entire test.

2.3.3 NASA-LANGLEY 0.18-SCALE FAN-POWERED MODEL (Reference 1: Langley Working Paper - 258)

Wing span = 5.400 feet.

The model consisted of a wing equipped with single-slotted flaps, ailerons and a lift fan unit mounted in the inboard section of each wing, a fuselage with a pitch control fan mounted in the nose, a "Tee"-type empennage with movable rudder and horizontal tail, and a tricycle landing gear without doors.

Each wing fan was geometrically scaled and consisted of a 36-blade rotor, a 40-blade exit stator, and an inlet frame. The exit louver assembly consisted of 14 movable louvers which were remotely controlled by actuators. Butterfly-type closure doors were mounted above each wing fan by a chordwise strut on the fan centerline. They were used to close the wing fan inlets during the power-off tests.

The pitch fan was geometrically scaled. It had fixed inlet vanes and fan thrust modulator doors which were mounted below the fan unit. These pitch fan doors were adjustable to obtain pitch trim.

The fans were driven by compressed air through tip turbines to simulate more closely the high-mass-flow characteristics of the full-scale fan drive system. The compressed air used to drive the fans passed through an ejector system located at the engine inlet. This helped to simulate the inflow to the turbojets of the full-scale aircraft.

The model was originally built as a flying model to study the stability and control characteristics of a fan-in-wing VTOL-type aircraft. Ailerons and flaps were manually adjustable. The landing gear and the horizontal tail were removable.

2.3.4 NASA-AMES FULL-POWERED MODELS

2.3.4.1 NASA-Ames Full-Scale Facsimile Powered Model

Ames Test 173, July 1962.

Wing span = 29.800 feet.

The model consisted of a wing equipped with single-slotted flaps and a lift fan unit located in the inboard section of each wing, a slab-sided fuselage with rounded corners, and an empennage with high-mounted horizontal tail. The model did not have either a landing gear or a pitch fan for this test. It is important to note here that the model was similar in size and configuration to the XV-5A but was not geometrically scaled from the XV-5A aircraft.

The basic General Electric X-353-5B Convertible V/STOL Propulsion System (Reference 2: General Electric Specification Number 112, January 15, 1962) was used except for the omission of interconnecting crossover ducting between the two wing fans and the two gas generators. In this case, each wing fan lift unit received all of its power from only one gas generator. Each fan unit had a 36-blade rotor and an 88-blade exit stator. The exit louvers were mounted below the stator and extended across the tip-turbine exhaust section. Alternate louvers were connected together to provide fan thrust modulation. The louvers were remotely controlled by actuators to provide both stagger (thrust spoiling) and vector (thrust vectoring) control. In the full aft position the louvers acted as closures for the wing fan exits. Butterfly-type closure doors were mounted on the upper surfaces of the wings on the wing fan centerlines. They were used to seal the wing fan inlets during power-off tests.

The horizontal tail, vertical tail, and the butterfly-type wing-fan-inlet doors were removable.

2.3.4.2 NASA-Ames Full-Scale Facsimile Powered Model

Ames Test 177, December 1962.

Wing span = 29.800 feet.

The model was essentially the same as that used for the Ames Test 173, except for limited testing of split flaps on the outboard wing panels to simulate drooped ailerons, the addition of a pitch control fan mounted in the nose of the fuselage, and a modification of the wing-fan-exit louvers to reduce hot gas reingestion at the gas generator and fan inlets. The model did not have a landing gear.

The General Electric X-376 Pitch Fan (Reference 3: General Electric Specification Number 113, March 1, 1962) was installed in the nose of the model. It is aerodynamically similar to the wing fan lift units of the X-353-5B Propulsion System and was designed to be operated with the system. Power was supplied by a modified T-58 gas generator rather than the J-85 gas generators which powered the wing fan units. The T-58 was mounted in

the forward section of the fuselage with the inlet facing aft. Air was supplied to the T-58 gas generator through small ports in the side of the fuselage and from the interior of the fuselage. Thrust modulator doors were mounted below the pitch fan and were remotely controlled. The pitch fan inlet did not have vanes or louvers to simulate the XV-5A inlet closure. Fairings enclosed the pitch fan installation when it was not used.

During the first part of the test, as in the Ames Test 173, the wing-fan-exit louvers and the part of the louvers which extended over the exhaust turbine section of the wing fans, functioned as one-piece louvers. In an attempt to reduce hot gas reingestion at the gas generator and fan inlets in ground effect at low speed, the section of the louvers which extended across the exhaust turbine section was fixed at a 30-degree aft vector setting with respect to the main louvers. This fix was used during the remainder of the test.

2.3.5 XV-5A AIRCRAFT, S/N 62-4505

Ames Test 210, 20 May-18 June 1964

Wing span = 29.833 feet.

The XV-5A aircraft is a mid-wing flight research vehicle with a "Tee"-type empennage configuration, has a tricycle landing gear retracting into the fuselage, and is powered by two General Electric X353-5B convertible V/STOL Propulsion Systems (Reference 2: General Electric Specification Number 112, January 15, 1962) and one General Electric X376 Pitch Fan (Reference 3: General Electric Specification Number 113, March 1, 1962). The aircraft is capable of conventional wing-supported flight at high subsonic speeds and V/STOL operation in the fan-supported flight mode, as described in the XV-5A specification 62B124.

In fan-supported flight, power to drive the tip-turbine lift fans is supplied by two J-85 gas generators, pneumatically coupled so that each lift fan derives half of its required power from each gas generator. Approximately 13 percent of the gas flow is required to drive the pitch fan. A gas diverter valve on each gas generator is used to direct the engine gas flow to the fans for VTOL operation or to a tailpipe for the conventional mode.

In the hover mode, pitch trim and control are obtained by modulating the pitch fan thrust reverser doors. Directional and lateral trim and control are obtained by differential vectoring and staggering of the wing-fan-exit louvers, respectively. Altitude control is obtained by symmetrical staggering of the wing-fan-exit louvers. During transition flight, forward thrust is obtained by symmetrical vectoring of the wing-fan-exit louvers aft. As the conventional aerodynamic controls become effective, the fan controls are progressively phased out by a mechanical mixer box.

In conventional flight the wing fan inlets are closed by butterfly-type doors mounted on the chordwise centerline strut of the fans. The wing-fan-exit louvers are vectored aft to fair into the lower wing surface and to close the wing fan exits. The pitch fan inlet vanes provide a closure for the inlet and fair into the upper forward surface of the fuselage. The pitch fan modulator doors close off the pitch fan exit and fair into the lower forward fuselage.

During the Ames Test 210, all fan mode testing was conducted with the landing gear retracted to prevent overheating of the structure in the main landing gear bay area. Pitch fan-off testing was accomplished by blocking the gas flow normally used by the pitch fan. No tail-off testing was accomplished during these tests.

2.3.6 XV-5A AIRCRAFT, S/N 62-4505

Edwards AFB Vertical Thrust Stand Test.

20-22 October 1965

Wing span = 29.833 feet.

The aircraft was basically the same as it was when tested in the Ames Full-Scale Wind Tunnel, Ames Test 210, except for the following modifications:

1. Stiffening and strengthening of the wing-fan-exit louver system to preclude louver bending and torsional deflection and to provide for louver actuators of increased power. This was achieved by:

   a. applying a double skin to the louvers to prevent flexing, which also increased the actual thickness ratio of the louvers, and

   b. increasing the load capability of the wing fan louver actuators to prevent backing off of the louvers.

2. The landing gear was fixed in the extended position during the entire test. This required the removal of the main landing gear doors and the installation of a fairing to cover the main landing gear bay, thus reducing the possibility of overheating the structure in this area.

No pitch fan-off testing was accomplished during this period.

2.4 INSTRUMENTATION

The various parameters pertinent to the data correlation program which were either instrumented and recorded, or were manually adjusted, are listed in Table III.

The parameters to be measured came under the following main headings: basic airframe force and moment data obtained with the tunnel balance system; engine parameters; wing fan and pitch fan data; control positions; ambient pressure; and airspeed.

Power was recorded only for the 1/6-scale tests, where the power to the motor was measured, and for the thrust stand tests, which of course gave only hover power data.

2.5 DATA ACCURACY

Evaluation of the longitudinal data accuracy required examination of test techniques, stabilization times, number of data recordings per test point, and repeatability checks; tolerances, interactions, and repeatability of the force balance systems; wind tunnel characteristics, flow inclination, turbulence level, and 'q' distribution; model/aircraft instrumentation, measurement of power to fans, measurement of fan RPM and fan inlet temperatures, surface pressures, etc.; and review of test logs to identify failures occurring during runs which would invalidate the data obtained.

Several areas existed where the instrumentation and/or techniques used gave cause to question the data, if not to invalidate it altogether. Although considerable effort was spent in the attempt, it was impossible to reconcile differences in the moment data from the Ames 173 and 177 tests. In spite of the fact that both tests used the same model, the data showed a static margin difference of about 5%. Several possible sources of error were investigated, such as upflow caused by presence of a ground plane, strut corrections, and the moment center used in the data reduction routines. NASA records of these tests were not sufficient to resolve this difference. Examination of the data did tend to indicate, however, that the error was most apt to be in the 177 data, and the correlation effort proceeded on this premise. Tending to substantiate this conclusion was the fact that some of the 177 data showed sharp discontinuities which might have resulted from strut interference.

Fan inlet temperature data presented another problem area in data reduction because of hot gas reingestion. Fan inlet temperatures were recorded during the static fan calibration runs of the full-scale powered model (Ames Tests 173 and 177), but not during the entire tests. Therefore, it was necessary to compromise and reduce all but the calibration runs based on wind tunnel ambient conditions. Records indicate that hot gas reingestion by the fans can have significant effects under certain conditions. Figure 2 shows the relative effect of varying wing-fan-inlet

TABLE III
MODEL/AIRCRAFT INSTRUMENTATION

PARAMETER	1/8-SCALE UNPOWERED	1/6-SCALE POWERED	FULL-SCALE (NO PITCH FAN)	FULL-SCALE (PITCH FAN)	A/C, S/N 62-4505 AMES TEST	A/C, S/N 62-4505 VERT THRUST
ENGINE						
RPM	NA***	Yes	Yes	Yes	Yes	Yes
Inlet Temp	NA	NA	Yes	Yes	No	Yes
Inlet Press.	NA	NA	No	No	No	Yes
Power	NA	Motor Input Pwr	No	No	No	Yes
WING FAN						
RPM	NA	Yes	Yes	Yes	Yes	Yes
Inlet Temp	NA	No	Yes	Yes	Yes	Yes
Press. Data	NA	Yes	No	Yes	Yes	No
Louver Pos	NA	Yes	Yes	Yes	Yes	Yes
PITCH FAN						
RPM	NA	Yes	NA	Yes	Yes	Yes
Inlet Temp	NA	No	NA	Yes	Yes	Yes
Press. Data	NA	Yes	NA	No	No	Yes
Door Pos	NA	Man. Adjust.	NA	Yes	Yes	Yes
CONTROL POS.						
Flaps	Man. Adjust.	Man. Adjust.	Man. Adjust.	Man. Adjust.	Yes	Yes
Ailerons	Man. Adjust.	Man. Adjust.	NA	NA	Yes	Yes
Horiz Tail	Man. Adjust.	Man. Adjust.	Yes	Yes	Yes	Yes
Elevator	Man. Adjust.	Man. Adjust	NA	NA	Yes	Yes
Long. Stick	NA	NA	NA	NA	Yes	Yes
Collective Stick	NA	NA	NA	NA	Yes	Yes
Throttle	NA	NA	NA	NA	Yes	Yes
MISCELLANEOUS						
Out. Air Temp	Tun Amb Temp **	Tun Amb Temp	Tun Amb Temp	Tun Amb Temp	Tun Amb Temp	Yes
Airspeed	Tun Dyn Press.*	Tun Dyn Press.	Tun Dyn Press.	Tun Dyn Press.	Tun Dyn Press.	Yes

* Tunnel Dynamic Pressure
** Tunnel Ambient Temperature
*** Not Applicable

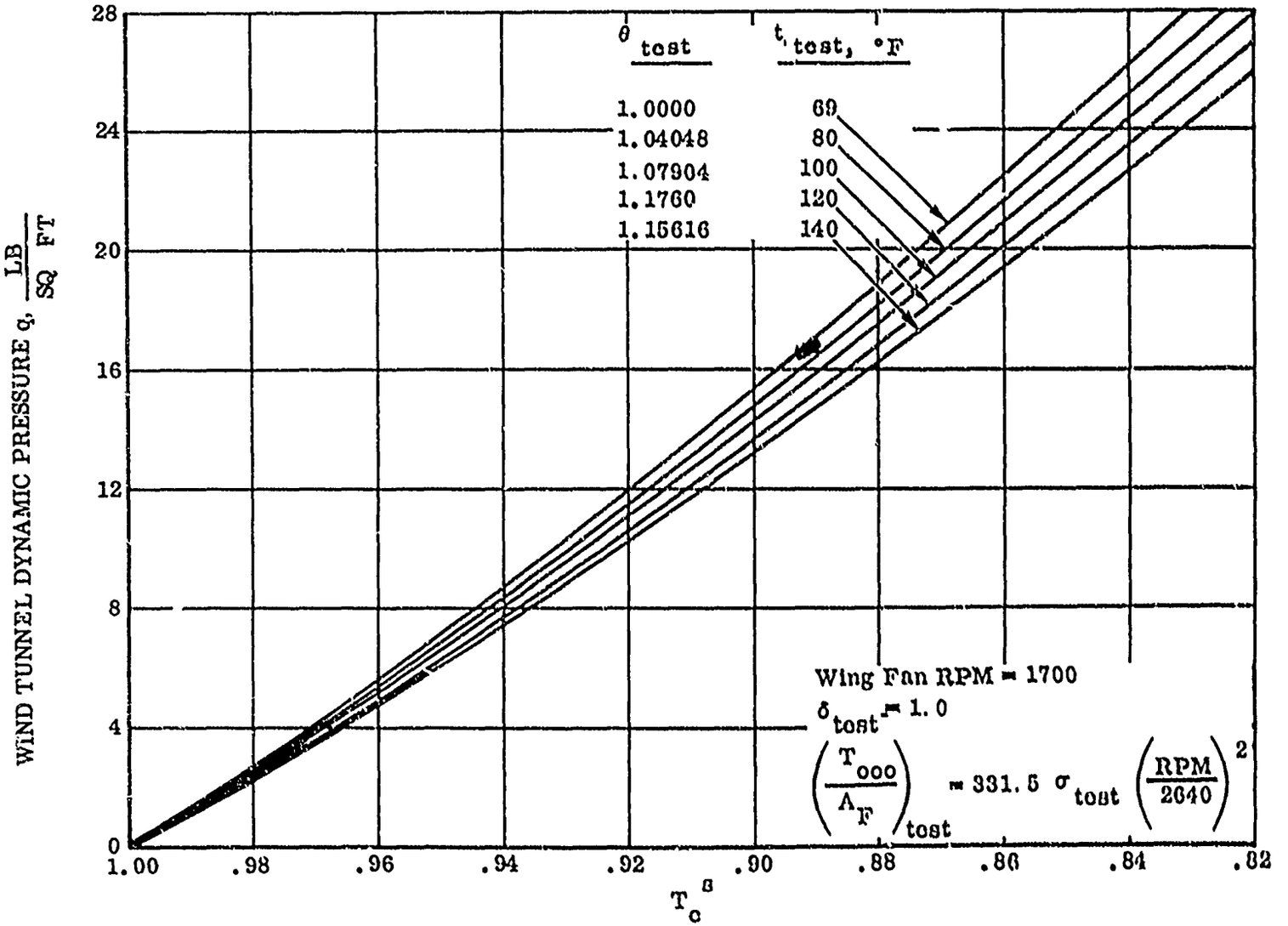

Figure 2. Fan Inlet Temperature Effect.

temperature on the speed parameter "T_c^s", assuming $\delta_{test} = 1.00$. Data from the XV-5A aircraft tests at Ames and Edwards Air Force Base were reduced based on both ambient conditions and wing-fan-inlet temperatures. Calibration and data accuracy of the wing-fan-inlet temperatures for these last two tests are of concern. This is because the instrumentation system recorded the average value of several fan inlet thermocouples. Thus, the failure of one thermocouple would result in an incorrect temperature being recorded.

A problem of reading wing-fan-exit louver position during a run existed for the full-scale powered model (Ames Test 173 and 177). The test logs indicate that at the end of several runs, all of the wing-fan-exit louvers were not at the positions called for. Thus, all the data for these particular runs must be considered suspect.

An electrical noise problem during the first half of the second test of the 1/6-scale powered model (CVAL 344A) may have resulted in incorrect right-hand wing-fan-exit louver settings for those runs which required changing the vector angle during the run. Additional runs were made to provide a check on the earlier data.

The fan power required data for the 1/6-scale tests is somewhat in question so far as magnitude is concerned due to the manner in which they were obtained. This is because the power delivered to the electric motors was measured and calibration curves were used to arrive at the motor output. The shafting and gear losses were estimated rather than measured.

It would be expected that the trends indicated by the 1/6-scale power data would be valid, although these trends did not agree with the variations in power with forward speed indicated by a large fan-in-wing model of another configuration. There were no other data for the XV-5A configuration that could be used for comparison.

Some of the factors influencing the accuracy of the data from the various tests are summarized in Table IV.

FACTORS AFFECTING DATA ACCURACY	RYAN 1/8-SCALE UNPOWERED TESTS CVAL 343 AND 343A 8-x-12 FT TEST SECTION	RYAN 1/6-SCALE POWERED TESTS CVAL 344 AND 344A 12-x-20 FT TEST SECTION
SUPPORT CORRECTIONS		
Aerodynamic Tares	An image support system was used to determine the aerodynamic tares for the fuselage alone and the wing-fuselage combination. An image sting was used on the wing alone to obtain the tares.	No aerodynamic tares were determin for the sting support system.
Interference Tares	Obtained by the image system.	No interference tares were determined for the sting support system.
Deflection Corrections	Not applicable.	Based on static loading of sting suppo
TUNNEL CALIBRATIONS		
q - Distribution	—	Data available for q = 1.4 psf and q = 9.0 psf, fair to poor.
q - Measurement	—	q measured in 8-x-12 ft section and calibrated for 16-x-20 ft section
Flow Inclination	Data corrected for flow inclination.	No correction applied to data.
Turbulence Level	Turbulence factor less than 1.1 at test velocity.	Turbulence factor approximately 1.5 for power-off test velocity.
q - Control	Good, ± 1/4-percent.	Good, ± 1/4-percent.
BALANCE ACCURACIES	—	Good, within one percent including interactions.

DATA ACCURACY

AMES FULL-SCALE (WITH PITCH FAN) AMES TEST 177 40-x-80 FT TEST SECTION	A/C S/N 62-4505 AMES TEST 210 40-x-80 Ft TEST SECTION	NASA-AME EDWAR STATIC TH
ections based on lift, drag, and pitch- of strut support system alone. Moment ct. Same corrections were applied sitions.	Support corrections based on drag and pitching moment of strut support system alone.	Not applicable. Tests co wind conditions.
states, "All longitudinal data were the influence of struts." Indications aerodynamic tares were applied to the	No interference tares were obtained for the strut support system.	No interference tares wer support system.
e.	Not applicable	Not applicable.
e for q = 20 psf, q = 60 psf, and good, (less than 1/2-percent variation n).	Data available for q = 20 psf, q = 60 psf and q = 120 psf, good, (less than 1/2-percent variation from the mean)	Not applicable.
—	—	Not applicable.
flow inclination correction applied data only. Flow may be cambered o or three degrees.	No correction applied to data.	Not applicable.
—	—	Not applicable.
considerably during a given run.	Poor varied considerably during a given run.	Not applicable.
ment, ± 250 ft-lb	Quoted: Lift, ± 20 lb Drag, ± 2 lb Pitching moment, ± 250 ft-lb	Accuracy questionable due t from fan efflux.

C

A/C S/N 62-4505 AMES TEST 210 40-x-80 FT TEST SECTION	NASA-AMES TEST AT EDWARDS AFB STATIC THRUST STAND
Support corrections based on drag and pitching moment of strut support system alone.	Not applicable. Tests conducted at or near zero wind conditions.
No interference tares were obtained for the strut support system.	No interference tares were obtained for the cradle support system.
Not applicable	Not applicable.
Data available for q = 20 psf, q = 60 psf and q = 120 psf, good, (less than 1/2-percent variation from the mean)	Not applicable.
—	Not applicable.
No correction applied to data.	Not applicable.
—	Not applicable.
Poor varied considerably during a given run.	Not applicable.
Quoted: Lift, ± 20 lb Drag, ± 2 lb Pitching moment, ± 250 ft-lb	Accuracy questionable due to heating of load cells from fan efflux.

D

3.0 BASIS FOR CORRELATION OF POWERED DATA

A series of specialized coefficients for expressing force, moment, and power data and a corresponding correlating parameter have been used almost exclusively in performing the work discussed herein. These special coefficients are an outgrowth of data correlation procedures developed during early submerged fan application studies, and were used in their present form throughout the XV-5A program for reduction and correlation of aerodynamic-propulsion characteristics. The theoretical basis, purpose, and practical applicability of the system of coefficients are discussed in this section.

The methods which were used in development of the basic data correlation procedures are described in Reference 5. In this parent document, the technique of dimensional analysis and the fundamentals of model theory were used to develop a series of coefficients and a correlating parameter which were shown to have general applicability to any propeller or rotor system. The form of the force and moment coefficients and the correlating parameter was recognized as being identical to a system of coefficients introduced by Mr. R. E. Kuhn of NASA-Langley and used by NASA-Langley in reduction of deflected slipstream and tilt-wing V/STOL model data. A power coefficient compatible with the system of force and moment coefficients was proposed in Reference 5 as an added item.

This system of coefficients in its basic form makes use of the propeller (or rotor) loading parameter T/A as a fundamental quantity in the algebraic expressions defining the coefficients. The value of T/A used in the expressions is based on actual propeller thrust measured for the specific test point.

During the XV-5A design phase, a modification of this system was necessary in order to correlate data from small-scale and full-scale powered wind tunnel tests. The need for modifications arose because of the inability to obtain actual lift fan rotor thrust data from wind tunnel tests of the full-scale models. Anticipation of future correlations of wind tunnel data with flight test results further encouraged the modification.

A simple revision in coefficient expressions was made to circumvent the absence of rotor thrust data. The revision was based on consideration of the requirements for dynamic similarity of the aerodynamic system and consisted of the substitution of total lift fan thrust existing under static (zero-speed) operating conditions at the measured fan speed for the actual rotor thrust. It was further necessary to specify reference thrust conditions for an installed lift fan with exit louvers positioned for zero flow vectoring and zero louver stagger.

While this is acknowledged as a major modification of the basic correlation procedure, it nevertheless provides a technically accurate basis for precise correlation of data from two systems <u>which are dynamically similar</u>. It may be recognized that the values of the coefficients will be equal

under those conditions where the ratios of the substituted static thrust and the actual rotor thrust for the two systems are identical, which is, in fact, required for dynamic similarity to exist. Thus for any specified operating conditions, the two values of thrust differ by a constant, and the value of the constant is of no consequence in applying the coefficients as long as the exact reverse of the data reduction procedure is used.

Thus, the basic and the modified coefficients are of the same form but have terms defined differently. For example, the definitions of the lift coefficients and the correlating parameter are written as follows:

Basic Form	Modified Form
$C_L'' = \frac{L}{((T/A)+ q)A}$	$C_L^s = \frac{L}{((T_{ooo}/A)+ q)A}$
$T_c'' = \frac{T/A}{(T/A)+ q}$	$T_c^s = \frac{T_{ooo}/A}{(T_{ooo}/A)+ q}$

The superscript "s" in the modified system is used to denote the static reference used for the thrust value, and the triple-zero subscript denotes the condition of zero freestream velocity, vector angle, and stagger angle.

Having discussed some apparent truths regarding dynamically similar systems, it is now important to explore the effect of a lack of dynamic similarity on the correlation of data.

The original and derivative data reduction procedures have numerous data handling advantages for V/STOL aircraft applications. The techniques are considered to meet the requirements for a satisfactory data correlation procedure as outlined below:

1. A data nondimensionalizing procedure suitable for expressing the aerodynamic-propulsion characteristics for a variety of V/STOL aircraft configurations.

2. A method for expressing aerodynamic-propulsion characteristics and providing operating condition correlation on a common and compatible basis.

3. A system which provides coefficients and condition correlation applicable throughout the aircraft operating envelope and adaptability to nonstandard operating conditions such that evaluation of special effects such as ground effects, propulsion system conversion between VTOL and CTOL operating modes, etc., are facilitated.

4. Coefficients which maintain reasonable and predictable numerical values over the complete operating envelope of the vehicle.

5. A system which represents minimum departure from more commonly used nondimensionalizing procedures.

Dynamic similarity of aerodynamic systems is assured when kinematic similarity of flow exists. Geometric similarity is a prime prerequisite for achieving kinematic similarity. Likewise, based on model theory, kinematic similarity of flow can exist only if viscous and compressibility effects in the fluid flow are identical.

While a test program designed for the specific purpose of evaluation of system differences could be expected to provide data for evaluations of these model geometric or flow effects, such testing is not normally performed in an aircraft developmental testing program. Thus, data to provide a means for the correlations of results from wind tunnel tests of non-geometrically similar models are usually not available. It is important to point out that the aerodynamic systems under consideration encompass the wind tunnel test section(s) and all other flow-influencing factors.

From the above discussion, then, to achieve dynamic similarity between two lift fan systems, kinematically similar flows must exist at all points within the system. A lack of similarity of flow through the fans can thus be expected to produce differences in rotor loading and duct inflow and exit patterns. These effects can modify the model pressure distributions external to the lift fans even when similarity of the external geometry exists.

Based upon consideration of the points in the above discussion, it may be stated that of the two methods of expressing aerodynamic-propulsion characteristics, the original form of data reduction system would be expected to provide the more exacting basis for correlation of lift fan mode data. Unfortunately, such data are either very difficult or impossible to obtain, and during the correlation efforts discussed in later sections, attempts have been made to develop and apply corrections for rotor loading differences.

In an ideal data correlation effort concerned with external aerodynamic characteristics, tailoring of fan inlet and rotor might be accomplished as required in order to obtain specially measured rotor flows. Model scale effects might thus be established under these circumstances. The correlation of data might then be accomplished on the basis of representative fan flow and freestream velocity ratio--a more fundamental quantity for depicting the operating conditions.

4.0 DATA CORRELATION

4.1 COLLECTION OF DATA

Collection and cataloging of the data required contacting the various test facilities to determine the validity of data on hand, types of corrections applied to the data, wind tunnel characteristics, and any additional information pertinent to data use and interpretation. The data were identified by test and run numbers for easy reference.

Run logs were studied to determine which data would be useful to this program. In the case of the 1/6-scale tests, all data included tunnel wall corrections. Since the examination of wall corrections was to be a part of the correlation study, it was necessary to have the data without corrections. Accordingly, the test facility was asked to remove the wall corrections from the specific runs that were to be used for correlation purposes.

At the beginning of this program, the 0.18-scale data which had been obtained in three different NASA-Langley test sections by NASA personnel specifically for data correlation purposes were anticipated to provide a unique foundation for the data comparison efforts. This model was regarded as the most representative of the aircraft with close geometric scaling and tip-driven fans. In the time that elapsed between the planning of this program and the initiation of work on it, review of the 0.18-scale data by NASA-Langley convinced them that their confidence level in the data was too low to allow the data to be released to an outside organization. Some 0.18-scale data from more recent tests (Ref. 1) were released to Ryan, but an insufficient number of parameters had been recorded to permit conversion to slipstream notation for correlation purposes. These data were utilized, however, in comparison with the calculated stability derivatives as discussed in Section 6.2.

The models and test programs whose data were reviewed for the data correlation program were:

1. Ryan 1/8-scale model, conventional flight mode, low-speed wind tunnel tests (CVAL 343 and 343A).

2. Ryan 1/6-scale fan-powered model, low-speed wind tunnel tests (CVAL 344 and 344A).

3. NASA-Ames full-scale fan-powered model, low-speed wind tunnel tests (Ames 173 and 177).

4. NASA-Ames XV-5A aircraft low-speed wind tunnel test (Ames 210), Edwards AFB XV-5A aircraft vertical thrust stand test.

5. NASA-Langley 0.18-scale fan-powered model, low-speed model tests (Ref. 1).

4.2 PREPARATION OF DATA

Preparation of the longitudinal data for correlation required that all data be reduced to one common nondimensional form. The specialized slipstream notation was selected because the majority of the data involved was already available in this form. Considerable effort, however, was expended in reducing the data from the NASA-Ames Tests 173 and 177. Punched data cards were no longer available, requiring all information to be first tabulated from an assortment of engine run records, run schedules, load test records, and IBM print-out sheets. The data were plotted and cross-plotted so that comparison of various tests could be made for identical conditions and similar configurations.

Once the data were in comparable form so that the actual data to be used for correlation could be selected, it became apparent that there was insufficient comparable data to allow correlation of tail-on data. As discussed under Section 2.5.7, the Ames Test 177 data were considered to be questionable for use. The result was that the final correlation was limited to wing-body 1/6-scale data and the Ames Test 173 data. Data from the other test programs were used, however, to establish some of the correction factors.

4.3 CORRECTION FACTORS

4.3.1 CONFIGURATION EFFECTS

4.3.1.1 Wing Geometry

A tabulated comparison of wing geometric parameters is presented in Table II. The 1/6-scale model wing represented the actual aircraft quite accurately. The most notable differences were outer wing panel dihedral and wing thickness.

The outer wing panel dihedral of the 1/6-scale model was -6 degrees compared to +4 degrees for the XV-5A aircraft and zero for the NASA-Ames full-scale model. The difference in dihedral was not considered to affect longitudinal characteristics significantly; therefore, no corrections were made.

The 1/6-scale model wing thickness-to-chord ratio was 20 percent greater than that of the aircraft in order to accommodate the model wing fans. At moderate angles of attack, the difference in thickness was considered to be negligible for power-off conditions, and the effect with power on was not known. No corrections were attempted.

The NASA-Ames full-scale model wing was representative of the XV-5A, but there were numerous differences in geometry. A comparison of the two-wing planforms is shown in Figure 3. It was felt that most of the geometric differences were too small to make meaningful corrections to the Ames data, especially since the effects of planform on power-on characteristics have not been clearly established.

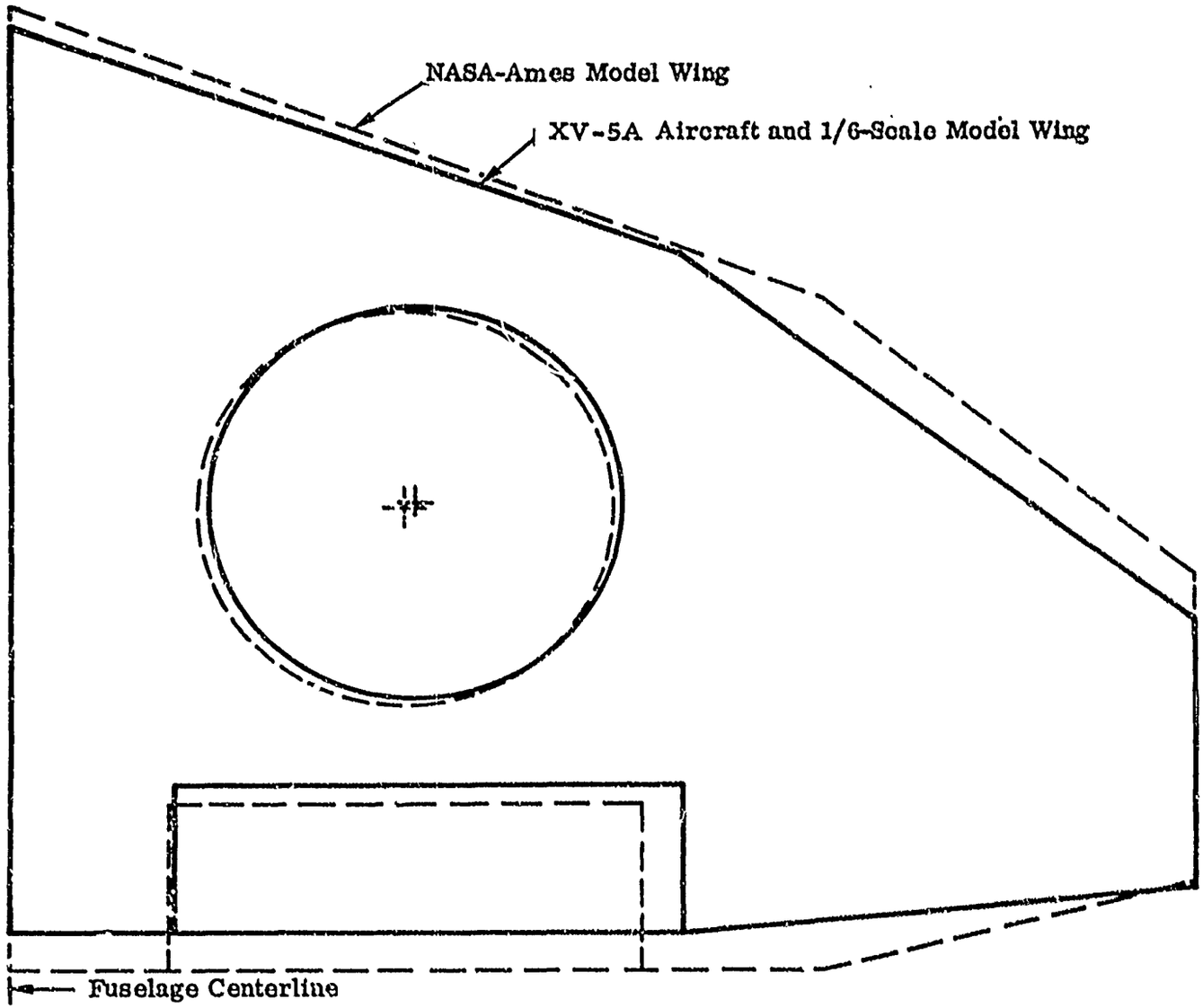

Figure 3. Comparison of NASA-Ames Model and XV-5A Wing Planforms.

The Ames model wing had 9.7 percent greater area than the XV-5A and no twist or dihedral in the outboard panel. These differences were examined since the Ames model would be expected to produce proportionately greater lift (dimensionally) in power-off conventional flight and at low thrust coefficients with power on. The power-off aerodynamic coefficients based on wing area would be expected to be about the same for the Ames and 1/6-scale models, since the greater forces are nondimensionalized with respect to a greater wing area. The slipstream coefficients based on fan area would not be the same, because both models had properly scaled fan areas so that the Ames model had a 9.7 percent greater wing-to-fan area ratio than the Ryan 1/6-scale model.

A comparison of the Ryan 1/6-scale and Ames 173 power-off characteristics is shown in Figure 4. The lift and moment coefficients at zero angle of attack and zero flap are in fairly good agreement, but the 1/6-scale drag coefficient is considerably less than that of the Ames model. The 1/6-scale drag coefficient data have the appearance of a laminar bucket at low angles of attack, which may be possible since the test Reynolds number was very low and no turbulence simulation was used on the model. However, the scatter in the 1/6-scale data was too great to be able to tell if a laminar bucket really existed. At least part of the power-off drag difference was due to the faired engine inlet on the 1/6-scale model, and to the open inlet and the windmilling engines on the Ames model.

The power-off lift and drag coefficients for zero flaps compare favorably at the higher angles of attack, considering the amount of scatter in the 1/6-scale data. The pitching moment coefficient indicates the 1/6-scale wing-body to be more unstable than the Ames model. The reason for the difference in stability was not established.

If the effects of power on the wing-body aerodynamics were the same for the 1/6-scale and Ames models, then the data presented in Figure 4 would indicate that the slipstream lift and drag coefficients of the Ames model at zero angle of attack in transition should be greater than the Ryan 1/6-scale. This should be particularly true at low thrust coefficients where wing lift becomes most significant. Actually, the reverse was true. The Ames model lift and drag slipstream coefficients at zero angle of attack and zero exit louver angle were less than the 1/6-scale. These results suggested that the effect of the larger than full-scale wing area and the lack of outboard panel twist of the Ames model were negligible, or they were offset by the multitude of other small geometric differences, or the induced effects due to power were much greater than all of the differences in wing geometry combined.

Another consequence of the Ames model wing being out of scale was the lower wing fan chord cutout ratio, D_F/c, due to the larger chord. Reference 6 shows the fan induced pitching moment to be sensitive to this parameter and indicates that the Ames model induced pitching moment should be reduced about 6 percent. Applying the correction to the Ames 173 test data would increase the disparity between those data and the Ryan 1/6-scale model data at zero louver angle. Since there were so many other geometric differences in the wing and flap, it was not considered practical to apply a correction for chord cutout ratio.

No logical corrections could be found which would account for the differences in wing geometry and improve correlation of the 1/6-scale and Ames model data in the fan-powered mode.

4.3.1.2 Flap Geometry

The flap chord of the NASA-Ames model was the same percent of local wing chord as the XV-5A aircraft and the 1/6-scale model. The span of the Ames model flap was about 3-percent wing span shorter. The Ames flap was a single-slotted type, but slot geometry could not be determined because detailed drawings were not available.

The effectiveness of the 1/6-scale and Ames model flap in the conventional, power-off mode is indicated in Figure 4. The Ames flap obtained only 65 percent of the lift and moment coefficient increment of the 1/6-scale model and had about the same increment in drag coefficient. The small difference in flap span would hardly be expected to account for the large difference in effectiveness. The reason for the difference in power-off flap effectiveness could not be determined from the information available. While they are not quantitatively defined differences in flap section geometry, nonoptimum gap and chordwise position and an actuator cutout in the flap leading edge were known to exist.

The Ames data could be corrected for the difference in power-off flap effectiveness if it were known that the effect of fan operation on the flap was proportionately the same for both models. This correction would amount to assuming that the difference in effectiveness was due to geometric differences or Reynolds number.

A comparison of power-on flap effectiveness is shown in Figure 5. With the fans operating, the 1/6-scale model flap was less effective than the Ames flap even though it was more effective with power off. Flap increments for the 1/6-scale model were available at only three values of thrust coefficient for zero exit louver angle. More data would have been very desirable because the lift and drag increments appear to be very nonlinear.

The data of Figures 4 and 5 point to the conclusion that the effect of fan operation on flap effectiveness was very much different for the small-scale and full-scale models. Whether the difference was due to scale effect, geometry, or some other reason could not be determined. A correction to account for the difference in power-off flap effectiveness would result in an increase in the power-on flap effectiveness of the Ames model, which was already greater than the 1/6-scale flap. Therefore, no correction for flap geometry or effectiveness could be justified.

4.3.1.3 Landing Gear

The NASA-Ames full-scale model had no landing gear, and the actual aircraft tests were run almost entirely with the gear retracted. The 1/6-scale model tests were conducted almost entirely with the main landing gear on and without a nose gear. To correlate the small-scale and full-scale test results, it was necessary to remove the effect of the landing gear from the 1/6-scale data.

The only 1/6-scale model power-on data available to show the effect of landing gear were at 50 degrees vector angle and zero angle of attack for three values of thrust coefficient. Those data were too meager and inconclusive, as the effect of the landing gear appeared no larger than the scatter in the data.

The landing gear increments are probably a function of vector angle, with power on, since the fan efflux impinges on the gear. However, that effect was unobtainable, and it was felt that the power-off dynamic pressure effect was probably the major part of the landing gear contribution. The incremental effect of the landing gear in conventional, power-off flight is shown in Figure 6 for both the 1/6-scale and 1/8-scale models. The 1/6-scale model data were very erratic, but at some conditions compared favorably with 1/8-scale model data even though the 1/6-scale model had no nose gear. The 1/8-scale data were quite smooth and were considered to be the most reliable. Since the total landing gear correction in slipstream coefficients is small and since power-off data are being applied to power-on conditions, the 1/8-scale model data were used to correct 1/6-scale data to landing gear up.

The landing gear increments shown in Figure 6 are due to the landing gear's being down. Those conventional coefficients were converted to slipstream notation and added to the 1/6-scale data using the following equations:

$$\Delta C_L{}^s = -\Delta C_L \left(1-T_c{}^s\right) \frac{S}{A_F} = -6.11\Delta C_L \left(1-T_c{}^s\right)$$

$$\Delta C_D{}^s = -\Delta C_D \left(1-T_c{}^s\right) \frac{S}{A_F} = -6.11\Delta C_D \left(1-T_c{}^s\right)$$

$$\Delta C_m{}^s = -\Delta C_m \left(1-T_c{}^s\right) \frac{S\bar{c}}{A_F D_F} = -11.05\Delta C_m \left(1-T_c{}^s\right)$$

4.3.1.4 Pitch Fan Closure

The NASA-Ames model did not have a pitch fan or any opening in the nose during Test 173, while the 1/6-scale model pitch fan inlet and exit were always open when the wing fans were running. The 1/6-scale model pitch fan-off data had to be corrected for the effect of the open inlet and exit in order to compare them with Ames 173 test data.

The effect of the open pitch fan cavity on the 1/6-scale model could be obtained only from power-off, conventional flight data. While it was realized that those data were not strictly applicable to the wing fans on condition, it is reasonable to expect the major contributions to be included. The conventional flight increments due to the pitch fan cavity's being open are in Figure 7. Those increments were converted to slipstream notation and added to the 1/6-scale model data using the same equations used previously for the landing gear effect.

4.3.2 WALL EFFECTS

A thorough discussion of wind tunnel wall effects and currently used techniques of correcting for them are presented in Appendix III. A sample calculation illustrating the method used in this report is also given.

The wall effect corrections to power-on test data shown in this report were based on Heyson's linearized theory (Reference 7). Wall effects were judged to be negligible for the 1/6-scale model tests because of the very large tunnel size relative to the model.

Data from NASA-Ames Test 173 are shown in Figures 8 through 10 both uncorrected and corrected for wall effects. The effect of these wall corrections on correlation with 1/6-scale model data is shown in subsequent sections of this report.

4.3.3 STRUT TARES

The 1/8-scale conventional flight model test was the only one in which aerodynamic interference tares were determined for the support system. Support system corrections were included in the 1/8-scale model tabulated data received from the test facility.

The 1/6-scale model was sting-mounted, and the only correction applied to the test data was an angle-of-attack correction due to sting deflection. The tabulated 1/6-scale model data as received from the test facility included the sting corrections, and no further support system corrections were made for this study.

The tabulated data received from the NASA-Ames Research Center for Test 173 were not corrected for strut system tares. Strut tare corrections were applied to those data as necessary using the tares from the Ames Test 210. Those tares were considered applicable since they account only for the direct force contribution of the isolated struts, and the same strut system was used for both tests. The strut tare corrections added to the Ames 173 test data are, in slipstream notation,

$$\Delta C_D{}^{s} = -0.093\ (1-T_c{}^{s})$$

$$\Delta C_m{}^{s} = (0.0735 + 0.135\ \sin\alpha)\ (1-T_c{}^{s})$$

NASA-Ames Test 177 used the variable height support system. The tabulated test data received from the test facility presented the data with and without the support system tare corrections applied. The tares used are given below in slipstream coefficients. The values given are for the contribution of the isolated support system, as model interference tares were unknown.

$$\Delta C_L^{\ s} = -0.0338\ (1-T_c^{\ s})$$

$$\Delta C_D^{\ s} = \left[-0.7562 + 0.3551 \sin\alpha\right]\ (1-T_c^{\ s})$$

$$\Delta C_m^{\ s} = \left[0.6667 + 0.6025 \sin\alpha\right]\ (1-T_c^{\ s})$$

4.3.4 FAN FLOW AND POWER CORRECTIONS

The most important and most difficult model differences to account for were those of the propulsion-lift system. While the 1/6-scale and Ames full-scale model lift fans were conceptually the same, there were a number of geometric differences. In addition to the fan differences, the two models used a different type of power source which affected the forces and moments acting on the model. A brief description of the power transmission systems is in order.

4.3.4.1 Wing Fan System

The 1/6-scale model wing fans were individually driven by an electric motor through a right-angle drive and gearbox arrangement. The power input to the motors was measured and converted to motor shaft horsepower output through reference to a calibration curve. The 1/6-scale model power source and transmission system were completely internal to the model and did not contribute to the external forces or moments.

The NASA Ames model used full-scale hardware as the main elements of the propulsion-lift system. Each wing fan was driven by a tip turbine which was powered by exhaust gas delivered from a J-85 turbojet engine through internal ducts. Unlike the 1/6-scale model, the power source and gas transmission system of the Ames model contribute to the forces on the model. The hot gas which drives the wing fan tip turbine is exhausted at the inboard periphery of the fan through exit louvers which are merely an extension of the normal fan louver system. The turbine efflux contributes a thrust which is vectored along with the wing fan thrust. The additional thrust is obtained at the expense of gas generator ram drag.

4.3.4.2 Wing Fan Geometry Considerations

Wing fan flow characteristics at the same thrust coefficient are basically a function of fan geometry including inlet and exit. The most significant geometric differences between the 1/6-scale model wing fans and the Ames full-scale fans were in fan thickness, inlet vanes, mass flow area (hub-to-diameter ratio), direction of rotation, and possibly exit louver zero reference.

The excess wing thickness required to accommodate the 1/6-scale model fans was discussed in Section 4.3.1.1. The effect on fan performance of the greater depth of the fan for the 1/6-scale model was not known, nor was it considered feasible to attempt to estimate the effect.

The inlet vane system of the 1/6-scale model, as initially installed, was the same as the full-scale configuration. However, the circular vane and four lateral straight vanes were removed very early in the test program. Initial 1/6-scale model tests indicated that the vanes excessively reduced the fan static thrust While removal of the inlet vanes improved static fan performance of the 1/6-scale model, the effect on fan performance in crossflow was not known. Experimental data were not obtained in crossflow with the vanes installed, and estimation of the effect was considered unfeasible.

The exit louvers were of cambered design on the 1/6-scale model, NASA-Ames model, and the XV-5A aircraft. The louver cross sections were identical for the Ames model and the aircraft; they were of simplified design in the case of the 1/6-scale model consisting of radius leading edges and beveled trailing edges.

The zero louver angle reference could not be positively established for all of the models. The Ames model louver angle was reportedly measured with a propeller protractor, and it was supposed that the reference was a plane tangent to the aft side of the louver. Such a measurement would correspond to the method used on the actual XV-5A aircraft.

The 1/6-scale model louver angle was measured with a template designed for that purpose; however, the actual zero reference was not recorded. Reference 7 implies the louver zero reference to have been the chord plane of the louver. Nevertheless the static test data of Reference 8 indicate a louver deflection approximately 2.5 degrees forward (negative vector) for zero horizontal force, which is identical to that louver angle quoted for zero horizontal force for the X353-5 fan by General Electric. Therefore, no corrections to account for exit louver differences were attempted.

The Ames full-scale model was unique in that both wing fans rotated in the same direction, while all other models and the XV-5A aircraft had counter-rotating fans. The right-hand fan rotated counterclockwise on the Ames model instead of clockwise. The direction of rotation could be expected to change the spanwise distribution of lift over the fan and possibly the induced effect of the fan on the wing in crossflow. The net flow field of the fan plus wing is too complex and the net effect probably too small to even attempt to estimate the effect of the wing fans rotating in the same direction.

The hub diameter of the 1/6-scale model fan was larger than the full-scale fan, resulting in a mass flow (compressor) area 10.7 percent less than full-scale. The ratio of mass flow area to gross fan area (including the hub) was 0.75 for the 1/6-scale model and 0.84 full-scale.

Some implications of the difference in mass flow area between the 1/6-scale and full-scale fans which have the same gross area, after accounting for scale factors, can be illustrated by comparing the fan static thrust performance. The disk loading of the 1/6-scale model and full-scale fans given below is that which was used for reduction of wind tunnel and flight test data to slipstream notation. The full-scale disk loading given was used for both the Ames model and the actual XV-5A aircraft.

$$\frac{T_{000}}{A_F} = 0.03315\,\sigma N_F^2 \qquad \text{(full-scale)}$$

$$\frac{T_{000}}{A_F} = 0.02675\,\sigma N_F^2 \qquad \text{(1/6-scale model)}$$

The reference area for the disk loadings above is the gross fan area based on the overall diameter of the fan rotor. The fan speed is expressed in percent such that at the same percent of fan speed, the 1/6-scale and full-scale fans have the same rotor tip velocity. The corresponding fan speeds at 100-percent RPM are 2640 RPM full-scale and 15,840 RPM for the 1/6-scale model.

The small-scale and full-scale disk loadings are not given above on a comparable basis because the full-scale value includes the fan turbine thrust. The turbine thrust was estimated to be 10 percent of the total fan rotor plus turbine thrust. That value was obtained from fan performance calculations by the General Electric Company in 1962. Removing the turbine thrust contribution from the full-scale disk loading, we obtain a comparison of the average disk loading of the fan alone. These values are

$$\frac{T_{000}}{A_F} = 0.02984\,\sigma N_F^2 \qquad \text{(full-scale)}$$

$$\frac{T_{000}}{A_F} = 0.02675\,\sigma N_F^2 \qquad \text{(1/6-scale)}$$

The disk loading of the full-scale fan, based on gross area, is about 11.5 percent greater than the 1/6-scale model at the same tip speed. If we compare the disk loadings based on the mass flow area of the rotor, an entirely different result is obtained. That comparison is given below:

$$\frac{T_{ooo}}{A} = 0.03551\ \sigma N_F^2 \qquad \text{(full-scale)}$$

$$\frac{T_{ooo}}{A} = 0.03566\ \sigma N_F^2 \qquad \text{(1/6-scale)}$$

From the very close agreement of disk loading above, it can be concluded that the overall aerodynamic performance of the rotor mass flow area is the same for the full-scale and 1/6-scale model fans. The radial load distribution and the performance in crossflow could, however, be different due to the differences in fan hub, absence of 1/6-scale model inlet vanes, etc.

It was stated in Section 3.0 that geometric similarity is a prerequisite to achieving complete dynamic similarity between two systems. Therefore, geometric differences between full-scale and 1/6-scale model fans will preclude the possibility of finding a condition where the fan flows are completely dynamically similar. In order to correlate full-scale and 1/6-scale model data, it is necessary to try to compare test conditions which are as nearly dynamically similar as possible. In achieving this end, consideration was given to using the disk loading based on fan mass flow area instead of gross area for reducing the data to slipstream coefficients. The reason for this was simply that the relationship between disk loading and percent of fan speed was the same for full-scale and 1/6-scale on a mass flow area basis, whereas it was not using gross fan area. Therefore, if the mass flow area was used at the same adjusted value of thrust coefficient, the crossflow or advance ratio ($V/_{\omega}R$) would also be the same for both 1/6-and full-scale. If gross fan area were used, then the crossflow ratio would be different for the two models at the same values of thrust coefficient using the basic definition.

In order to resolve the question of fan reference area, it was necessary to examine a more fundamental quantity, the momentum jet velocity ratio, V_o/V_j. Jet velocity ratio is discussed in detail in Reference 5, where it is shown that to achieve kinematically similar flows, the ratio of local velocity to freestream velocity must be the same in both flow fields. The magnitude and distribution of the fan momentum jet velocity are of fundamental importance because they directly affect the local velocities induced on various parts of the model. In the correlation of test data, an average momentum jet velocity is used as the correlating parameter, and disk loading corresponds directly to an average momentum velocity. The choice of disk loading reference area then merely determines the area over which the momentum jet velocity is averaged. Thus,

at the same thrust coefficient, the small-scale and full-scale models would have the same velocity ratio based on the average jet velocity over the total fan disk or over the mass flow area, depending on the reference area. Whether one reference is more correct than the other is argumentative. If the difference in mass flow to gross fan area ratio is very large for two models, the mere choice of reference area will not account for the dynamic dissimilarity because the inherent difference in jet velocity distribution cannot be accounted for. In the case of the study, a check indicated that the correlation of the 1/6-scale and Ames model data would not be significantly affected by changing from fan reference area to mass flow area. Therefore, to retain properly scaled reference areas, the gross fan area, based on overall rotor diameter, was used throughout.

4.3.4.3 Wing Fan Turbine Thrust Correction

The wing fan tip-turbine thrust is included in the full-scale disk loading without fan reference area revision. Adding a representative turbine thrust to the 1/6-scale model disk loading was considered appropriate. The contribution of the turbine thrust to the forces and moments acting on the model was treated as a direct, vectored force acting at the fuselage station and waterline of the fan center. The turbine efflux can actually be expected to alter the local induced velocities on the underside of the wing and fuselage, but no reasonable way of correcting for the induced effect is known. The direct force contribution of the turbine is probably the major part of the total effect.

As stated in the preceding section, the wing fan turbine thrust was estimated to be 10 percent of the total fan plus turbine thrust. The turbine thrust variation with thrust coefficient was not known, so the static thrust contribution was used for all calculations. The incremental static thrust due to the turbine is

$$\Delta T_{ooo} = 0.1 \, (T_{ooo})_{corr}$$

$$(T_{ooo})_{corr} = (T_{ooo})_{fan} + \Delta T_{ooo}$$

The incremental lift, drag, and moment due to fan turbine exhaust are

$$\Delta L = \Delta T_{ooo} \cos (\beta_v - \alpha) \qquad (1)$$

$$\Delta D = -\Delta T_{ooo} \sin (\beta_v - \alpha) \qquad (2)$$

$$\Delta M = -\Delta T_{ooo} \cos\beta_v \, (x_{WF} - x_{cg}) + \Delta T_{ooo} \sin\beta_v \, (z_{WF}) \qquad (3)$$

$$(x_{WF}-x_{cg}) = 0.833 \text{ ft} \tag{4}$$

$$z_{WF} = 1.0 \text{ ft} \tag{5}$$

Since the turbine thrust effectively adds to the disk loading, the 1/6-scale model thrust coefficient and slipstream dynamic pressure must be corrected in this exercise. The corrected values were obtained from the following equations where the subscript, corr, denotes the value corrected for fan turbine thrust.

$$\left(\frac{T_{coo}}{A_F}\right)_{corr} = \frac{1}{0.9}\left(\frac{T_{ooo}}{A_F}\right) = 1.111\left(\frac{T_{ooo}}{A_F}\right)$$

$$\left(T_c{}^s\right)_{corr} = \frac{\left(T_{ooo}/A_F\right)_{corr}}{\left(T_{ooo}/A_F\right)_{corr} + q_o}$$

$$\left(T_c{}^s\right)_{corr} = \frac{1}{1 + 0.9\left(\frac{1-T_c{}^s}{T_c{}^s}\right)} \tag{6}$$

$$q^s{}_{corr} = \left(\frac{T_{ooo}}{A_F}\right)_{corr} + q_o$$

$$\frac{q^s}{(q^s)_{corr}} = \frac{1}{1 + 0.111\ T_c{}^s} \tag{7}$$

The corrected thrust coefficient and dynamic pressure ratio are shown in Figure 11.

The total corrected value of lift, drag, and pitching moment slipstream coefficients was obtained by using Equations (1) through (7). The resulting equations are

$$\left(C_L{}^s\right)_{corr} = C_L{}^s\left(\frac{1}{1 + 0.111\ T_c{}^s}\right) + 0.1\ (T_c{}^s)_{corr} \cos(\beta_v - \alpha)$$

$$\left(C_D{}^s\right)_{corr} = C_D{}^s\left(\frac{1}{1 + 0.111\ T_c{}^s}\right) - 0.1\ (T_c{}^s)_{corr} \sin(\beta_v - \alpha)$$

NOTES:

Conventions: Flight, Power Off, Tail Off, No Landing Gear
All Fan Inlets and Exits Closed

SYM	MODEL	REMARKS
○	Ames 173	Corrected For Strut Tares And Wall Effects
△	Ryan 1/6-Scale	Corrected For Wall Effects

Unflagged Symbols are $\delta_f = 0°$, $\delta_d = 0°$

Flagged Symbols are $\delta_f = 45°$, $\delta_d = 0°$

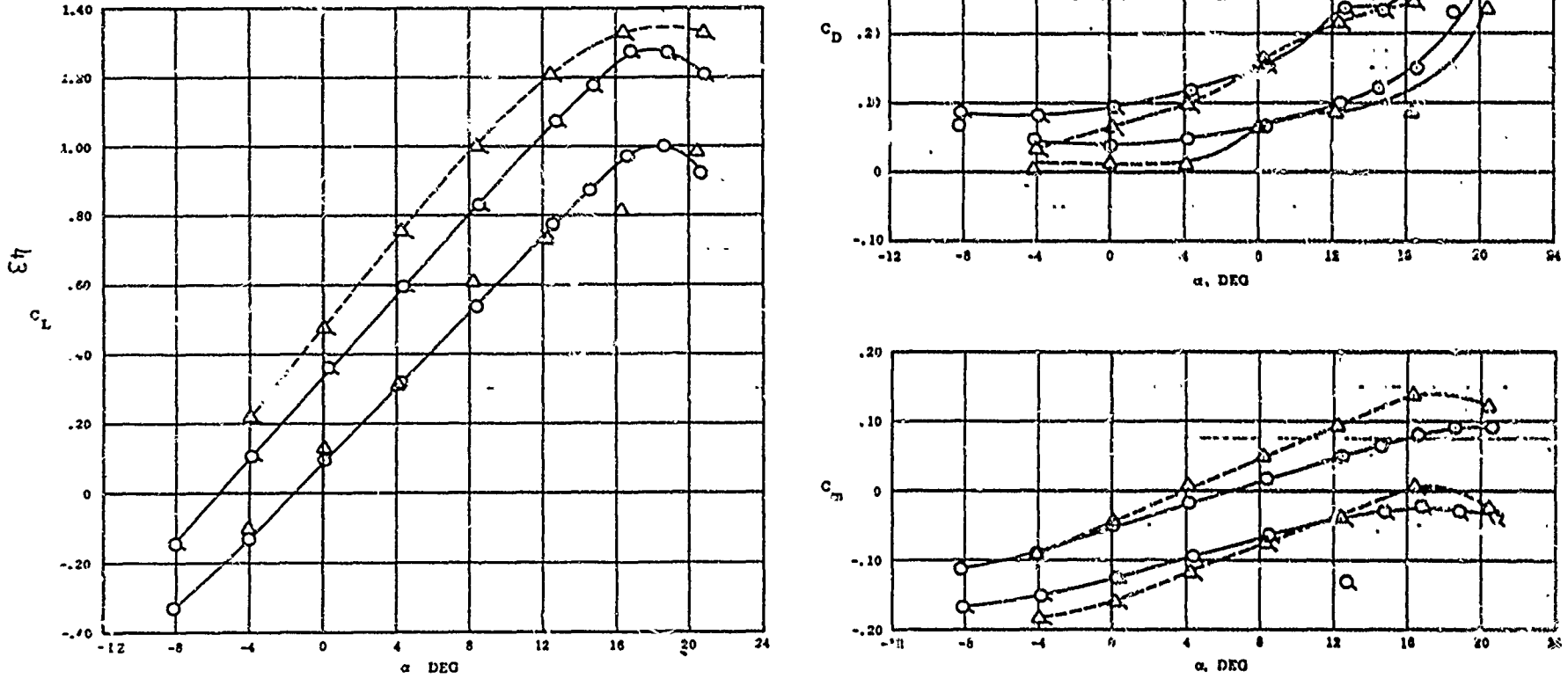

Figure 4. Wing-Body Characteristics of NASA-Ames and Ryan 1/6-Scale Models, Power Off.

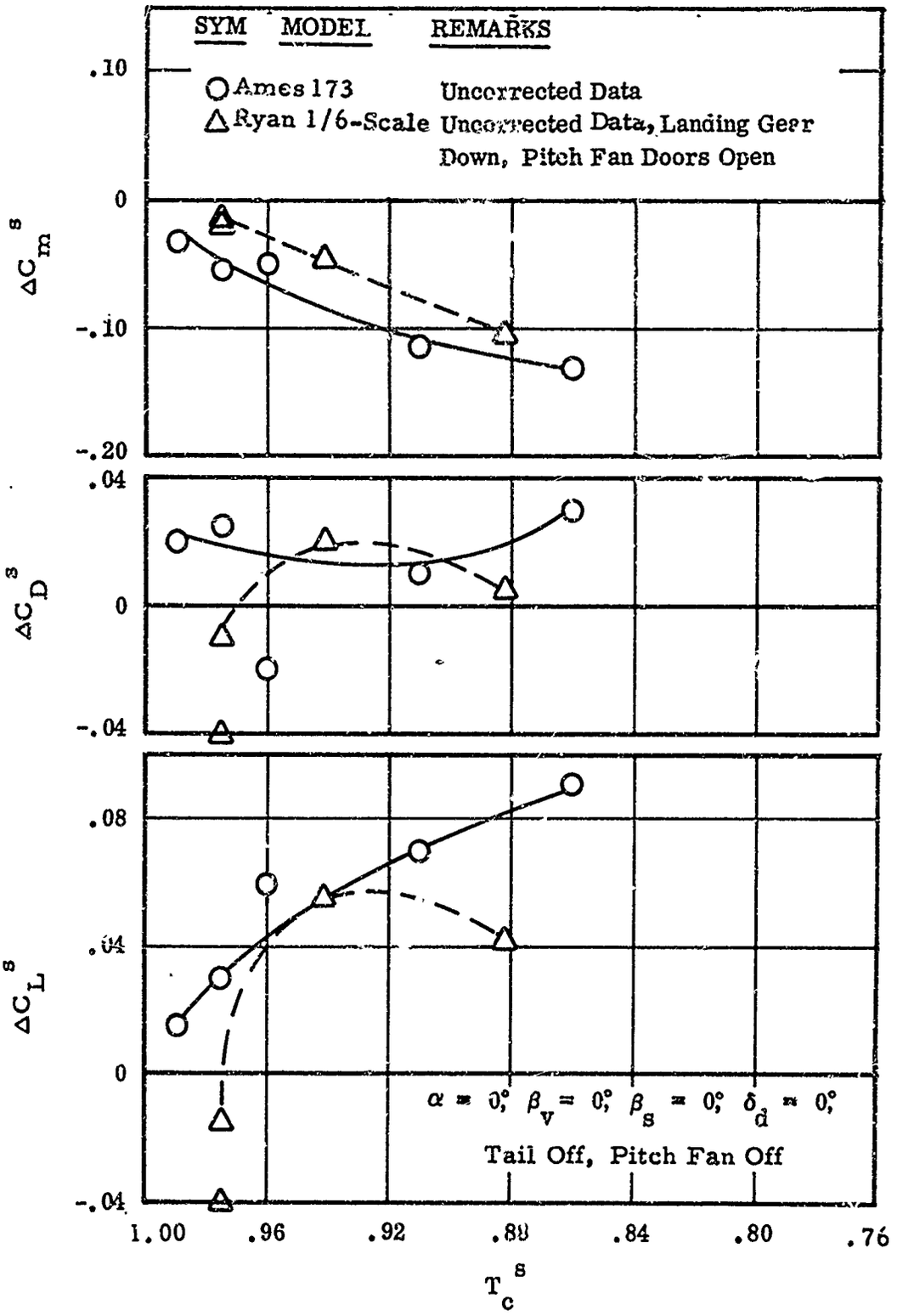

Figure 5. Comparison of Power On Flap Effectiveness, NASA-Ames and Ryan 1/6-Scale Models.

NOTES:

1. $\delta_f = 45°$, $\delta_d = 0°$.
2. 1/8-Scale Model Data Used for Configuration Corrections
3. O 1/8-Scale Conventional Flight Model, Tail Off
   □ 1/6-Scale Conventional Flight Model

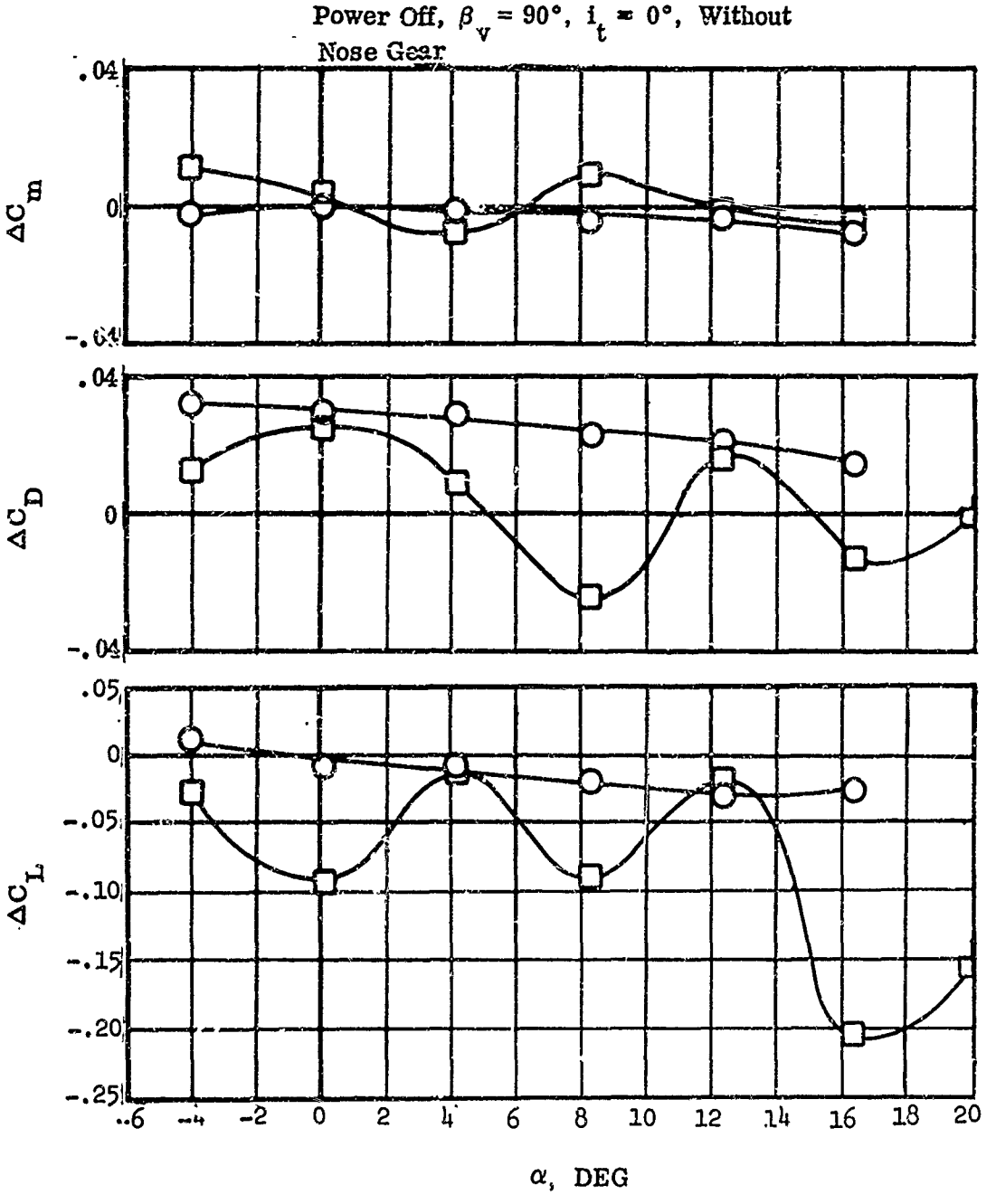

Figure 6. Incremental Aerodynamic Coefficients Due to Landing Gear Down, Power Off.

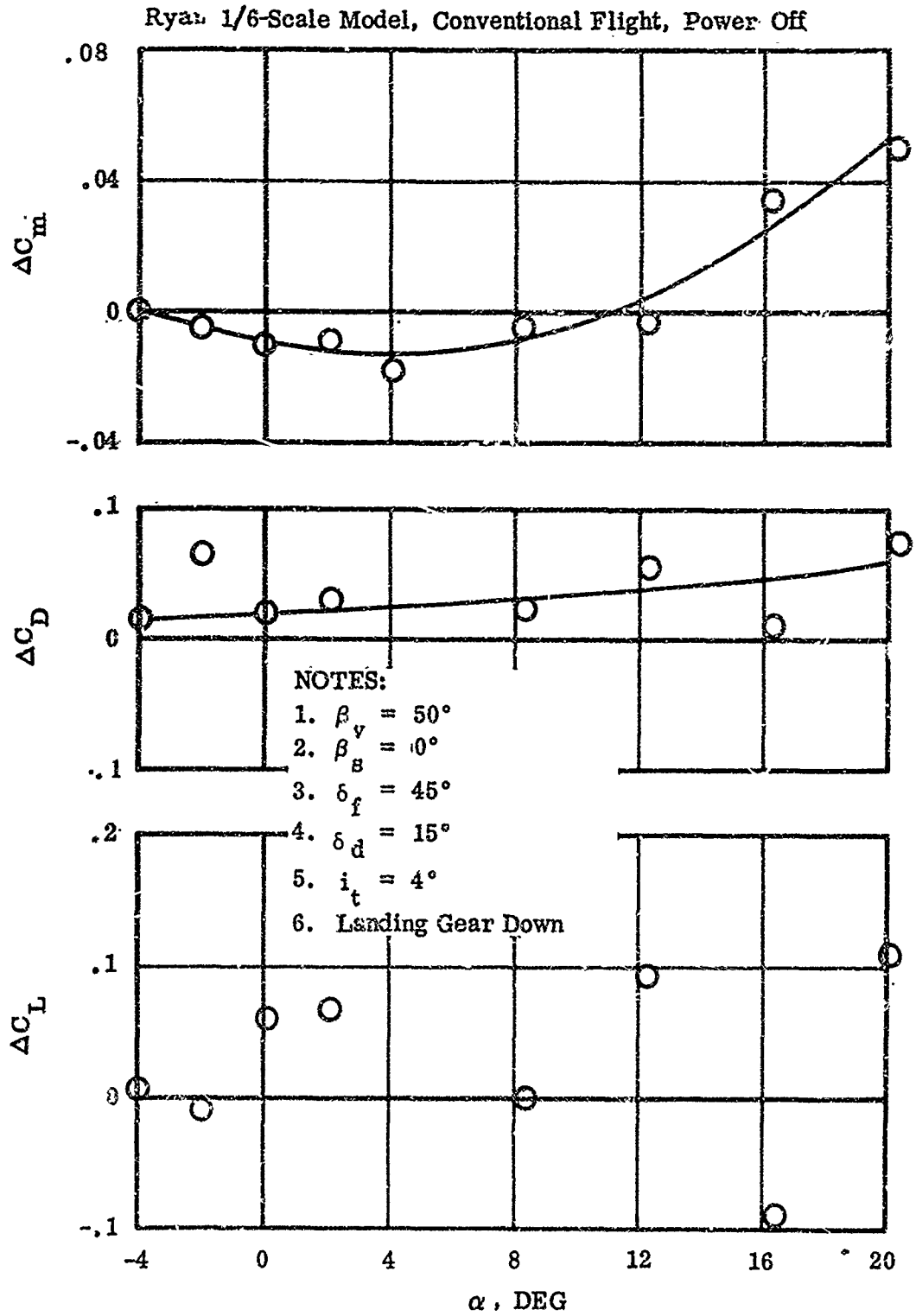

Figure 7. Incremental Aerodynamic Coefficients Due to Open Pitch Fan Inlet and Exit, Power Off.

NOTES:
$\beta_v = 0°, \beta_s = 0°, \delta_f = 45°, \delta_d = 0°$ Tail Off, Pitch Fan Off

SYM	T_c^*	$(T_c^*)_{corr}$
○	0.856	0.861
□	0.964	0.968
△	0.990	0.991

Flagged Symbols Are Corrected For Wall Effect.
T_c^* is Average Value

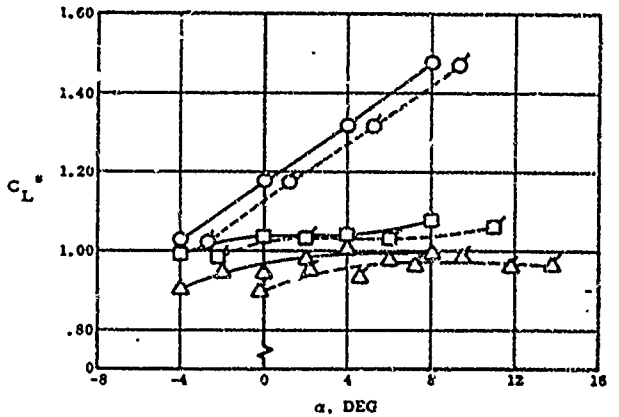

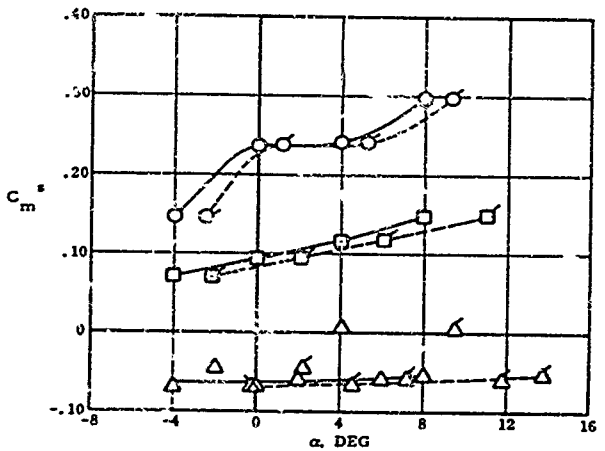

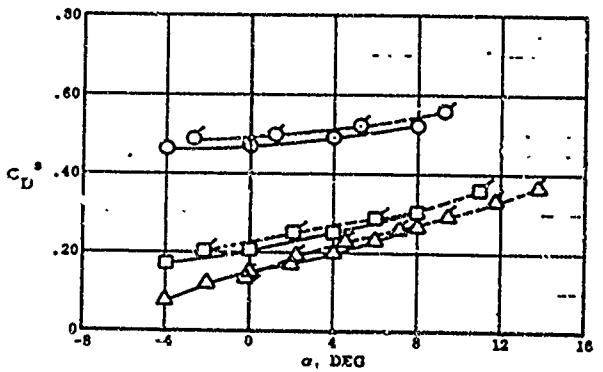

Figure 8. Wind Tunnel Wall Effect Corrections, NASA-Ames Model, Power On, $\beta_v = 0°$, $\beta_s = 0°$.

NOTES:

$\beta_v = 0°, \beta_s = 0°, \delta_f = 45°, \delta_d = 0°$ Tail Off, Pitch Fan Off

SYM	T_c^*	$(T_c^*)_{corr}$
◇	0.914	0.917
○	0.979	0.981

Flagged Symbols Are Corrected For Wall Effect.
T_c^* is Average Value.

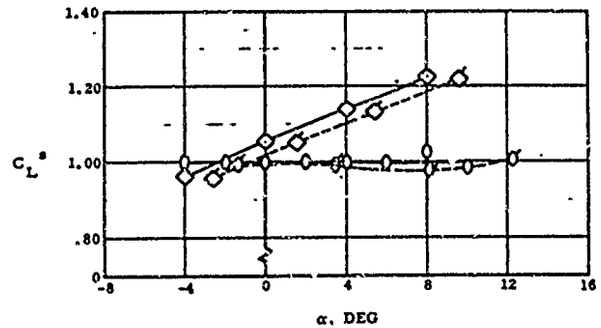

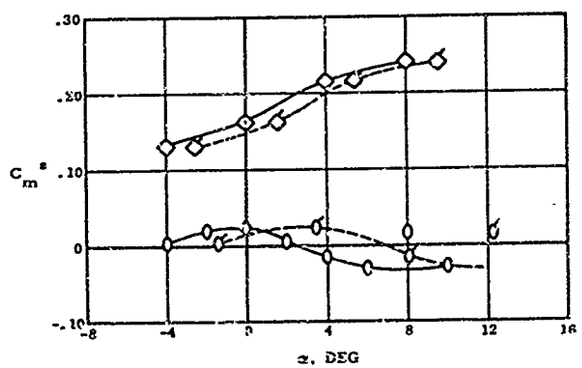

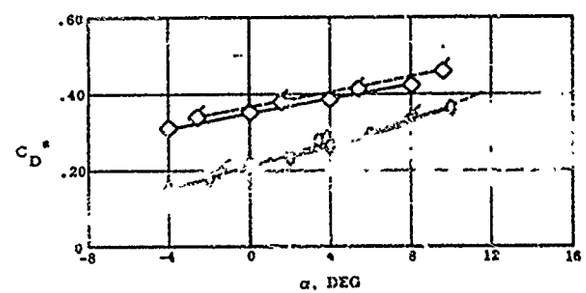

Figure [illegible] and Tunnel Wall Effect Corrections, NASA-Ames Model, Power On, $\beta_v = 0°$, $\beta_s = 0°$.

NOTES:

$\beta_v = 20°$, $\beta_s = 0°$, $\delta_f = 45°$ $\delta_d = 0°$, Tail Off, Pitch Fan Off

SYM	T_c^*	$(T_c^*)_{corr}$
—O—	0.959	0.961

Flagged Symbols are Corrected For Wall Effects.
T_c^* is Average Value

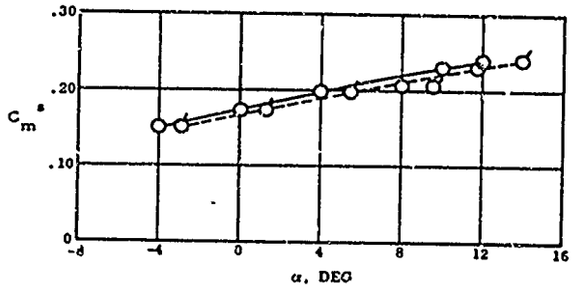

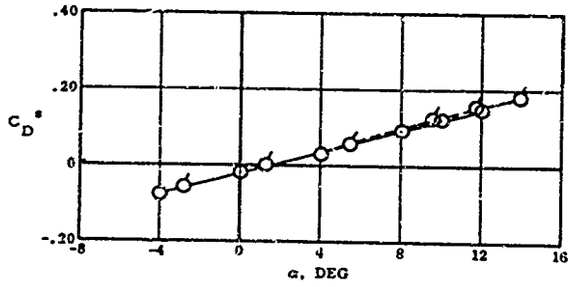

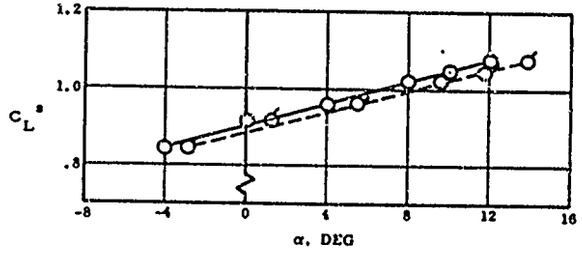

Figure 10. Wind Tunnel Wall Effect Corrections, NASA-Ames Model, Power On, $\beta_v = 20°$, $\beta_s = 0°$.

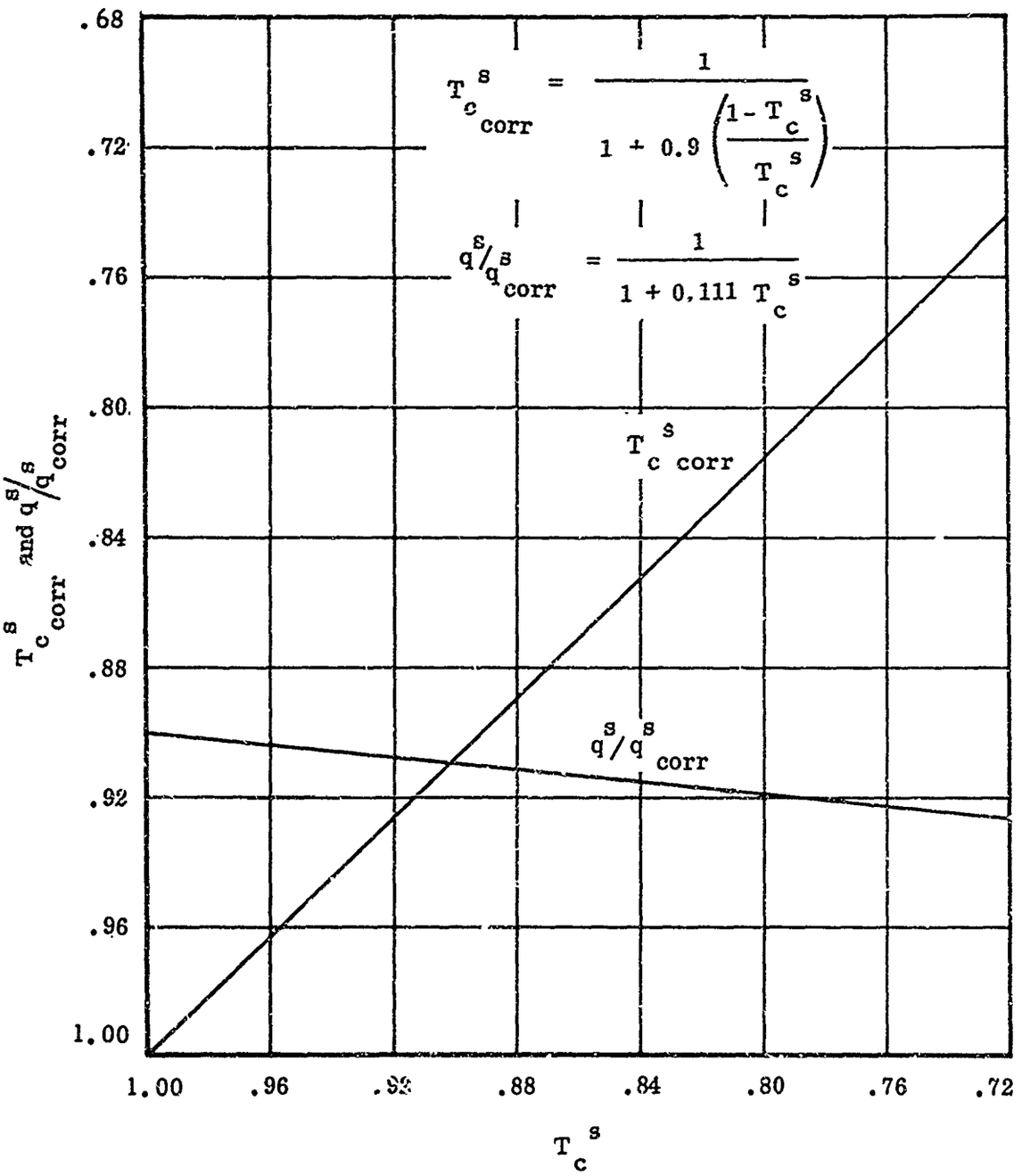

Figure 11. Correction Factors for Wing Fan Turbine Thrust.

$$\left(C_m^s\right)_{corr} = C_m^s\left(\frac{1}{1 + 0.111\ T_c^s}\right) + 0.1\ (T_c^s)_{corr}\ (-0.16\ \cos\beta_v + 0.192\ \sin\beta_v)$$

4.3.4.4 Gas Generator Ram Drag Correction

Since the benefit of the wing fan turbine thrust was added to the 1/6-scale model data, the penalty of gas generator ram drag must also be included. The estimated ram drag level of the Ames 173 test was used to correct the 1/6-scale data.

The 1/6-scale model had streamlined plugs which sealed off the engine inlets. With no mass flow through the engine ducts, the difference in drag due to engine inlets was largely ram drag. Since the ram drag correction was necessarily approximate, other possible differences, such as induced flow over the canopy, were neglected.

Coefficient parameters were not measured during the Ames 173 and 177 tests to calculate engine airflow, nor was the overall ram drag correction large enough to require accurate airflow data.

The theoretical ram drag of the fans can be expressed as a function of thrust coefficient only. The engine ram drag was not so easily handled because it is a function of both power setting and freestream velocity. In order to avoid tying each data point to a specific velocity or power setting, several assumptions were necessary to generalize the engine ram drag correction. The magnitude of the correction was not considered great enough to justify a more accurate estimation.

By relating the airflow through the engine to the airflow through the fan, the engine ram drag coefficient can be related to the fan ram drag coefficient and hence to thrust coefficient. The general expression for ram drag and the corresponding coefficient is

$$D_R = \dot{m}V_o$$

$$\left(\Delta C_D^s\right)_R = \frac{D_R}{q^s A_F}$$

The engine ram drag coefficient is then related to the fan ram drag coefficient by the equation given below:

$$\Delta C_D{}^s{}_{R_g} = \frac{\dot{m}_g}{\dot{m}_F}\Delta C_D{}^s{}_{R_F}$$

$$\Delta C_{D_{R_g}}^{s} = \frac{\dot{m}_g}{\dot{m}_F}\sqrt{2T_c^{s}(1-T_c^{s})} \tag{8}$$

The wing fan corrected mass flow can be estimated from momentum considerations and is given by the following equations for the full-scale fans:

$$\frac{\dot{m}_F\sqrt{\theta}}{\delta} = A_F\sqrt{\rho_o K_F}\left(\frac{N_F}{\sqrt{\theta}}\right)$$

$$K_F = \frac{T_{ooo}}{A_F\sigma N_F^{2}} = 0.03315 \text{ lb/ft}^2, \text{ (full-scale)}$$

$$\frac{\dot{m}_F\sqrt{\theta}}{\delta} = 0.378\left(\frac{N_F}{\sqrt{\theta}}\right)\text{slugs/sec, (two fans)} \tag{9}$$

The engine corrected airflow used for this report is shown in Figure 12 as a function of corrected engine speed. The basis for those data is the calculated, installed performance of the J-85 engine in the XV-5A as published in Reference 9. Since the fan mass flow is related to fan speed and engine flow to engine speed, it was necessary to relate engine speed to fan speed. The data used for this were taken from static tests of the Ames full-scale model during Test 177 and are shown in Figure 13. An apparent failure of engine speed instrumentation occurred during the static runs of Ames Test 173, so those data were not used.

Cross plotting the data of Figures 12 and 13 gives the relationship in Figure 14 between engine airflow and wing fan speed used for calculating the engine ram drag correction in this report. The relationship was linear for the range of corrected fan speed from 40 to 70 percent, but became nonlinear above that range. Since nearly all of NASA-Ames Tests 173 and 177 were run in the low fan speed range, the use of the curve in Figure 14 was considered justified. The equation expressing the relationship between engine airflow and fan speed from Figure 14 is given below:

$$\frac{W_{a_g}\sqrt{\theta}}{\delta} = 9.3 + 0.36\frac{N_F}{\sqrt{\theta}}, \text{ lb/sec/engine} \tag{10}$$

If Equations(9)and (10)are combined, the ratio of engine airflow to fan flow is obtained as shown in the following equations:

$$\frac{\dot{m}_g}{\dot{m}_F} = \frac{2\left(0.289 + 0.0112\frac{N_F}{\sqrt{\theta}}\right)}{0.378\,\frac{N_F}{\sqrt{\theta}}}$$

$$\frac{\dot{m}_g}{\dot{m}_F} = \left(2\,\frac{0.764}{N_F/\sqrt{\theta}} + 0.0296\right) \qquad (11)$$

It should be noted that Equation (11) is valid only in the range of corrected fan speed from 40 to 70-percent. When Equation (11) is substituted into Equation (8), the complete expression for the incremental drag coefficient due to engine ram drag is obtained:

$$\Delta C_D{}^{s}_{R_g} = 2\left(\frac{0.764}{N_F/\sqrt{\theta}} + 0.0296\right)\sqrt{2T_c{}^{s}\,(1-T_c{}^{s})} \qquad (12)$$

The high location of the engine inlet results in a pitching moment correction due to the ram drag. The application of the ram drag force was taken as the center of the face of the inlet, which was located 5.85 feet forward and 2.85 feet above the reference center of gravity. The pitching moment coefficient then is given by the equation below:

$$\Delta C_m{}^{s}_{R_g} = (0.548\cos\alpha + 1.125\sin\alpha)\Delta C_D{}^{s}_{R_g} \qquad (13)$$

The ram drag corrections given by Equations (12) and (13) are plotted in Figure 15 for 40-, 60-, and 70-percent corrected fan speed. The difference in the coefficient between 40-and 70-percent fan speed was considered small enough that the value for 60-percent fan speed could be used as a sufficiently accurate approximation. The ram drag correction was thereby simplified to a function of thrust coefficient only.

4.3.4.5 Wing Fan Power Correction

The wing fan power coefficients of the 1/6-scale model were based on the shaft horsepower output of the model drive motor. The power delivered to the fan rotor was not measured, but would be less due to friction losses in the mechanical power transmission system. It was observed in the 1/6-scale model power coefficient data taken during static operation that the power coefficient varied as a function of power input and fan speed.

Ideally, the power coefficient should have remained constant if power were indeed directly proportioned to the cube of the fan speed. Reference 10 attributed the static variation in power coefficient to system friction losses which are proportioned to the square of the fan speed. Reference 10 then developed a correction to the 1/6-scale model power coefficient data to remove the friction losses and thereby produce a power coefficient which did not vary with fan speed at a thrust coefficient of 1.0. The power coefficient correction for friction losses developed by Reference 10 was used to correct all 1/6-scale model power coefficient data in this report. That correction is given by the following equation:

$$\Delta C_p{}^s = \frac{0.1046}{N_F}$$

The friction coefficient correction might be expected to vary with thrust coefficient because of friction loss variation with changes in fan rotor loading due to crossflow at constant fan RPM. The variation with thrust coefficient is probably a relatively minor effect compared to the fan speed effect.

Power coefficients could not be calculated for the Ames 173 or 177 tests, because the necessary parameters to perform the calculations were not measured. A qualtitative indication of power required, however, may be obtained from gas generator RPM alone, but tests were run at essentially constant fan speed so that the variation in fan speed with thrust coefficient at constant power setting was not available. Measurement of change in fan speed with change in tunnel speed with power held constant may be used to obtain an indication of the ratio of power coefficient to the static power coefficient.

Horsepower calculations were made for the Ames 210 test of the actual XV-5A aircraft, but those data were all obtained with values of exit louver vector and stagger associated with normal control system rigging, not directly comparable with zero louver vector or stagger data. The horsepower calculated was the ideal horsepower available at the turbine exit of the gas generator, and therefore does not include the ducting losses or fan turbine efficiency factor. As a matter of interest, similar data were measured during flight test evaluation of the aircraft.

A correlation of 1/6-scale model and full-scale wing fan power required should be made on the basis of power delivered to the fan rotor. Correlation of the power delivered at the power source would be meaningful only if the difference between mechanical and gas power transmission loss from the source to the fan rotor could be adequately accounted for. There were not sufficient test data to determine the losses, and theoretical analysis of the system losses was beyond the scope of this study. Therefore, correlation of 1/6-scale and full-scale wing fan power required was not attempted.

While an accurate correlation of fan power required was not possible, the effect of flight speed on apparent power absorption was so grossly different for the 1/6-scale and full-scale fans that there was little doubt that the difference existed. The difference in apparent power absorption in crossflow was one of the greatest disparities noted between the 1/6-scale and full-scale wing fan data. The effect of exit louver vector and stagger angle on fan power absorption was qualitatively the same for both sets of fans.

The effect of crossflow on fan power absorption can be expressed as the ratio of the power coefficient at some value of thrust coefficient to the static power coefficient. Thus,

$$\frac{C_p^s}{C_{p_o}^s} = \frac{P}{P_o}\left[\frac{\left(T_{ooo}/A_F\right)_o}{\left(T_{ooo}/A_F\right)}\right]^{3/2}$$

$$\frac{C_p^s}{C_{p_o}^s} = \frac{P}{P_o}\left[\frac{N_{F_o}}{N_F}\right]^3$$

If the exit louver angle and the angle of attack are assumed to be constant, the variation of power coefficient ratio with thrust coefficient expresses the variation in power at constant fan speed or the variation in fan speed at constant power. The power coefficient ratio, in theory, is not subject to the large errors that absolute power coefficient is because it is only a measure of the relative change in power, or fan speed, from the static value. However, in practice, the accuracy of the ratio is determined by such effects as the exactness with which power changes with flight speed variation can be measured and the effects of fan and engine reingestion on power developed and fan speed.

A comparison of the power coefficient ratio for the 1/6-scale and full-scale wing fans is shown in Figure 16 for zero exit louver angle and zero angle of attack. The full-scale values shown are the same as those used for flight simulator studies of the XV-5A. They were obtained from Reference 11 and based on a NASA-Ames test of a high wing, fan-in-wing model using original General Electric X353-5 fans. While those data are not exactly applicable to the XV-5A aircraft, they are quite representative of the actual full-scale fan characteristics.

The significant factor evident in Figure 16 is the variation in power coefficient ratio with thrust coefficient. The 1/6-scale model data indicate that at constant fan speed, greater power is required with decreasing thrust coefficient, while the full-scale data indicate the opposite trend. The difference could also be stated as at constant power the 1/6-scale model fan speed would decrease with decreasing thrust coefficient and the full-scale fan speed would increase. This discrepancy

was never satisfactorily resolved during the development of the XV-5A.

If the variation in power coefficient ratio were the same for both models, it would be of little concern in correlating aerodynamic coefficients. The important question which arises from the difference in 1/6-scale and full-scale power coefficient ratio is: how does the actual fan thrust vary at constant power or at constant fan speed? It was shown in Reference 5 and in Section 3.0 of this report that the more valid correlation parameter is really thrust coefficient based on actual thrust. In this study and in the development and flight test of the XV-5A, the fan static thrust was used for the correlation parameter because of its measurability and unique relationship to fan speed and, hence, its convenience. Correlation of small- and full-scale model data would be valid using static fan thrust if, at any condition, the ratio of actual fan thrust to static thrust is the same for both models. If, however, the ratio is different for small-scale and full-scale, then at the same test thrust coefficient based on static thrust, the two models would be at different thrust coefficients based on actual fan thrust.

The variation of power coefficient ratio with thrust coefficient as shown in Figure 16 has been attributed to two plausible explanations. One explanation is that the gross fan thrust remains relatively constant at constant fan speed, and the efficiency of the fan or distribution of rotor loading changes in crossflow. The difference in 1/6-scale and full-scale characteristics would affect the correlation of test data, but it would be virtually impossible to make any corrections because only the induced or interference effects of fan flow would be involved. Gross fan thrust would remain a unique function of fan speed, and thrust coefficient based on static thrust would be valid for data correlation purposes. The second explanation is that fan efficiency remains relatively constant, and a constant power delivered produces a constant actual fan thrust even though fan speed may vary. If the latter explanation were true, then data correlation could be significantly affected by the difference in 1/6-scale and full-scale power coefficient characteristics, because power would be the true measure of actual fan thrust and fan speed would not. It is most likely that a combination of the two explanations is the reason for power coefficients varying with thrust coefficient. Measured fan momentum thrust in crossflow would be required to support either of the two explanations.

The only measured momentum thrust in crossflow was obtained during the NASA-Ames full-scale tests. The results are reported in Reference 12. Those data show that the wing fan momentum thrust decreased with decreasing thrust coefficient at constant fan speed. The power required was not determined during those tests, but according to the data of Figure 16, the power must also decrease with thrust coefficient at constant fan speed. The Ames data lend support to the assumption that the actual fan thrust in crossflow varies with power at constant fan speed. Whether or not the actual fan thrust is constant at constant power could be determined only if power-required data were available. The accuracy of the Ames variation of momentum thrust in crossflow was not established because it was not known if the data were corrected for hot gas reingestion into the fan inlet.

In spite of the many unknown factors concerning wing fan characteristics in crossflow, an attempt was made to correct the 1/6-scale and full-scale test data to account for the difference in the variation of power coefficient ratio in crossflow. The power correction was based on the assumption that actual gross fan thrust, in crossflow, was constant at constant power and not at constant fan speed. There was not sufficient data available to establish that such an assumption was entirely valid or invalid, and it was at best partially substantiated by the comparison of power coefficient ratio and momentum thrust measurement.

If actual fan disk loading is assumed to be constant at constant power, then the power coefficient ratio based on actual disk loading would be equal to 1.0 for the case of zero exit louver deflection.
The power correction then amounts to adjusting the data reduction disk loading to a value corresponding to a power coefficient ratio of one.
The disk loading corrected to constant power is given by the following equation:

$$\left(\frac{T}{A_F}\right)_P = \frac{T_{ooo}}{A_F}\left(\frac{C_p^s}{C_p^s{}_o}\right)^{2/3}$$

The thrust coefficient and slipstream dynamic pressure must be corrected to the adjusted value of reference disk loading. Those corrections are given by the following equations:

$$(T_c^s)_P = \frac{1}{1+\left(\frac{C_p^s{}_o}{C_p^s}\right)^{2/3}\left(\frac{1-T_c^s}{T_c^s}\right)}$$

$$\frac{q^s}{(q^s)_P} = \frac{1}{1+T_c^s\left(\frac{C_p^s}{C_p^s{}_o}\right)^{2/3}-T_c^s} \qquad (14)$$

The aerodynamic coefficients were then corrected by multiplying by the slipstream dynamic pressure ratio given in Equation (14).

In arriving at an illustration of the effect, the power correction was applied to a comparison of the 1/6-scale and full-scale data at zero exit louver only.

4.3.4.6 Pitch Fan System

The 1/6-scale model pitch fan was powered by a separate electric motor and gearbox arrangement in the same manner as the wing fans. The power to the pitch fan was not measured, and correlation with full-scale power data was not possible.

The Ames full-scale model was equipped with an XV-5A pitch fan. The full-scale pitch fan was driven by a tip turbine in the same manner as the wing fans. The Ames model pitch fan was powered by a separate T-58 gas generator, whereas the pitch fan in the actual XV-5A was driven by hot gas bleed from the J-85 gas generators used to drive the wing fans. Power data were not measured for the Ames full-scale model tests; therefore, correlation was not possible.

Since there were numerous differences between the 1/6-scale and full-scale wing fans in geometry and power characteristics which could not be adequately accounted for, a detailed analysis of pitch fan differences was not warranted. There were even less data available to define pitch fan characteristics than for the wing fans, and it was considered unlikely that differences between 1/6-scale and full-scale pitch fans could be resolved. Therefore, pitch fan data correlation was limited to examination of static thrust reverser door effectiveness.

4.3.4.7 Pitch Fan Thrust Reverser Door Geometry

The pitch fan thrust reverser doors presented two difficulties in correlating pitch fan effectiveness. The 1/6-scale model and the XV-5A aircraft doors were so-called sugar scoop type, in that they had end plates normal to the door surface at the forward and aft ends of the door. The doors of the Ames model were curved metal plates with no end plates. The effect of that difference could not be determined. In addition to the end plates, the XV-5A aircraft had cascade doors which were never tested on a wind tunnel model.

Besides the differences in thrust reverser door configuration, the models used different door position references. The door positions for the actual aircraft and the 1/6-scale model were measured in degrees from fully closed, while on the NASA-Ames model the position was measured in degrees from the maximum thrust position. The maximum thrust door position of the Ames model was assumed to be 112 degrees from fully closed, which was considered a reasonably accurate estimate.

4.4 WING-BODY CORRELATION

Correlation of wing-body data was limited to the 45-degree flap configuration with no aileron droop, landing gear up, pitch fan off, and the pitch fan cavity closed. This limitation reduced the applicable test data to those of the 1/6-scale model test and NASA-Ames Test 173. The reasons for selecting the described configuration are given below:

1. The 1/6-scale wing-body was tested at only three values of thrust coefficient with zero flaps, which was not sufficient, considering the characteristics of the data.

2. Ames Test 210 had no tail-off (wing-body) data.

3. Ames Test 177 wing-body data were all obtained with the wing fan turbine louvers offset 30 degrees from the remainder of the fan louvers.

4. Ames Tests 173 and 177 did not accurately represent drooped ailerons.

5. Ames Test 173 had no pitch fan installed and no landing gear.

The chosen configuration was that most nearly represented by two different tests. The degree of success obtained with the wing-body correlation was considered to provide a measure of the extent to which further correlation attempts should be pursued.

4.4.1 ZERO ANGLE OF ATTACK, ZERO EXIT LOUVER

A comparison of the 1/6-scale and Ames full-scale model wing-body characteristics is shown in Figure 17. There the uncorrected test data were in poor agreement at thrust coefficients below about 0.95. At the high thrust coefficients, the drag and moment coefficients attained good agreement. The inherent nature of the general configuration indicates that the drag and moment coefficients must come into reasonably good agreement as the thrust coefficient approaches 1.0. The drag coefficient must approach a value close to zero, since thrust vectoring is zero, the moment coefficient must approach approximately -0.16, which is the nondimensional moment arm between the center of gravity and the fan center.

The uncorrected lift coefficients of the two models shown in Figure 17 were generally in poor agreement at all thrust coefficients. The variation of lift coefficient with thrust coefficient was about the same for both models below a thrust coefficient of about 0.92; however, the magnitude of the 1/6-scale model lift coefficient was 5 to 7 percent greater than that of the Ames full-scale model. At thrust coefficients above 0.92, the magnitude and variation of lift coefficient with thrust coefficient disagreed significantly. It would be well to note here that the maximum level-flight speed of the XV-5A aircraft, at zero angle of attack with the pitch fan on, corresponds to a thrust coefficient of approximately 0.90.

The rapid variations in lift coefficient at high thrust coefficients shown in Figure 17 caused some concern as to whether they actually existed or whether they were due to data inaccuracies such as bad test points. After examining other data with the tail on and different flap settings, it was concluded that the characteristic was typical of that actually obtained during the test.

No data were presented for static conditions because wind tunnel test data under those circumstances were considered to be highly questionable. Reference 13 presents some insight into the problem of very low speed testing, wherein a pattern of recirculation of the propulsion-lift system efflux can be set up in the tunnel. Reference 13 is discussed further in Appendix III with wall effects and wind tunnel limitations. The minimum test velocity above which test data could be considered certain to be valid was not established for any of the XV-5A model tests. There is insufficient experimental data currently available to evaluate the type of flow phenomena, discussed in Reference 13 , with respect to a particular configuration.

In addition to the comparison of uncorrected test data, the effect of data corrections successively applied to the Ames full-scale model is also shown in Figure 17 . The Ames data were corrected only for wall effects and strut system tares, which were not included in the basic data. The wall effect correction accounted for 20 percent of the difference in drag coefficient below a thrust coefficient of 0.95 with a diminishing effect at high thrust coefficients. The strut correction reduced the wall effect increment such that the total full-scale correction factors accounted for about 12 percent of the difference in drag coefficient.

Full-scale corrections to moment coefficient, shown in Figure 17, had only a minor effect on the correlation. Wall effects adversely affected the correlation, while the strut correction nearly cancelled out that due to the wall effect.

There was no lift correction due to the Ames 173 strut system. Wall effect corrections had a large adverse effect on the lift coefficient correlation below a thrust coefficient of 0.94. The wall correction increased the difference between the lift curves of the two models in Figure 17 by 50 to 100 percent. At high thrust coefficients, the wall correction diminished and had little overall effect on the correlation.

The effect of the corrections successively applied to the 1/6-scale model data is shown in Figure 18 compared to the final, corrected, full-scale model data. The fan turbine thrust correction reduced the 1/6-scale model drag coefficient even though there was no actual correction to the drag force at zero exit louver. This was due to the increased slipstream dynamic pressure resulting from including turbine thrust in the corrected fan disk loading the same as it is included in the full-scale disk loading. The derivation of the 1/6-scale model corrections was shown in Section 4.3, and the individual effects of the corrections shown in Figure 18 are self-explanatory. The total effect of all 1/6-scale model corrections on the data correlation was discouraging. Overall, the 1/6-scale model corrections adversely affected the lift and moment coefficient correlation, but only by about 0.01 in the magnitude of either coefficient. The total corrections to drag coefficient accounted for 15 to 25 percent of the difference between 1/6-scale and full-scale below a thrust coefficient of about 0.94.

An example of the effect of the assumed correction for wing fan power absorption discussed in Section 4.3 is shown in Figure 19. The correction was applied to the final corrected curves, excluding power, of Figure 18. It is evident that the correction had a very large effect, particularly on lift coefficient. The correlation of lift, drag, and pitching moment coefficient was improved in varying degrees depending upon the thrust coefficient.

A noteworthy effect of the power correction was that it overcorrected lift coefficient such that the full-scale lift coefficient was greater than the 1/6-scale model at all thrust coefficients. Without the power correction, the 1/6-scale model lift coefficient was greater than full-scale below a thrust coefficient of 0.95. Therefore, the wall effect corrections, which had an adverse effect on the correlation without the power correction, would enhance the lift coefficient correlation with the power correction applied.

The lack of measured fan momentum thrust data or a definitive relationship between actual thrust and power delivered makes the power correction, at best, an estimate. The large effect of the power correction on the data correlation, though, indicates that the actual momentum thrust, hence actual momentum jet velocity ratio, cannot be ignored if it is hoped to establish kinematically similar flow conditions between small-scale and full-scale models.

4.4.2 VARIABLE ANGLE OF ATTACK, 20 DEGREES VECTOR ANGLE

Of the wing-body data from the 1/6-scale model and Ames Test 173, there was only one angle-of-attack polar for which the thrust coefficient of the two models was close enough to permit a direct data comparison and for which the Ames model thrust coefficient did not vary significantly during the test run. Those data were obtained at an exit louver vector angle of 20 degrees and are shown in Figure 20.

The difference between the full-scale and 1/6-scale uncorrected test data at 20 degrees vector angle was of the same order of magnitude as that at zero vector angle for the same thrust coefficient. The thrust coefficients of the two models shown in Figure 20 were not exactly the same, but it will be seen that they are very nearly the same after all corrections have been applied.

Wind tunnel wall corrections and strut system tares applied to the full-scale model data, Figure 20, had a negligible effect on the drag and moment coefficients. The wall effect correction accounted for about 20 to 30 percent of the difference in lift coefficient, but increased the difference in lift curve slope.

The effect of the 1/6-scale model corrections on the data correlation is shown in Figure 21. Note that the fan turbine thrust correction changes the thrust coefficient of the 1/6-scale model data to within 0.001 of the full-scale thrust coefficient. The 1/6-scale model corrections had only a small effect on lift coefficient, but accounted for 25 to 30 percent of the difference in drag coefficient and 35 to 50 percent of the moment coefficient difference, depending on angle of attack. None of the applied corrections had any effect on the slope of the coefficients versus angle of attack. Although 25 to 50 percent of the difference between 1/6-scale and full-scale model data was accounted for, the remaining discrepancy was still too large to consider the correlation satisfactory.

4.4.3 EXIT LOUVER VECTOR EFFECTIVENESS

A comparison of the thrust vectoring effectiveness of the 1/6-scale and full-scale model wing fans is shown in Figure 22 for a thrust coefficient of 0.96. Actual test data from the Ames 173 test could not be shown because there were no wing-body vector effectiveness data at the same thrust coefficient as the 1/6-scale model. Therefore results from cross-plots of data are shown. Vector effectiveness is shown as the incremental change in the aerodynamic coefficients due to vectoring the exit louvers from zero. An advantage of comparing incremental effects is that most of the data corrections developed in Section 4.3 become identically zero. In fact, only two of the model corrections are applicable. The fan turbine thrust correction to the 1/6-scale model data is a function of vector angle and therefore applicable. The Ames 173 curve should actually have been corrected for the change in wall effect from zero vector angle, but the magnitude of the correction appeared to be too small to warrant the very large number of calculations required

The correlation of incremental vector effectiveness shown in Figure 22 was surprisingly good compared to the correlation of absolute coefficients in Sections 4.4.1 and 4.4.2. The greatest discrepancy was in drag coefficient at 40 degrees vector angle, where the Ames model obtained 11.5 percent less incremental drag coefficient than the 1/6-scale model. The 1/6-scale model fan turbine thrust correction was within the scatter of the 1/6-scale model test data.

The only direct comparison of actual test data for vectoring effectiveness of the 1/6-scale model and Ames Test 173 was at a thrust coefficient of about 0.978 with the horizontal tail on. Those data are shown in Figure 23. The correlation of uncorrected data from the two models was good, except for lift coefficient. The lift decrement of the two models due to vectoring differed by nearly a constant value above 10 degrees vector angle. Figure 23 indicates that the 1/6-scale model absolute lift coefficient at zero vector may have been in error, but it was not obvious from the test data.

The relatively good agreement between 1/6-scale and full-scale model vector effectiveness shown in Figures 22 and 23 created the suspicion that possibly comparisons had been made in the only range of thrust coefficient where the two models did agree. Vector effectiveness was further investigated for the effect of thrust coefficient. That effect is shown in Figures 24 and 25 for both models. The 1/6-scale model data shown in those figures are the difference between two actual test points, whereas the Ames 173 data are the difference between faired curves at constant vector angle. The approach with the Ames 173 test data was necessary because thrust coefficient varied too much from run to run and from data point to data point.

The trends in lift coefficient shown in Figures 24 and 25 agree quite well for the two models. The 1/6-scale model lift and moment coefficient increments are nearly within the scatter of the Ames data; however, sufficient 1/6-scale test data are sorely lacking.

The major discrepancy between the 1/6-scale and full-scale model vector effectiveness was in the variation of the incremental drag coefficient with thrust coefficient. In Figures 24 and 25, the 1/6-scale model drag coefficient increment remains constant or increases with decreasing thrust coefficient, while the Ames model data decreases. The reason for the discrepancy could not be determined.

4.4.4 EXIT LOUVER STAGGER EFFECTIVENESS

There were no exit louver stagger effectiveness data from the 1/6-scale model and Ames Test 173 which were directly comparable. A limited comparison is shown in Figure 26, where the 1/6-scale model curve was obtained by cross-plotting other test data. Note also that the Ames model had the horizontal tail on and the 1/6-scale model did not, but that difference should have a negligible effect.

The agreement in stagger effectiveness between the two models shown in Figure 26 was very good without attempting any corrections. As in the case of vector effectiveness, the stagger effectiveness may not compare so well at other thrust coefficients. There were not enough data for both models to correlate the effect of thrust coefficient on stagger effectiveness.

4.4.5 STATIC AERODYNAMIC DERIVATIVES

A general comparison of angle-of-attack effects for the full-scale and 1/6-scale models was not feasible, due to the lack of a common test thrust coefficient and to the full-scale model thrust coefficient's sometimes varying appreciably during a run. Therefore, it was decided to compare the lift, drag, and moment coefficient derivatives with respect to angle of attack. The derivatives were evaluated at zero angle of attack.

The variation of the aerodynamic derivatives with thrust coefficient at zero exit louver angle is shown in Figure 27. The corrections applied to the data in Figure 27 were obtained by simply taking the derivative, with respect to angle of attack, of the corrections derived in Section 4.3.

The greatest discrepancy between the 1/6-scale and full-scale model derivative was in the pitching moment or static stability derivative. The 1/6-scale model wing-body was 30 to 50 percent more unstable than the Ames full-scale model below a thrust coefficient of 0.94. It was pointed out in Section 4.3 that the same difference existed in the conventional flight configuration for both zero and 45 degrees flap deflection. As is evident in Figure 27, applying the data corrections generally increased the magnitude of the discrepancy. The reasons for the difference in static stability between the two models could not be identified.

The lift coefficient derivatives for the two models were in fair agreement, but not to the extent desirable for a correlation of test data. More data points would have been desirable for the Ames 173 wing-body to ascertain if any scatter existed in the derivative. The corrections applied to the lift coefficient derivative accounted for about 40 percent of the difference between the two models below a thrust coefficient of 0.91, and had a negligible effect at higher thrust coefficients.

Correlation of the drag coefficient derivative shown in Figure 27 was not conclusive due to considerable scatter in the data, particularly for the 1/6-scale model. As in the case of the lift coefficient derivative, more full-scale model wing-body data would have been desirable. The full-scale model uncorrected data were predominantly within the scatter of the 1/6-scale model data. Data corrections had no discernible effect.

The effect of exit louver vector angle on the aerodynamic derivatives is shown in Figure 28 for a thrust coefficient of 0.96. There was a severe shortage of Ames 173 test data at the same thrust coefficient as the 1/6-scale model. The 1/6-scale model data shown were the only data available for the variation of the derivatives with vector angle. Since there was only one data point available for the Ames full-scale model, a fairing was made to the value for zero vector angle from Figure 27.

The lift coefficient derivatives shown in Figure 28 were in good agreement at 20 degrees vector angle, but an apparent discrepancy existed at zero vector. The data corrections applied had a negligible effect on the correlation.

The same difference in static stability shown in Figure 27 at zero vector also is evident in Figure 28 at 20 degrees vector angle. The moment coefficient derivative of either model was not significantly affected by vector angle at a thrust coefficient of 0.96. The net effect of the 1/6-scale model data corrections was negligible compared to the difference between the two models.

Figure 28 shows an apparently large difference in the 1/6-scale and full-scale model drag coefficient derivative versus vector angle. The value for the 1/6-scale model at zero vector in Figure 28 can be seen to be considerably below the faired average in Figure 27. If the zero vector angle value was actually in error, it would mean that possibly the entire 1/6-scale model curve was low in drag coefficient derivative. In such a case, the correlation of the two models would be greatly improved. Since there were no other 1/6-scale model data with which to compare the effect of vector angle, the accuracy of the data shown in Figure 28 could not be verified.

4.5 DOWNWASH

A limited amount of wing-body downwash data is presented in Figure 29 for the 1/6-scale and full-scale models. The horizontal tail downwash angle was taken at the point of intersection of the tail-on and tail-off curves of pitching moment coefficient versus angle of attack. The Ames 173 downwash angles were difficult to determine more accurately than ±2 or 3 degrees because of data scatter and because the tail-on and tail-off curves were nearly parallel at their intersection. Comparison of downwash from other tests and models, such as Ames 210, was hampered by dissimilar test conditions and configuration differences which could not be adequately reconciled. From the data of Figure 29, it can only be concluded that the full-scale and 1/6-scale model downwash angles were of the same order of magnitude.

4.6 PITCH FAN

A comparison of the static pitch fan thrust reverser door effectiveness is shown in Figure 30 for the 1/6-scale model, the Ames full-scale model, and the XV-5A aircraft. The differences in door geometry were discussed in Section 4.3. The XV-5A aircraft with the cascade reverser doors would be expected to exhibit the greater effectiveness and reversing capability shown in Figure 30. The Ames model and the 1/6-scale model were most nearly the same geometrically, and they show about the same effectiveness or slope versus door position. The difference in zero thrust door position of the Ames and 1/6-scale models shown in Figure 30 may have been due to the inability to determine the pitch fan door reference position of the Ames model, which was discussed in Section 4.3.

Correlation of pitch fan door effectiveness in transition was not attempted, partially because of the lack of good correlation statically. The test data from models with different reverser doors would not be expected to correlate, and the differences due to door geometry and reference position could not be corrected. In addition, the ratio of pitch fan to wing fan speed for the 1/6-scale model was not the same as full-scale, so possible differences in interference effects would be introduced. Those differences could not be accounted for either.

4.7 POWER

Correlation of power data beyond that shown in Figure 16 was not attempted. There were known to be very large apparent differences in wing fan power absorption between the 1/6-scale and full-scale models. Comparison of power output at the power source would be incorrect because of the different methods of transmission of power to the fan rotor. There was not sufficient information available to determine the power delivered to the fan rotor; therefore, no common basis existed for correlation of absolute power data. Furthermore, there were no power data available from the Ames 173 or 177 tests. Some comparison of the ratio of power at any condition to the static power required in terms of coefficients, would have been possible, but would not have been meaningful in terms of data correlation. There is no way of correcting the power from one model, such as in Figure 16, to account for the difference in power required between two models. Such a correction should not be confused with the power correction derived in Section 4.3.4.5. In the so-called power correction of Section 4.3.4.5, power, per se, was not the significant parameter, but was used only as a device to establish the magnitude of possible adjustments to fan disk loading.

4.8 COMPLETE MODEL

Comparison of Ames 173 and 177 complete model data with 1/6-scale model data would not have been meaningful because of the rather poor correlation obtained with the wing-body data. Correlation of actual XV-5A aircraft data from Ames Test 210, which was all complete model data, with the 1/6-scale data would have been more appropriate because the airframe geometry was more similar. However, the apparent differences between the 1/6-scale model and full-scale wing fans were considered to be the most significant factors affecting data correlation, and those differences could not be reconciled. Therefore, it is unlikely that correlation using the Ames 210 data would have been any more meaningful than that using the Ames 173 or 177 data. For these reasons, no correlation of complete model data was made.

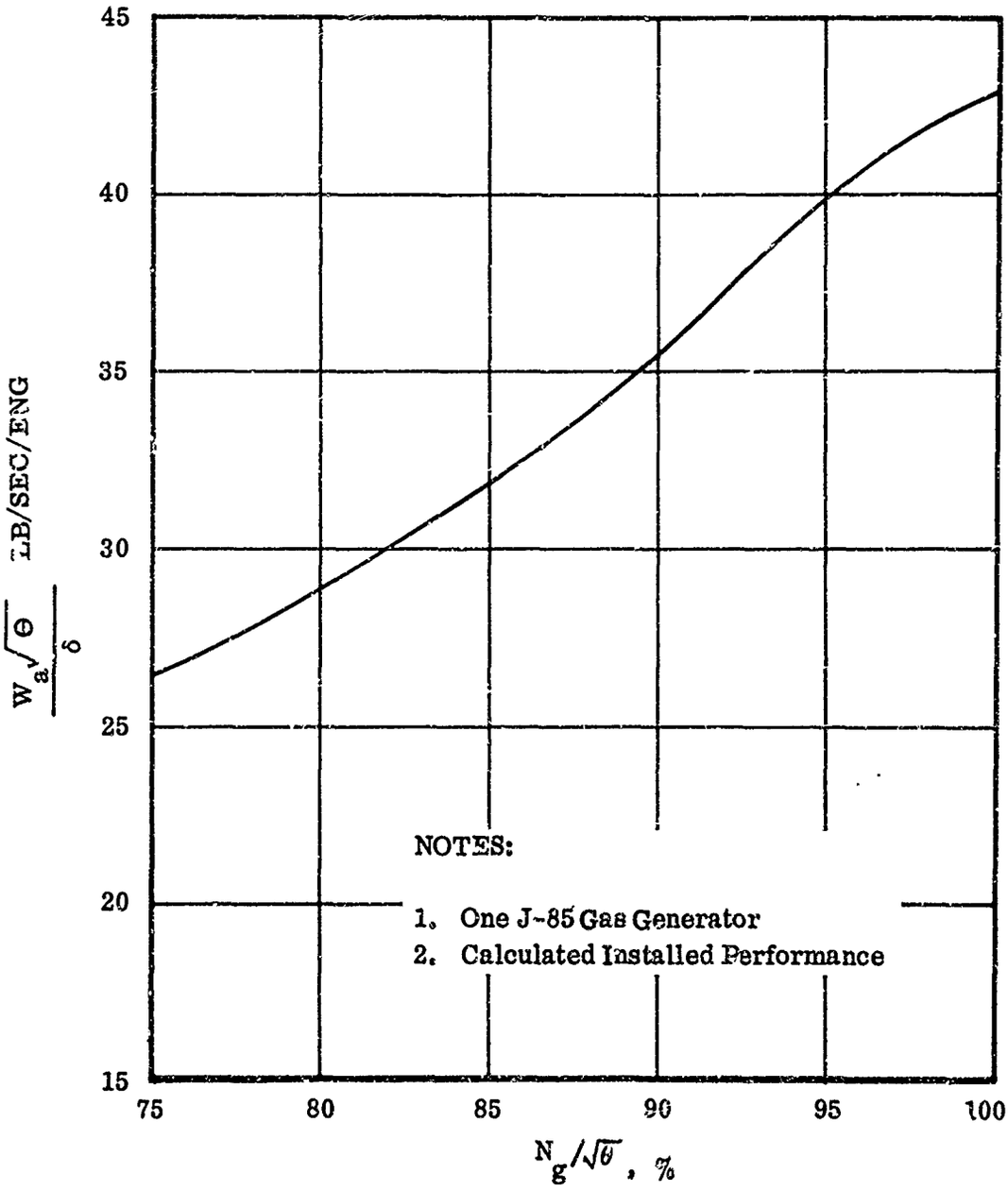

Figure 12. Gas Generator Estimated Airflow.

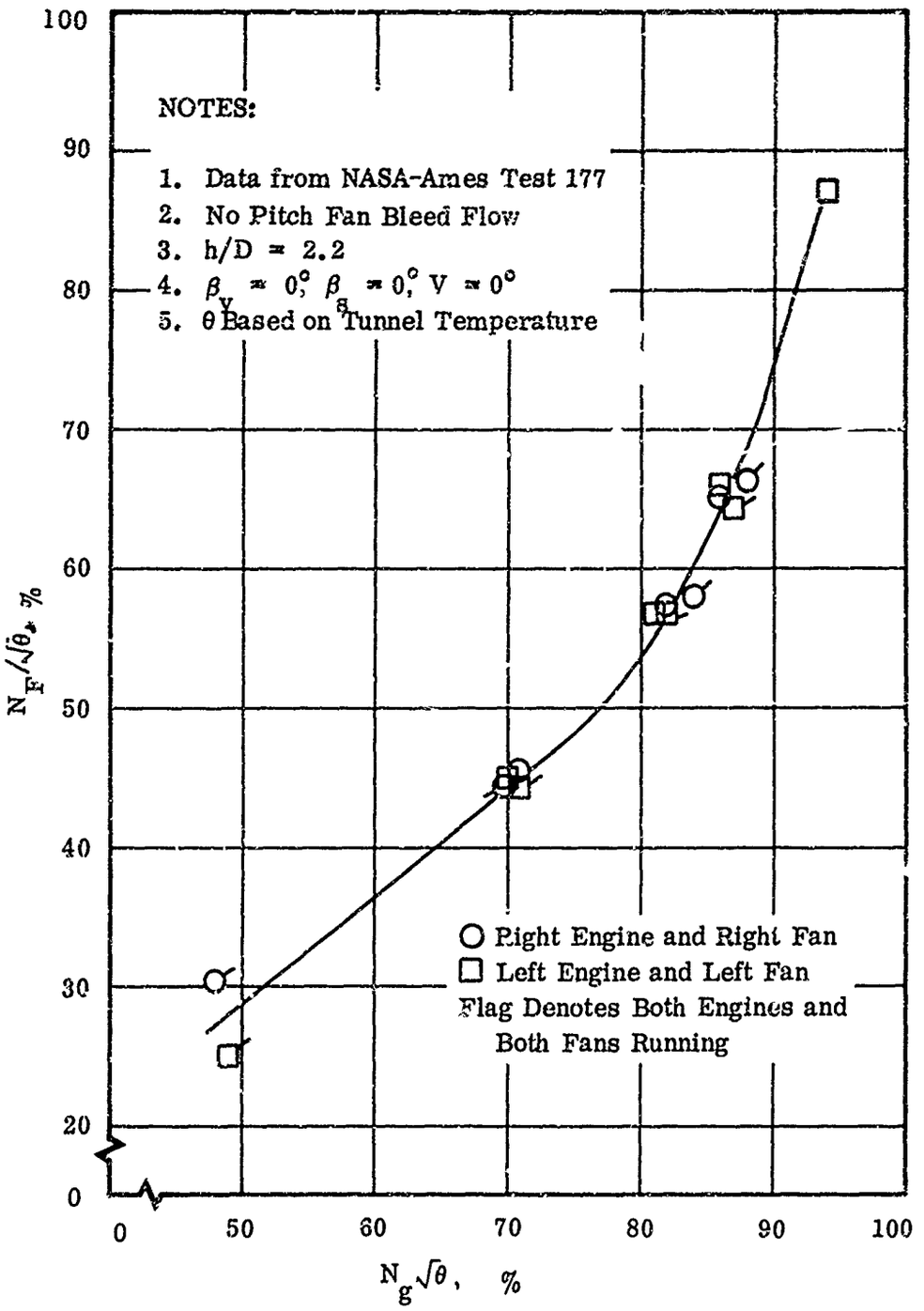

Figure 13. Variation of Wing Fan Speed With Gas Generator Speed, β_v=0°, β_s=0°, V=0°.

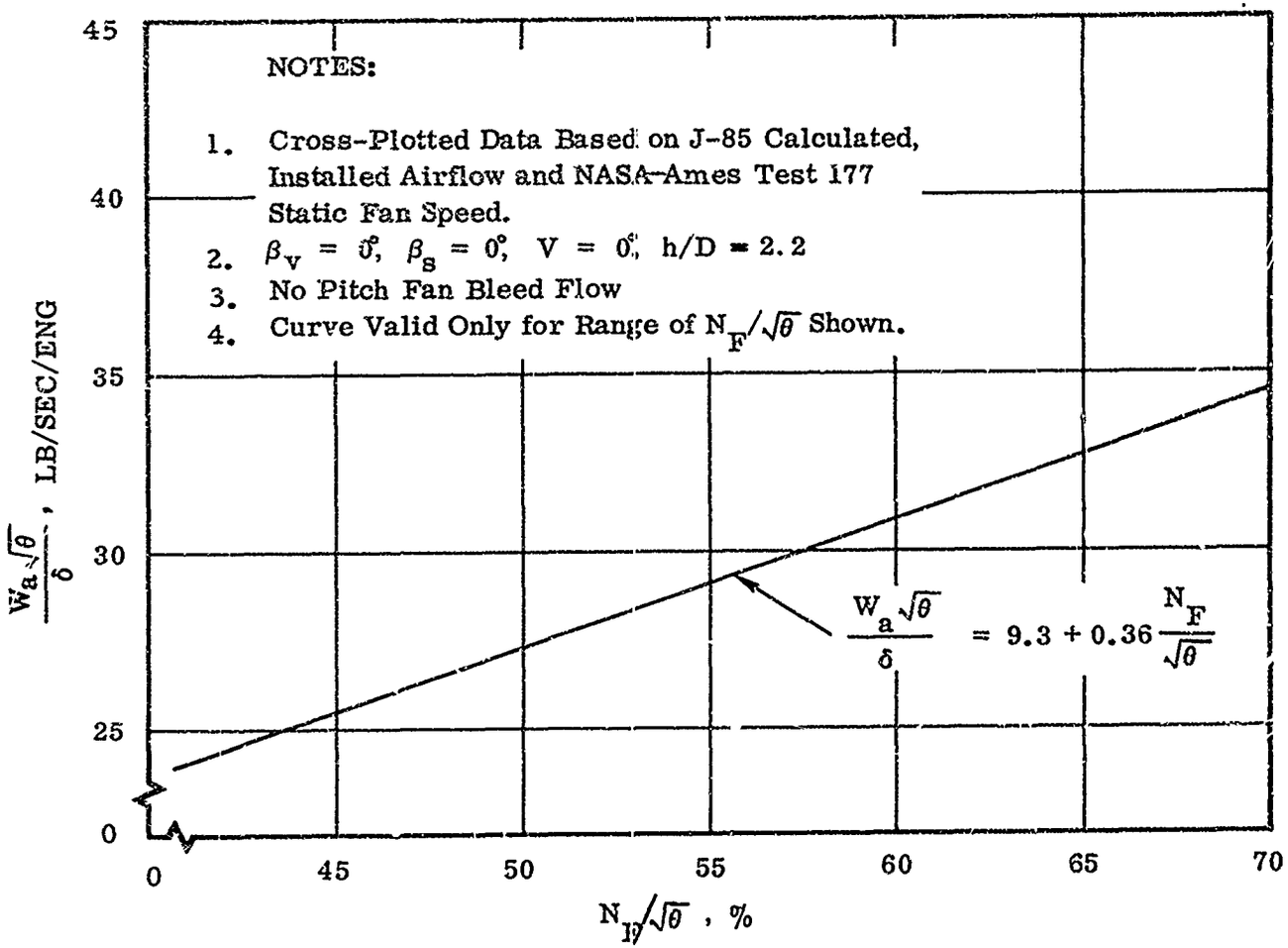

Figure 14. Estimated Variation of Gas Generator Airflow With Wing Fan Speed.

NOTES:

1. $\Delta C_m{}^s$ and $\Delta C_D{}^s$ for $N_F/\sqrt{\theta}$ = 60% Used For All 1/6-Scale Model Corrections

2. $\Delta C_D{}^s = 2\left(\frac{0.764}{N_F/\sqrt{\theta}} + 0.0296\right)\left[2T_c{}^s(1-T_c{}^s)\right]^{1/2}$

$\Delta C_m{}^s = (0.548 \cos\alpha + 1.125 \sin\alpha)\,\Delta C_D{}^s$

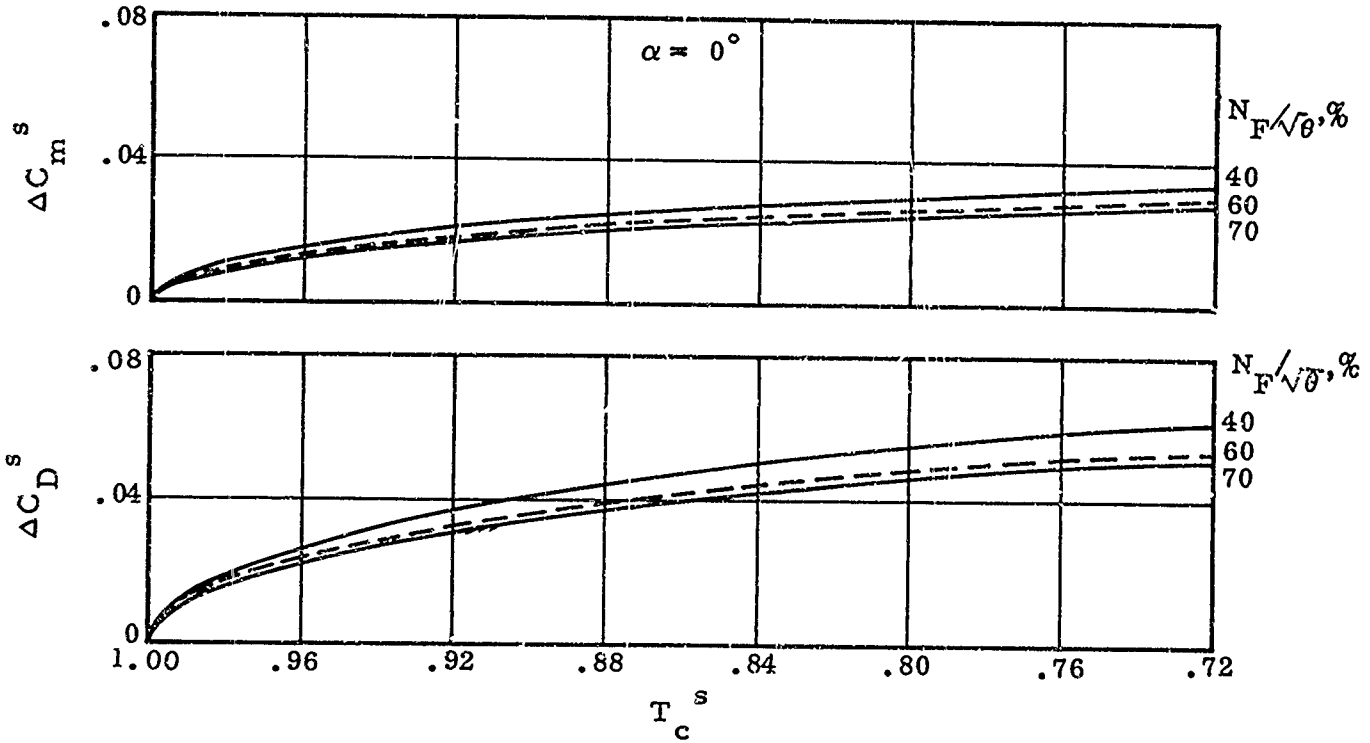

Figure 15. Estimated Drag and Moment Coefficients Due to Gas Generator Ram Drag.

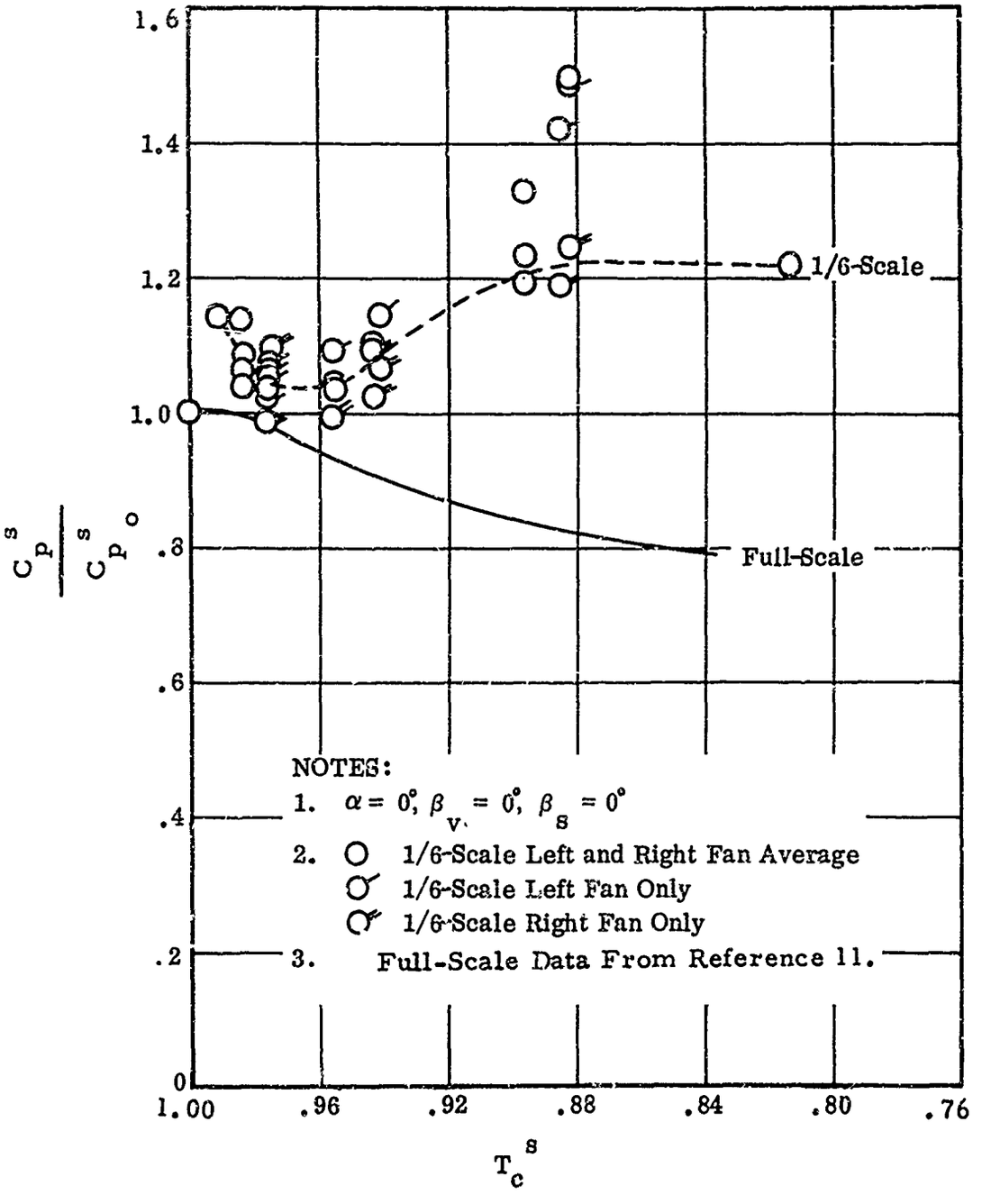

Figure 16. Comparison of Power Coefficient Ratio in Transition, Full-Scale and 1/6-Scale Models.

NOTES:

$\alpha = 0^{\circ}, \beta_V = 0^{\circ}, \beta_s = 0^{\circ}, \delta_f = 45^{\circ}, \delta_d = 0^{\circ}$, Tail Off, Pitch Fan Off

SYM	MODEL	REMARKS
—○—	Ames 173	Uncorrected Data, No Landing Gear, No Pitch Fan Doors
—○—	Ames 173	Data Corrected For Wall Effects
———	Ames 173	Data Corrected For Wall Effects and Strut Tares
—△—	1/6-Scale	Uncorrected Data, Landing Gear Down, Pitch Fan Doors Open

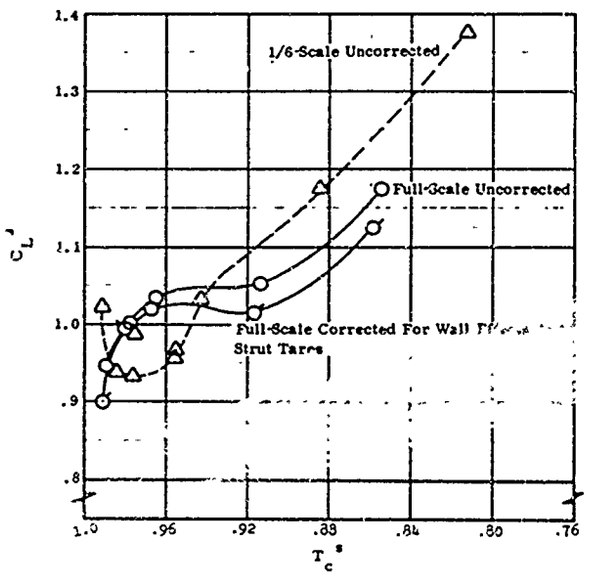

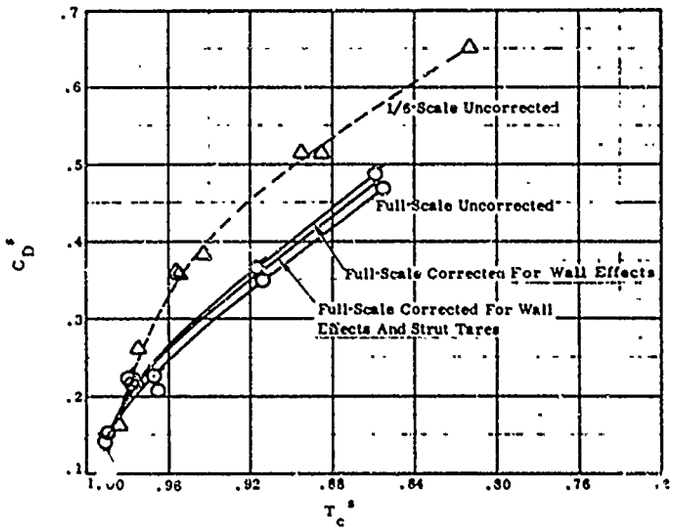

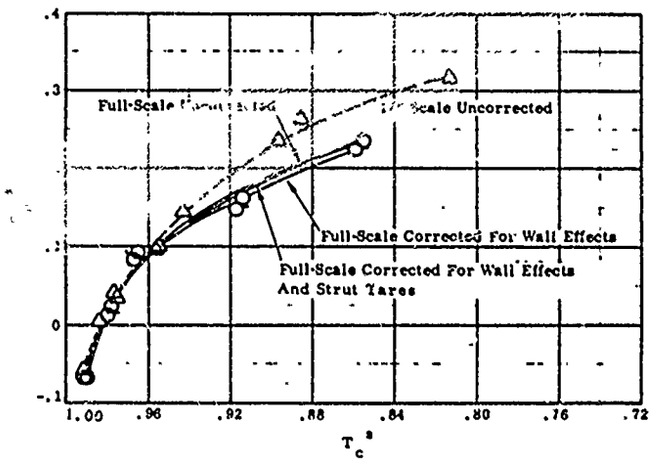

Figure 17. Effect of Full-Scale Data Corrections on Wing-Body Correlation, $\beta_V = 0^{\circ}$, $\beta_s = 0^{\circ}$, $\alpha = 0^{\circ}$.

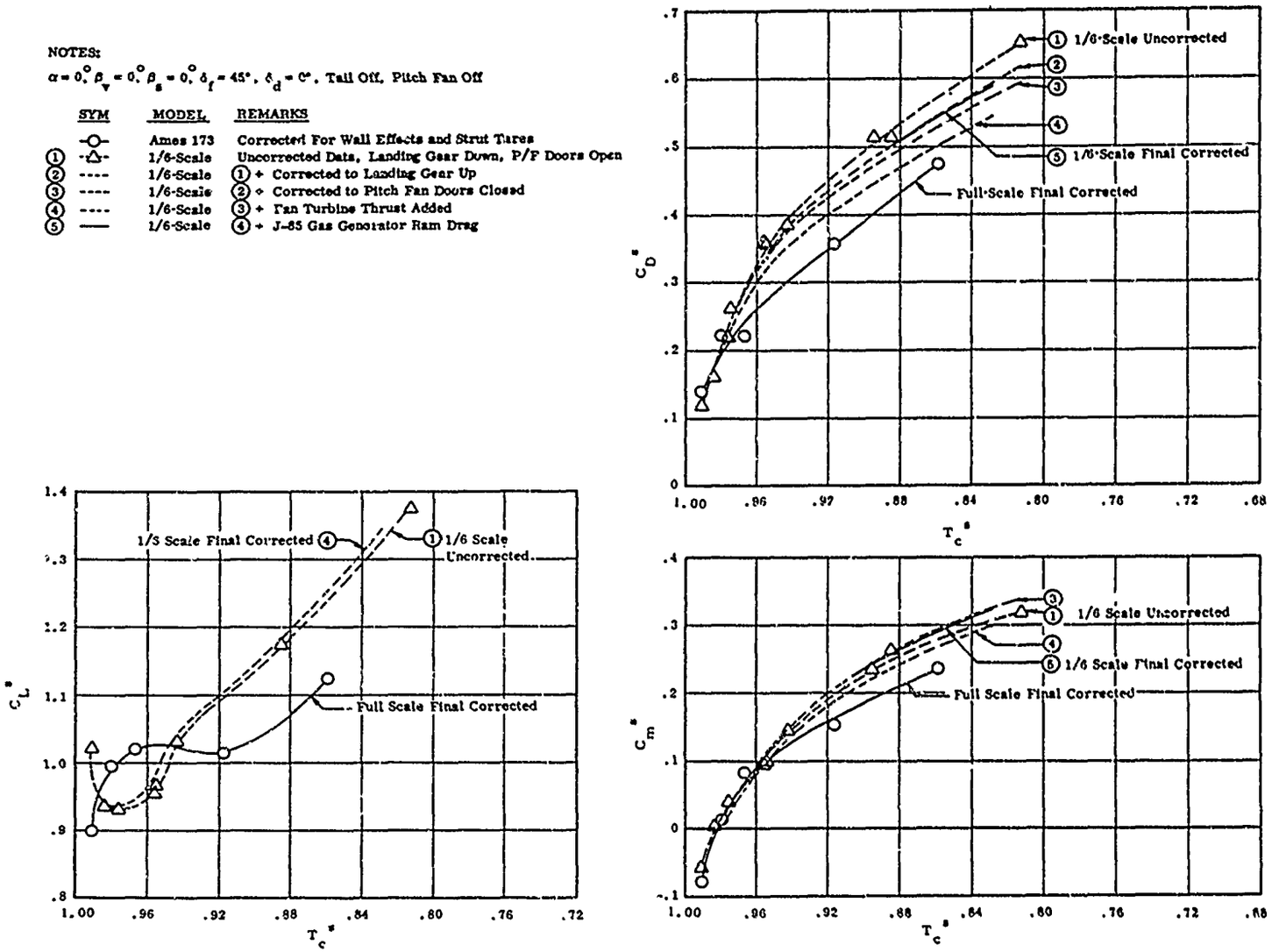

Figure 18. Effect of Ryan 1/6-Scale Model Data Corrections on Wing-Body Correlation, $\beta_v = 0^\circ$, $\beta_s = 0^\circ$, $\alpha = 0^\circ$.

NOTES:

$\alpha = 0^\circ$, $\beta_v = 0^\circ$, $\beta_s = 0^\circ$, $\delta_f = 45^\circ$, $\delta_d = 0^\circ$, Tail Off, Pitch Fan Off

SYM	MODEL	REMARKS
①——	Ames 173	Test Data Corrected For Wall Effects And Strut Tares
②——	Ames 173	① Corrected For Wing Fan Power
③----	1/6-Scale	Test Data Corrected For Landing Gear, Pitch Fan Doors, Fan Turbine Thrust, And Gas Generator Ram Drag.
④----	1/6-Scale	③ Corrected For Wing Fan Power

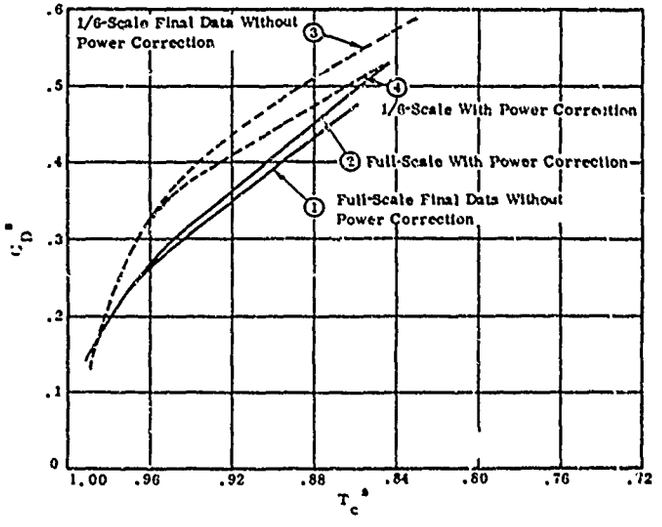

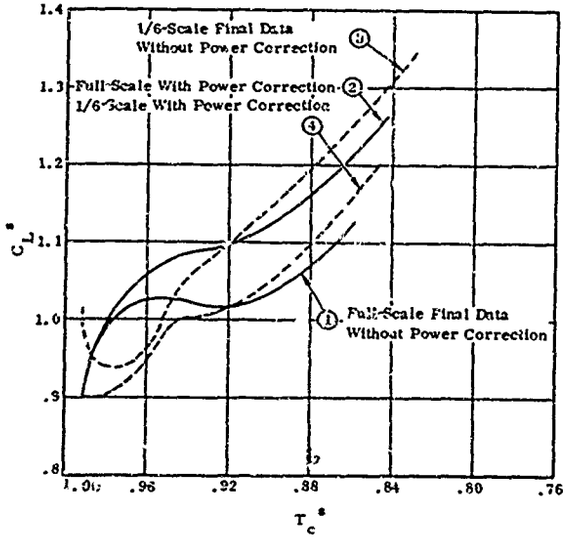

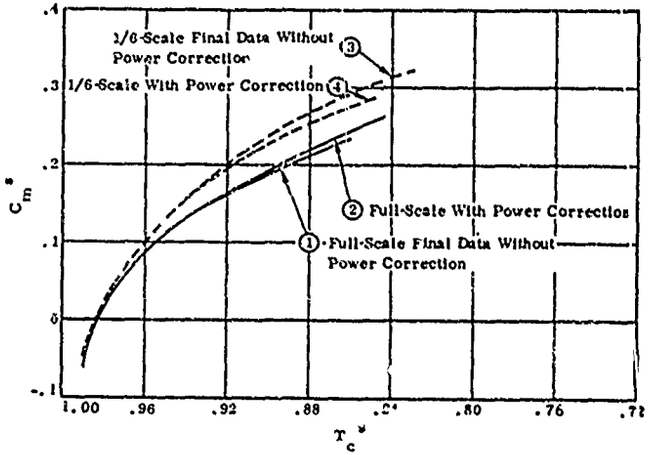

Figure 19. Effect of Wing Fan Power Correction on Wing-Body Correlation, $\beta_v = 0^\circ$, $\beta_s = 0^\circ$, $\alpha = 0^\circ$

NOTES:

$\beta_v = 20°$, $\beta_s = 0°$, $\delta_f = 45°$, $\delta_d = 0°$, Tail Off, Pitch Fan Off

SYM	MODEL	T_c^s	REMARKS
-○-	Ames 173	.959	Uncorrected Data
-○-	Ames 173	.961	Data Corrected For Wall Effects
—	Ames 173	.961	Data Corrected For Wall Effects And Strut Tares
-△-	1/6-Scale	.956	Uncorrected Data, Landing Gear Down, Pitch Fan Doors Open

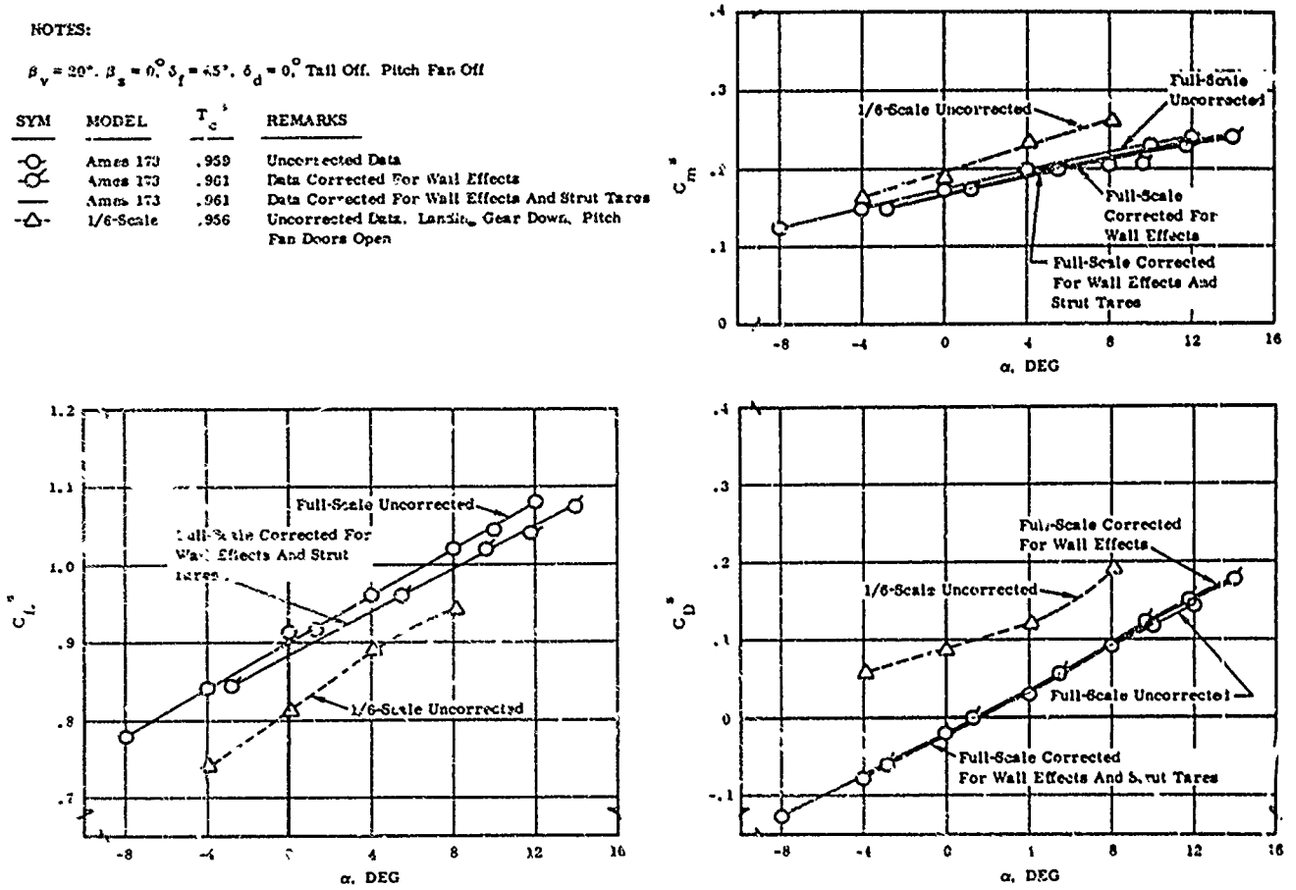

Figure 20. Effect of Full-Scale Data Corrections on Wing-Body Correlation, β_v=20°, β_s=0°, T_c^s=0.96.

NOTES:

$\beta_v = 20°$, $\beta_s = 0°$, $\delta_f = 45°$, $\delta_d = 0°$, Tail Off, Pitch Fan Off

SYM	MODEL	T_c^s	REMARKS
—○—	Ames 173	.961	Corrected For Wall Effects and Strut Tares
(1) --△--	1/6-Scale	.956	Uncorrected Data, Landing Gear Down, Pitch Fan Doors Open
(2) ———	1/6-Scale	.956	(1) + Corrected to Landing Gear Up
(3) ———	1/6-Scale	.956	(2) + Corrected to Pitch Fan Doors Closed
(4) ———	1/6-Scale	.960	(3) + Fan Turbine Thrust Added
(5) ———	1/6-Scale	.960	(4) + Engine Ram Drag Added

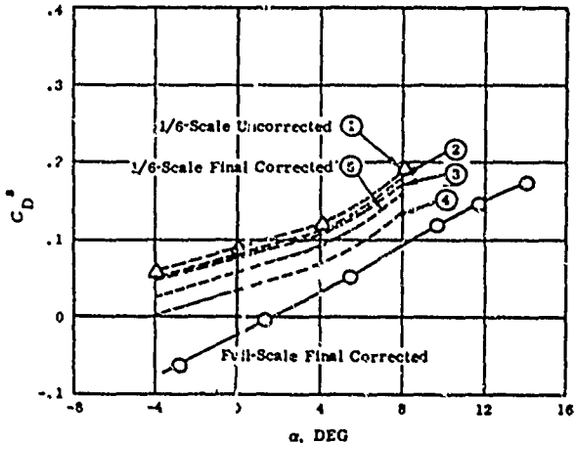

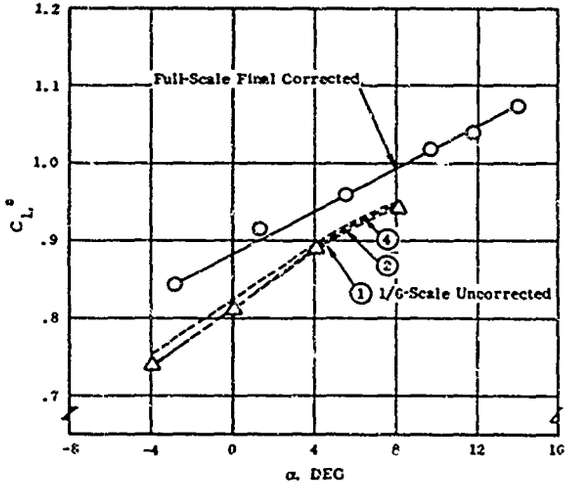

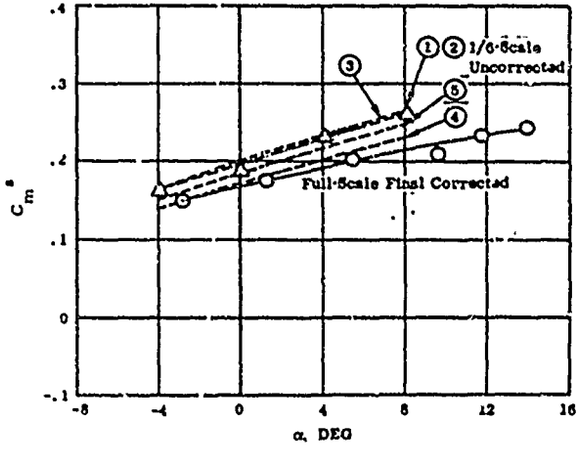

Figure 21. Effect of Ryan 1/6-Scale Model Data Corrections on Wing-Body Correlation, $\beta_v = 20°$, $\beta_s = 0°$, $\bar{T}_c^s = 0.96$.

NOTES:
$\alpha = 0°, \beta_s = 0°, \delta_f = 45°, \delta_d = 0°$, Tail Off, Pitch Fan Off

SYM	MODEL	T_c^s	REMARKS
-X-	Ames 173	0.96	Cross-Plotted From Uncorrected Data, Not Actual Test Points
-◇-	1/6-Scale	0.956	Uncorrected Data, Landing Gear Down, Pitch Fan Doors Open
-□-	1/6-Scale	0.955	Uncorrected Data, Landing Gear Down, Pitch Fan Doors Open
——	1/6-Scale	0.96	Data Corrected For Fan Turbine Thrust

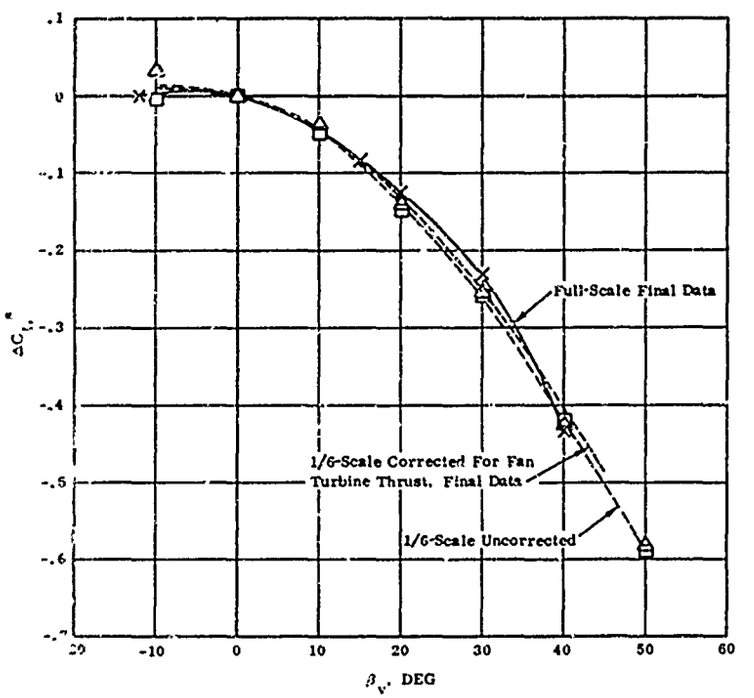

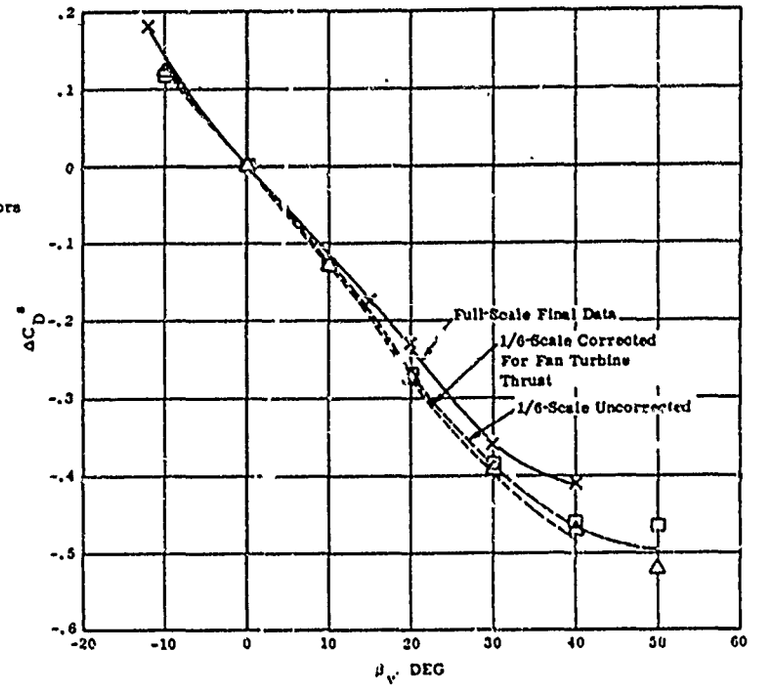

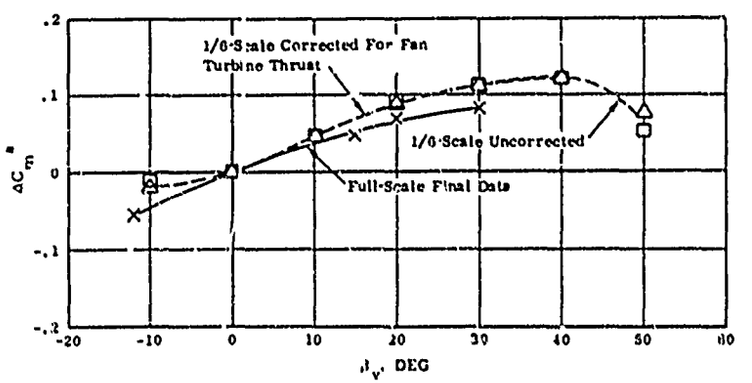

Figure 22. Correlation of Vector Effectiveness, NASA-Ames and Ryan 1/6-Scale Models, β_s=0°, α=0°, T_c^s=0.96.

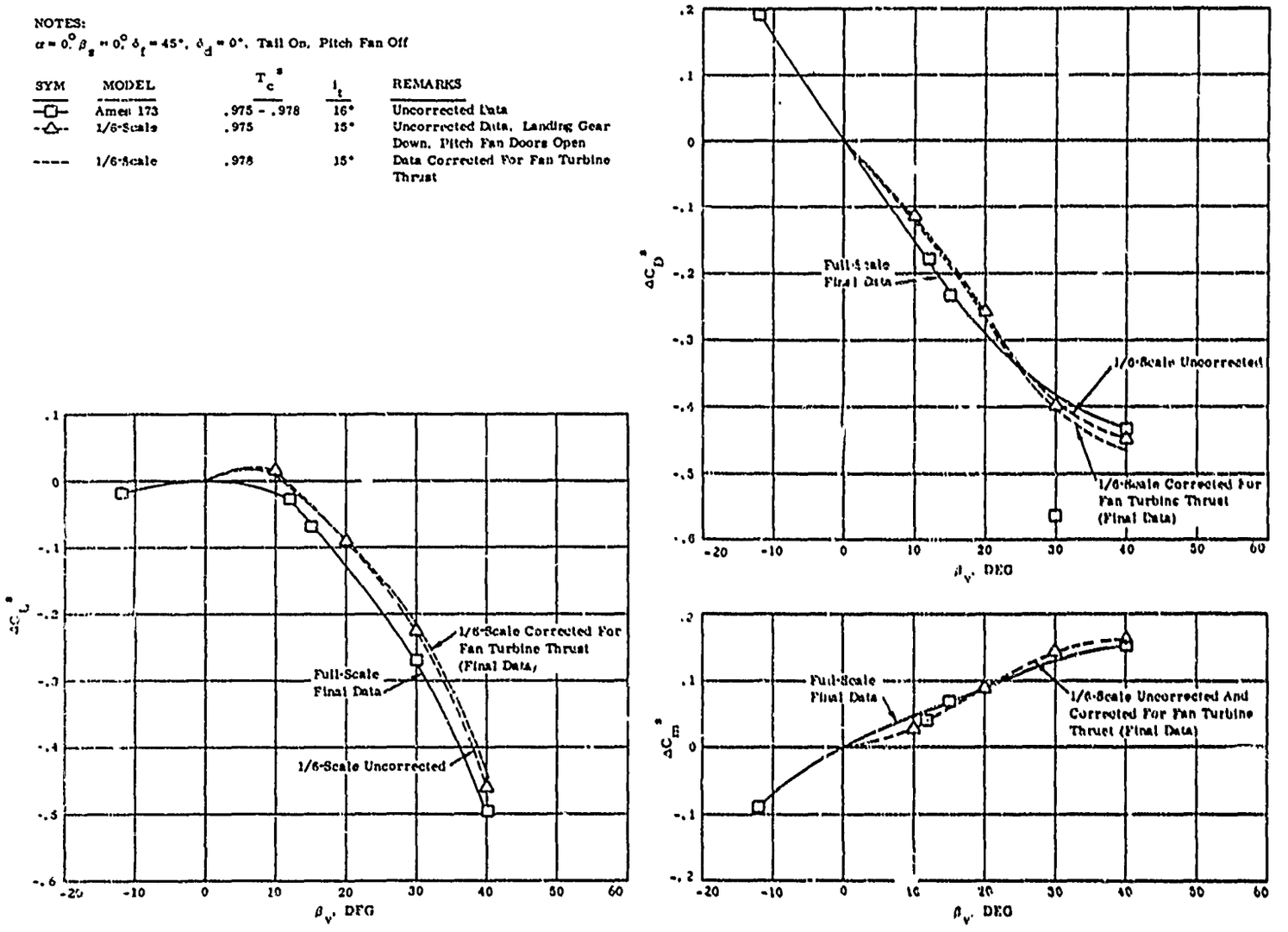

Figure 23. Correlation of Vector Effectiveness, NASA-Ames and Ryan 1/6-Scale Models, $\beta_s=0^\circ$, $\alpha=0^\circ$, $T_c^s=0.978$.

NOTES:
$\alpha = 0^{\circ}, \beta_s = 0^{\circ}, \delta_f = 45^{\circ}, \delta_d = 0^{\circ}$, Pitch Fan Off

SYM	MODEL	REMARKS
Solid	Ames 173	Cross-Plotted From Uncorrected Data Near Test T_c^* Not Actual Data Points
Open	1/6-Scale	Uncorrected Data, Landing Gear Down, Pitch Fan Doors Open
○	$\beta_v = 10^{\circ}$	Flagged Symbols = Tail On
□	$\beta_v = 15^{\circ}$	Unflagged Symbols = Tail Off
◇	$\beta_v = 30^{\circ}$	

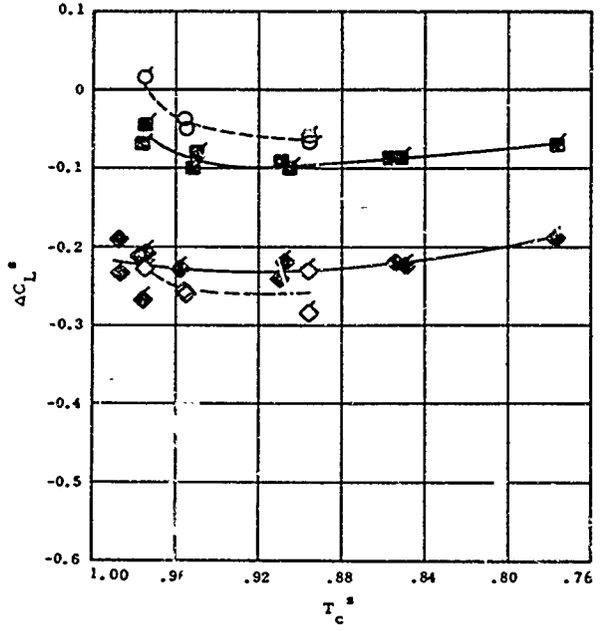

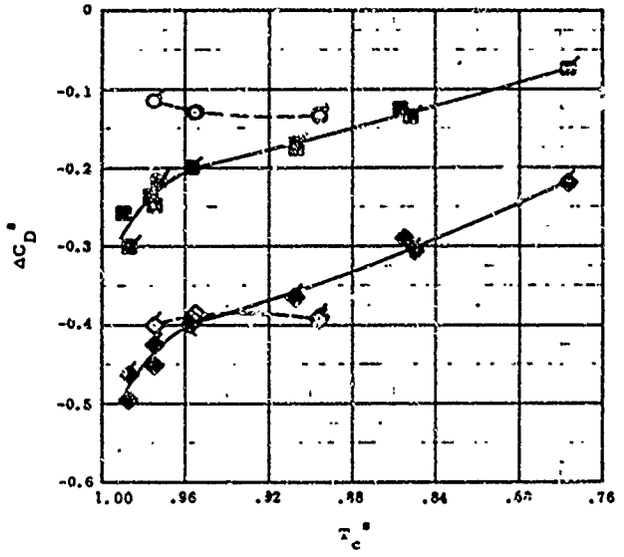

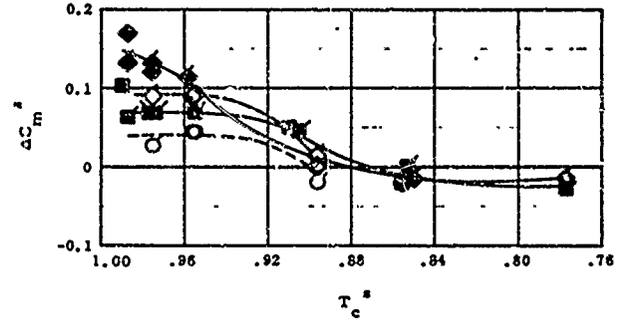

Figure 24. Effect of Thrust Coefficient on Vector Effectiveness, NASA-Ames and Ryan 1/6-Scale Models, β_v=10°, 15°, and 30°, β_s=0°, α=0°.

NOTES:

$\alpha = 0°, \beta_s = 0°, \delta_f = 45°, \delta_d = 0°$ Pitch Fan Off

SYM	MODEL	REMARKS
Solid	Ames 173	Cross-Plotted From Uncorrected Data Near Test T_c^*. Not Actual Data Points
Open	1/6-Scale	Uncorrected Data. Landing Gear Down, Pitch Fan Doors Open
—○—	$\beta_v = 20°$	Flagged Symbols = Tail On
—△—	$\beta_v = 40°$	Unflagged Symbols = Tail Off

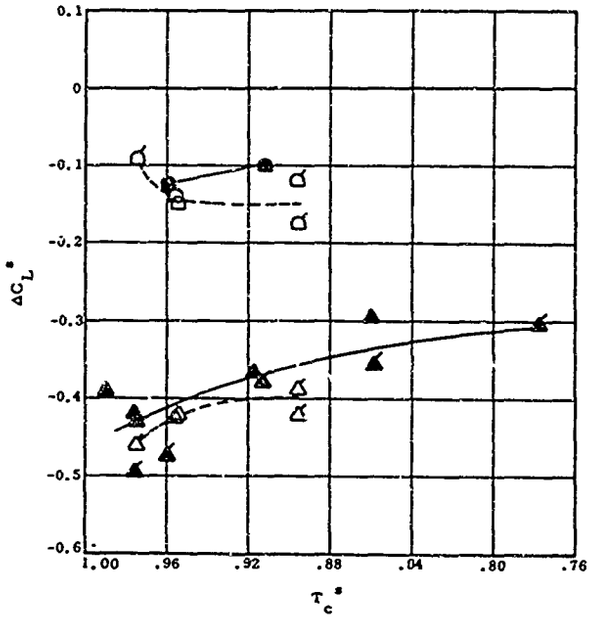

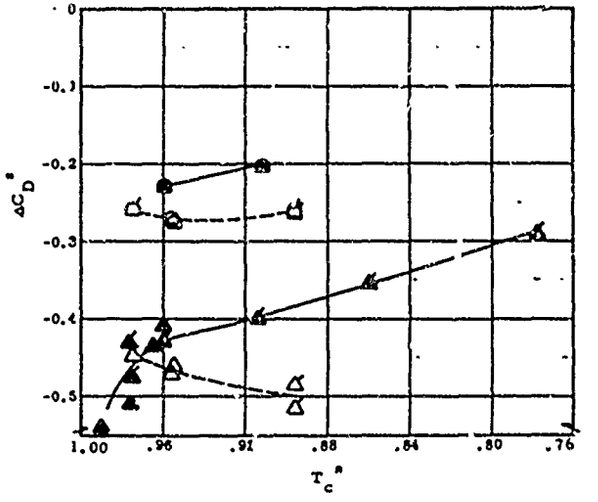

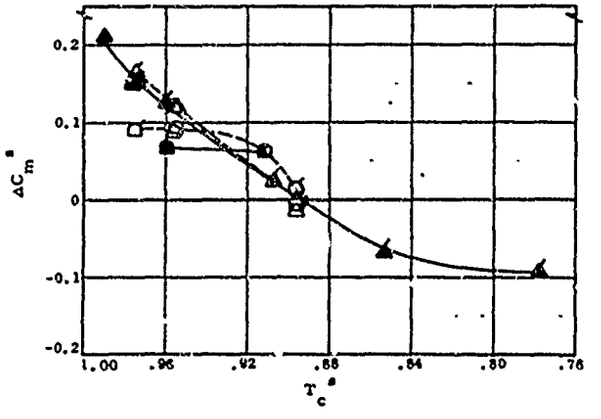

Figure 25. Effect of Thrust Coefficient on Vector Effectiveness, NASA-Ames and Ryan 1/6-Scale Models, β_V=20° and 40°, β_S=0°, α=0°.

NOTES:
$\alpha = 0^{\circ}$, $\beta_v = 18^{\circ}$, $\delta_f = 45^{\circ}$, $\delta_d = 0^{\circ}$, Pitch Fan Off

SYM	MODEL	T_c^s	i_t	REMARKS
-O-	Ames 173	.96	0°	Uncorrected Data
-X-	1/6-Scale	.956	Tail Off	Cross-Plotted From Uncorrected Data; Not Actual Data Points. Landing Gear Down, Pitch Fan Doors Open

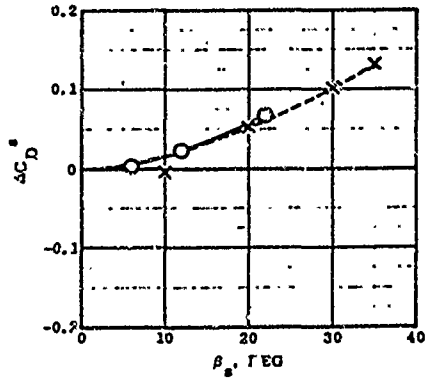

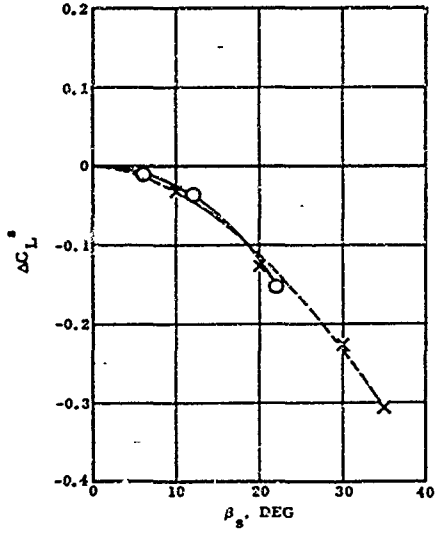

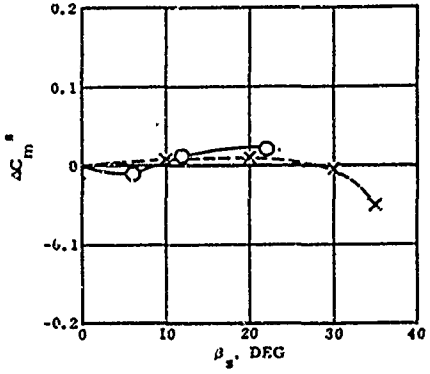

Figure 26. Correlation of Stagger Effectiveness, NASA-Ames and Ryan 1/6-Scale Models, β_v=18°, α=0°, T_c^s=0.96.

NOTES:

$\alpha = 0°, \beta_v = 0°, \beta_s = 0°, \delta_f = 45°, \delta_d = 0°$, Tail Off, Pitch Fan Off

SYM	MODEL	REMARKS
—○—	Ames 173	Uncorrected Data
①—△—	1/6-Scale	Uncorrected Data, Landing Gear Down, Pitch Fan Doors Open
②———	1/6-Scale	① + Corrected To Landing Gear Up
③———	1/6-Scale	② + Corrected To Pitch Fan Doors Closed
④———	1/6-Scale	③ + Fan Turbine Thrust Added
⑤———	1/6-Scale	④ + J-85 Gas Generator Ram Drag Added

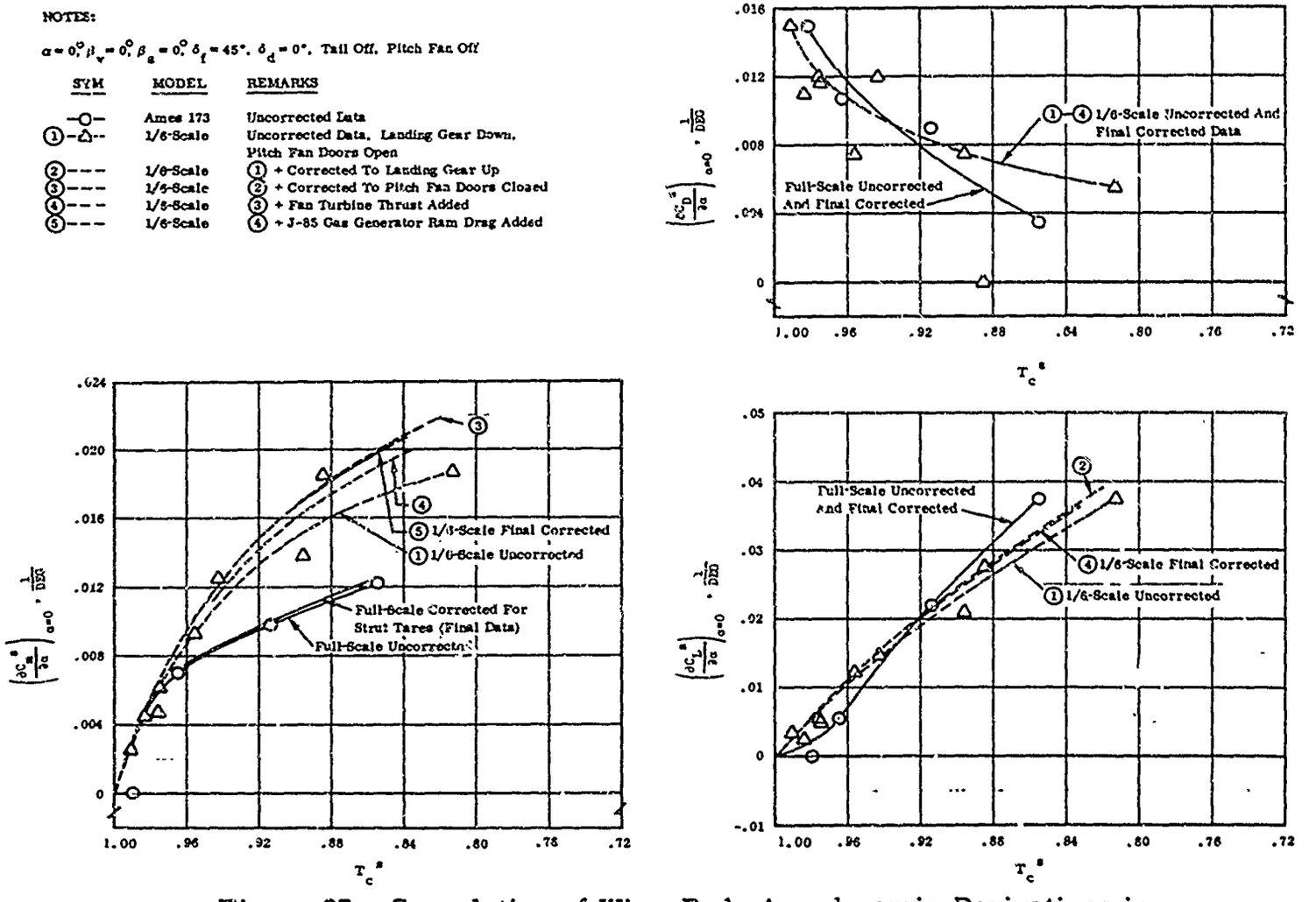

Figure 27. Correlation of Wing-Body Aerodynamic Derivatives in Transition, NASA-Ames and Ryan 1/6-Scale Models, $\beta_v = 0°$, $\beta_s = 0°$.

NOTES:

$\alpha = 0^{\circ}$, $\beta_s = 0^{\circ}$, $\delta_f = 45^{\circ}$, $\delta_d = 0^{\circ}$, Tail Off, Pitch Fan Off

SYM	MODEL	T_c^s	REMARKS
○	Ames 173	0.96	Uncorrected Data
① △	1/6-Scale	0.956	Uncorrected Data, Landing Gear Down, Pitch Fan Doors Open
② ----	1/6-Scale	0.956	① + Corrected To Landing Gear Up
③ ----	1/6-Scale	0.956	② + Corrected To Pitch Fan Doors Closed
④ ----	1/6-Scale	0.96	③ + Fan Turbine Thrust Added
⑤ ----	1/6-Scale	0.96	④ + J-85 Gas Generator Ram Drag Added

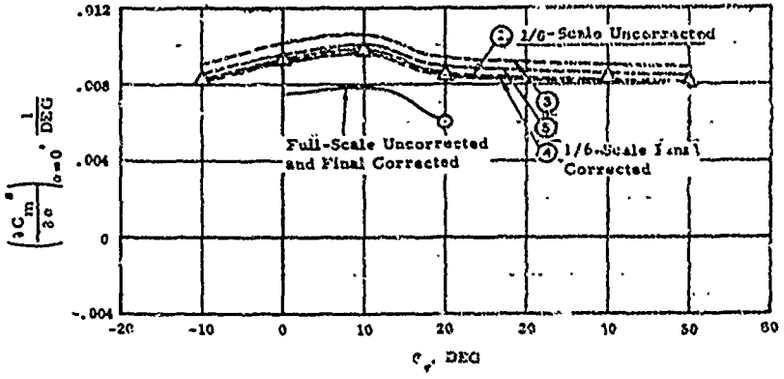

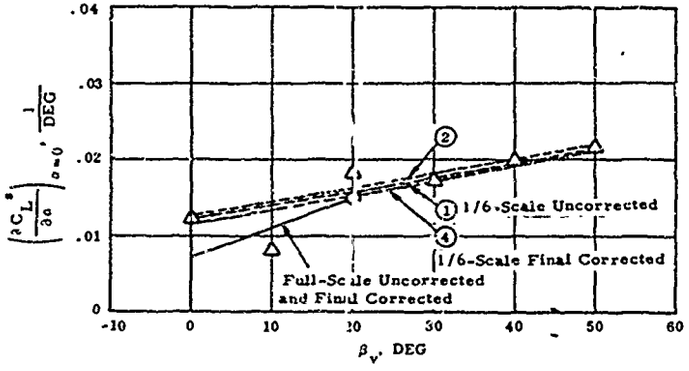

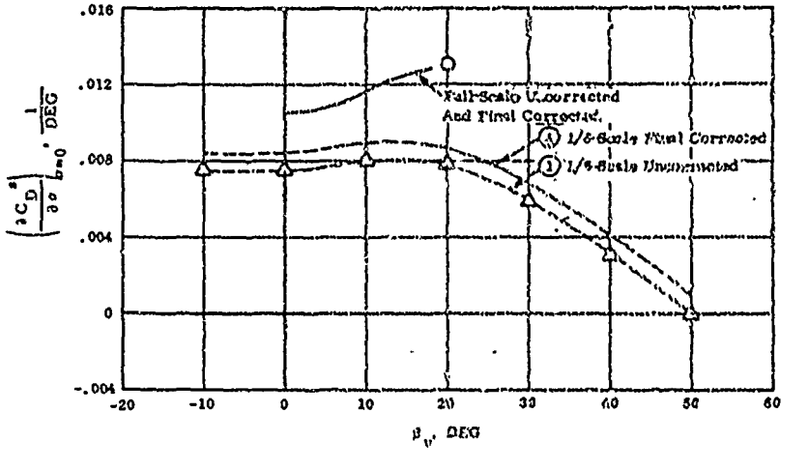

Figure 28. Effect of Vector Angle on Wing-Body Aerodynamic Derivatives, NASA-Ames and Ryan 1/6-Scale Models, $\beta_s = 0^{\circ}$; $T_c^s = 0.96$.

$\beta_v = 0°$, $\beta_s = 0°$, $\delta_f = 45°$, $\delta_d = 0°$, Pitch Fan Off

SYM	T_c^s
○	0.984
□	0.976
◇	0.943
◇	0.930
◺	0.913
◗	0.885
△	0.873
⬭	0.848

NOTES:

Unflagged symbols denote 1/6-scale model with landing gear down and pitch fan doors open.

Flagged symbols denote Ames 173 model without landing gear or pitch fan doors.

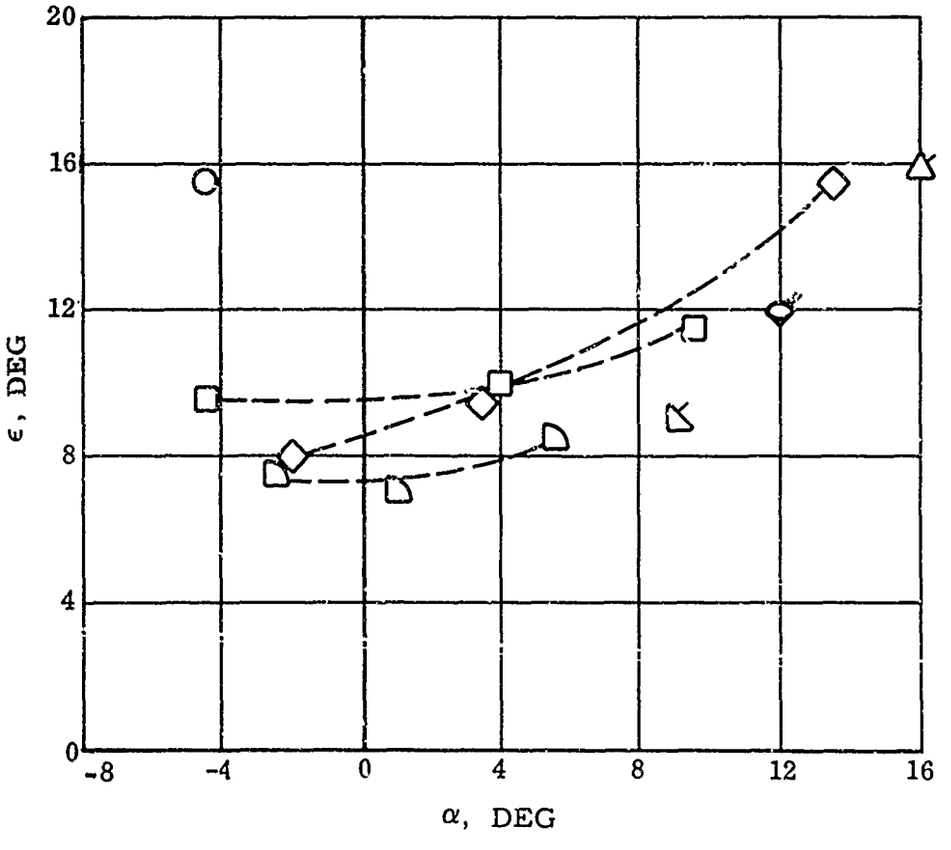

Figure 29. Correlation of Horizontal Tail Downwash, NASA-Ames and Ryan 1/6-Scale Models, $\beta_v = 0°$, $\beta_s = 0°$.

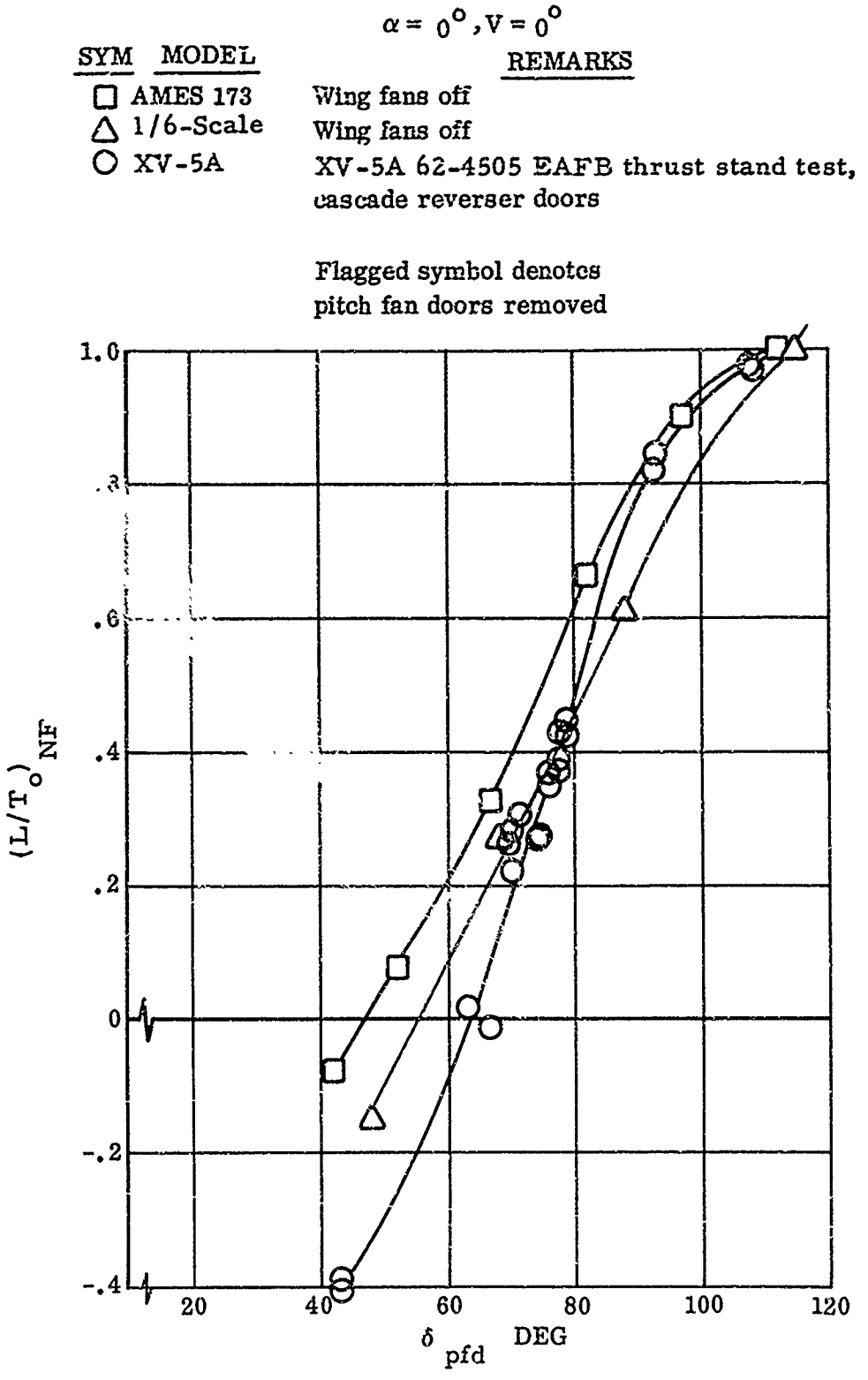

Figure 30. Correlation of Static Pitch Fan Door Effectiveness, NASA-Ames Model, Ryan 1/6-Scale Model and XV-5A Aircraft.

5.0 AIRCRAFT CHARACTERISTICS

5.1 SELECTION OF BASIC DATA

The basic data selected to represent the XV-5A aircraft characteristics for establishing equilibrium conditions in fan-mode flight were chosen from the full-scale tests of the aircraft in the Ames 40-x-80 foot Wind Tunnel (Ames Test 210). These data were considered to be superior to data obtained from other model tests, as the interrelated aerodynamic effects of the aircraft configuration, propulsion system, and control system settings were properly accounted for. Although test data were available with the nose fan inoperative, all tests were conducted with the horizontal tail installed, requiring corrections for the presence of the tail in order to arrive at the basic wing-body characteristics required for the development of the stability derivatives. This correction required the use of estimated tail effectiveness data, but the possible errors introduced are believed to be secondary to the considerations of total aircraft system representation discussed above.

5.1.1 CORRECTIONS TO OBTAIN WING-BODY CHARACTERISTICS

The longitudinal force and moment coefficients obtained from Ames Test 210 are shown in Figure 31 for zero geometric angle of attack with the nose fan inoperative. These data were corrected to zero exit louver stagger by use of limited stagger effectiveness data derived from the 210 test, and to the tail-off configuration by the estimated contributions of the horizontal tail shown in Figures 32 and 33. The tail increments were calculated from the equations given in Reference 14, page 123.

Finally, the basic data were corrected to the condition of 100 percent collective lift stick, which is the normal setting for this control in actual flight. The stagger effectiveness utilized for this correction was obtained from static thrust stand tests of the XV-5A at Edwards Air Force Base and is discussed in Reference 15, Routine Q. The thrust stand tests were conducted with modified stiffened exit louvers, which resulted in a larger lift variation with louver stagger angle than was obtained with the original louvers during the full-scale wind tunnel tests. The resulting corrections, due to the stagger washout schedule with vector angle at 100 percent collective lift stick, are shown in Figure 34 as a function of fan thrust coefficient. The final, corrected wing-body data, which are shown in Figure 35, served as the basic characteristics for developing the wing-body contributions to the stability derivatives.

5.1.2 CORRECTIONS TO OBTAIN COMPLETE AIRPLANE CHARACTERISTICS

The horizontal tail drag increment of Figure 32 and the nose fan drag contribution shown in Figure 36 were added to the basic data of Figure 35 to obtain the total airplane drag level, as shown in Figure 37. The tail drag for a constant incidence of 20 degrees was added for vector angles less than 30 degrees and for 15 degrees incidence for vector angles greater than 30 degrees. The nose fan contribution was calculated from the following equation derived from simple momentum theory in Reference 14, page 126:

$$\Delta C_D{}^s = T_c{}^s \left[\frac{2\,(1-T_c{}^s)}{T_c{}^s} \frac{T_{NF}}{T_{000}} \frac{A_{NF}}{A_F} \right]^{1/2} \qquad (15)$$

This expression has been shown to predict the nose fan momentum drag increment obtained from nose fan-on and-off wind tunnel data (Figure 36 and Reference 14).

5.2 LONGITUDINAL TRIM ANALYSIS

The drag curves of Figure 3[illegible] form a graphical method for determining the value of trimmed thrust coefficient for each vector angle at the intersection of the drag curves with the zero ordinate. The untrimmed values of pitching moment coefficient at the trimmed values of thrust coefficient are then set equal to zero for equilibrium about the Y-axis, and the corresponding untrimmed lift coefficients are corrected for the effects of balancing the pitching moment.

5.2.1 PITCHING MOMENT TRIM

The pitching moment coefficient obtained from Figure 35 at the trim values of thrust coefficient, when added to the appropriate tail moment increments, represents the total untrimmed pitching moment with the nose fan inoperative. In order to balance this moment with the controls, it was necessary to add the nose fan moment contribution at the thrust modulator door settings corresponding to a specified control stick position, and then to determine the change in control setting required to bring the moment into equilibrium. The nose fan moment contribution at zero longitudinal stick position was determined from comparisons of nose fan-on and nose fan-off data at approximately the same test conditions.

An untrimmed pitching moment parameter was developed in terms of nose fan and elevator control characteristics in the following form:

$$-\left(\frac{\Delta C_m{}^s}{\Delta \delta_{s_e}}\right) = \frac{\partial K_{NF}}{\partial \delta_{pfd}} \left[\left(\frac{T_{NF}}{T_{000}} \right) T_c{}^s \frac{x_{NF}}{D_F} \frac{\partial \delta_{pfd}}{\partial \delta_{s_e}} \right]$$

$$+ \frac{\partial C_m}{\partial \delta_e} (1-T_c{}^s) \frac{S\bar{c}}{A_F D_F} \frac{\partial \delta_e}{\partial \delta_{s_e}} \qquad (16)$$

where

$\frac{\partial K_{NF}}{\partial \delta_{pfd}}$ is the nose fan door effectiveness parameter, .024 per deg

$\frac{\partial \delta_{pfd}}{\partial \delta_{s_e}}$ is the nose fan door gearing, deg/in.

$\frac{\partial \delta_e}{\partial \delta_{s_e}}$ is the elevator gearing, 3.75 deg/in.

$\frac{\partial C_m}{\partial \delta_e}$ is the elevator effectiveness, -.01025 per deg

This equation was evaluated for a range of thrust coefficients for each vector angle, as shown in Figure 38. Nose fan door gearing characteristics are shown in Figure 39. Nose fan door effectiveness was obtained by calculating the nose fan lift from the lift coefficient of Equation (23) and normalizing by the nose fan static thrust. Typical results are shown in Figure 40 for two wind tunnel test conditions in comparison with static thrust stand test data.

The change in control positions for moment equilibrium was determined from the following relationships:

$$\Delta \delta_{s_e} = \frac{C_{m_{unt}}^{s}}{\left(\frac{\Delta C_m^s}{\Delta \delta_{s_e}} \right)} \tag{17}$$

$$\delta_{pfd} = \left(\frac{\partial \delta_{pfd}}{\partial \delta_{s_e}} \right) \Delta \delta_{s_e} + \delta_{pfd_o} \tag{18}$$

$$\delta_e = \frac{\partial \delta_e}{\partial \delta_{s_e}} \Delta \delta_{s_e} \tag{19}$$

The control settings required for trim drag and moment at the trim values of thrust coefficient are shown in Figure 42.

5.2.2 TRIMMED LIFT COEFFICIENT

The total airplane lift coefficient at trim was determined from the following summation:

$$C_L^s = C_{L_{WB}}^s + \Delta C_{L_t}^s + \Delta C_{L_{NF}}^s + \Delta C_{L_{INT}}^s + \Delta C_{L_{\delta_e}}^s \quad (20)$$

where

$C_{L_{WB}}^s$ is the basic wing-body value

$\Delta C_{L_t}^s$ is the tail lift contribution

$\Delta C_{L_{NF}}^s$ is the direct nose fan contribution

$\Delta C_{L_{INT}}^s$ is the nose fan interference contribution

$\Delta C_{L_{\delta_e}}^s$ is the elevator contribution, $.028\ (1-T_c^s)\Delta\delta_e$

The direct nose fan contribution was calculated from the lift parameter of Figure 36.

$$\Delta C_{L_{NF}}^s = \left(\frac{C_L^s}{K_{NF}}\right) \frac{\partial K_{NF}}{\partial \delta_{pfd}} (\delta_{pfd} - 62°) \quad (21)$$

The nose fan interference lift increment was calculated from the lift factors shown in Figure 41.

$$\Delta C_{L_{INT}}^s = \left(\Delta C_{L_{INT}}^s\right)_{\delta_{pfd}} = 60° + \left(\frac{\partial C_{L_{INT}}^s}{\partial \delta_{pfd}}\right)(\delta_{pfd} - 60°) \quad (22)$$

The nose fan interference effect was determined during the evaluation of nose fan-on/off data from comparison of measured and calculated lift increments. The lift required to produce the measured pitching moment increment due to the nose fan was calculated from

$$\Delta C_L^{\ s} = \frac{\Delta C_m^{\ s}}{\left| \frac{x_{HF}}{D_F} \right|} + \Delta C_D^{\ s} \, z/x_{HF} \qquad (23)$$

The interference lift from the difference between the measured and calculated quantities was calculated from

$$\Delta C_{L_{INT}}^{\ s} = \Delta C_{L_{meas.}}^{\ s} - \Delta C_L^{\ s} \qquad (24)$$

This lift increment is shown in Figure 41 in terms of nose fan door position from several sources of wind tunnel data. Although there is considerable scatter in the data, definite trends are indicated which show an apparent lift loss on the wing due to nose fan operation near neutral lift, which is larger than the direct nose fan lift force, and a slight increase in the lift loss with increasing nose fan door angle in the positive lift direction.

The curves faired through the data points of Figure 41 represent the values of interference lift increments used in Equation (20).

5.2.3 TRIM AIRSPEED IN TRANSITION

The true airspeeds for equilibrium flight at each vector angle were calculated for a gross weight of 10,000 pounds from the following equation:

$$V_{KN} = \frac{1}{1.689} \sqrt{\frac{2}{\sigma \rho_o} \frac{W/A_F}{C_L^{\ s}} (1-T_c^{\ s})} \qquad (25)$$

where $C_L^{\ s}$ and $T_c^{\ s}$ are the equilibrium values. Lift coefficient and airspeed are shown in Figure 43 as a function of vector angle. The required wing fan reference static thrust was determined from

$$T_{000} = \frac{T_c^{\ s} \, q \, A_F}{(1-T_c^{\ s})} \qquad (26)$$

and is shown in Figure 52.

NOTES:
$\alpha = 0°$, $\delta_{se} = 0$ In., $i_t = 1°$, CG 240, $\delta_{sc} = 60\%$

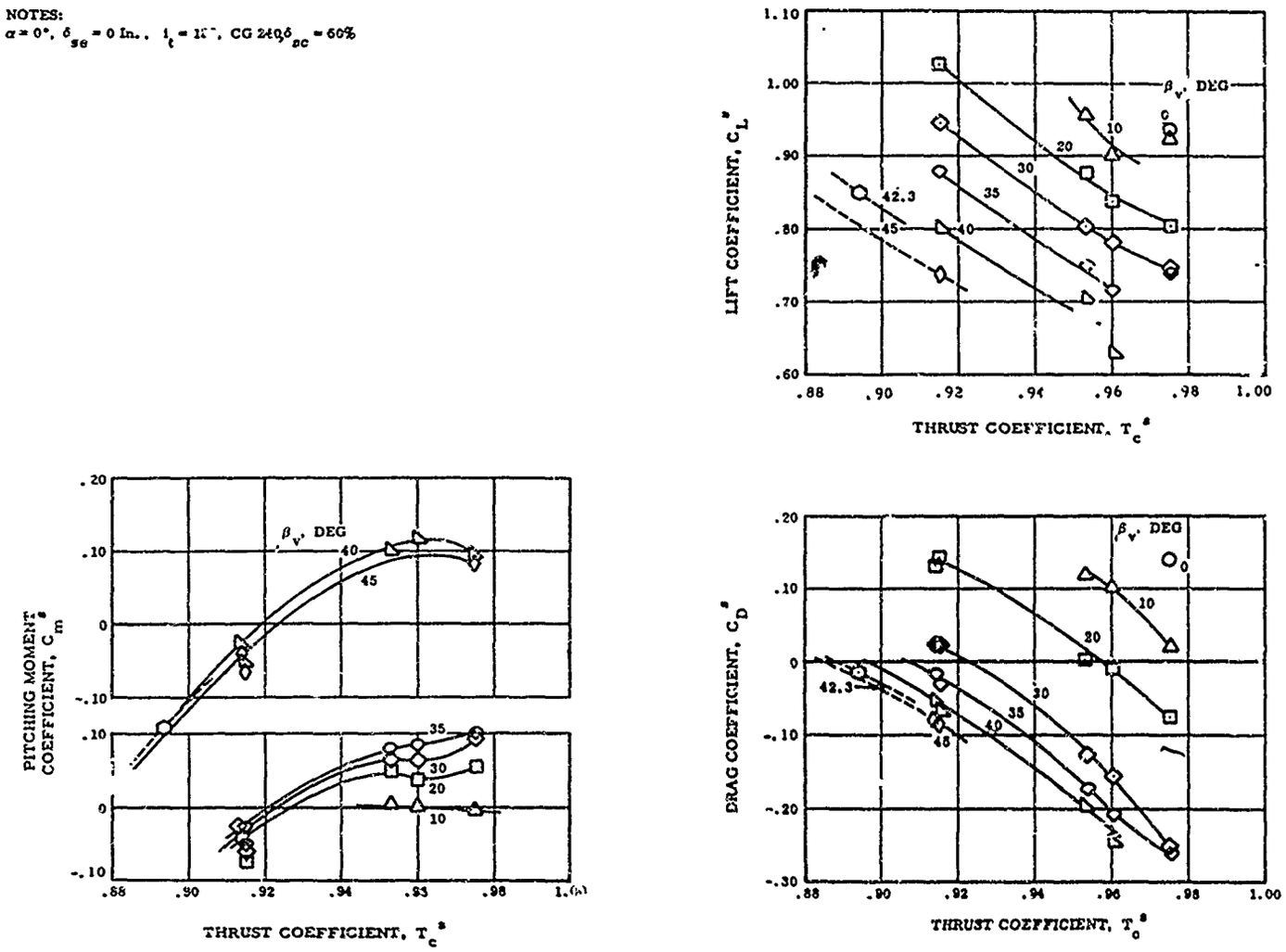

Figure 31. Longitudinal Characteristics of XV-5A Full-Scale Wind Tunnel Tests With Nose Fan Off.

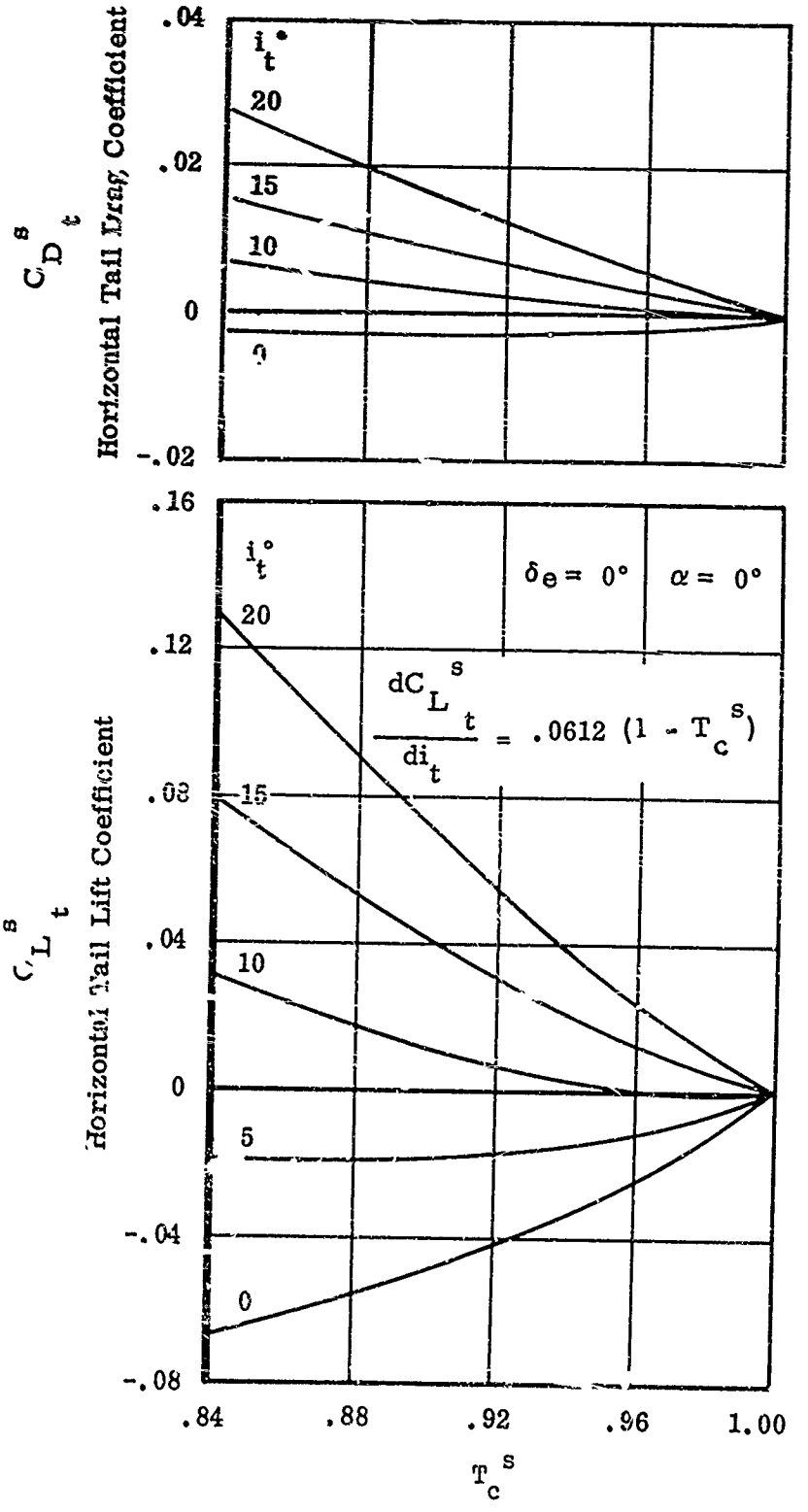

Figure 39 Estimated Horizontal Tail Lift and Drag Increments.

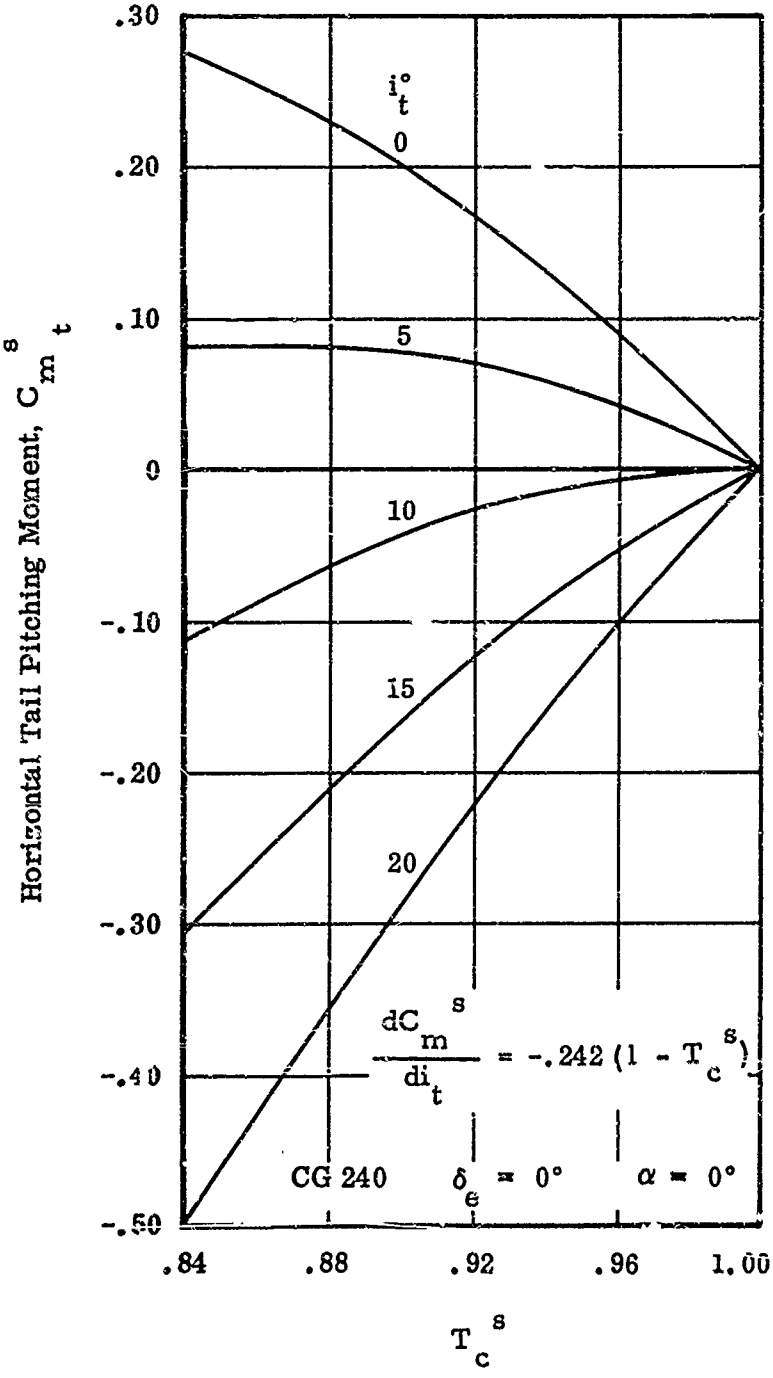

Figure 33. Estimated Horizontal Tail Pitching Moment Increment.

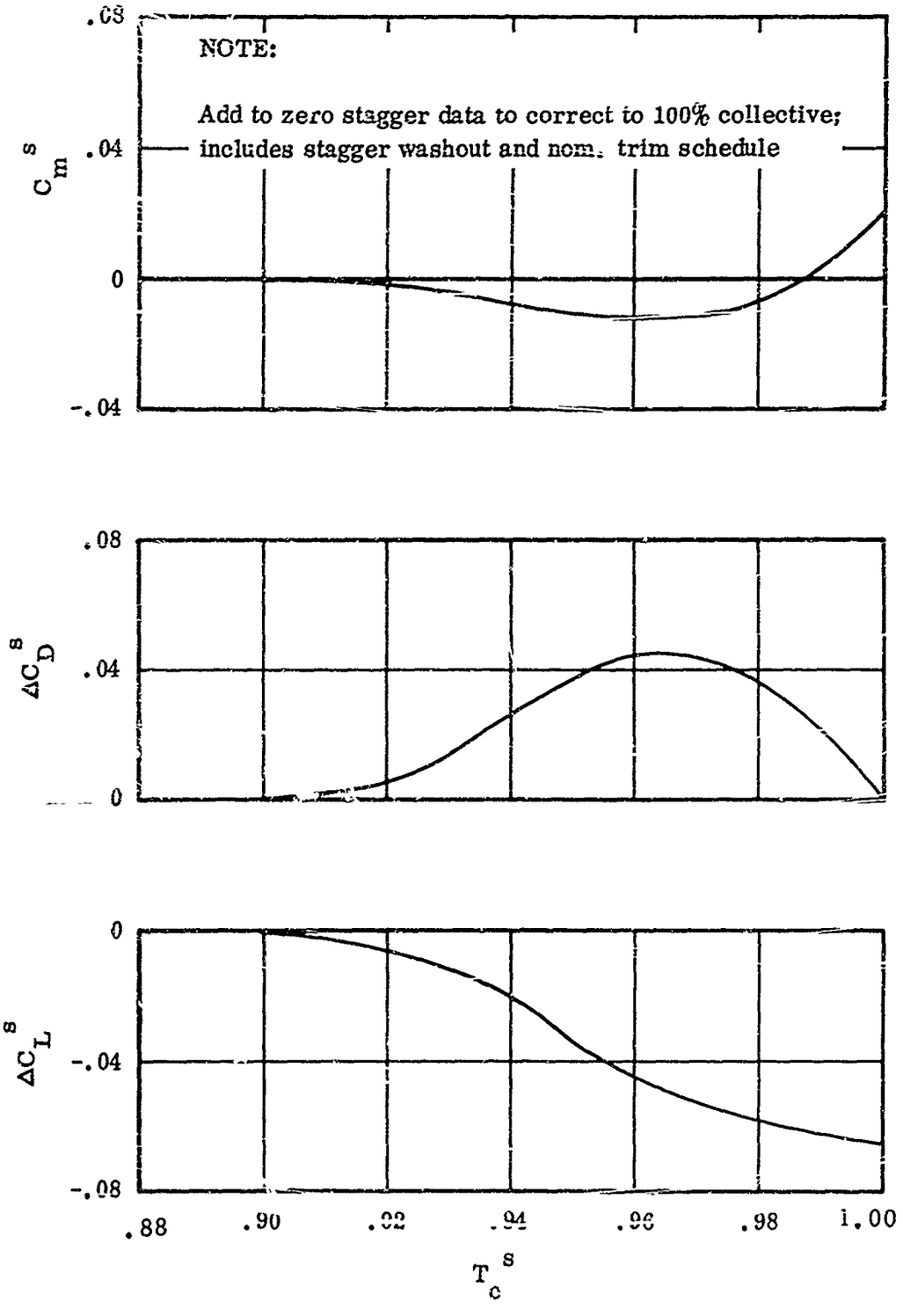

Figure 34. Stagger Corrections for 100% Collective Lift Stick Position.

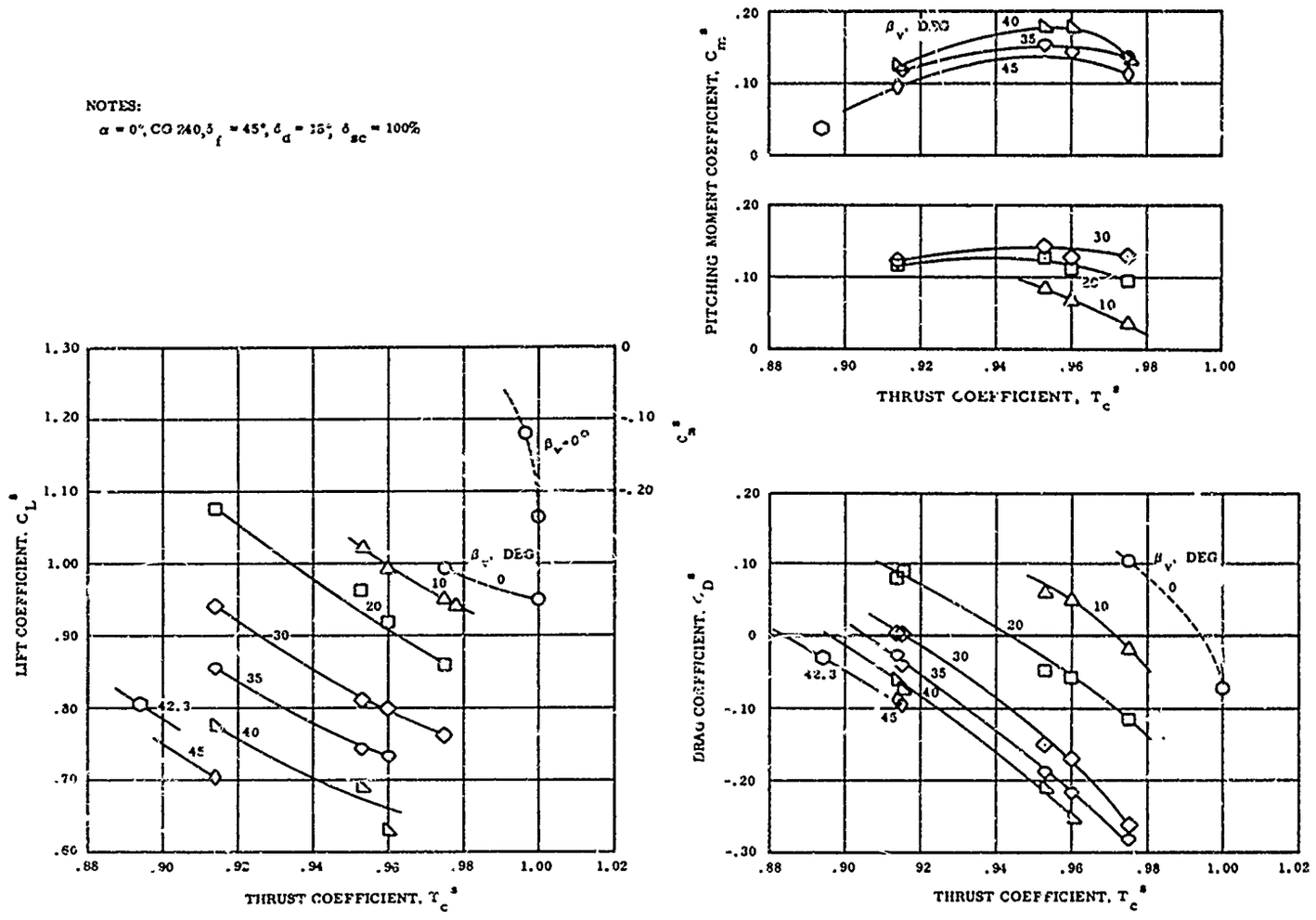

Figure 35. Estimated Wing-Body Characteristics.

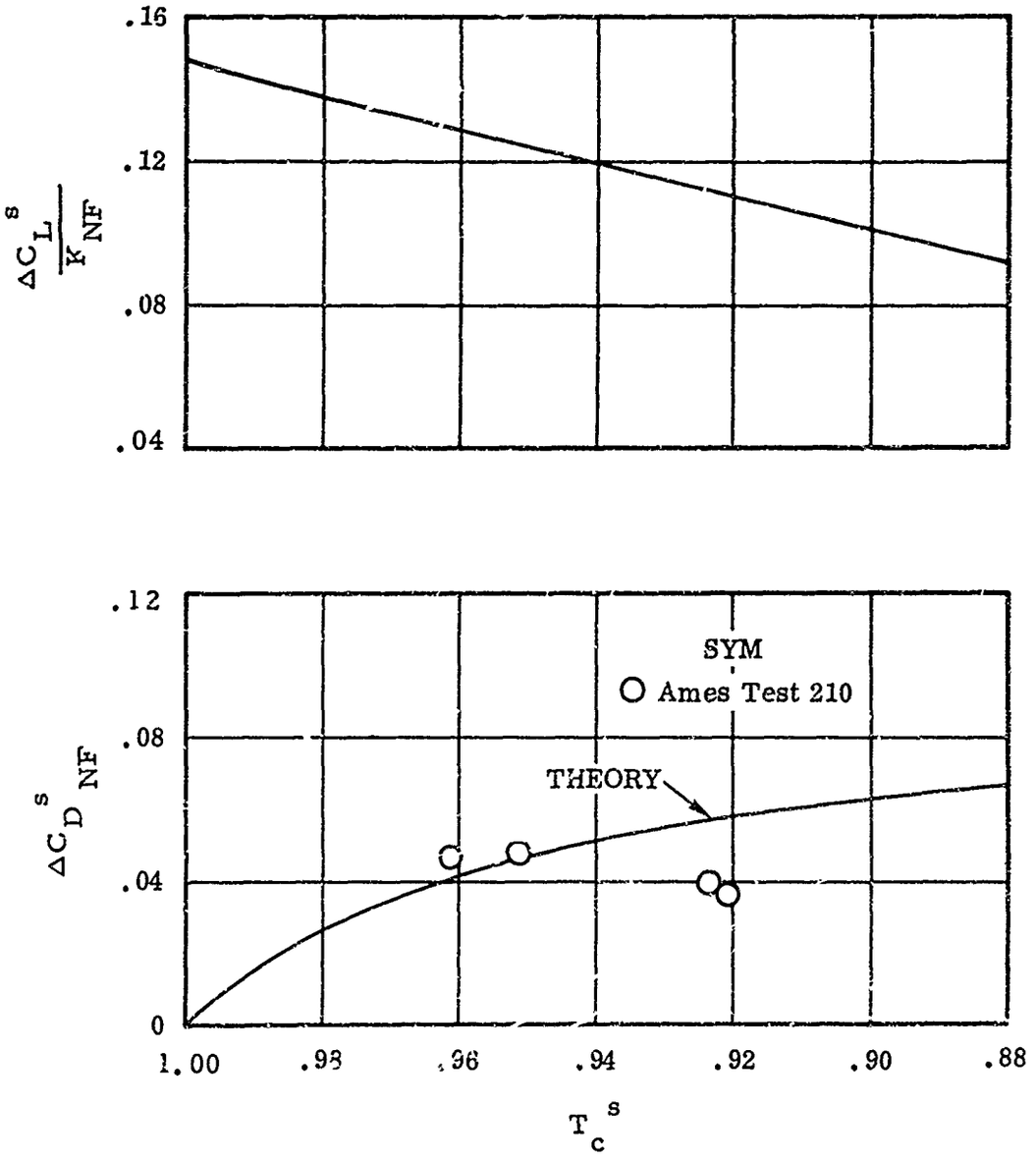

Figure 36. Nose Fan Direct Lift and Drag Contributions.

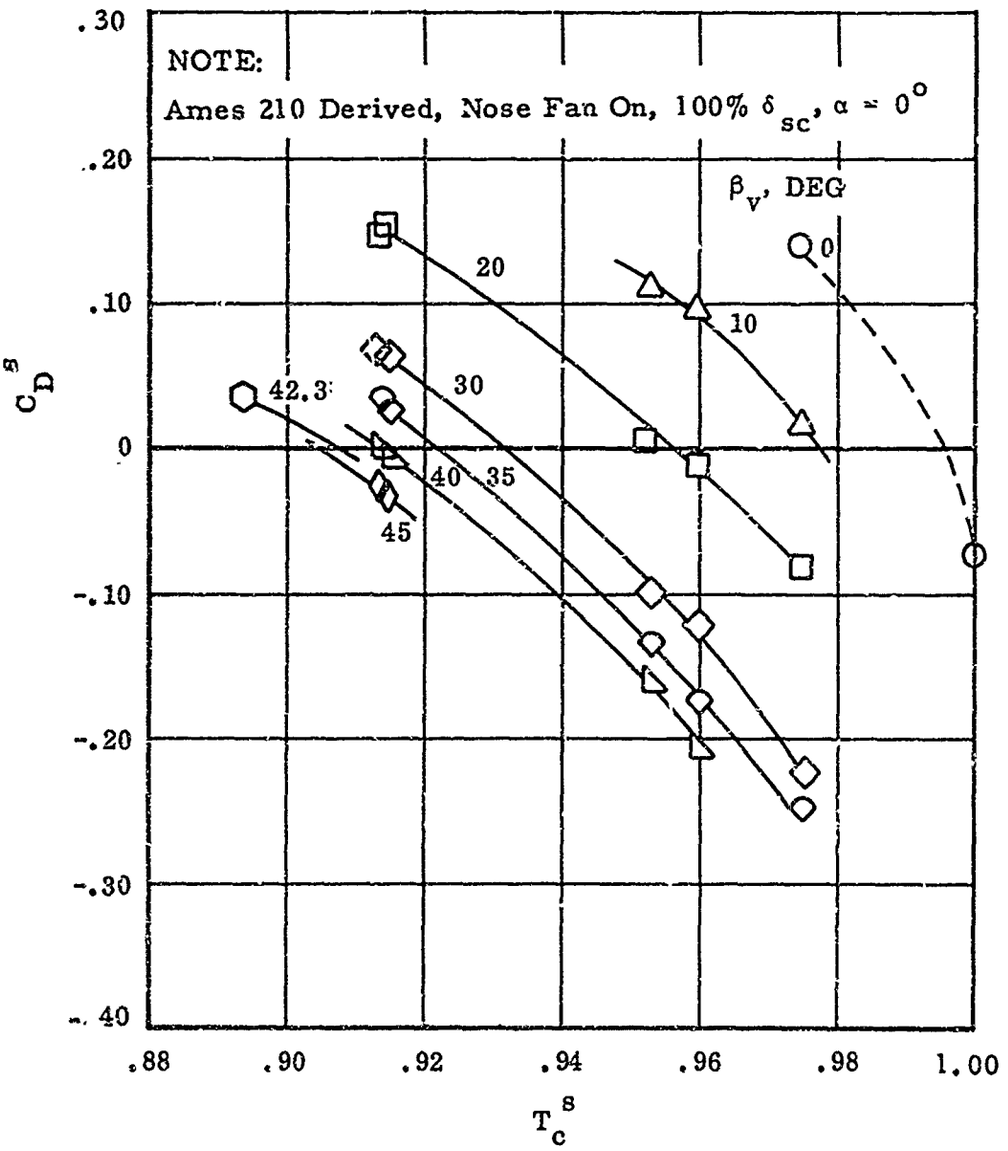

Figure 37. Drag Plot for Determining Trim Thrust Coefficient.

NOTE: CG STA 240

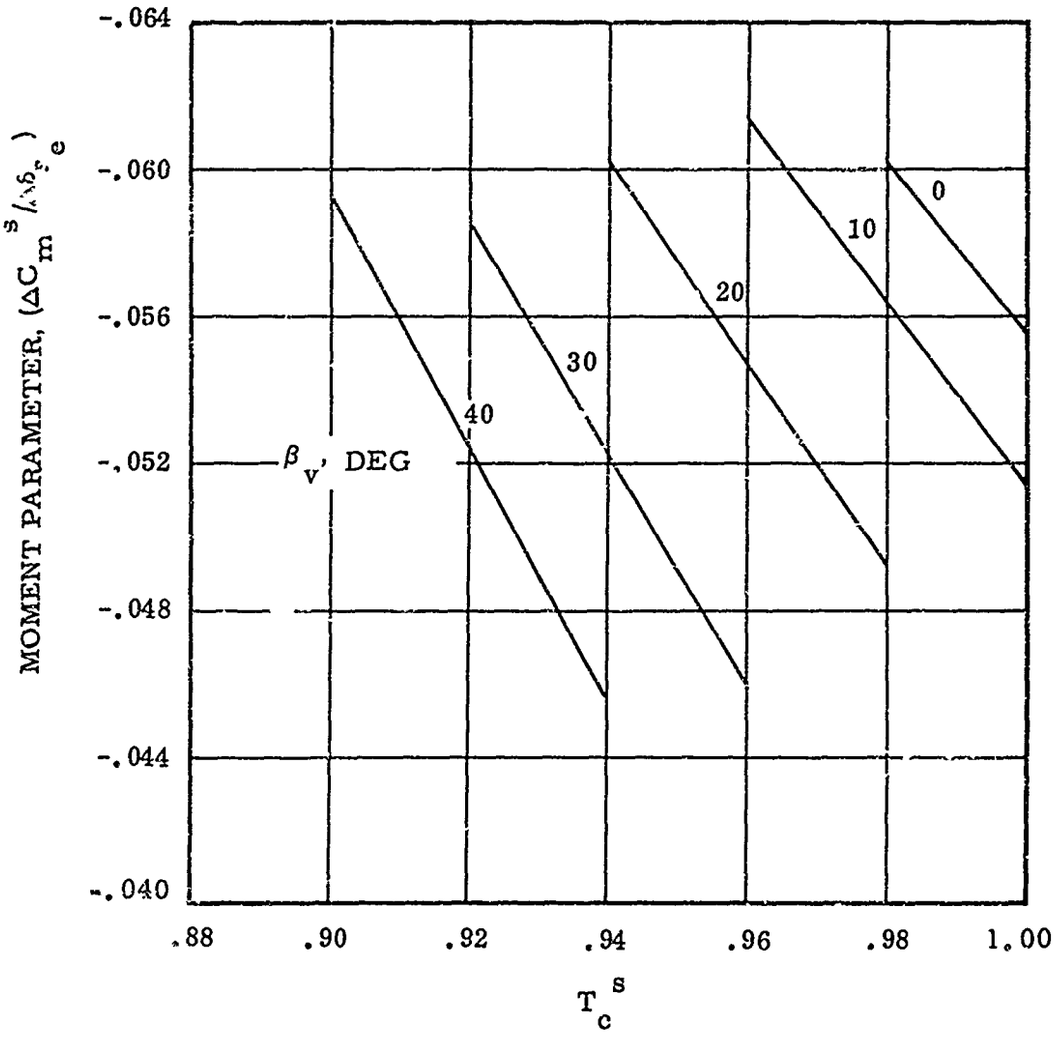

Figure 38. Pitching Moment Trim Parameter.

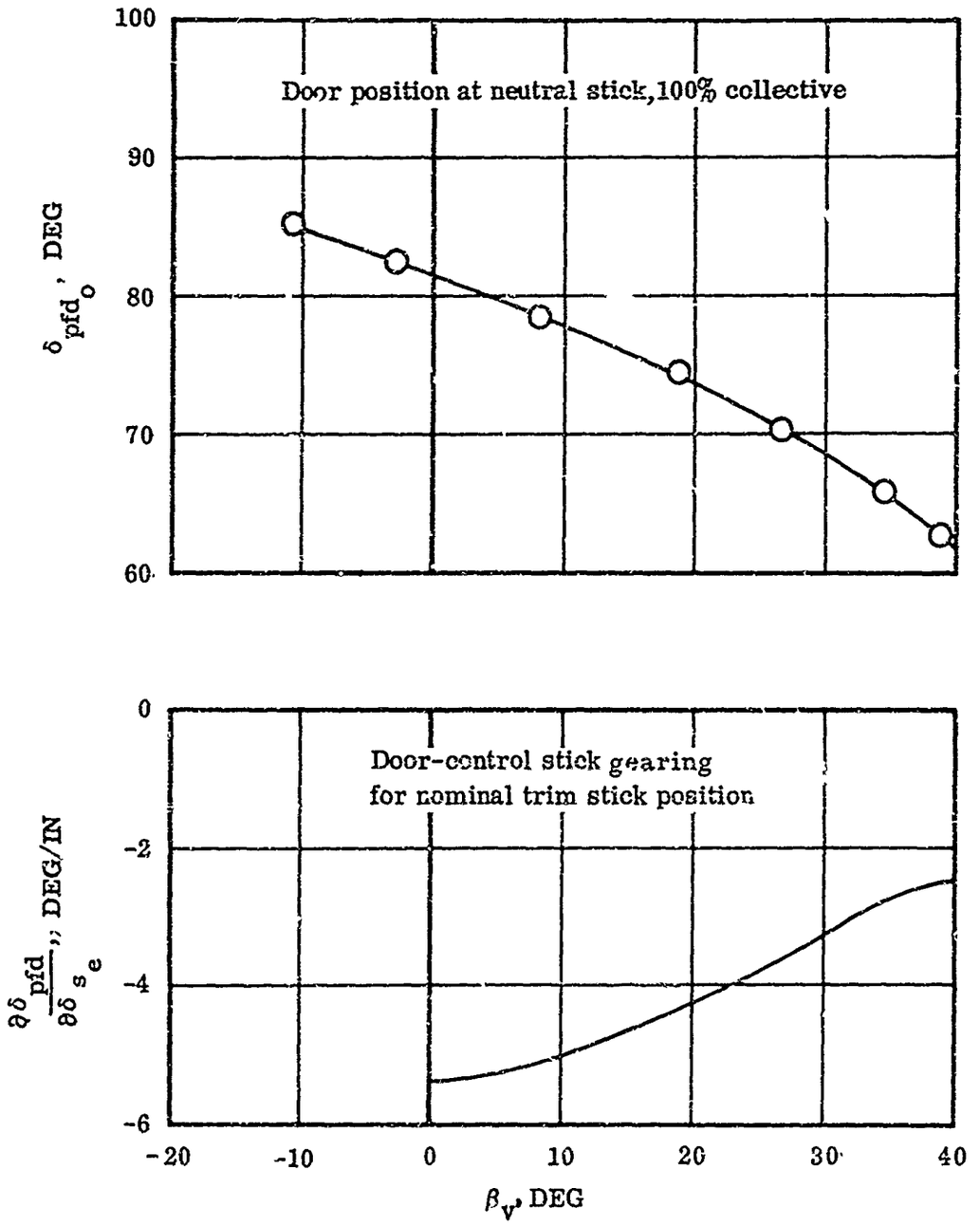

Figure 39. Nose Fan Door-Control Gearing.

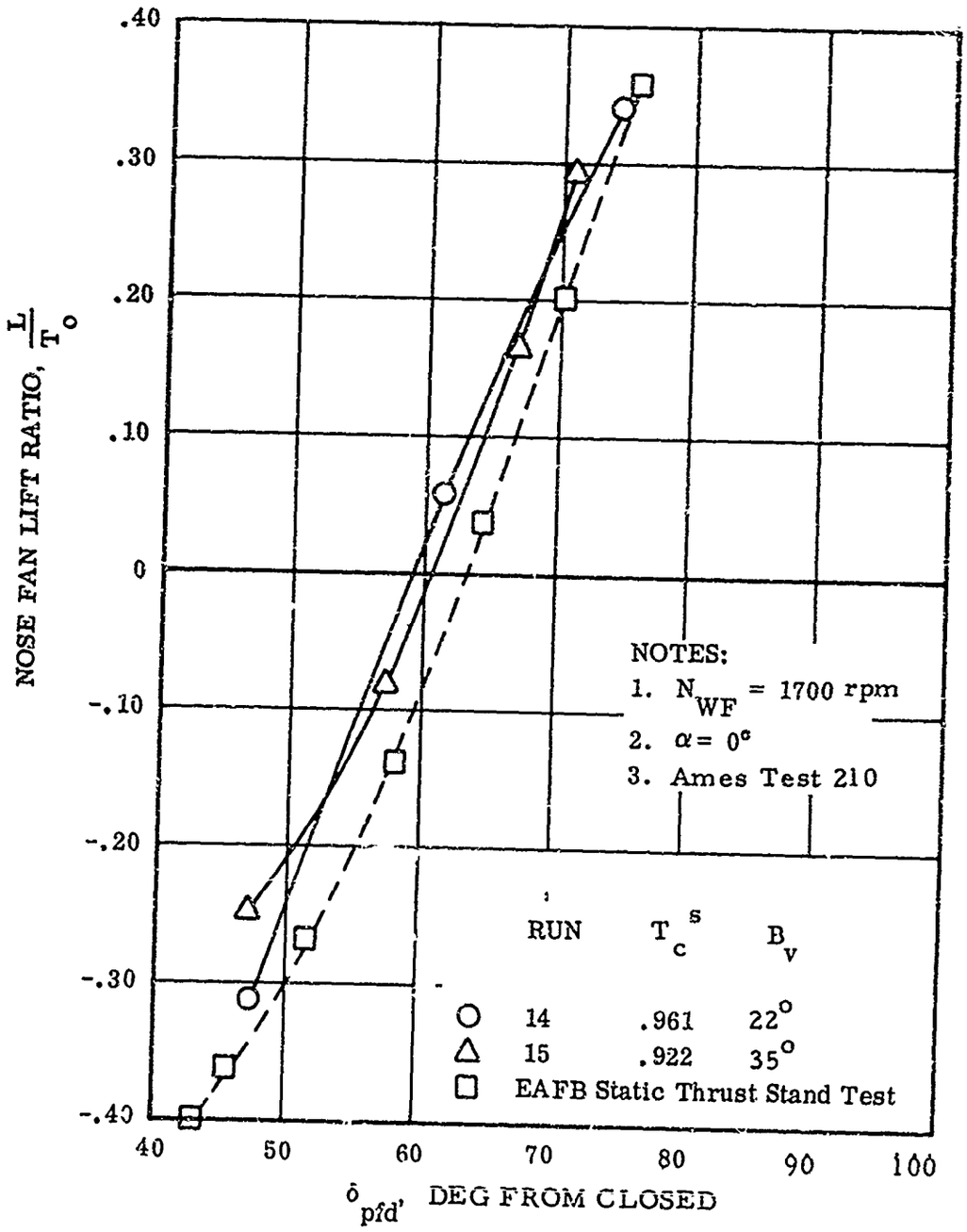

Figure 40. Nose Fan Lift Effectiveness.

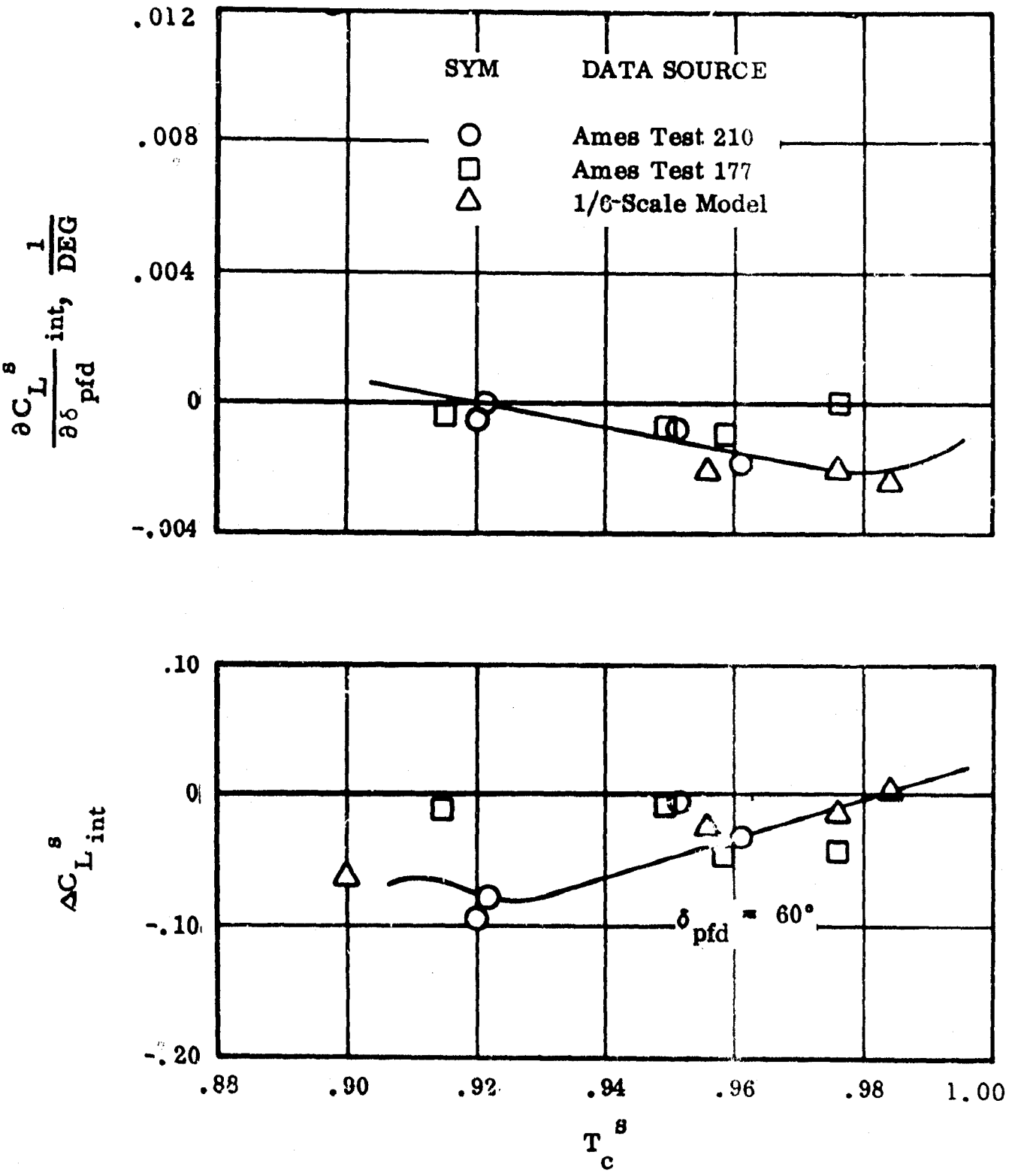

Figure 41. Nose Fan Lift Interference Factors.

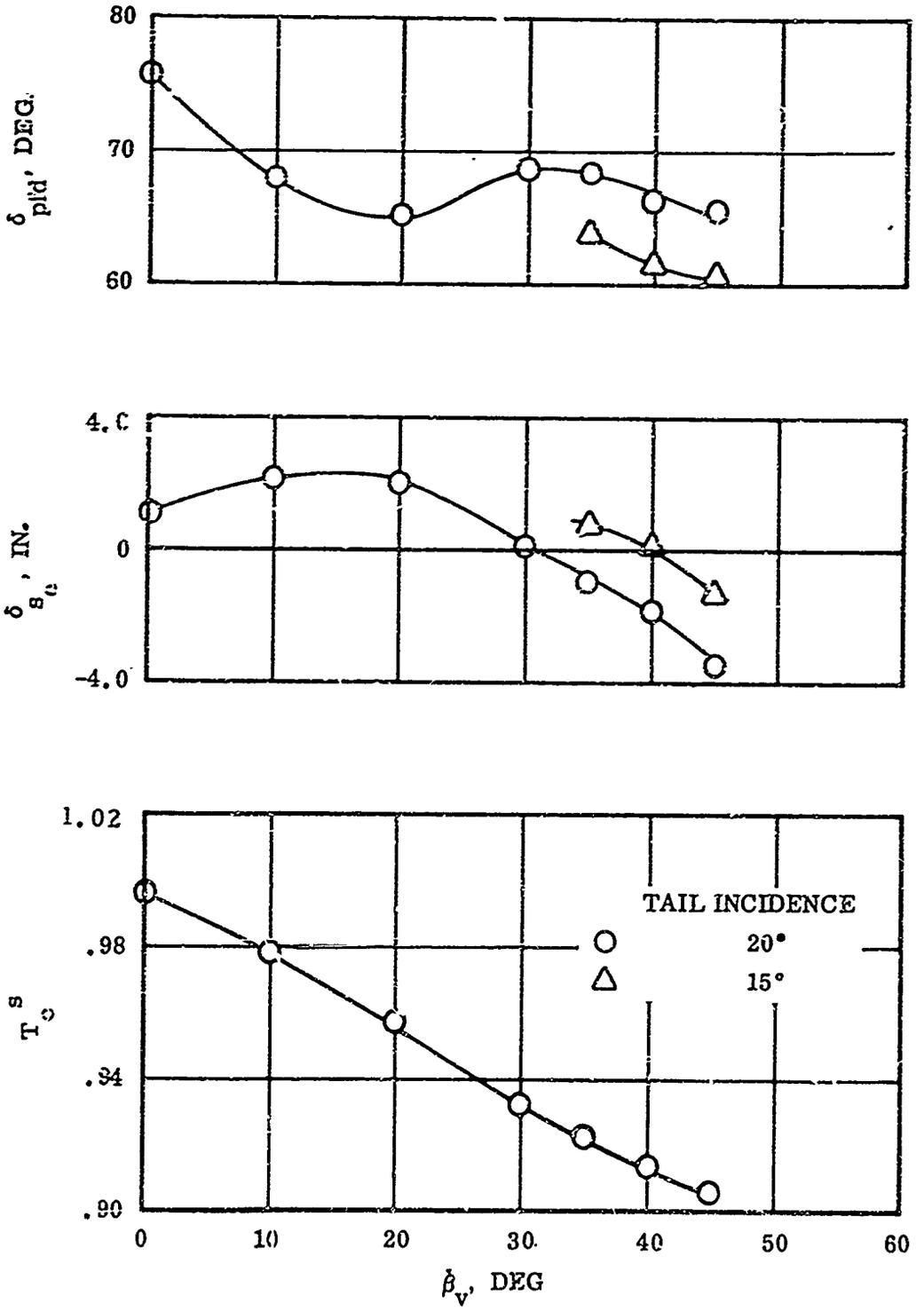

Figure 42. Control Settings Required for Trim Drag and Moment.

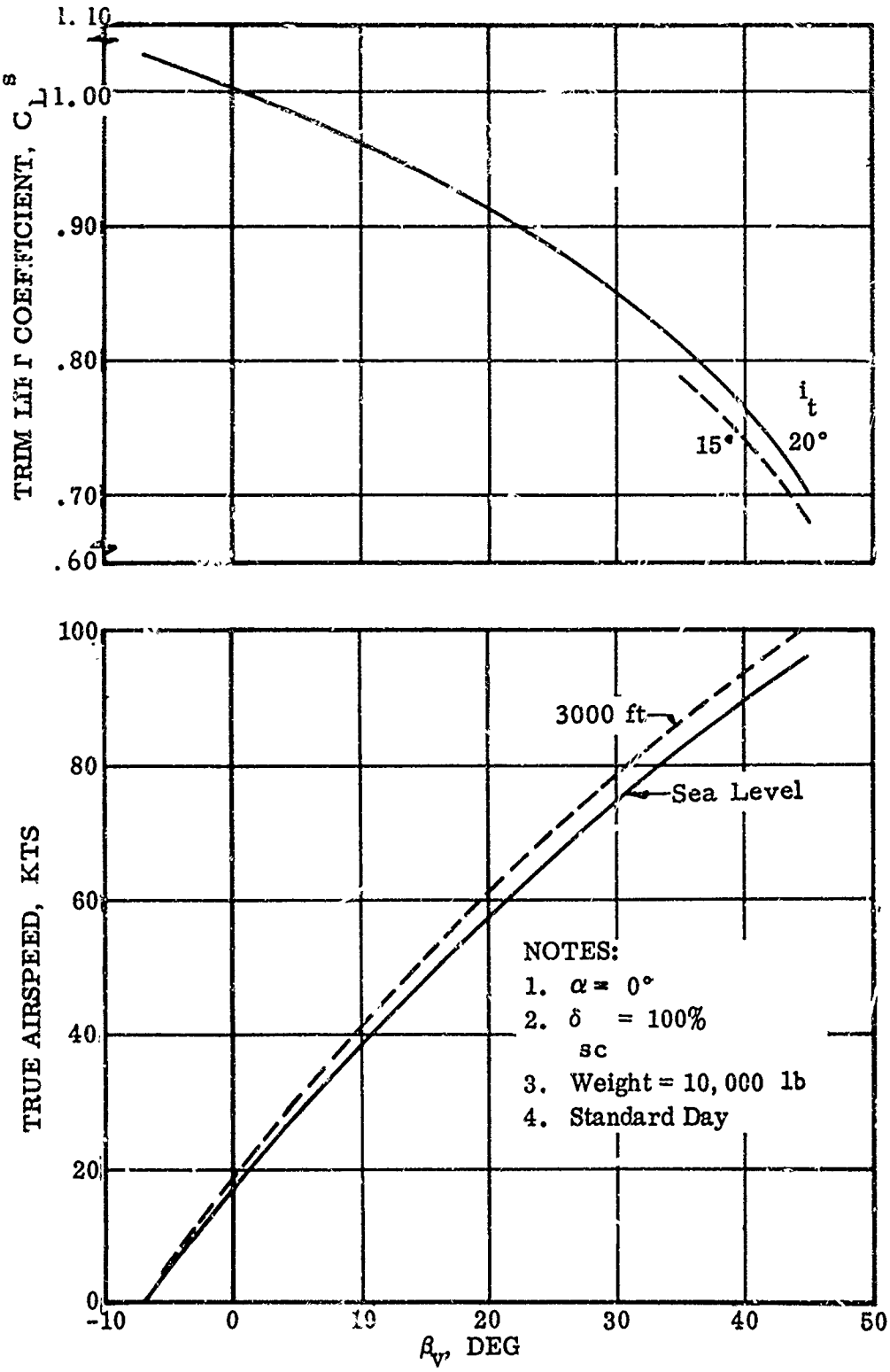

Figure 43. Trim Lift Coefficient and Airspeed in Transition.

6.0 STABILITY AND CONTROL DERIVATIVES

6.1 DERIVATION OF EQUATIONS

6.1.1 GENERAL DESCRIPTION OF THE STABILITY DERIVATIVES

The longitudinal stability derivatives originated herein were developed in dimensional form for a system of body axes so as to be suitable for use with conventional linear equations of motion for small perturbation stability and control analyses of flight characteristics in the fan mode.

6.1.2 METHOD OF APPROACH

The equations for the stability derivatives were developed independently to express the contributions of the horizontal tail, the wing-body combination, and the nose fan. This procedure enabled an assessment of the relative magnitudes of the principal contributions to the aircraft stability characteristics and is compatible with the normal wind tunnel test technique of model data buildup methods. This approach further permits the omission of certain terms, depending upon the condition being analyzed, such as the nose fan terms for pitch fan-diverted flight or the tail terms at very low speeds.

The derivatives were developed for transition flight at trimmed flight conditions corresponding to exit louver vector angles of about 10 degrees and above. This procedure permitted the utilization of stability axes data in coefficient form, and the derivatives are analogous to conventional stability derivatives for small excursions in angle of attack.

The flight condition of very low speeds near hovering, where angle of attack is undefined or may attain very large values, was considered as a special case, and those derivatives are referred to as "hovering derivatives". Under these conditions, the forces and moments are predominantly generated by the changes in mass flow of the fan systems and are predictable by momentum theory and by consideration of the resulting induced effects of the mass flow on the aircraft structure.

In the development of the derivatives, small-angle approximations were generally not made except for the product of small terms. Some of the terms which are retained are small by inspection, however, and can be neglected for angles of attack near zero.

The equations were developed by writing expressions for the longitudinal forces and moments and performing the differentiation of these expressions with respect to the velocity perturbations, u, w, and q. The resulting equations are simple expressions in terms of the nondimensional coefficients and static stability derivatives obtainable from wind tunnel test data.

The detailed derivations of the derivative equations and special considerations involving the assumptions which govern the source or applicability of the derivatives are contained in Appendix I .

6.1.3 TRANSITION DERIVATIVE EQUATIONS

The stability and control derivative expressions for the transition flight speed range which were developed in Appendix I for the general case are given in Appendix II, Table IX, for the condition of zero angle of attack. The wing-body terms include the effects of constant power input to the fans, as discussed in Appendix I. The control derivatives are given as two parts representing the elevator and nose fan thrust modulator doors.

6.1.4 HOVERING DERIVATIVE EQUATIONS

The hovering derivative equations which are independent of angle of attack are given in Appendix II, Table X. The derivatives with respect to vertical velocity and pitch rate include aerodynamic terms due to the fuselage and horizontal tail, which approximate their damping contributions by linearizing the expression in terms of the maximum value of the perturbation velocity.

6.2 CALCULATION OF STABILITY AND CONTROL DERIVATIVES

The stability derivative equations given in Appendix II were evaluated at each trim airspeed determined as a function of vector angle, as shown in Figure 43. The required inputs for calculation of the contributions of the horizontal tail, wing-body, and nose fan are discussed in the following sections.

6.2.1 HORIZONTAL TAIL

The values of the required inputs for calculation of the horizontal tail derivatives are given in Table V, where the values of tail lift and drag coefficient and downwash characteristics were obtained from Figures 44 and 45. The tail force coefficients were derived from the tail increments discussed in Section 5.1. The downwash characteristics were obtained from tests of the 1/6-scale model of the XV-5A (References 10 and 14).

6.2.2 WING-BODY

The values of the required inputs for the wing-body derivatives are given in Table VI and Figures 46 through 53. The lift, drag and pitching moment coefficients shown in Figure 46 were obtained from Figure 35 at the trim values of thrust coefficient discussed in Section 5.2. Lift coefficients are shown for the nose fan inoperative and for the nose fan on, with only the interference lift increments of Figure 41 included. The latter values of lift coefficient were used in computing the wing-body derivatives.

The angle-of-attack derivatives are shown in Figures 47 through 49. The lift and drag characteristics were obtained from data of Reference 14 and include the influence of drooped ailerons. The pitching moment derivative was obtained from comparisons of 1/6-scale model and full-scale model tests (Ames 173). The full-scale data were corrected for an apparent discrepancy in the power-off pitching moment curve slope prior to comparing with the small-scale data. The test data, which had been obtained at c.g. station

246, were then corrected to c.g. station 240, which was the reference moment center chosen for the development of the stability derivatives.

Slopes of the lift, drag, and pitching moment coefficient curves with thrust coefficient at the trim values were obtained from Figure 35 and are shown in Figures 50 and 51.

Wing fan thrust required at each trim point was determined by the method of Section 5.2.3 and is shown in Figure 52. The fan speed parameters for constant power are shown in Figure 53 and were developed from fan speed data of Ames 210 full-scale tests of the XV-5A.

6.2.3 NOSE FAN

The inputs for the nose fan derivatives are included in Table VII. The nose fan thrust and the thrust modulator door-control derivatives were calculated from the relationships given in Appendix I.

6.2.4 CALCULATED DIMENSIONAL DERIVATIVES

The individual contributions to the stability and control derivatives calculated for equilibrium conditions for sea level standard day and 10,000 pounds gross weight are tabulated in Appendix II, Tables XI and XII. The sum of the derivatives representing the complete airplane is shown in Figures 54 through 58 as a function of trim airspeed. The transition derivatives at low speeds were faired into the values calculated by the hovering derivative equations at zero airspeed. There were no large discontinuities in the derivatives between the lowest transition speed calculated (17 knots) and the hovering condition, which tends to validate both sets of equations.

The derivatives were also evaluated for a 3,000-foot standard day atmosphere at the same gross weight and are included in Appendix II. Reducing air density has only a small effect on the magnitude of the derivatives, except for those with respect to pitching velocity.

6.3 SUBSTANTIATION OF EQUATIONS

6.3.1 LANGLEY MODEL DYNAMIC TESTS

Static and forced oscillation dynamic tests conducted with the Langley 0.18-scale model of the XV-5A provided an opportunity to compare the results of those tests with the stability derivatives calculated in this report. Although the work of the model tests is currently reported in a limited-distribution Langley Working Paper, it is listed as a reference (1) because of its importance to the investigation of this report.

6.3.2 COMPARISONS OF MODEL [illegible] WITH CALCULATED DERIVATIVE MODEL SCALE FACTORS

A comparison of the trim characteristics of the model and those calculated for the XV-5A airplane, as developed in Section 5, is shown in Figure 59 for a full-scale lift of 10,000 pounds at zero angle of attack. The model scaled velocity was calculated as that required for the full-scale wing loading with the equilibrium lift coefficients of the model at each vector angle. The lift coefficients are in good agreement at the lower vector angles, but the model values are higher at vector angles above 25 degrees and the corresponding model airspeeds are lower. The nose fan door positions for moment trim differ because of differences in door configuration and because of the lack of an elevator control on the model.

In order to scale the model dimensional derivatives for comparison with the calculated full-scale values, it was necessary to develop special scaling factors, because the model lift and velocity did not scale by the geometric model scale factor. The scaled lift and velocity ratios are shown in Figure 60 in comparison with the appropriate functions of the model geometric scale factor, and the model scaling factors developed for each derivative are given in Table VII.

6.3.2.1 DERIVATIVES WITH RESPECT TO VELOCITY, u

The derivatives with respect to the velocity perturbation along the X-axis are compared in Figure 61. Symbols are used for the calculated derivatives to denote the velocity points at which they were calculated.
The model derivatives were determined from the slopes of cross plots of the static data obtained on either side of the equilibrium point for each vector angle. While qualitative agreement was expected, the degree of quantitative agreement is quite encouraging, considering the differences in models and model tests which provided the sources for the two sets of data.

The pitching moment derivative, which is a measure of speed stability, is positive at hover and in transition below about 50 knots. Above this speed the derivative becomes negative, indicating negative or unstable speed stability.

6.3.2.2 DERIVATIVES WITH RESPECT TO ANGLE OF ATTACK

The force and moment derivatives with respect to angle of attack are compared in Figure 62. The calculated values were derived from the derivatives with respect to w, shown in Figure 55. While the vertical force derivatives are in good agreement, the longitudinal force and pitching moment agreement is only fair. The calculated horizontal force derivative is sensitive to the magnitude of the drag curve slope, which is difficult to measure because of its nonlinear nature.

Based on the calculated derivatives, the airplane is statically stable above 70 knots, whereas the model data remains unstable to higher speeds, with a sudden change in stability above 70 knots. The pitching moment derivative is discussed in more detail in a later section.

6 3.2.3 DERIVATIVES WITH RESPECT TO PITCH RATE

Force derivatives with respect to pitch rate are shown in Figure 63. Inspection of the elements of the vertical force derivative showed the same magnitude for the horizontal tail contributions, but the model derivative with the tail off was negative in sign compared with a positive calculated increment for the wing-body nose fan. Therefore, the model total derivative is more negative than the calculated total derivative. However, qualitative agreement is indicated, and the force derivatives with pitch rate are not considered as important factors in dynamic stability.

The pitch damping derivative comparison is shown in Figure 64. Good agreement is evident, especially at the lower flight speeds; however, the calculated derivatives do not include derivatives with respect to $\dot{\alpha}$. The effect of $\dot{\alpha}$ on the tail contribution is discussed in the following section.

6.3.2.4 FACTORS AFFECTING CORRELATION OF DERIVATIVES

Tests of the 0.18-scale model with the horizontal tail on and off afforded the opportunity to assess the relative magnitudes of the tail and wing-body contributions to the stability derivatives.

Figure 65 shows a comparison of the hovering pitch damping derivative as a function of full-scale pitch rate. The calculated tail increment was taken as the local slope of the derivative, which for the model would correspond to zero pitch angle where the pitch rate is maximum. The total derivative is seen to increase with pitching velocity, and the calculated and test values are in closer agreement at the higher angular velocities.

A comparison of the vertical force damping derivative in hovering flight is shown in Figure 66, where the linearized calculated values are shown for two values of the perturbation velocity, w. The calculated vertical force is slightly higher than the test data at a velocity of 25 ft/sec, but the local slopes at a given velocity are in good agreement.

A comparison of the contributions to the pitching moment derivative with angle of attack is shown in Figure 67. The scatter in the model data for the wing-body nose fan is equivalent to the calculated nose fan increment. The nose fan increment in coefficient form is compared in Figure 68 with full-scale wind tunnel data which substantiates the calculated value.

The 0.18-scale model tail increment shown in Figure 67 was increased by 15 percent to account for differences in tail area and aspect ratio. The tail contribution is still lower than the calculated values after the correction, but the agreement in the total derivative is improved compared with that of Figure 62. The tail contributions were further investigated by placing

the increments in conventional coefficient notation, as shown in Figure 69. The 0.18-scale model data, corrected for tail geometry, are shown for both fan power on and off in comparison with the calculated derivatives of this report, and with 1/6-scale model data on which the calculated values are based. The 0.18-scale model with power off shows the same level of stability as the 1/6-scale model with power on. The effect of power on the 0.18-scale model reduces the tail derivative by about 18 percent and is apparently due to a higher rate of change of downwash with angle of attack or lower dynamic pressure at the tail, or both. The majority of the 1/6-scale downwash data were obtained with the nose fan inoperative, and detailed testing with and without the nose fan would be required to determine the effect of nose fan operation on the flow characteristics at the tail.

The model pitch damping derivative shown in Figure 64 includes the derivative with respect to rate of change of angle of attack. Although $\dot{\alpha}$ terms were not included in the calculated derivatives, the effect of this derivative on the correlation with model test data was evaluated.

The total horizontal tail theoretical damping derivative, $\frac{\partial M}{\partial q} + \frac{\partial M}{\partial \dot{\alpha}}$, is equal to the pitch damping derivative increased by the quantity $1 + d\varepsilon/d\alpha$. The comparison of the tail static stability level in Figure 69 shows the 0.18-scale model tail to be about 18 percent lower than the calculated value, after correcting the model for differences in tail area and lift curve slope. Based on the static stability comparison, the value of the quantity $\eta_t(1-d\varepsilon/d\alpha)$ for the model was determined and a correction factor in terms of $\eta_t(1 + d\varepsilon/d\alpha)$ was developed for the model data. This correction is shown in Figure 70 along with the calculated tail derivative which includes the theoretical $\dot{\alpha}$ contribution. The correction factor, if determined at the same value of $d\varepsilon/d\alpha$ as for the calculated derivative, is the ratio of dynamic pressure ratios. It is conceivable that the model $d\varepsilon/d\alpha$ could be higher than that assumed, but any reduction in the downwash derivative made for comparison purposes will decrease the magnitude of the correction required for agreement of the tail derivative.

Therefore, it appears that the 0.18-scale model has a lower value of dynamic pressure ratio at the horizontal tail than that used in the calculated derivatives. This reduction in q at the tail is probably due to the nose fan and results in smaller tail contributions to the static and dynamic stability derivatives.

TABLE V. INPUTS FOR CALCULATION OF TAIL DERIVATIVES

VARIABLES

U or V_T (ft/sec)	ϵ (deg)	$\frac{\partial \epsilon}{\partial \alpha}$	C_{L_t}	C_{D_t}
28	10.7	0.443	0.506	0.041
67	10.1	0.409	0.530	0.044
97	9.5	0.377	0.558	0.046
126	8.8	0.353	0.590	0.049
152	8.4	0.341	0.349	0.027

CONSTANTS

$\eta_t = 0.910$

$\partial C_{L_t}/\partial \alpha_t = 3.04 \frac{1}{rad}$

$\alpha_w = 0^o$

$\partial C_{L_t}/\partial \delta_e = 1.42 \frac{1}{rad}$

$\rho = 0.002377$ slug/cu ft

$S_t = 52.86$ sq ft

$K_i = 0.100$

$\ell_t = 21.12$ ft

$z_t = -7.83$ ft

TABLE VI. INPUTS FOR CALCULATION OF WING-BODY DERIVATIVES

VARIABLES

U or V_t (ft/sec)	T_c^s	C_L^s	C_D^s	C_m^s	$\frac{\partial C_L^s}{\partial \alpha}$ $(\frac{1}{rad})$	$\frac{\partial C_D^s}{\partial \alpha}$ $(\frac{1}{rad})$
28	0.996	0.952	-0.017	-0.120	0.10	0.965
67	0.978	0.918	-0.033	0.025	0.52	0.739
97	0.957	0.865	-0.046	0.122	0.90	0.586
126	0.932	0.783	-0.058	0.135	1.35	0.513
152	0.914	0.715	-0.066	0.120	1.75	0.460

U or V_T (ft/sec)	$\frac{\partial C_m^s}{\partial \alpha}$ $(\frac{1}{rad})$	$\frac{\partial C_L^s}{\partial T_c^s}$	$\frac{\partial C_D^s}{\partial T_c^s}$	$\frac{\partial C_m^s}{\partial T_c^s}$	$\frac{C_p^s}{C_{p_o}^s}$	$\frac{\partial (C_{p_o}^s / C_p^s}{\partial V}$
28	0.100	-1.0	-9.0	-14.0	0.983	0.00073
67	0.27[illegible]	-0.9	-6.3	- 4.2	0.973	0.00166
97	0.361	-[illegible].6	-3.[illegible]	- 1.3	0.898	0.00179
126	0.430	-[illegible].3	-3.6	0.5	0.809	0.00151
152	0.462	-3.2	-3.6	2.0	0.772	0.00102

CONSTANTS

α_w = 0°

ρ = 0.002377 slug/cu ft

A_p = 42.6 sq ft.

D_F = 5.2 ft

$\bar{z}$ = 1.00 ft

$(x_{cg} - x_{WF})$ = -1.353 ft

TABLE VII. INPUTS FOR CALCULATION OF NOSE FAN DERIVATIVES

VARIABLES

U or V_T (ft/sec)	T_c^s	T_{ooo} (lb)	T_{NF} (lb)
28	0.996	9,890	1,450
67	0.978	10,130	1,421
97	0.957	10,470	1,392
126	0.932	11,010	1,367
152	0.914	12,250	1,444

CONSTANTS

$\alpha = 0^o$

$\rho = 0.002377$ slug/cu ft

$A_{NF} = 7.07$ sq ft

$x_{NF} = 15.1$ ft

$z = 1.0$ ft

$\frac{\partial \Delta C_L^s}{\partial \delta_{pfd}^o} = 0.0024$

$\frac{\partial \Delta C_D^s}{\partial \delta_{pfd}^o} = 0.001$

$\frac{\partial (N/T_o)}{\partial \delta_{pfd}^o} = 0.024$

TABLE VIII. MODEL SCALING FACTORS FOR DIMENSIONAL STABILITY DERIVATIVES

DERIVATIVE	UNITS	SCALE FACTOR
$\frac{\partial Z/\partial u}{L_o}$	$\frac{\text{sec}}{\text{ft}}$	$\frac{L_{om}}{L_{o_{FS}}} \times \frac{V_m}{V_{FS}} \times N^3$
$\frac{\partial X/\partial u}{L_o}$	$\frac{\text{sec}}{\text{ft}}$	$\frac{L_{om}}{L_{o_{FS}}} \times \frac{V_m}{V_{FS}} \times N^3$
$\frac{\partial M/\partial u}{L_o \bar{c}}$	$\frac{\text{sec}}{\text{ft}}$	$\frac{L_{om}}{L_{o_{FS}}} \times \frac{V_m}{V_{FS}} \times N^3$
$\frac{\partial Z/\partial \alpha}{L_o}$	rad	Unity
$\frac{\partial X/\partial \alpha}{L_o}$	rad	Unity
$\frac{\partial M/\partial \alpha}{L_o \bar{c}}$	rad	Unity
$\frac{\partial Z/\partial q}{L_o}$	$\frac{\text{sec}}{\text{rad}}$	$\frac{L_{om}}{L_{o_{FS}}} \times \frac{V_{FS}}{V_m} \times N^3$
$\frac{\partial X/\partial q}{L_o}$	$\frac{\text{sec}}{\text{rad}}$	$\frac{L_{om}}{L_{o_{FS}}} \times \frac{V_{FS}}{V_m} \times N^3$
$\frac{\partial M/\partial q}{L_o \bar{c}}$	$\frac{\text{sec}}{\text{rad}}$	$\frac{L_{om}}{L_{o_{FS}}} \times \frac{V_{FS}}{V_m} \times N^3$
$\frac{Z}{L_o}$	-	$\frac{L_{cm}}{L_{o_{FS}}} N^3$

NOTES:

1. $\alpha_w = 0°$, $\delta_e = 0°$
2. Coefficients Based on Tail Area

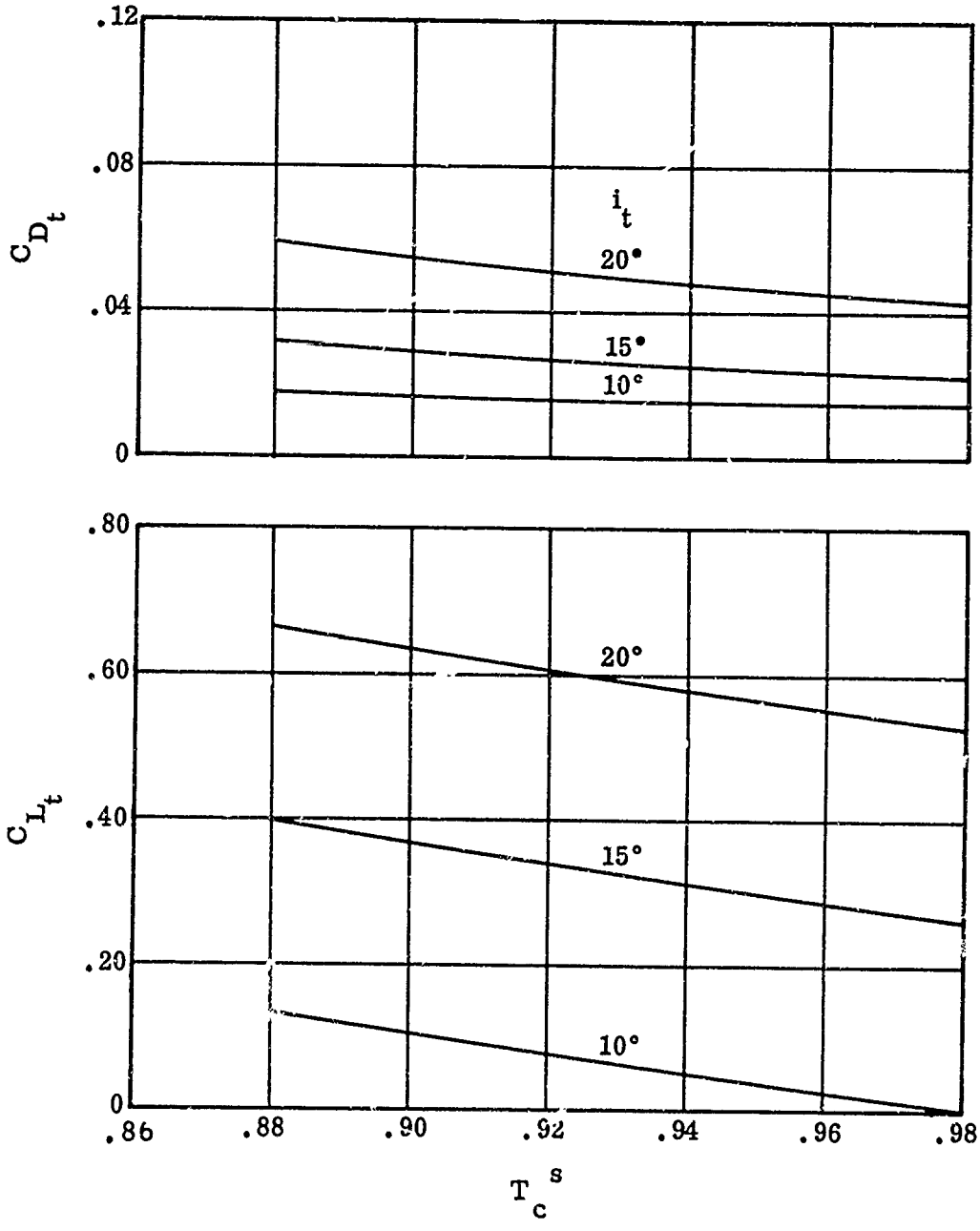

Figure 44. Horizontal Tail Lift and Drag Coefficient.

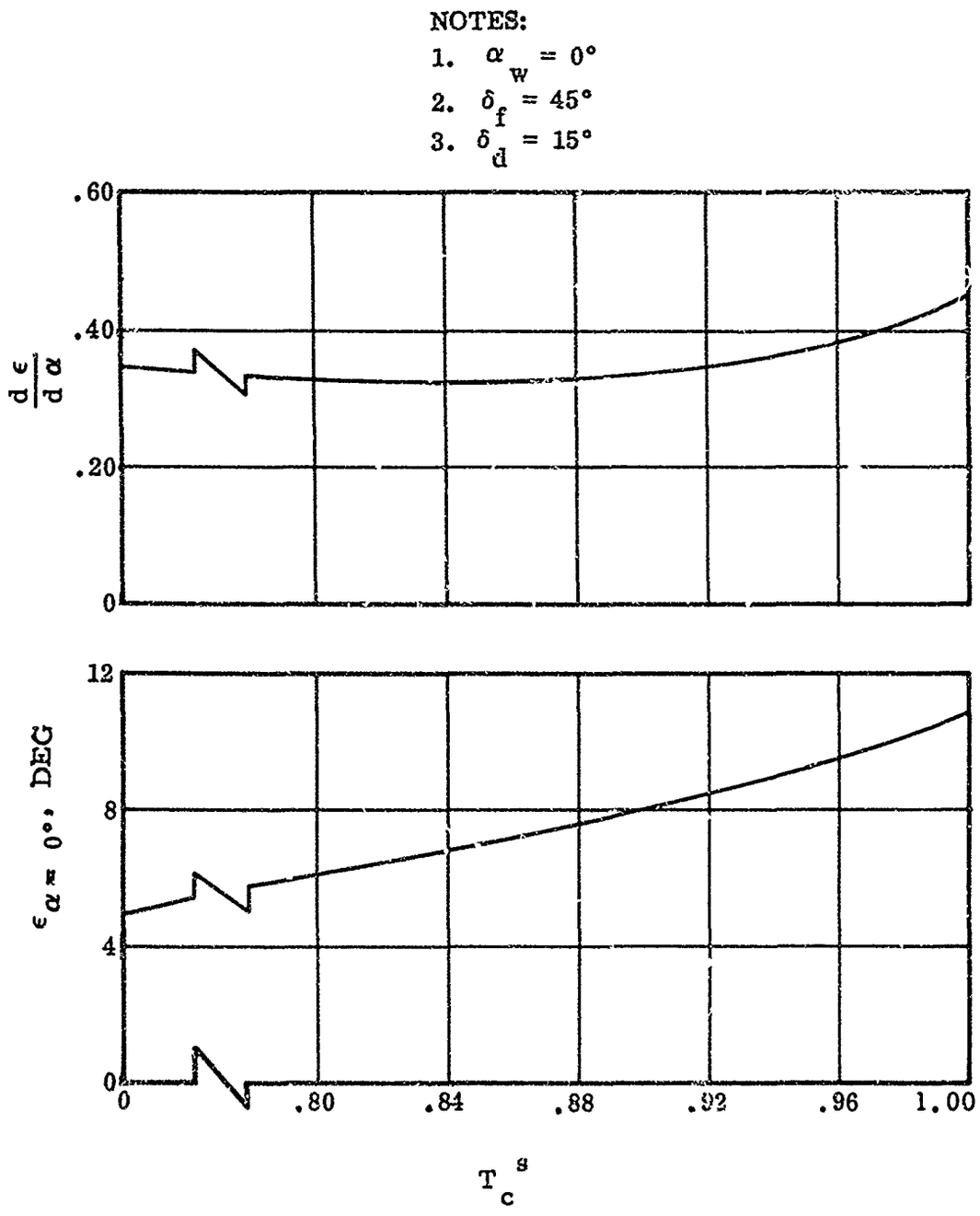

Figure 45. Downwash Characteristics at Horizontal Tail.

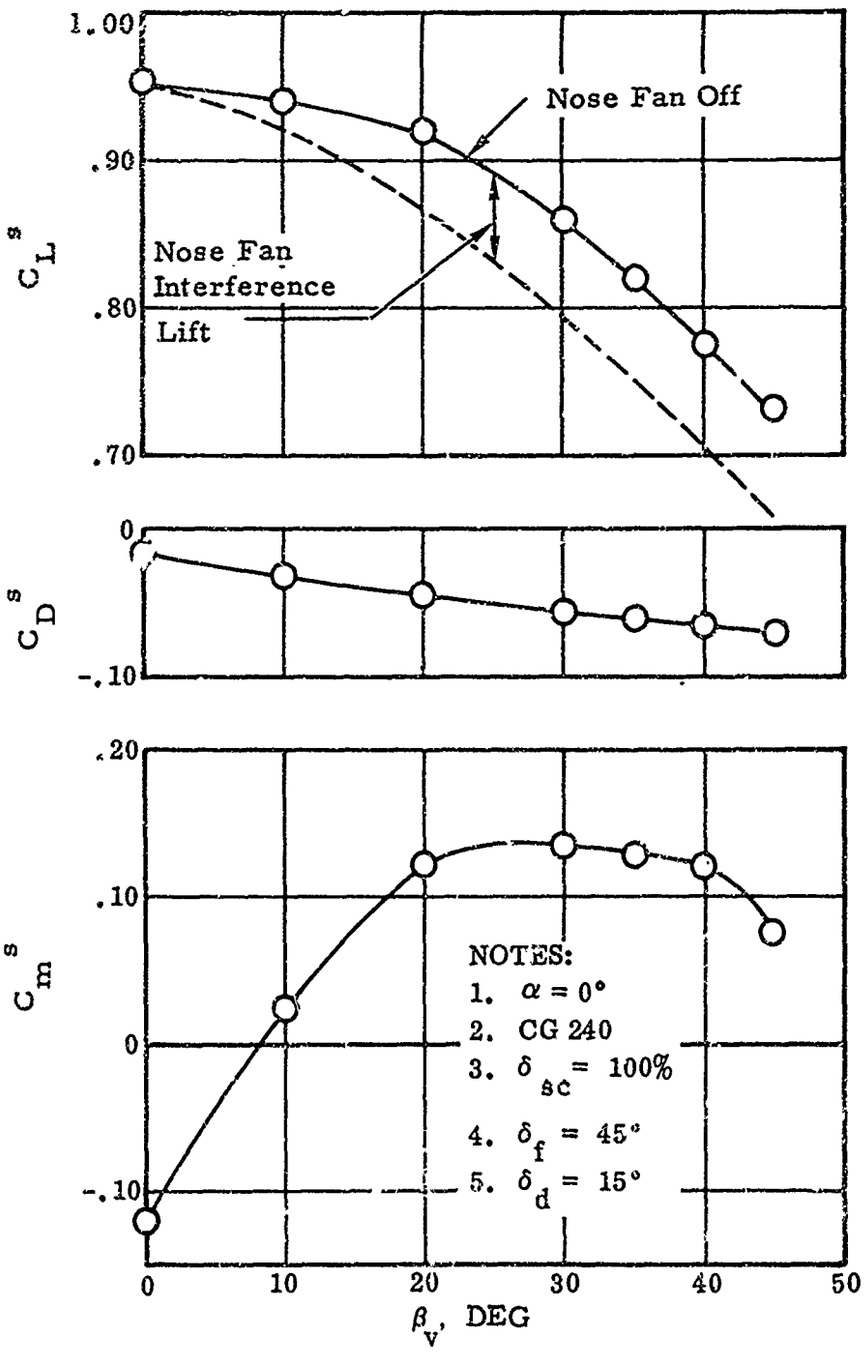

Figure 46. Wing-Body Force and Moment Coefficients at Trim.

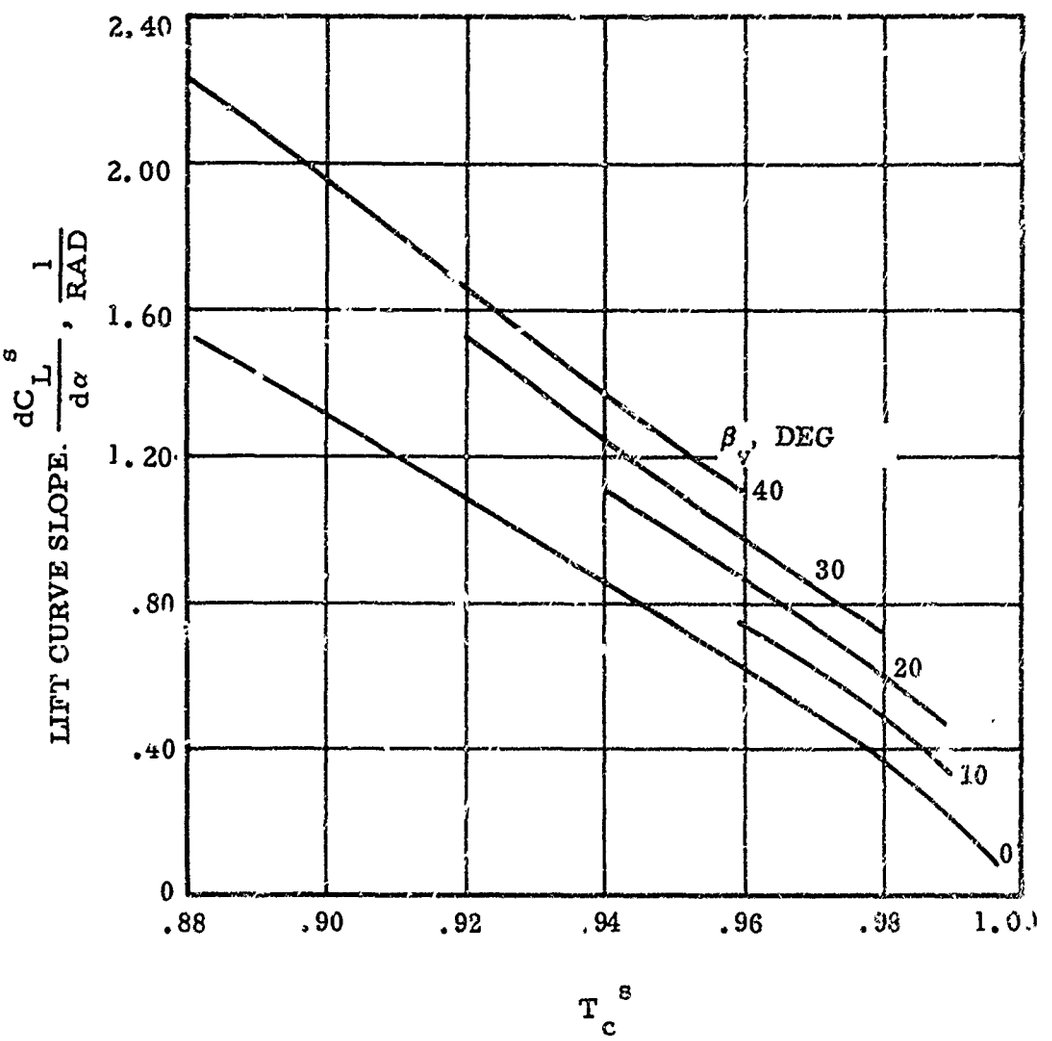

Figure 47. Wing-Body Lift Curve Slope.

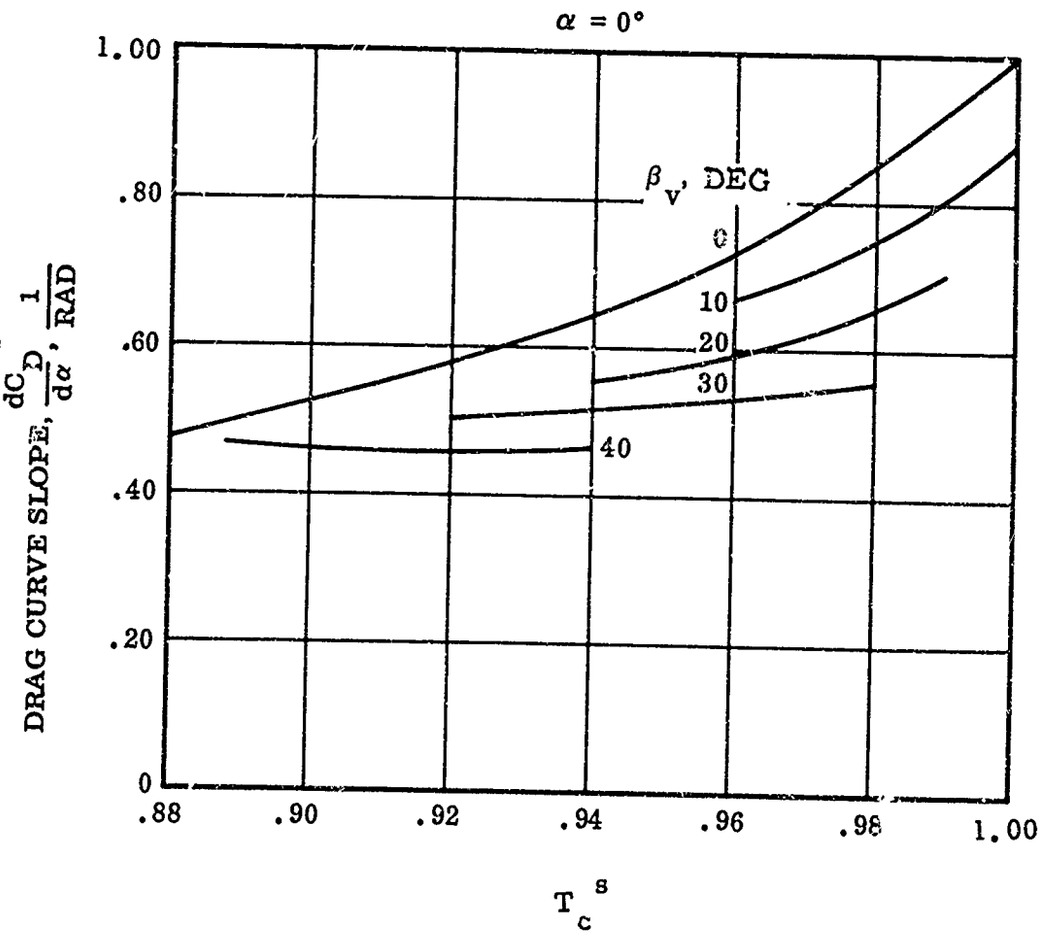

Figure 48. Wing-Body Drag Curve Slope.

NOTES:

1. CG STA 240
2. WL 112
3. Source: 1/6 Scale and Ames 173

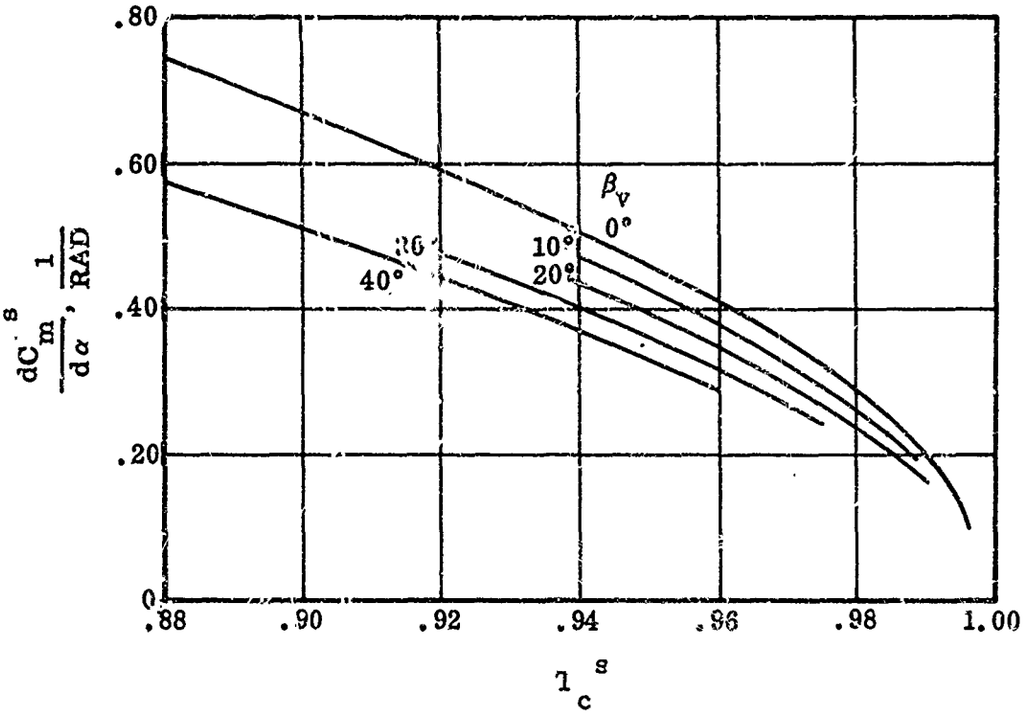

Figure 49. Wing-Body Pitching Moment Curve Slope.

NOTES:

1. $\alpha = 0°$
2. $\delta_{sc} = 100\%$
3. $\delta_f = 45°$
4. $\delta_d = 15°$

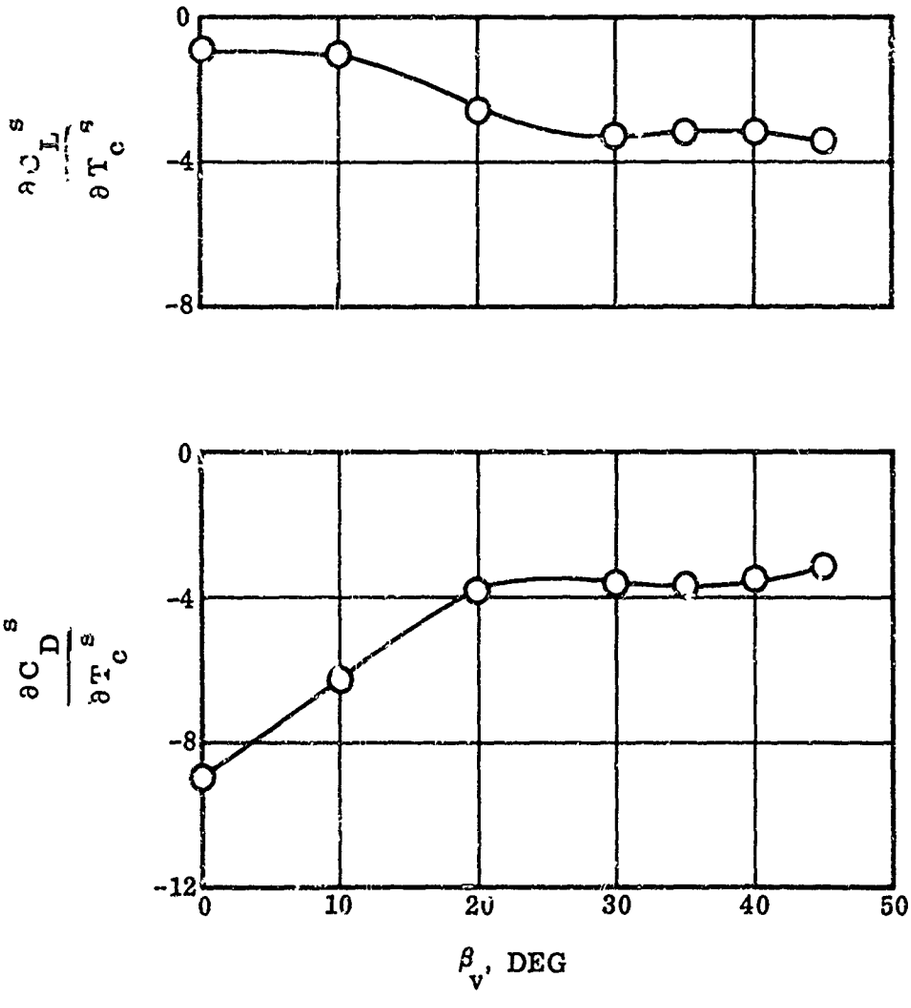

Figure 50. Wing--Body Force Coefficient Derivatives With Thrust Coefficient.

NOTES:

1. $\alpha = 0°$
2. CG 240
3. $\delta_{sc} = 100\%$
4. $\delta_f = 45°$
5. $\delta_d = 15°$

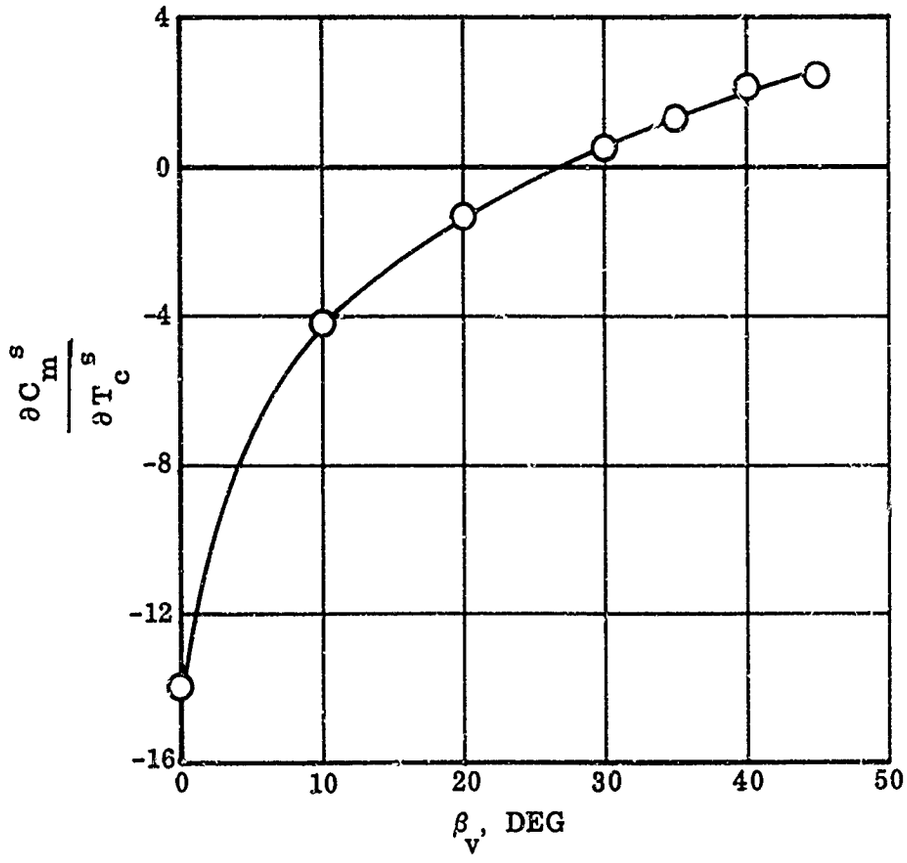

Figure 51. Wing-Body Moment Coefficient Derivative With Thrust Coefficient.

NOTES:

1. $\alpha = 0°$, CG 240, $\delta_{sc} = 100\%$
2. Weight = 10,000 lb
3. Sea Level Standard Day

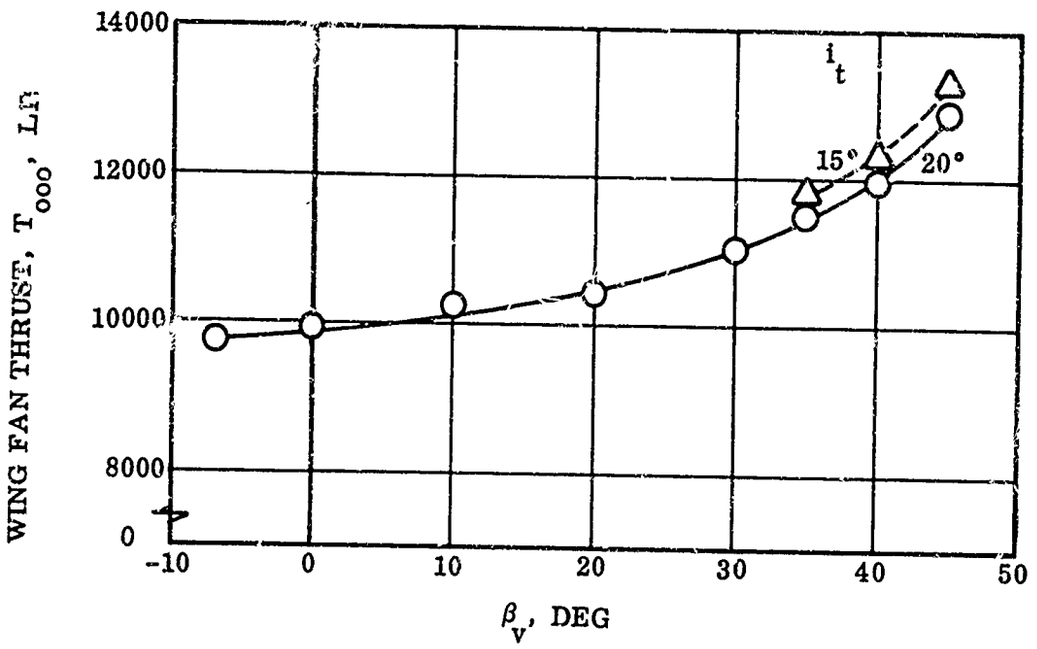

Figure 52. Wing Fan Reference Thrust Required at Trim.

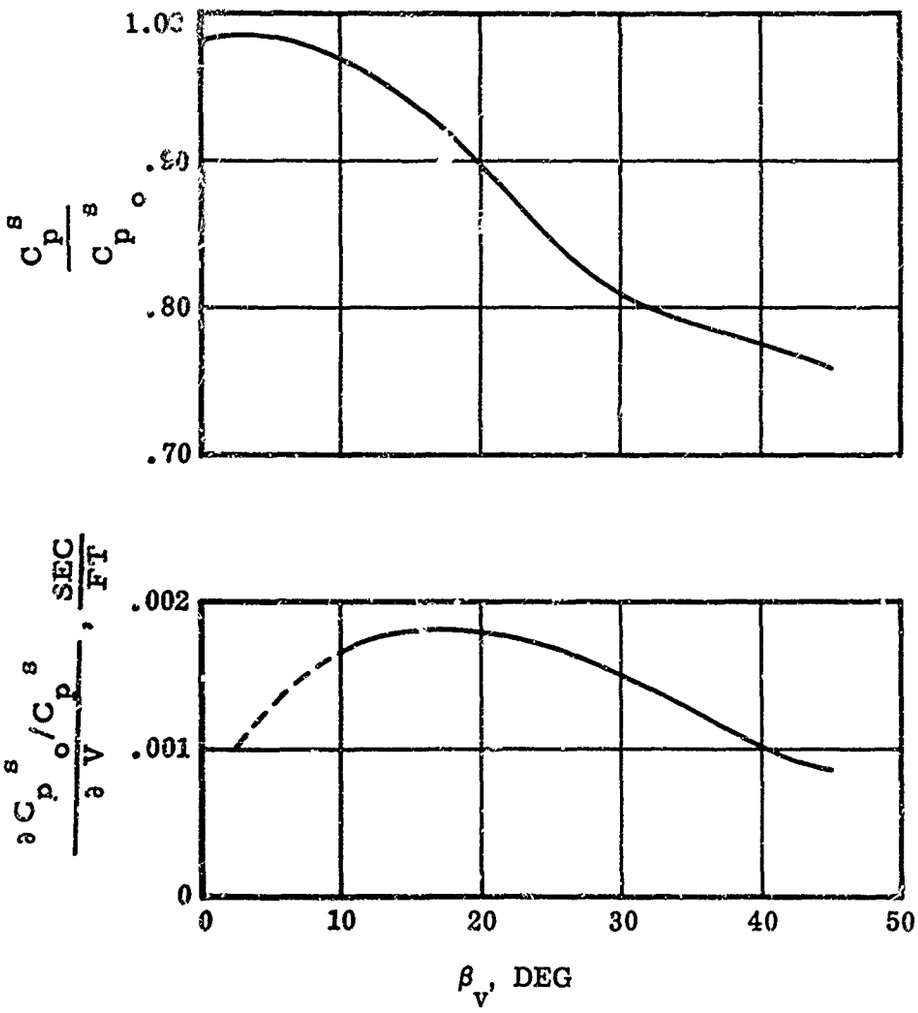

Figure 53. Wing Fan Speed Parameters for Constant Power.

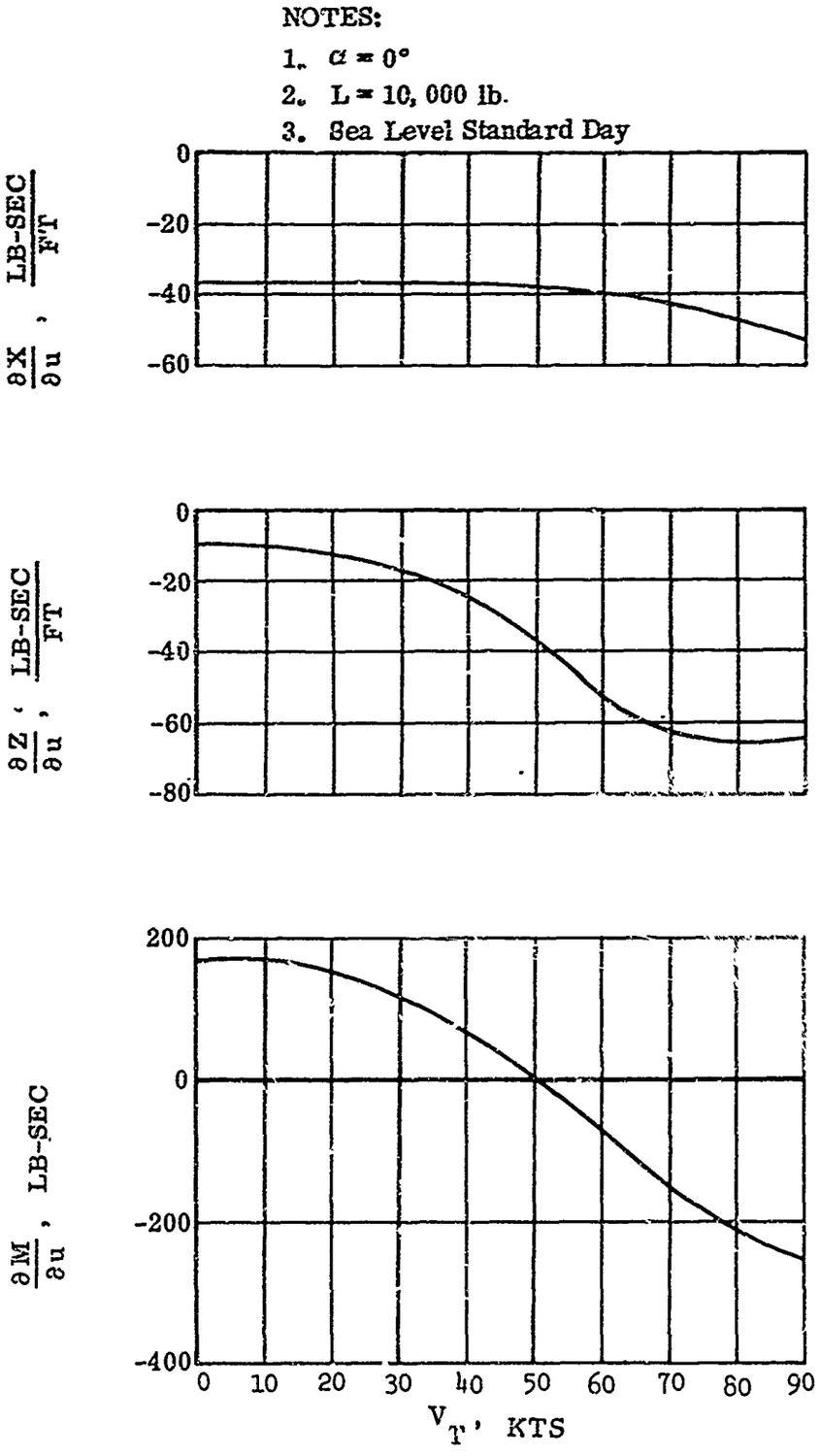

Figure 54. Stability Derivatives With Respect to Velocity Along the X-Axis.

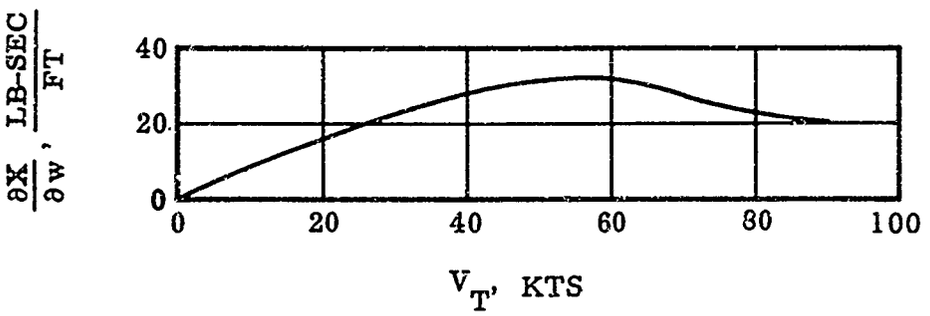

NOTES:
1. $\alpha = 0°$
2. L = 10,000 lb
3. Sea Level Standard Day

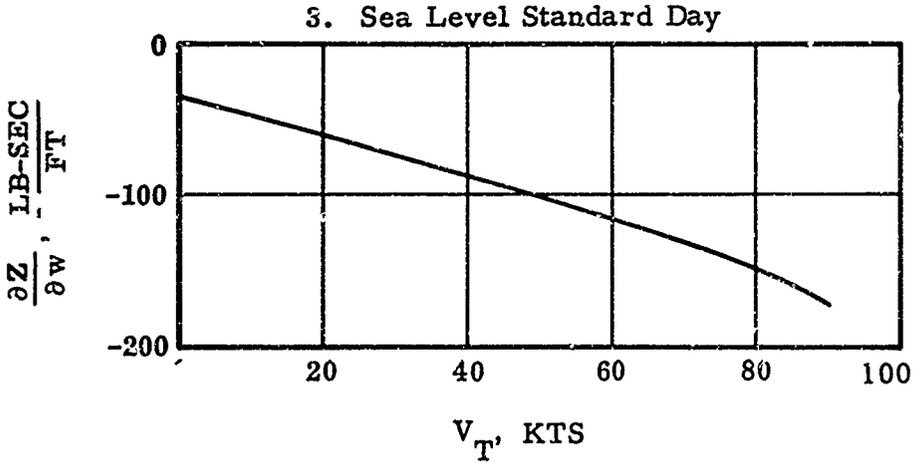

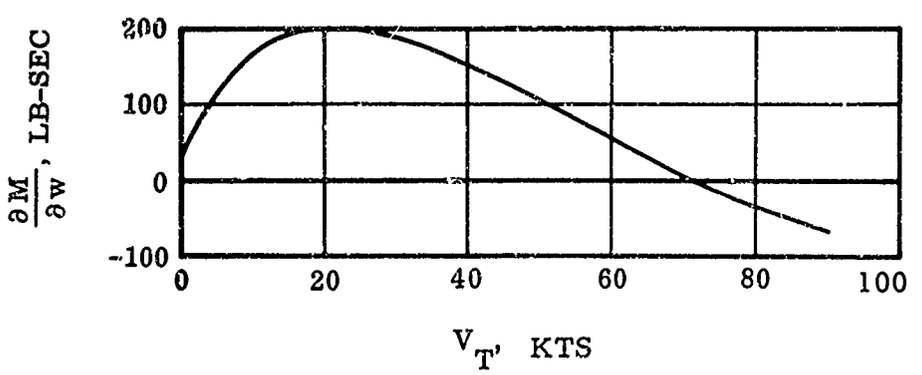

Figure 55. Stability Derivatives With Respect to Velocity Along the Z-Axis.

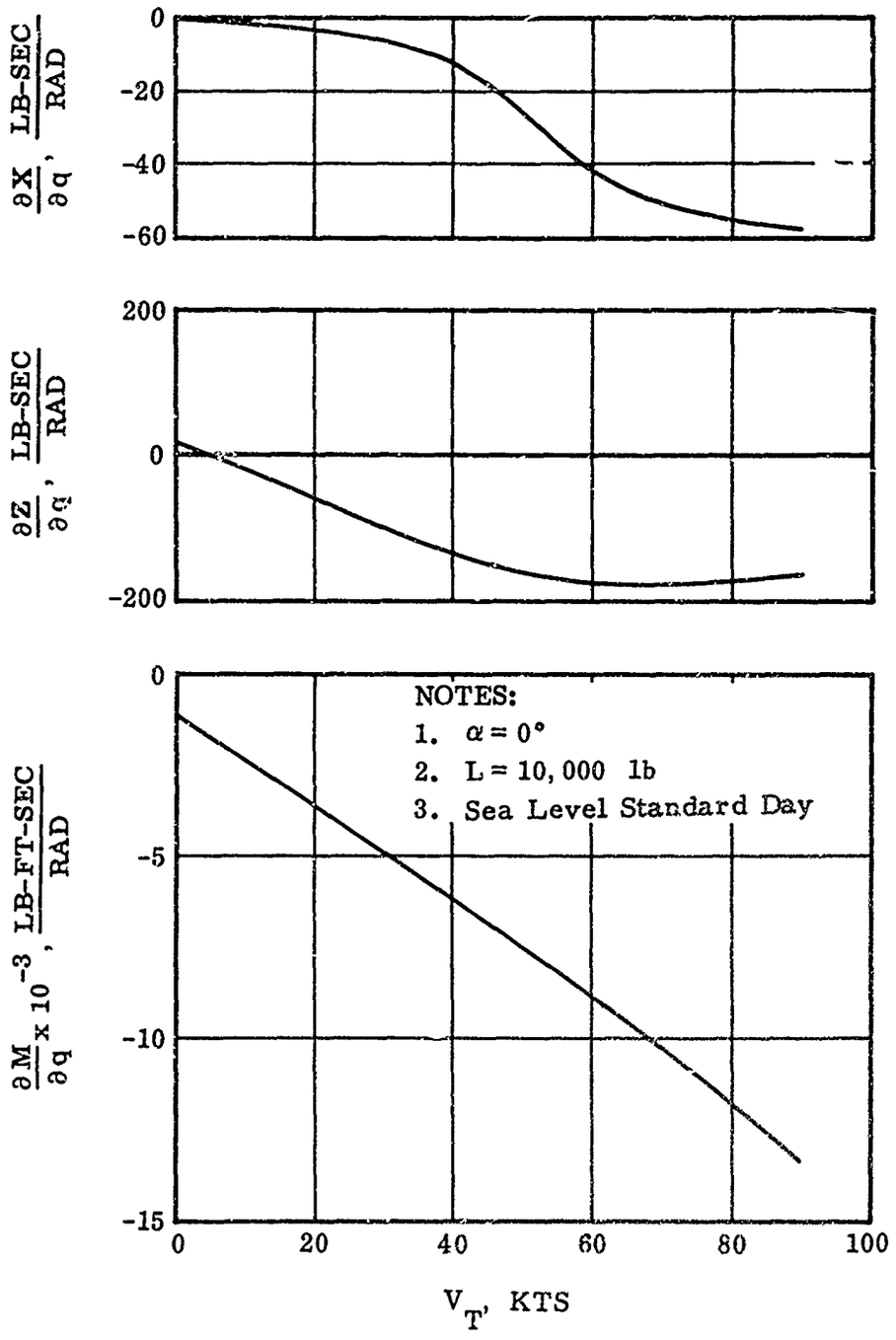

Figure 56. Stability Derivatives With Respect to Pitching Velocity.

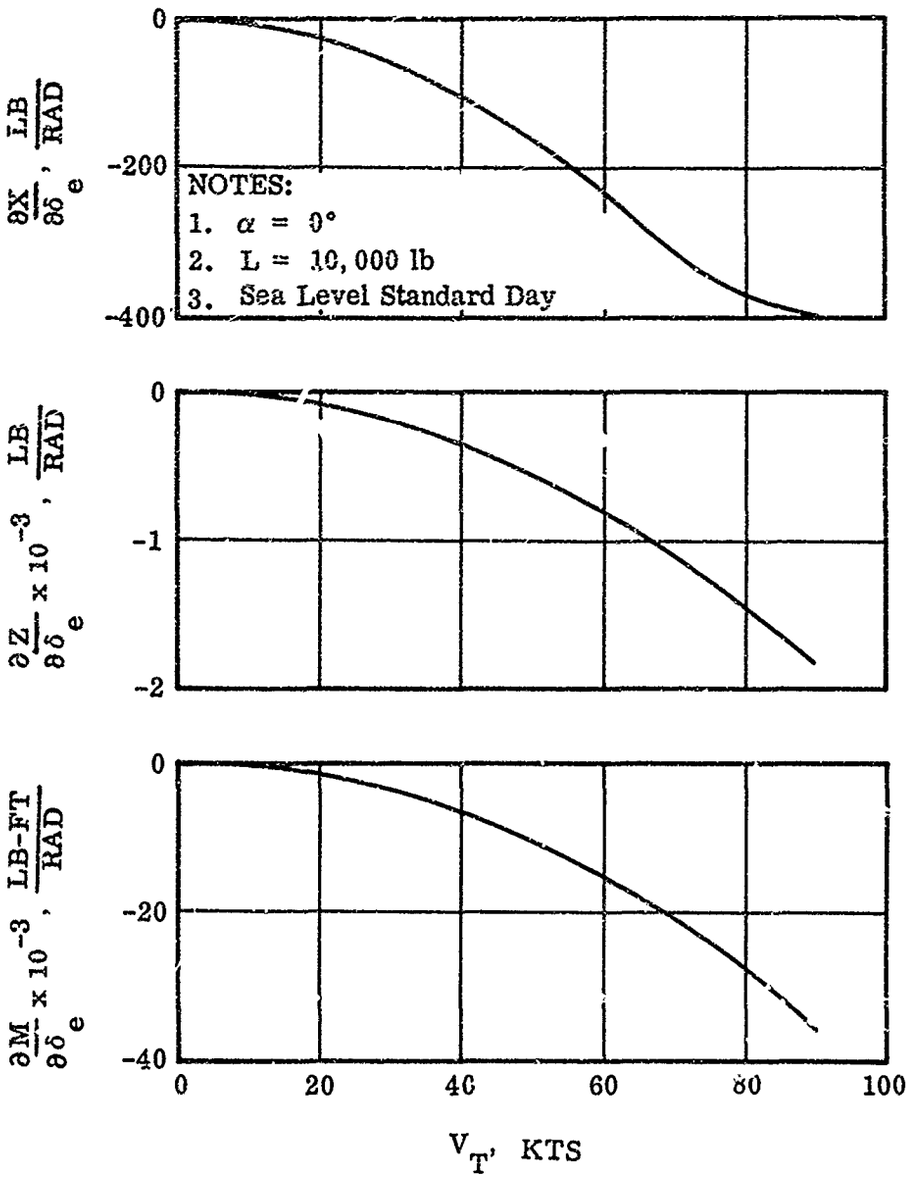

Figure 57. Control Derivatives With Respect to Elevator Deflection.

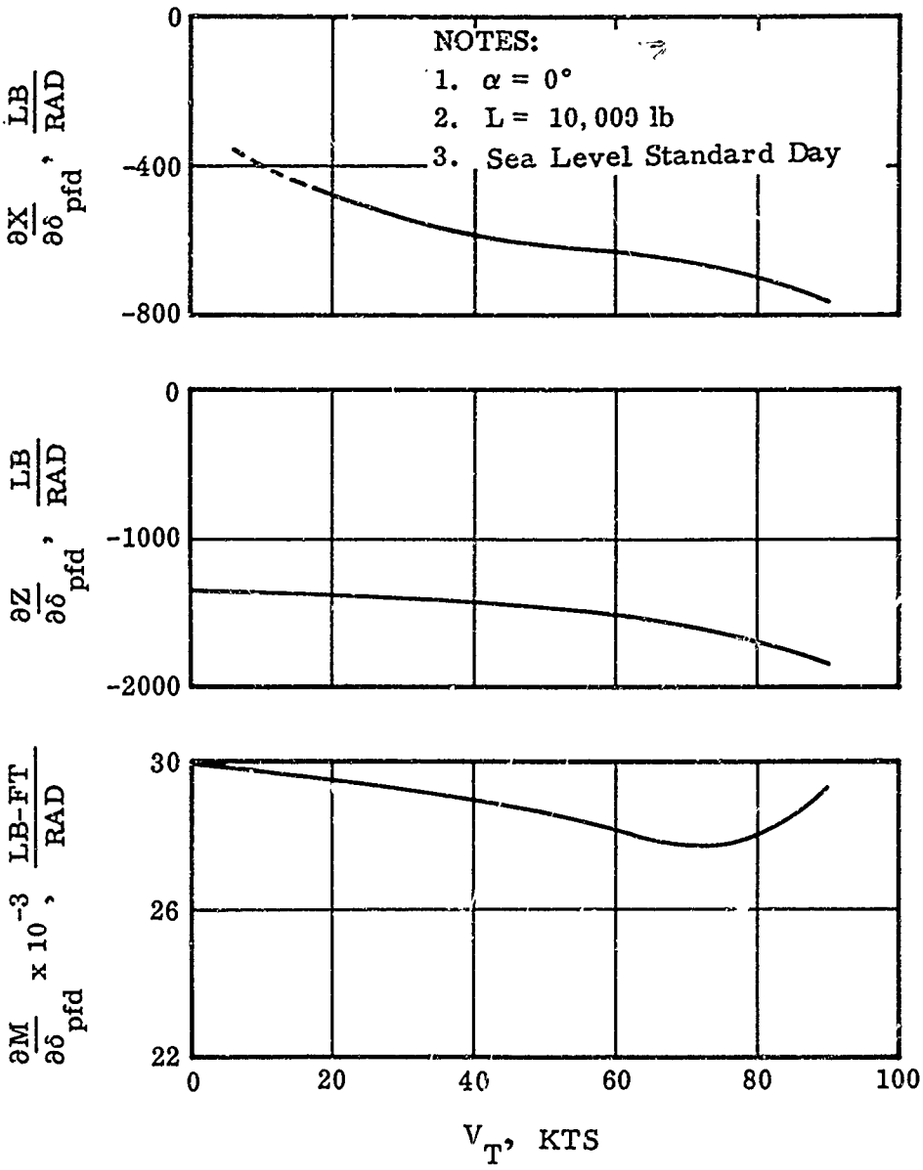

Figure 58. Control Derivatives With Respect to Nose Fan Door Position.

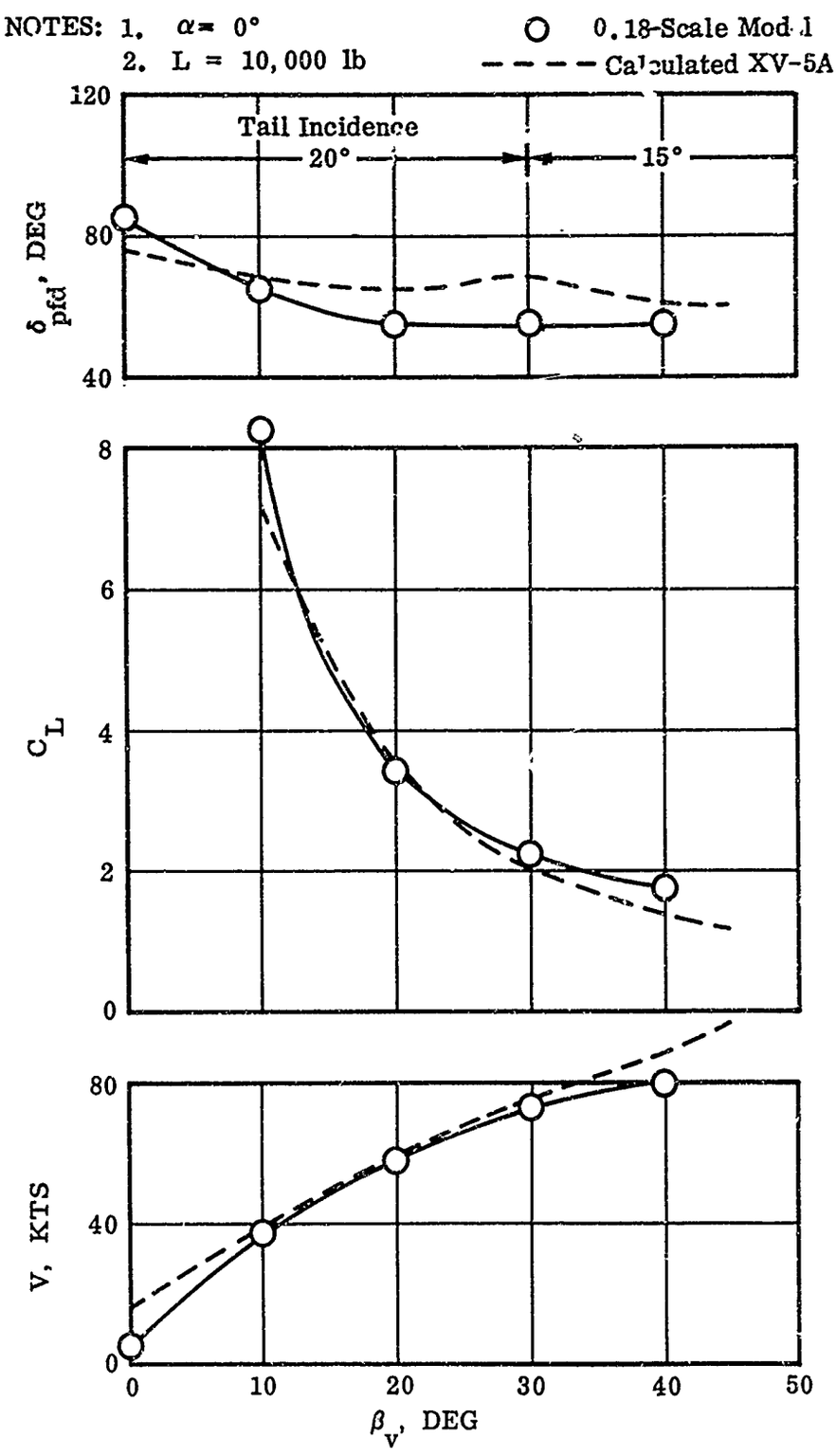

Figure 59. Comparison of Trim Characteristics.

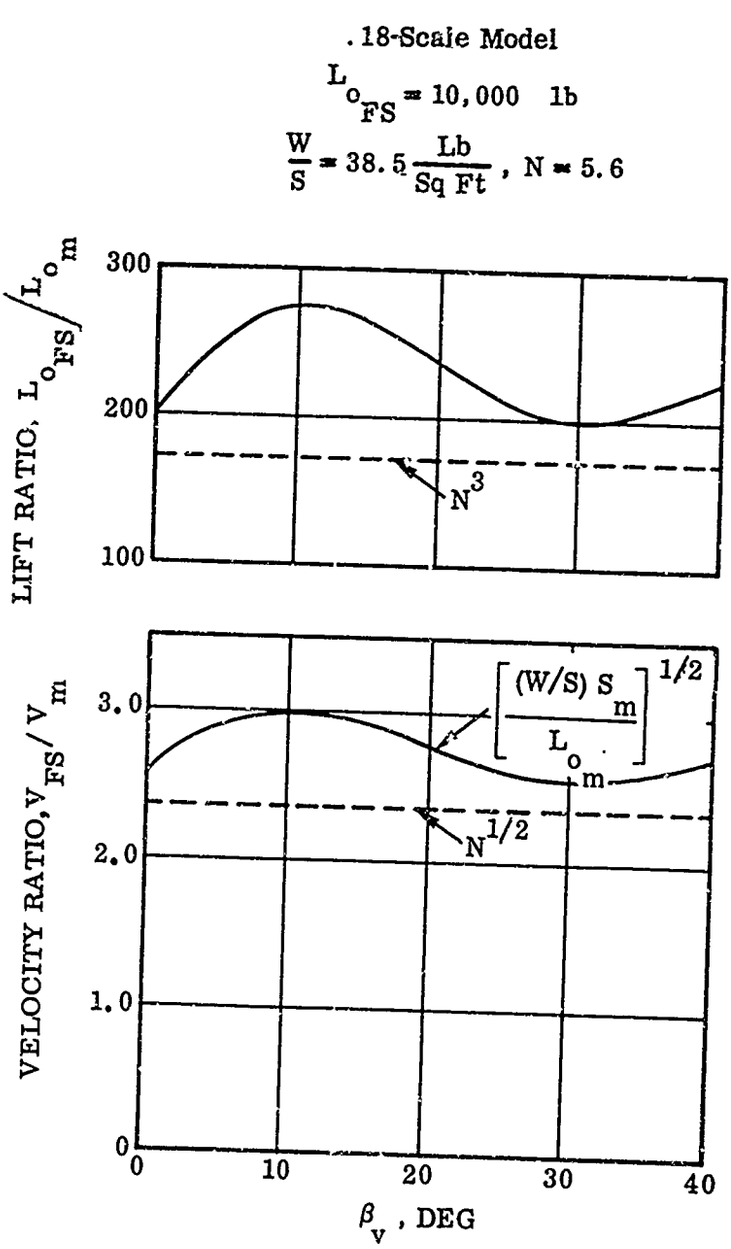

Figure 60. Parameters for Development of Model Scaling Factors.

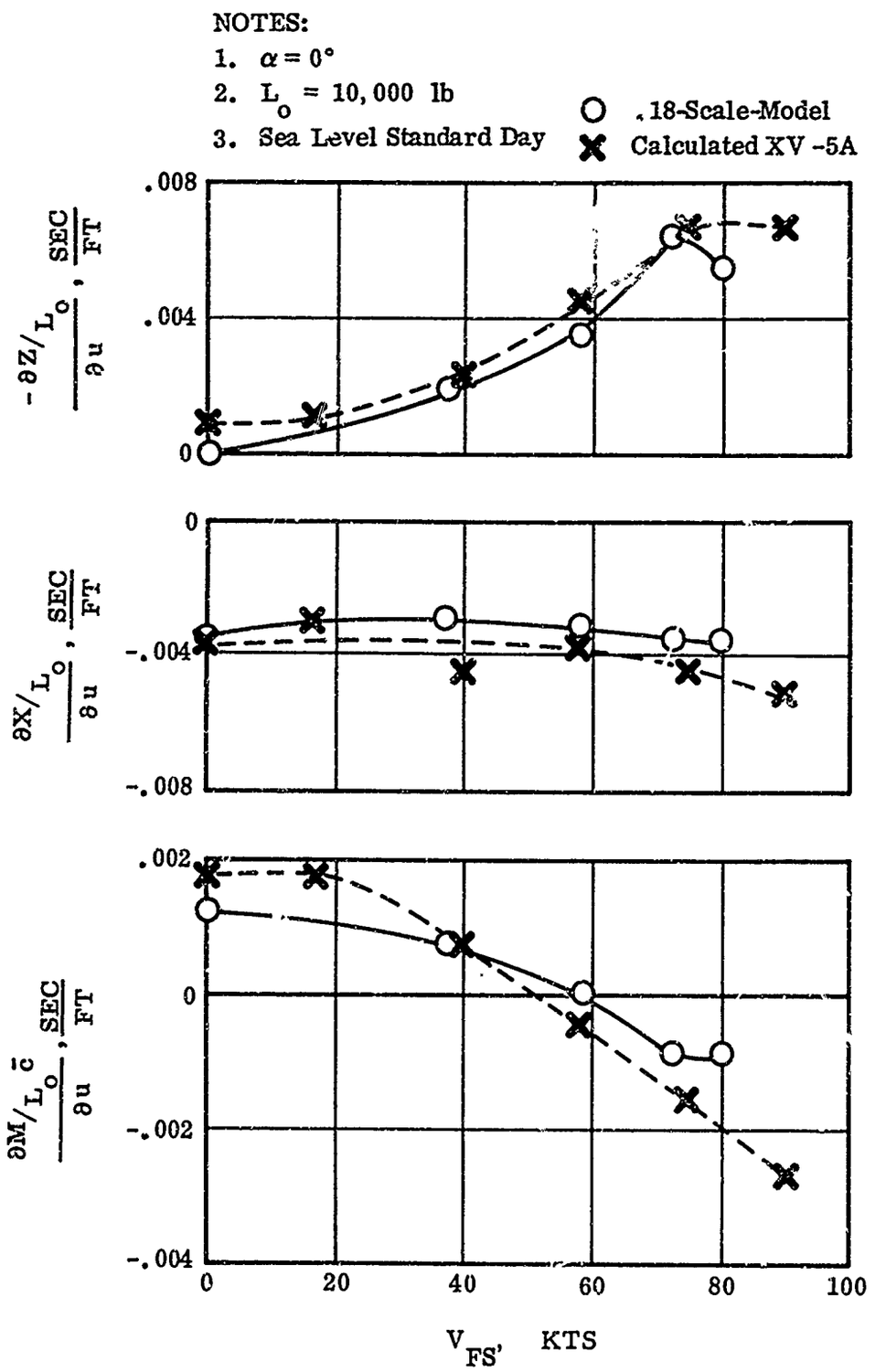

Figure 61. Comparison of Derivatives With Respect to Velocity Along the X-Axis.

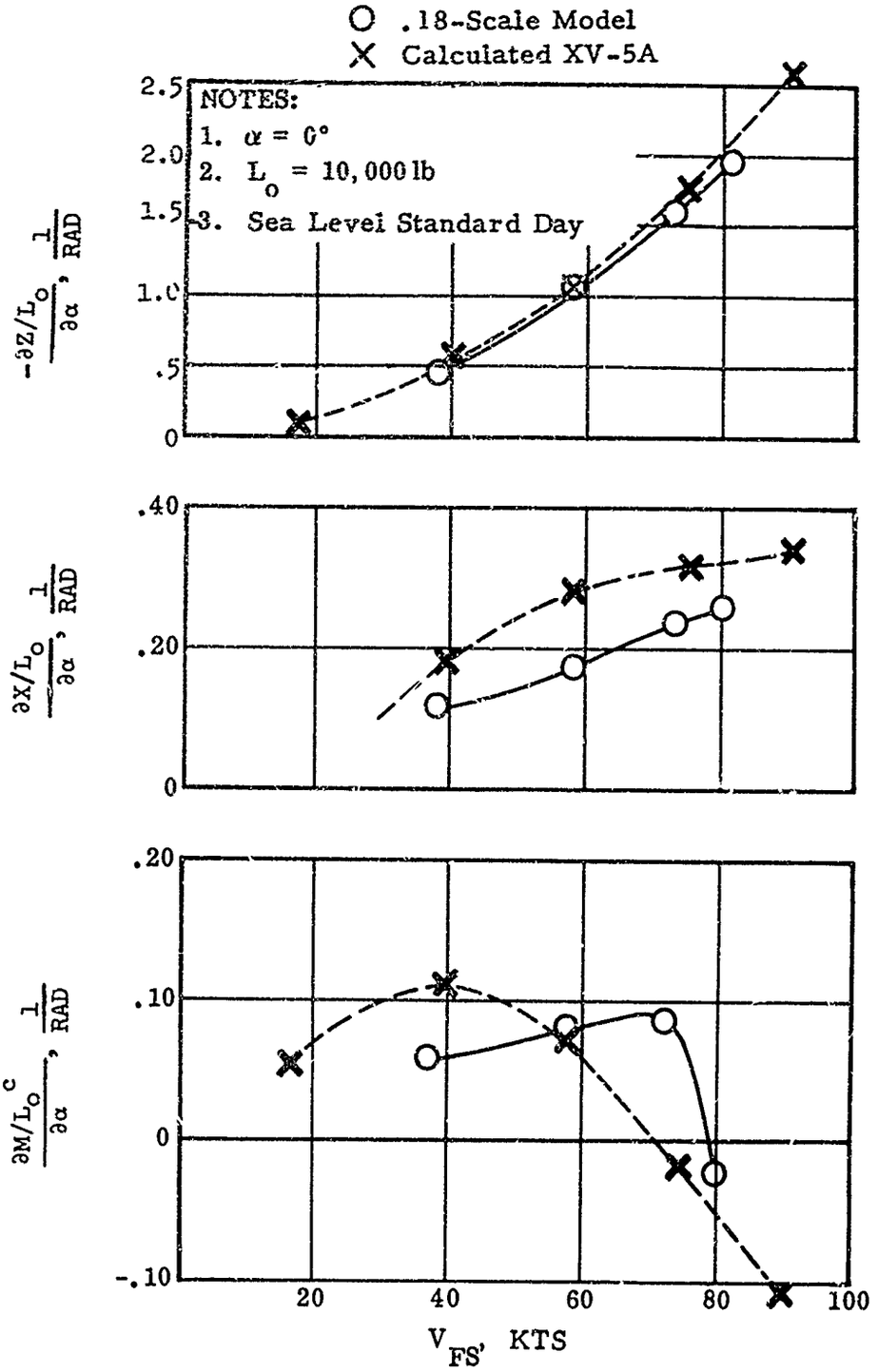

Figure 62. Comparison of Derivatives With Respect to Angle of Attack.

NOTES:

1. $\alpha = 0°$
2. $L_o = 10,000$ lb
3. Sea Level Standard Day

Model Derivatives are $\left[\frac{\partial F_{x,z}}{\partial q} + \frac{\partial F_{x,z}}{\partial \dot{\alpha}}\right] \frac{1}{L_o}$

○ .18 Scale-Model
✕ Calculated XV-5A

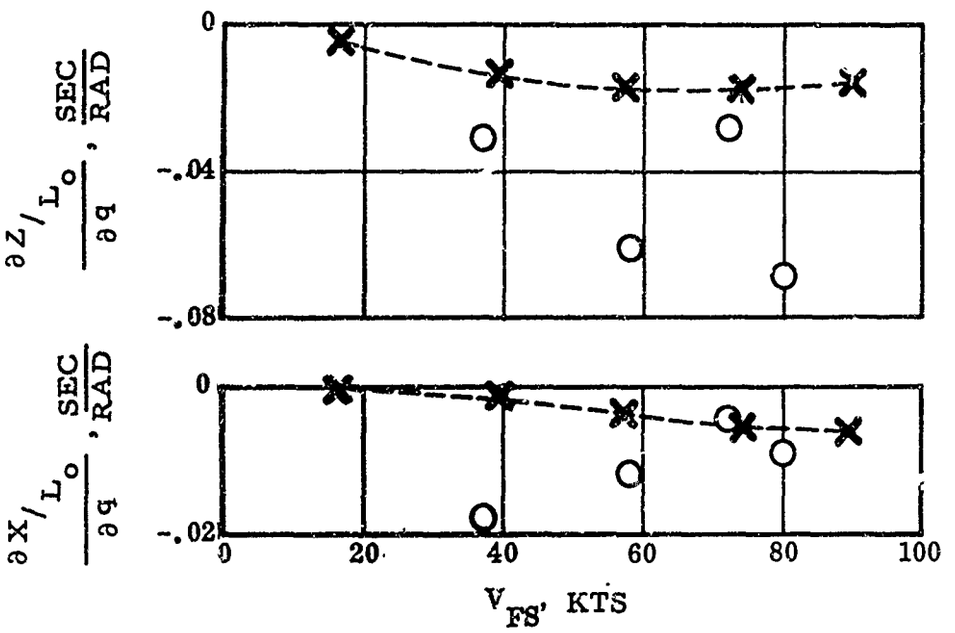

Figure 63. Comparison of Force Derivatives With Respect to Pitch Rate.

NOTES:

1. L_o = 10,000 lb
2. α = 0°
3. Sea Level Standard Day

○ .18-Scale Model

✕ Calculated XV-5A

Model Derivative is $\frac{M_q + M_{\dot{\alpha}}}{L_o \bar{c}}$

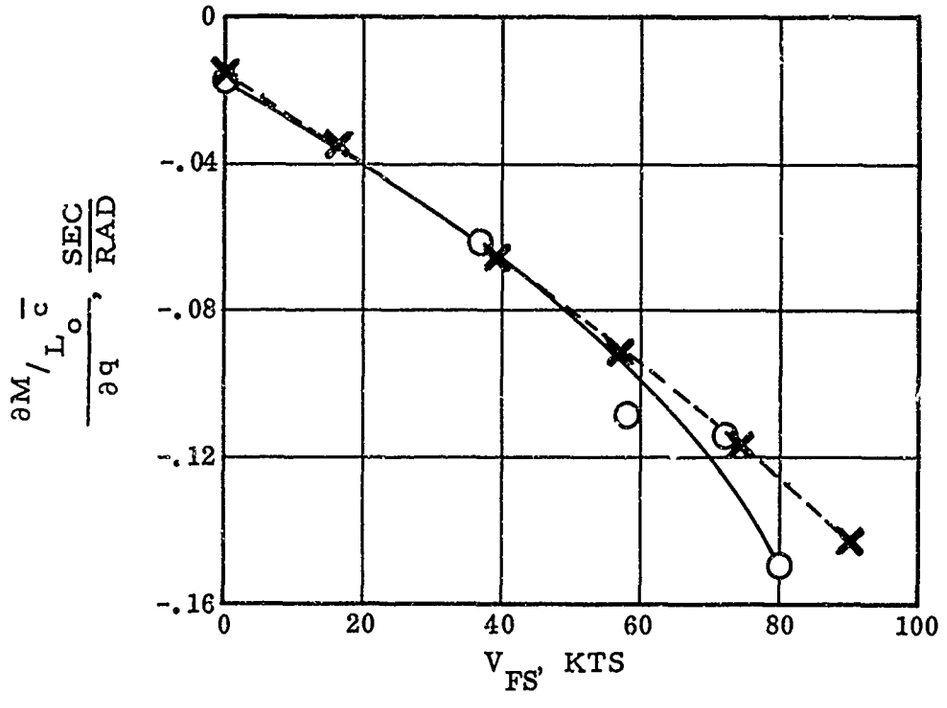

Figure 64. Comparison of Pitch Damping Derivative.

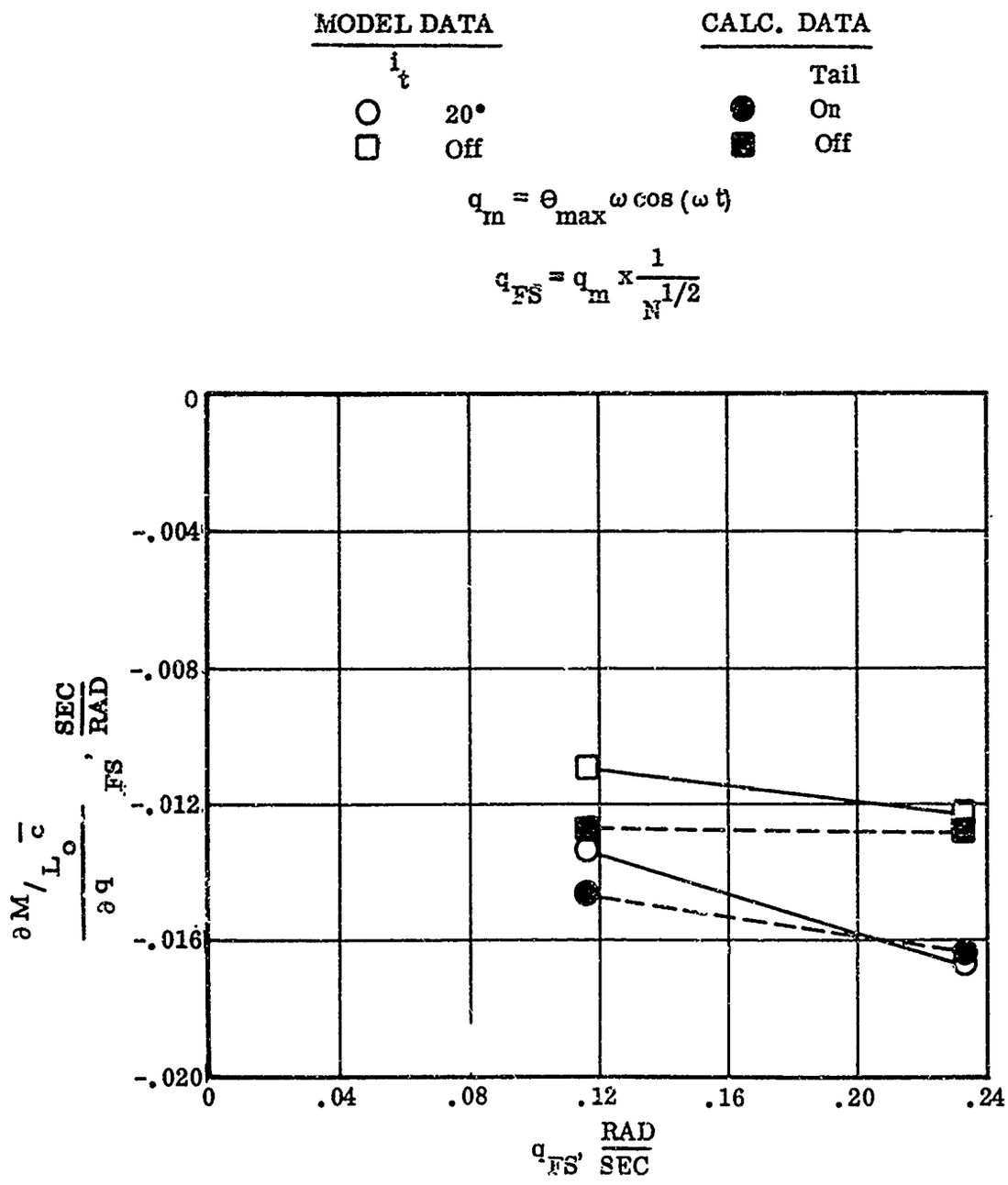

Figure 65. Comparison of Pitch Damping in Hovering Flight.

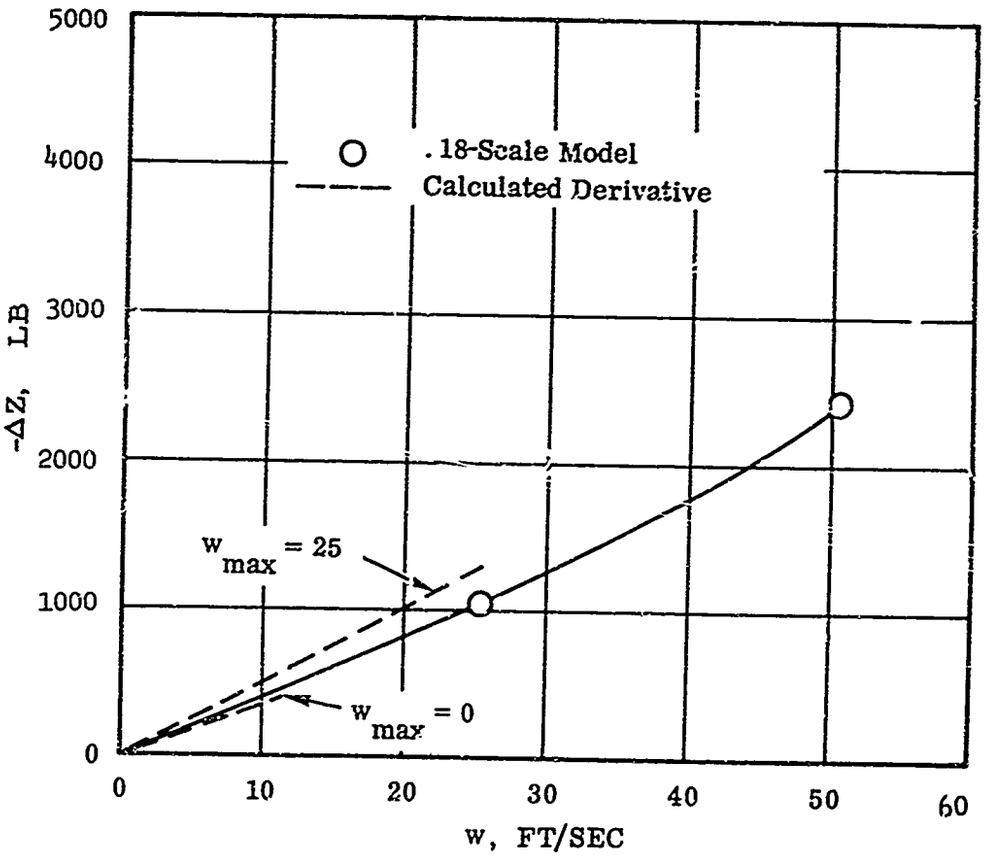

Figure 66. Comparison of Vertical Damping Forces in Hovering Flight.

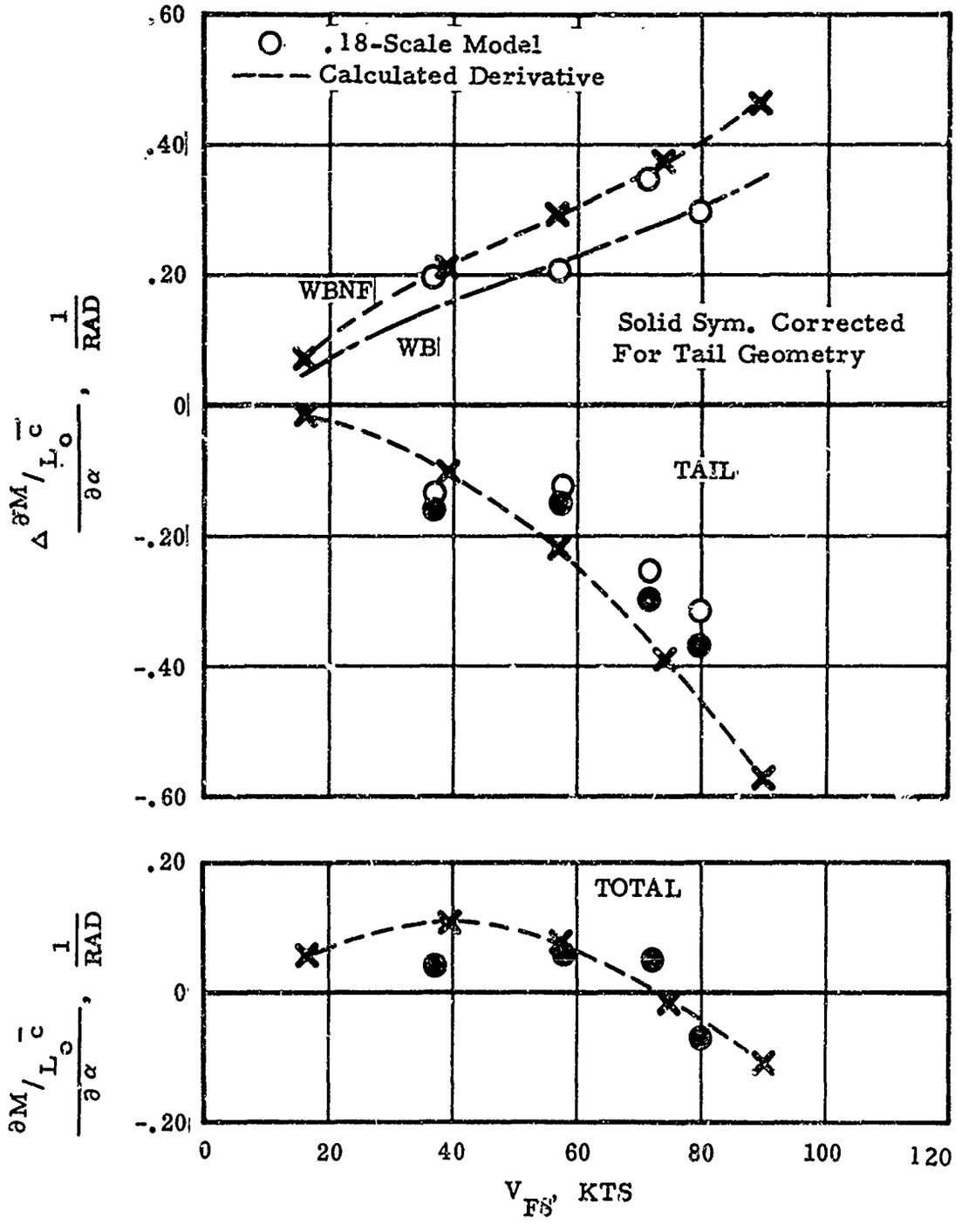

Figure 67. Comparison of M_α Derivative Components.

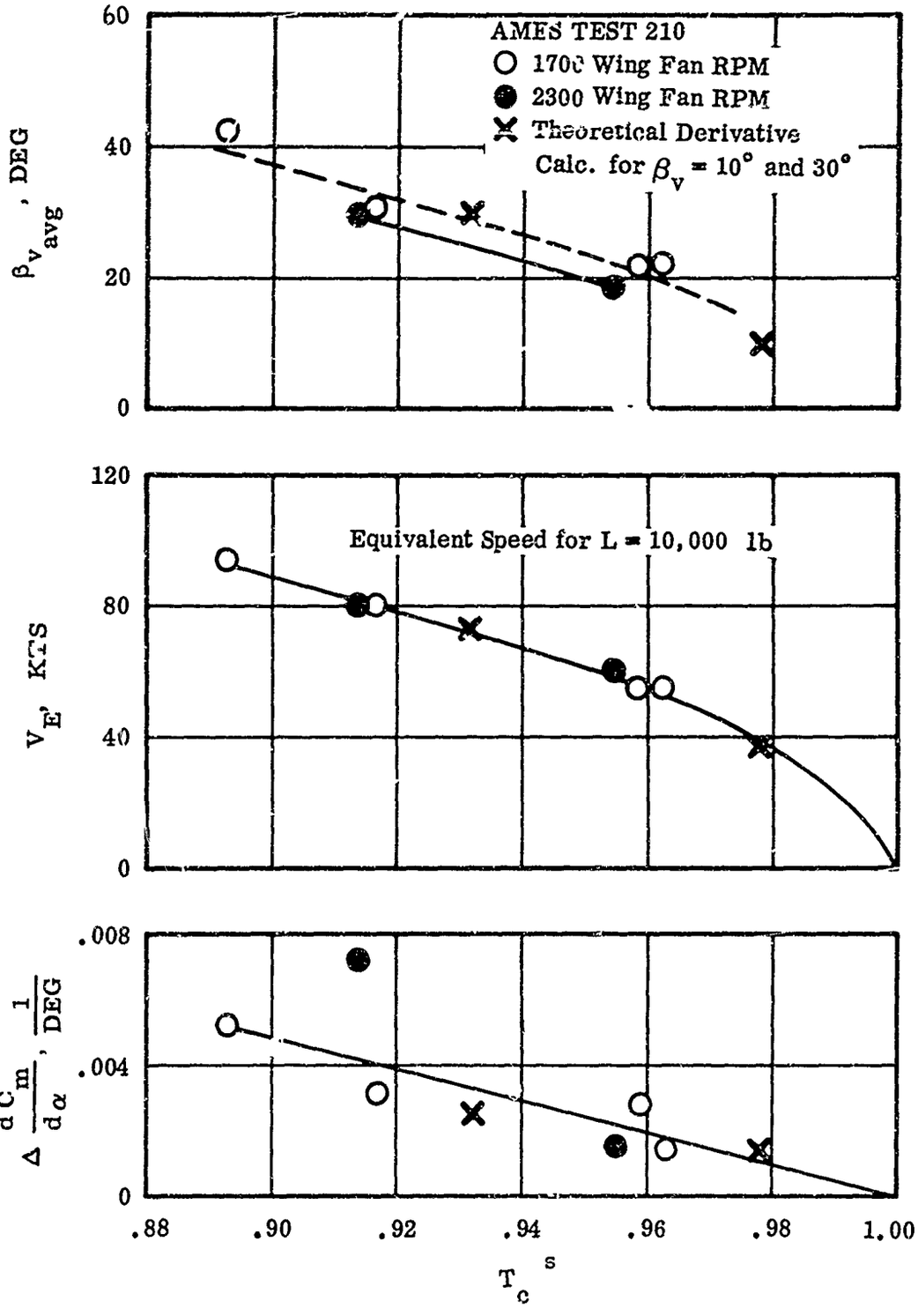

Figure 68. Comparison of Nose Fan Contribution to Stability.

$\delta_f = 45°$ $\delta_d = 15°$

.18-SCALE MODEL:

○ Power On Corrected to Full-Scale Config.
– – – Power Off Corrected to Full-Scale Config.

1/6-SCALE MODEL:

△ Test Data Power On (Wing Fans Only)
✕ Calc. Derivative
—— Power Off

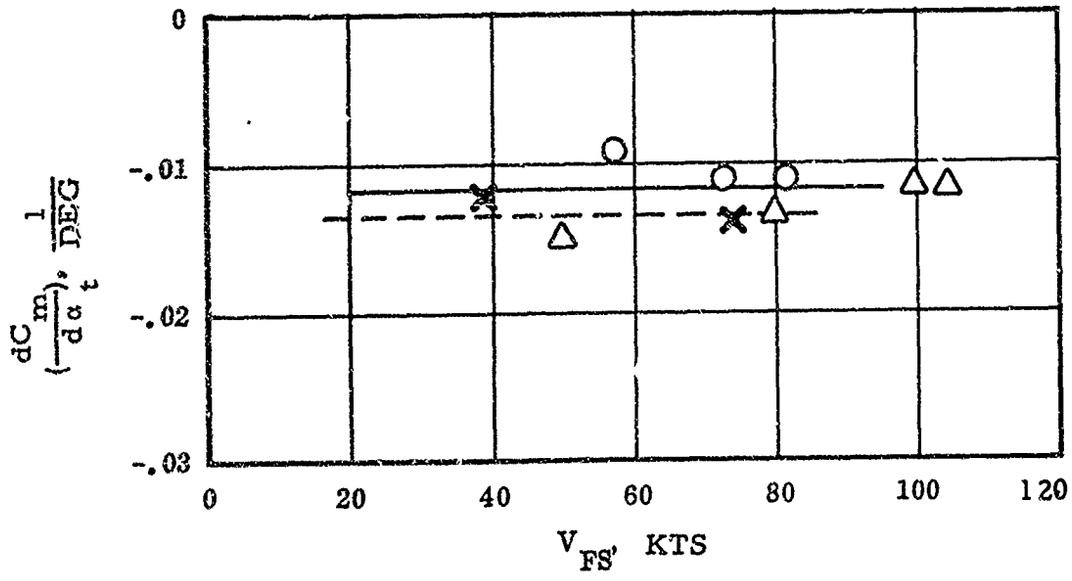

Figure 69. Comparison of Horizontal Tail Contribution to Static Stability.

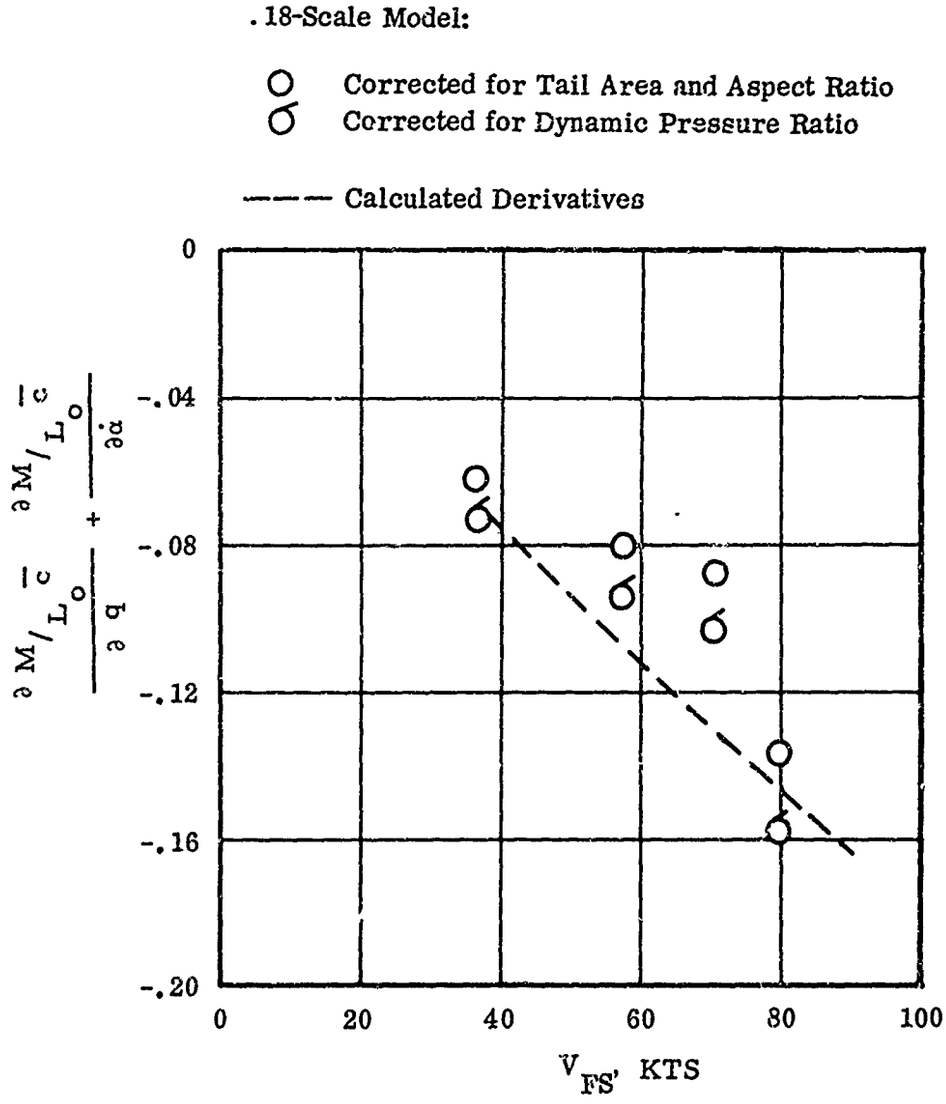

Figure 70. Comparison of Horizontal Tail Damping Derivatives.

7.0 SUMMARY OF RESULTS

1. Final correlation of 1/6-scale and Ames full-scale wing-body data was poor. The disagreement between the two sets of data generally increased with decreasing thrust coefficient (increasing flight speed).

2. Correction factors were derived to account for configuration and propulsion system differences where those differences could be identified and adequate information was available to develop the correction.

3. Correlation of the incremental effect of exit louver vector angle was good at thrust coefficients of 0.96 and 0.978 (approximately 55 and 41 knots, respectively). Correlation of the incremental drag coefficient was poor at lower thrust coefficients, while incremental lift and moment coefficients were in fairly close agreement for the 1/6-scale and Ames full-scale models.

4. Correlation of the 1/6-scale and Ames full-scale model incremental effect of exit louver stagger angle was good at a thrust coefficient of 0.96 (approximately 55 knots). Correlation at other thrust coefficients could not be made because of insufficient data.

5. Correlation of the wing-body static longitudinal stability derivative, $\partial C_m{}^s/\partial\alpha$, for the 1/6-scale and Ames full-scale model was poor at thrust coefficients below 0.96 (approximately 55 knots).

6. Correlation of horizontal tail downwash was inconclusive because of insufficient test data. The downwash angles for the 1/6-scale and Ames full-scale model were of the same order of magnitude at zero exit louver deflection.

7. Correlation of static pitch fan thrust reverser door effectiveness was not possible because of uncorrectable differences in door geometry between the 1/6-scale and Ames full-scale models and the XV-5A aircraft. In addition, the absolute door position on the Ames model could not be established.

8. The correction factors developed for data correlation generally accounted for less than half of the differences between the Ames full-scale and 1/6-scale model wing-body test data.

9. Many differences in geometry and apparent differences in wing fan characteristics existed between the 1/6-scale and full-scale models, which could not be corrected for because of complexity and insufficient experimental data.

10. Comparable configuration and test conditions for the 1/6-scale and Ames models, which would permit a direct comparison of data points, were a rare occurrence. There was only one instance in which direct comparison of angle-of-attack polars could be made.

11. The effect of vector angle was available at only one thrust coefficient for the 1/6-scale model wing-body and at only three thrust coefficients for the full-scale model for both wing-body and complete model. These were not sufficient to establish possible data scatter.

12. Correlation of wing fan power required could not be made for the 1/6-scale and full-scale fans because of different methods of power transmission from the source to the fan rotor. There was not enough information to account for the system differences.

13. A very large apparent discrepancy in 1/6-scale and full-scale wing fan power absorption led to the suspicion that the variation of actual fan thrust in crossflow may be significantly different for the two fans. Lack of measured momentum fan thrust data prevented substantiation. Actual fan momentum thrust or actual momentum jet velocity ratio must be known if it is hoped to establish nearly kinematically similar flow conditions between small-scale and full-scale fans. Static fan thrust or fan speed does not appear to be adequate unless it is known that the fans under consideration are, in fact, dynamically similar.

14. This correlation study did not yield conclusive results concerning scale effects, except that turbulence simulation would be desirable on small-scale models. The 1/6-scale model did not have turbulence simulation.

15. Application of wind tunnel wall corrections to the Ames full-scale model data did not yield clearly defined results. The wall corrections, using Hyeson's linearized theory, had little effect on drag or moment correlation. The effect on lift correlation depended upon the particular data to which the corrections were applied.

16. Simple expressions were derived in terms of the force and moment coefficients and the static stability derivatives to represent the small perturbation longitudinal static and dynamic stability derivatives for the XV-5A in transition flight.

17. Expressions were developed in terms of lift-fan mass flow from simple momentum theory to represent small perturbation longitudinal stability derivatives for hovering flight.

18. Numerical values of the hovering dimensional stability derivatives compare favorably with those in transition flight at the lowest airspeed evaluated.

19. Fair quantitative agreement was obtained between all of the calculated derivatives and test data obtained from dynamic tests of the Langley 0.18 scale-model of the XV-5A.

20. The 0.18-scale model data indicate a lower dynamic pressure ratio at the horizontal tail than the value used for the calculated derivatives, and result in smaller tail contributions to the stability derivatives for the model.

21. The reduction in dynamic pressure at the horizontal tail is probably due to the nose fan, and additional wind tunnel testing will be required with specific tests to determine the effect of nose fan operation on the flow characteristics at the tail.

8.0 CONCLUSIONS

Based on the results of this report, the following general conclusions are made regarding the correlation of wind tunnel test data of V/STOL aircraft models:

1. Correlation of wind tunnel data representing a range of wind tunnel to model size relationships can be performed meaningfully only if the data have been obtained in a consistent manner and for this particular purpose. The model configuration must be exactly the same for each series of tests. If this is not the case, much more data are needed in order to allow proper configuration corrections.

2. It is felt that knowledge of tunnel wall corrections required for testing of V/STOL configurations could best be obtained by using relatively simple models rather than models representing a flight article. For instance, a lift-fan aircraft could be represented by a wing-fuselage-tail model having two wing fans with one fixed louver setting. When the testing of such a model in various sized and shaped test sections has led to a sufficient understanding of the necessary wind tunnel corrections, then an attempt to apply these corrections to wind tunnel data for a configuration for which there is comparable flight test data may be undertaken. Quite possibly, the wind tunnel corrections will require some further modification when the attempt is made to correlate the wind tunnel data to the flight test data, but in the initial efforts there should not be confusion between wall effects and configuration effects.

3. Test section shape as well as size, must be considered in establishing suitable tunnel wall corrections and test limitations.

9.0 RECOMMENDATIONS

1. It is recommended that the effects of the tunnel to model size relationship on testing of VTOL-type aircraft be investigated with a model and a test program specifically established for that purpose. A separate program should be pursued for each basic type of vertical lift system; i.e., fan-in-wing, wing and propeller, and lift jet.

2. Wind tunnel cross section shape and proportions, as well as size, are variables which should be investigated.

3. The model designed for a data correlation study should be as simple as is consistent with the configuration being tested.

4. Some form of flow visualization should be employed to understand better the mechanisms of tunnel interferences and to determine the testing limitations they impose.

5. Since an aircraft configuration always undergoes considerable evolution during the design process, it follows that a wind tunnel model tested early in a design program invariably does not represent the configuration of the flight article. If adequate understanding of the configuration effects exists, the early data may be modified so as to be useful throughout the program. Unfortunately, this knowledge does not exist for fan-in-wing-type aircraft. It is needed not only to predict the effects of design changes but also for preliminary design purposes so that existing data can be used to predict the characteristics of new designs. It is therefore recommended that a test program be initiated to evaluate configuration effects for the fan-in-wing-type aircraft. Typical of the parameters that should be investigated are:

   Fan Area to Wing Area Ratio

   Fan Diameter to Wing Chord Ratio

   Fan Hub to Fan Diameter Ratio

   Total Mass Flow to Turbine Mass Flow Ratio
   (Tip-Turbine Fans)

   Wing Flap Geometry

10.0 LIST OF REFERENCES

References

1 Chambers, Joseph R., and Grafton, Sue B.: Static and Dynamic Longitudinal Stability Derivatives of a Powered 0.18-Scale Model of a Fan-in-Wing VTOL Aircraft; NASA LWP-258, August 5, 1966 (Limited distribution).

2 Anon: Lift Fan Flight Research Aircraft Program, X353-5B Propulsion System Specification; General Electric Specification No. 112, January 15, 1962.

3 Anon: Lift Fan Flight Research Aircraft Program, X376 Pitch Fan Specification; General Electric Specification No. 113, March 1, 1962.

4 Davis, W.B., and Mendenhall, D.C.: Detail Aircraft Specification XV-5A Flight Research Aircraft; Ryan Report No. 62B125A, December 30, 1964.

5 Davis, Walter B.: Procedures for Correlation of the Aerodynamic Characteristics of V/STOL Aircraft; Presented at the IAS National Meeting on the "Future of Manned Military Aircraft" in San Diego, California, August 1-3 1960.

6 James, H.A.: Estimate of Forces and Moments Due to Ducted Fans in Cross Flow at Various Tilt and Vector Angles and with Wings; Ryan Report No. 65B008A, August 23, 1966.

7 Heyson, Harry H.: Linearized Theory of Wind-Tunnel Jet-Boundary Corrections and Ground Effect for VTOL-STOL Aircraft; NASA TR R-124, 1962.

8 Reynolds, H.A.: Additional Low Speed Wind Tunnel Tests of a 1/6-Scale Powered Model of the Ryan Model 173 Airplane to Investigate Static Performance and Low Speed Aerodynamic Characteristics at a Variety of Model Attitudes and Test Conditions; General Dynamics/Convair Report CVAL 344A, July 15, 1963.

9 Ela, B.W.: Calculated Installed Power Plant Performance for U.S. Army XV-5A Lift Fan Research Aircraft; Ryan Report No. 64B015, August 10, 1964.

10.0 LIST OF REFERENCES - Continued

References

10 Parks, W.C., and Schattschneider, D.G.: Wind Tunnel Test Report, One-Sixth Scale Powered Lift-Fan Model, U.S. Army XV-5A Lift-Fan Research Aircraft; Ryan Report No. 63B092, September 11, 1963.

11 Smith, E.G.: Summary of XV-5A (VZ-11) Aerodynamic Performance Obtained During Ames Tests - July 1962; General Electric Memorandum, December 14, 1962.

12 Kirk, Jerry V., Hickey, David H., and Hall, Leo P.: Aerodynamic Characteristics of a Full-Scale Fan-in-Wing Model Including Results in Ground Effect with Nose-Fan Pitch Control; NASA TN D-2368, 1964.

13 Rae, William H., Jr.: An Experimental Investigation of the Effect of Test Section Geometry on the Maximum Size Rotor That Can Be Tested in a Closed Throat Wind Tunnel; AIAA Paper No. 66-736, September 21-23, 1966.

14 XV-5A Stability and Control Group: Estimated Static Stability and Control Characteristics of the U.S. Army XV-5A Lift Fan Research Aircraft; Ryan Report No. 64B031, March 6, 1964.

15 Technical Sciences Section (Aircraft): XV-5A Flight Test Data Reduction Procedures; Ryan Report No. 29745-3, June 30, 1966.

16 Anon: Fundamentals of Design of Piloted Aircraft Flight Control Systems, Vol. II, Dynamics of the Airframe; BuAer Report AE-61-4, February 1953.

17 Advanced Engine and Technology Department: Full-Scale Wind Tunnel Test Report, XV-5A Lift Fan Flight Research Aircraft; General Electric Co. Report No. 153, December 1964.

18 Goldsmith, Robert H., and Hickey, Davis H.: Characteristics of Aircraft with Lifting Fan Propulsion Systems for V/STOL; IAS Paper 63-27, 1963.

19 Heyson, Harry H.: Wings, Wakes, Wind Tunnels, and Wall Effects, NASA LWP-341, December 15, 1966.

20 Correlation of Wind-Tunnel and Flight-Test Data for V/STOL Aircraft; NASA LWP-348, January 9, 1967.

10.0 LIST OF REFERENCES - Continued

References

21 Pope, Alan, and Harper, John J.: Low Speed Wind Tunnel Testing, John Wiley and Sons, New York, 1966, pp.175-183, 309-326, 386-389.

22 Kirkpatrick, David L.I.,: Wind Tunnel Corrections for V/STOL Model Testing; M.A.E. Thesis, University of Virginia, August 1962.

23 Black, E.L., and Brownrigg, W.E.: Factors Affecting the Correlation of V/STOL Wind Tunnel Data Obtained From Several Test Facilities; AIAA Paper No. 66-737, September 21-23, 1966.

24 Davenport, Edwin E., and Kuhn, Richard E.: Wind-Tunnel-Wall Effects and Scale Effects on a VTOL Configuration With a Fan Mounted in the Fuselage; NASA TN D-2560, January 1965.

25 Cook, Woodrow L., and Hickey, David H.: Comparison of Wind-Tunnel and Flight-Test Aerodynamic Data in the Transition-Flight Speed Range for Five V/STOL Aircraft; Paper No. 26, NASA SP-116, 1966, pp.447-467.

26 Goodson, Kenneth W.: Comparison of Wind Tunnel and Flight Results on a Four-Propeller Tilt-Wing Configuration; Paper No. 5, NASA SP-116, 1966, pp.51-62.

27 Grunwald, Kalman J.: Experimental Study of Wall Effects and Wall Corrections for a General Research Tilt-Wing Model with Flap; NASA TN D-2887, 1965.

28 Ganzer, Victor M., and Rae, William H., Jr.: An Experimental Investigation of the Effect of Wind-Tunnel Walls on the Aerodynamic Performance of a Helicopter Rotor; NASA TN D-415, 1960.

29 Kuhn, Richard E., and Naeseth, Rodger L.: Tunnel-Wall Effects Associated with VTOL-STOL Model Testing; AGARD Report 303, 1959.

30 Heyson, Harry H.: "Wind-Tunnel Wall Interference and Ground Effect for VTOL-STOL Aircraft;"J. Am. Helicopter Society, Vol. 6, No. 1, January 1961, pp.1-9.

10.0 LIST OF REFERENCES - Continued

References

31 Heyson, Harry H.: Nomographic Solution of the Momentum Equation for VTOL-STOL Aircraft; NASA TN D-814, 1961. (Also available as V/STOL Momentum Equations, Space/Aeron., Vol. 38, No. 2, July 1962, pp.B-18 to B-20.)

32 Heyson, Harry H., and Grunwald, Kalman J.: Wind-Tunnel Boundary Interference for V/STOL Testing; Paper No. 24, NASA SP-116, 1966, pp.409-434.

33 Heyson, Harry H.: Equations for the Application of Wind-Tunnel Wall Corrections to Pitching Moments Caused by the Tail of an Aircraft Model; NASA TN D-3738, November 1966.

34 Heyson, Harry H.: Tables of Interference Factors for Use in Wind-Tunnel and Ground Effect Calculations for VTOL-STOL Aircraft; Part I - Wind Tunnel Having Width-Height Ratio of 2.0; NASA TN D-933, 1962.

35 Heyson, Harry H.: Tables of Interference Factors for Use in Wind-Tunnel and Ground Effect Calculations for VTOL-STOL Aircraft; Part II - Wind Tunnels Having Width-Height Ratio of 1.5; NASA TN D-934, 1962.

36 Priestley, R.T.: Estimated Performance Characteristics U.S. Army XV-5A Lift-Fan Research Aircraft; Ryan Report No. 64B058, April 24, 1964.

37 Kirby, Robert H., and Chambers, Joseph R.: Flight Investigation of Dynamic Stability and Control Characteristics of a 0.18-Scale Model of a Fan-in-Wing VTOL Airplane; NASA TN D-3412, August 1966.

APPENDIX I
DERIVATION OF DIMENSIONAL LONGITUDINAL STABILITY DERIVATIVES

CONTRIBUTIONS OF THE HORIZONTAL TAIL

The horizontal tail is considered as an isolated surface affected by the free stream at the tail, and the derivatives are of the same form as the conventional aerodynamic expressions of Ref.16. However, due to the choice of axes system and to the high downwash angles, the tail lift and drag force must be resolved through the angle $(\alpha_w - \epsilon)$.

VARIATION OF THE TAIL NORMAL FORCE WITH VELOCITY ALONG THE X-AXIS, $\frac{\partial N_t}{\partial u}$

The tail normal force is expressed by

$$N_t = C_{N_t} \rho/2 \; V_T^2 \eta_t \; S_t \tag{27}$$

Differentiating with respect to velocity, u,

$$\frac{\partial N_t}{\partial u} = \eta_t S_t \; C_{N_t} \rho/2 \frac{\partial V_T^2}{\partial u} + \eta_t S_t \; \rho/2 \; V_T^2 \frac{\partial C_{N_t}}{\partial u} \tag{28}$$

The total velocity along the flight path may be written as

$$V_T = \sqrt{U_o^2 + 2 U_o u + u^2 + W^2} \tag{29}$$

$$V_T^2 = U_o^2 + 2 U_o u + u^2 + W^2$$

Taking the partial derivative with respect to u,

$$\frac{\partial V_T^2}{\partial u} = 2U_o + 2u = 2 (U_o + u) = 2U \tag{30}$$

From geometry of angles,

$$C_{N_t} = C_{L_t} \cos(\alpha_w - \epsilon) + C_{D_t} \sin(\alpha_w - \epsilon) \tag{31}$$

Differentiating with respect to u,

$$\frac{\partial C_{N_t}}{\partial u} = C_{L_t} \frac{\partial \cos(\alpha_w - \epsilon)}{\partial u} + \cos(\alpha_w - \epsilon) \frac{\partial C_{L_t}}{\partial u} + C_{D_t} \frac{\partial \sin(\alpha_w - \epsilon)}{\partial u} + \sin(\alpha_w - \epsilon) \frac{\partial C_{D_t}}{\partial u} \tag{32}$$

The terms of this equation may be developed as follows:

(1) $$\frac{\partial \cos(\alpha_w - \epsilon)}{\partial u} = -\sin(\alpha_w - \epsilon) \frac{\partial(\alpha_w - \epsilon)}{\partial u} = -\sin(\alpha_w - \epsilon) \left[\frac{\partial \alpha_w}{\partial u} - \frac{\partial \epsilon}{\partial u}\right]$$

(2) $$\frac{\partial C_{L_t}}{\partial u} = \frac{\partial C_{L_t}}{\partial \alpha_t} \frac{\partial \alpha_t}{\partial u}$$

where $\alpha_t = \alpha_w + i_t - \epsilon$

and $$\frac{\partial \alpha_t}{\partial u} = \frac{\partial \alpha_w}{\partial u} - \frac{\partial \epsilon}{\partial u} = \frac{\partial \alpha_w}{\partial u} - \frac{\partial \epsilon}{\partial \alpha_w} \frac{\partial \alpha_w}{\partial u} = \frac{\partial \alpha_w}{\partial u} \left(1 - \frac{\partial \epsilon}{\partial \alpha_w}\right)$$

$$\therefore \quad \frac{\partial C_{L_t}}{\partial u} = \frac{\partial C_{L_t}}{\partial \alpha_t} \frac{\partial \alpha_w}{\partial u} \left(1 - \frac{\partial \epsilon}{\partial \alpha}\right)$$

(3) $$\frac{\partial \sin(\alpha_w - \epsilon)}{\partial u} = \cos(\alpha_w - \epsilon) \frac{\partial(\alpha_w - \epsilon)}{\partial u}$$

(4) $$\frac{\partial C_{D_t}}{\partial u} = \frac{\partial C_{D_t}}{\partial \alpha_t} \frac{\partial \alpha_t}{\partial u} = \frac{\partial C_{D_t}}{\partial \alpha_t} \frac{\partial \alpha_w}{\partial u} \left(1 - \frac{\partial \epsilon}{\partial \alpha}\right)$$

Common to all terms is the partial of α_w with respect to velocity u, which can be written as

$$\frac{\partial \alpha_w}{\partial u} = \frac{-\sin \alpha_w}{V_T}$$

Substituting and collecting terms,

$$\frac{\partial C_{N_t}}{\partial u} = C_{L_t} \sin(\alpha_w - \epsilon) \frac{\sin\alpha_w}{V_T}\left(1 - \frac{\partial\epsilon}{\partial\alpha}\right) - \cos(\alpha_w - \epsilon) \frac{\partial C_{L_t}}{\partial \alpha_t}\left(1 - \frac{\partial\epsilon}{\partial\alpha}\right) \frac{\sin\alpha_w}{V_T}$$

$$- C_{D_t} \cos(\alpha_w - \epsilon)\left(1 - \frac{\partial\epsilon}{\partial\alpha}\right) \frac{\sin\alpha_w}{V_T} - \sin(\alpha_w - \epsilon) \frac{\partial C_{D_t}}{\partial \alpha_t}\left(1 - \frac{\partial\epsilon}{\partial\alpha}\right) \frac{\sin\alpha_w}{V_T} \quad (33)$$

Eliminating the product of sine terms,

$$\frac{\partial C_{N_t}}{\partial u} = - \frac{\partial C_{L_t}}{\partial \alpha_t}\left(1 - \frac{\partial\epsilon}{\partial\alpha}\right) \cos(\alpha_w - \epsilon) \frac{\sin\alpha_w}{V_T}$$

$$- C_{D_t}\left(1 - \frac{\partial\epsilon}{\partial\alpha}\right) \cos(\alpha_w - \epsilon) \frac{\sin\alpha_w}{V_T} \quad (34)$$

Substituting Equations (30), (31), and (34) into Equation (28),

$$\frac{\partial N_t}{\partial u} = \eta_t S_t \rho U \left[C_{L_t} \cos(\alpha_w - \epsilon) + C_{D_t} \sin(\alpha_w - \epsilon)\right]$$

$$+ \eta_t S_t \rho/2 V_T^2 \left[- \frac{\partial C_{L_t}}{\partial \alpha_t} - C_{D_t}\right]\left(1 - \frac{\partial\epsilon}{\partial\alpha}\right)\cos(\alpha_w - \epsilon) \frac{\sin\alpha_w}{V_T}$$

$$\frac{\partial N_t}{\partial u} = \eta_t S_t \rho U \left[C_{L_t} \cos(\alpha_w - \epsilon) + C_{D_t} \sin(\alpha_w - \epsilon)\right]$$

$$+ \eta_t S_t \rho/2 V_T\left(1 - \frac{\partial\epsilon}{\partial\alpha}\right) \sin\alpha_w \cos(\alpha_w - \epsilon) \left[- \frac{\partial C_{L_t}}{\partial \alpha_t} - C_{D_t}\right] \quad (35)$$

This equation can be further simplified but is left in this form for convenience. If the angle of attack is zero or the small angle assumption is made so that $\sin\alpha_w = 0$, the second term disappears.

VARIATION OF THE TAIL LONGITUDINAL FORCE WITH VELOCITY ALONG THE X-AXIS, $\frac{\partial X_t}{\partial u}$

The tail longitudinal force is expressed by

$$X_t = C_{x_t} \rho/2 \, V_T^2 \, \eta_t \, S_t \tag{36}$$

and the partial with respect to u is

$$\frac{\partial X_t}{\partial u} = C_{x_t} \eta_t S_t \rho/2 \frac{\partial V_T^2}{\partial u} + \eta_t S_t \rho/2 V_T^2 \frac{\partial C_{x_t}}{\partial u} \tag{37}$$

Also,

$$C_{x_t} = C_{L_t} \sin(\alpha_w - \epsilon) - C_{D_t} \cos(\alpha_w - \epsilon) \tag{38}$$

Performing operations similar to those done for the tail normal force, the following expression is obtained for the partial of longitudinal force coefficient with velocity.

$$\frac{\partial C_{x_t}}{\partial u} = C_{L_t} \left(1 - \frac{\partial \epsilon}{\partial \alpha}\right) \cos(\alpha_w - \epsilon) \left(\frac{-\sin\alpha_w}{V_T}\right) - \cos(\alpha_w - \epsilon) \cdot \frac{\partial C_{D_t}}{\partial \alpha_t} \left(1 - \frac{\partial \epsilon}{\partial \alpha}\right) \left(\frac{-\sin\alpha_w}{V_T}\right) \tag{39}$$

The variation of tail drag coefficient with tail angle of attack may be eliminated as follows:

$$\frac{\partial C_{D_t}}{\partial \alpha_t} = \frac{\partial C_{D_t}}{\partial C_{L_t}} \frac{\partial C_{L_t}}{\partial \alpha_t}$$

From $C_{D_t} = C_{D_{O_T}} + K_i C_{L_t}^2$

$$\frac{\partial C_{D_t}}{\partial C_{L_t}} = 2K_i C_{L_t}$$

$$\therefore \frac{\partial C_{D_t}}{\partial \alpha_t} = 2K_i C_{L_t} \frac{\partial C_{L_t}}{\partial \alpha_t}$$

Substituting in Equation (39) and rearranging,

$$\frac{\partial C_{x_t}}{\partial u} = \cos(\alpha_w - \epsilon)\frac{\sin\alpha_w}{V_T}\left(1 - \frac{\partial \epsilon}{\partial \alpha}\right)\left[-C_{L_t} + 2K_i C_{L_t}\frac{\partial C_{L_t}}{\partial \alpha_t}\right]$$

$$= \cos(\alpha_w - \epsilon)\frac{\sin\alpha_w}{V_T}\left(1 - \frac{\partial \epsilon}{\partial \alpha}\right) C_{L_t}\left[2K_i \frac{\partial C_{L_t}}{\partial \alpha_t} - 1\right] \tag{40}$$

Substituting Equations (30), (38), and (40) into Equation (37),

$$\frac{\partial \dot{X}_t}{\partial u} = \eta_t S_t \rho U\left[C_{L_t}\sin(\alpha_w - \epsilon) - C_{D_t}\cos(\alpha_w - \epsilon)\right]$$

$$+ \eta_t S_t \rho/2 V_T \cos(\alpha_w - \epsilon)\sin\alpha_w\left(1 - \frac{\partial \epsilon}{\partial \alpha}\right) C_{L_t}\left[2K_i \frac{\partial C_{L_t}}{\partial \alpha_t} - 1\right] \tag{41}$$

Again, the second term may be neglected if the small angle assumption is made for $\sin\alpha_w$.

VARIATION OF THE TAIL PITCHING MOMENT WITH VELOCITY

ALONG THE X-AXIS, $\frac{\partial M_t}{\partial u}$

The tail pitching moment derivative with respect to u is readily obtained from the moment equation about the aircraft c.g.

$$M_t = -N_t \ell_t + X_t z_t \tag{42}$$

$$\frac{\partial M_t}{\partial u} = -\ell_t \frac{\partial N_t}{\partial u} + z_t \frac{\partial X_t}{\partial u} \tag{43}$$

VARIATION OF THE TAIL NORMAL FORCE WITH VELOCITY ALONG THE Z-AXIS, $\frac{\partial N_t}{\partial w}$

Using Equations (27) and (31), the tail normal force may be written as

$$N_t = \rho/2\ V_T^2\ \eta_t\ S_t \left[C_{L_t} \cos(\alpha_w - \epsilon) + C_{D_t} \sin(\alpha_w - \epsilon)\right] \tag{44}$$

Taking the partial derivative with respect to velocity w and assuming that w is small with respect to U,

$$\frac{\partial N_t}{\partial w} = \rho/2\ V_T^2\ \eta_t\ S_t \left[\frac{\partial C_{L_t}}{\partial w} \cos(\alpha_w - \epsilon) + C_{L_t} \frac{\partial \cos(\alpha_w - \epsilon)}{\partial w} + \frac{\partial C_{D_t}}{\partial w} \sin(\alpha_w - \epsilon) + C_{D_t} \frac{\partial \sin(\alpha_w - \epsilon)}{\partial w}\right] \tag{45}$$

The partial derivatives in this expression may be evaluated as follows:

(1) $$\frac{\partial C_{L_t}}{\partial w} = \frac{\partial C_{L_t}}{\partial \alpha_w} \frac{\partial \alpha_w}{\partial w}$$

For small angles, $\sin\alpha_w = \alpha_w = \frac{w}{U}$

$$\frac{\partial \alpha_w}{\partial w} = \frac{1}{U}$$

$$\therefore \quad \frac{\partial C_{L_t}}{\partial w} = \frac{\partial C_{L_t}}{\partial \alpha_w} \frac{1}{U} = \frac{\partial C_{L_t}}{\partial \alpha_t} \left(1 - \frac{d\epsilon}{d\alpha}\right) \frac{1}{U}$$

(2) $$\frac{\partial \cos(\alpha_w - \epsilon)}{\partial w} = \frac{\partial \cos(\alpha_w - \epsilon)}{\partial \alpha_w} \frac{\partial \alpha_w}{\partial w} = -\sin(\alpha_w - \epsilon) \frac{\partial(\alpha_w - \epsilon)}{\partial \alpha_w} \frac{1}{U}$$

$$= -\sin \frac{(\alpha_w - \epsilon)\left(1 - \frac{d\epsilon}{d\alpha}\right)}{U}$$

$$(3)\quad \frac{\partial C_{D_t}}{\partial w} = \frac{\partial C_{D_t}}{\partial \alpha_w}\frac{\partial \alpha_w}{\partial w} = \frac{\partial C_{D_t}}{\partial \alpha_w}\frac{1}{U} = \frac{\partial C_{D_t}}{\partial \alpha_t}\left(1-\frac{d\epsilon}{d\alpha}\right)\frac{1}{U}$$

$$(4)\quad \frac{\partial \sin(\alpha_w-\epsilon)}{\partial w} = \frac{\partial \sin(\alpha_w-\epsilon)}{\partial \alpha_w}\frac{\partial \alpha_w}{\partial w} = \cos(\alpha_w-\epsilon)\left(1-\frac{d\epsilon}{d\alpha}\right)\frac{1}{U}$$

Replacing the tail drag variation with tail angle of attack by $2K_iC_{L_t}\frac{\partial C_{L_t}}{\partial \alpha_t}$ and substituting terms (1) through (4) into Equation (45),

$$\frac{\partial N_t}{\partial w} = \rho/2\, V_T^2\, \eta_t S_t \left\{ \frac{\partial C_{L_t}}{\partial \alpha_t}\left(1-\frac{d\epsilon}{d\alpha}\right)\frac{1}{U}\cos(\alpha_w-\epsilon) - C_{L_t}\sin(\alpha_w-\epsilon)\left(1-\frac{d\epsilon}{d\alpha}\right)\frac{1}{U} \right.$$
$$\left. + 2K_iC_{L_t}\frac{\partial C_{L_t}}{\partial \alpha_t}\left(1-\frac{d\epsilon}{d\alpha}\right)\frac{1}{U}\sin(\alpha_w-\epsilon) + C_{D_t}\cos(\alpha_w-\epsilon)\left(1-\frac{d\epsilon}{d\alpha}\right)\frac{1}{U} \right\} \qquad (46)$$

If the assumption is made that $V_T = U$, this equation reduces to

$$\frac{\partial N_t}{\partial w} = \rho/2\, V_T \eta_t S_t \left(1-\frac{d\epsilon}{d\alpha}\right)\left\{ \left[\frac{\partial C_{L_t}}{\partial \alpha_t} + C_{D_t}\right]\cos(\alpha_w-\epsilon) \right.$$
$$\left. + C_{L_t}\sin(\alpha_w-\epsilon)\left[2K_i\frac{C_{L_t}}{\partial \alpha_t} - 1\right] \right\} \qquad (47)$$

VARIATION OF THE TAIL LONGITUDINAL FORCE WITH VELOCITY ALONG THE Z-AXIS, $\frac{\partial X_t}{\partial w}$

The tail longitudinal force may be expressed by

$$X_t = \rho/2\ V_T^2\ \eta_t S_t \left[C_{L_t} \sin(\alpha_w - \epsilon) - C_{D_t} \cos(\alpha_w - \epsilon)\right] \tag{48}$$

Taking the partial derivative with respect to velocity w,

$$\frac{\partial X_t}{\partial w} = \rho/2\ V_T^2\ \eta_t S_t \left[C_{L_t} \frac{\partial \sin(\alpha_w - \epsilon)}{\partial w} + \frac{\partial C_{L_t}}{\partial w} \sin(\alpha_w - \epsilon) - C_{D_t} \frac{\partial \cos(\alpha_w - \epsilon)}{\partial w} - \frac{\partial C_{D_t}}{\partial w} \cos(\alpha_w - \epsilon)\right] \tag{49}$$

This expression is seen to contain the same partial derivatives as the equation for tail normal force variation with w. Making the same substitutions results in

$$\frac{\partial X_t}{\partial w} = \rho/2\ V_T^2\ \eta_t S_t \left[C_{L_t}\left(1 - \frac{d\epsilon}{d\alpha}\right) \cos(\alpha_w - \epsilon)\ \frac{1}{U} + \frac{\partial C_{L_t}}{\partial \alpha_t}\left(1 - \frac{d\epsilon}{d\alpha}\right) \frac{1}{U} \sin(\alpha_w - \epsilon) + C_{D_t}\left(1 - \frac{d\epsilon}{d\alpha}\right) \sin(\alpha_w - \epsilon)\ \frac{1}{U} - 2K_i C_{L_t} \frac{\partial C_{L_t}}{\partial \alpha_t}\left(1 - \frac{d\epsilon}{d\alpha}\right) \frac{1}{U} \cos(\alpha_w - \epsilon)\right] \tag{50}$$

Collecting terms and rearranging, this reduces to

$$\frac{\partial X_t}{\partial w} = \rho/2\ V_T\ \eta_t S_t \left(1 - \frac{d\epsilon}{d\alpha}\right) \left\{ C_{L_t}\left[1 - 2K_i \frac{\partial C_{L_t}}{\partial \alpha_t}\right] \cos(\alpha_w - \epsilon) + \left[\frac{\partial C_{L_t}}{\partial \alpha_t} + C_{D_t}\right] \sin(\alpha_w - \epsilon) \right\} \tag{51}$$

VARIATION OF THE TAIL PITCHING MOMENT WITH VELOCITY

ALONG THF Z-AXIS, $\frac{\partial M_t}{\partial w}$

The tail pitching moment with respect to w is obtained from the moment equation about the c.g.

$$M_t = -N_t \ell_t + X_t z_t$$

$$\frac{\partial M_t}{\partial w} = -\ell_t \frac{\partial N_t}{\partial w} + z_t \frac{\partial X_t}{\partial w} \tag{52}$$

VARIATION OF THE TAIL NORMAL FORCE WITH PITCHING VELOCITY, $\frac{\partial N_t}{\partial q}$

Rewriting the tail normal force as in Equation (44),

$$N_t = \rho/2 \; V_T^2 \; \eta_t S_t \left[C_{L_t} \cos(\alpha_w - \epsilon) + C_{D_t} \sin(\alpha_w - \epsilon) \right]$$

The derivative with respect to pitch rate q is

$$\frac{\partial N_t}{\partial q} = \rho/2 \; V_T^2 \; \eta_t S_t \left[\frac{\partial C_{L_t}}{\partial q} \cos(\alpha_w - \epsilon) + \frac{\partial C_{D_t}}{\partial q} \sin(\alpha_w - \epsilon) \right] \tag{53}$$

The partial of C_{L_t} with respect to q may be written as

$$\frac{\partial C_{L_t}}{\partial q} = \frac{\partial C_{L_t}}{\partial \alpha_t} \frac{\partial \alpha_t}{\partial q}$$

and the tail angle of attack as

$$\Delta \alpha_t = \frac{\ell_t q}{U} \quad \text{in radians}$$

and

$$\frac{\partial \alpha_t}{\partial q} = \frac{\ell_t}{U}$$

Therefore,

$$\frac{\partial C_{L_t}}{\partial q} = \frac{\partial C_{L_t}}{\partial \alpha_t} \frac{\ell_t}{U}$$

and

$$\frac{\partial C_{D_t}}{\partial q} = \frac{\partial C_{D_t}}{\partial \alpha_t} \frac{\ell_t}{U} = 2K_i C_{L_t} \frac{\partial C_{L_t}}{\partial \alpha_t} \frac{\ell_t}{U}$$

Substituting in Equation (53),

$$\frac{\partial N_t}{\partial q} = \rho/2 \; V_T^2 \eta_t S_t \left[\frac{\partial C_{L_t}}{\partial \alpha_t} \frac{\ell_t}{U} \cos(\alpha_w - \epsilon) + 2K_i C_{L_t} \frac{\partial C_{L_t}}{\partial \alpha_t} \frac{\ell_t}{U} \sin(\alpha_w - \epsilon) \right] \tag{54}$$

or

$$\frac{\partial N_t}{\partial q} = \rho/2 \; V_T \eta_t S_t \ell_t \frac{\partial C_{L_t}}{\partial \alpha_t} \left[\cos(\alpha_w - \epsilon) + 2K_i C_{L_t} \sin(\alpha_w - \epsilon) \right] \tag{55}$$

VARIATION OF THE TAIL PITCHING MOMENT WITH PITCHING VELOCITY, $\frac{\partial M_t}{\partial q}$

Rewriting the equation for tail pitching moment about the c.g.,

$$M_t = -\ell_t N_t + X_t z_t$$

$$\frac{\partial M_t}{\partial q} = -\ell_t \frac{\partial N_t}{\partial q} + z_t \frac{\partial X_t}{\partial q} \tag{56}$$

The variation of tail longitudinal force with pitch rate is small and generally not considered in dynamic stability analyses. Therefore, this term has been neglected, and the tail pitch damping is considered due to the normal force only.

CONTRIBUTIONS OF THE WING-BODY

The wing-body combination includes the fuselage, wing, wing fans, and interrelated effects as would be represented by wind tunnel data with the horizontal tail off and nose fan inoperative. In order to simplify the derivations, the assumption will be made initially that fan speed is constant, and then the effect of constant power on the derivatives will be evaluated.

VARIATION OF WING-BODY NORMAL FORCE WITH VELOCITY ALONG THE X-AXIS, $\frac{\partial N}{\partial u}$

The normal force in terms of slipstream-based quantities is

$$N = C_N{}^s q^s A_F \tag{57}$$

and the derivative with respect to velocity u is

$$\frac{\partial N}{\partial u} = C_N{}^s \frac{\partial q^s}{\partial u} A_F + q^s A_F \frac{\partial C_N{}^s}{\partial u} \tag{58}$$

By definition, slipstream dynamic pressure and thrust coefficient are

$$q^s = \frac{T_{000}}{A_F} + \rho/2 \, V_T{}^2 \tag{59}$$

$$T_c{}^s = \frac{T_{000}/A_F}{T_{000}/A_F + \rho/2 \, V_T{}^2} \tag{60}$$

With the assumption of constant fan speed and, thus, constant reference disk loading,

$$\frac{\partial q^s}{\partial u} = \rho U \tag{61}$$

$$\frac{\partial T_c^{\,s}}{\partial u} = \frac{-\left(T_{ooo}/A_F\right)\rho U}{\left[T_{ooo}/A_F + \rho/2\, V_T^{\,2}\right]^2} \tag{62}$$

Returning to Equation (58) and writing the normal force coefficient as

$$C_N^{\,s} = C_L^{\,s} \cos\alpha + C_D^{\,s} \sin\alpha \tag{63}$$

$$\frac{\partial C_N^{\,s}}{\partial u} = C_L^{\,s} \frac{\partial \cos\alpha}{\partial u} + \cos\alpha \frac{\partial C_L^{\,s}}{\partial u} + C_D^{\,s} \frac{\partial \sin\alpha}{\partial u} + \sin\alpha \frac{\partial C_D^{\,s}}{\partial u} \tag{64}$$

The partial derivatives in the expression are expanded as follows:

$$\frac{\partial \cos\alpha}{\partial u} = \frac{\sin^2\alpha}{V_T}$$

$$\frac{\partial \sin\alpha}{\partial u} = \cos\alpha \frac{d\alpha}{du} = \cos\alpha \left(\frac{-\sin\alpha}{V_T}\right)$$

$$\frac{\partial C_L^{\,s}}{\partial u} = \frac{\partial C_L^{\,s}}{\partial T_c^{\,s}} \frac{\partial T_c^{\,s}}{\partial u}$$

$$\frac{\partial C_D^{\,s}}{\partial u} = \frac{\partial C_D^{\,s}}{\partial T_c^{\,s}} \frac{\partial T_c^{\,s}}{\partial u}$$

Since the drag coefficient is near zero for equilibrium flight, the product of $C_D^{\,s}$, $\sin\alpha$, and $\sin^2\alpha$ terms is neglected. Substitution of the above quantities in Equation (64) yields

$$\frac{\partial C_N^{\,s}}{\partial u} = \left[\cos\alpha \frac{\partial C_I^{\,s}}{\partial T_c^{\,s}} + \sin\alpha \frac{\partial C_D^{\,s}}{\partial T_c^{\,s}}\right] \frac{\partial T_c^{\,s}}{\partial u} \tag{65}$$

Substituting Equations (61), (62), (63), and (65) into Equation (58),

$$\frac{\partial N}{\partial u} = \rho U A_F \left[C_L^{\,s} \cos\alpha + C_D^{\,s} \sin\alpha \right] + q^s A_F \left[\frac{\partial C_L^{\,s}}{\partial T_c^{\,s}} \cos\alpha + \sin\alpha \frac{\partial C_D^{\,s}}{\partial T_c^{\,s}} \right] \cdot$$

$$\frac{\left(\frac{-T_{ooo}}{A_F} \right) \rho U}{\left[\frac{T_{ooo}}{A_F} + \rho/2 \, V_T^{\,2} \right]^2} = \rho U A_F \left[C_L^{\,s} \cos\alpha \right] + A_F \left[\frac{\partial C_L^{\,s}}{\partial T_c^{\,s}} \cos\alpha \right.$$

$$\left. + \sin\alpha \frac{\partial C_D^{\,s}}{\partial T_c^{\,s}} \right] \frac{\left(\frac{-T_{ooo}}{A_F} \right) \rho U}{q^s} \qquad (66)$$

From the definition of thrust coefficient,

$$\frac{-\left(\frac{T_{ooo}}{A_F} \right)}{q^s} = -T_c^{\,s}$$

Making this substitution and collecting terms,

$$\frac{\partial N}{\partial u} = \rho U A_F \left\{ \left[C_L^{\,s} - \frac{\partial C_L^{\,s}}{\partial T_c^{\,s}} (T_c^{\,s}) \right] \cos\alpha - \frac{\partial C_D^{\,s}}{\partial T_c^{\,s}} (T_c^{\,s}) \sin\alpha \right\} \qquad (67)$$

The variation of normal force with velocity u, then, is dependent upon both the magnitude of the lift coefficient and the slope of lift coefficient versus thrust coefficient. Since this slope is normally negative in sign, both terms are additive.

VARIATION OF WING-BODY LONGITUDINAL FORCE WITH VELOCITY

ALONG THE X-AXIS, $\frac{\partial X}{\partial u}$

The detailed steps for the derivation of longitudinal force derivative with velocity u are not shown for the sake of brevity. The terms involved are the same as for the normal force, differing only by the definition of C_x^s. Using the same procedure, the following expression is derived for the longitudinal force derivative:

$$\frac{\partial X}{\partial u} = \rho U A_F \left\{ \left[\frac{\partial C_D^s}{\partial T_c^s} T_c^s - C_D^s \right] \cos\alpha + \left[\frac{C_L^s (1-2T_c^s)}{2(1-T_c^s)} - \frac{\partial C_L^s}{\partial T_c^s} T_c^s \right] \sin\alpha \right\} \quad (68)$$

Since the drag coefficient is small, the predominant term in this equation is the slope of drag coefficient versus thrust coefficient, which is indicative of the change in momentum drag with forward velocity.

VARIATION OF WING-BODY PITCHING MOMENT WITH VELOCITY ALONG THE X-AXIS, $\frac{\partial M}{\partial u}$

From the pitching moment,

$$M = C_m{}^s \, q^s A_F D_F,$$

$$\frac{\partial M}{\partial u} = C_m{}^s \, A_F D_F \frac{\partial q^s}{\partial u} + q^s A_F D_F \frac{\partial C_m{}^s}{\partial u} \tag{69}$$

$$\text{where } \frac{\partial C_m{}^s}{\partial u} = \frac{\partial C_m{}^s}{\partial T_c{}^s} \frac{\partial T_c{}^s}{\partial u}$$

Substituting Equations (61) and (62) into Equation (69),

$$\frac{\partial M}{\partial u} = A_F D_F \left[C_m{}^s \rho U + q^s \frac{\partial C_m{}^s}{\partial T_c{}^s} \frac{\left(\frac{-T_{000}}{A_F} \right) \rho U}{\left(\frac{T_{000}}{A_F} + \rho/2 V_T{}^2 \right)^2} \right]$$

$$= \rho U \, A_F D_F \left[C_m{}^s - \frac{\partial C_m{}^s}{\partial T_c{}^s} (T_c{}^s) \right] \tag{70}$$

This is the principal derivative affecting speed stability. At low speeds where $\partial C_m{}^s / \partial T_c{}^s$ is negative, the sign of the derivative is positive, denoting the pitch-up tendency with forward velocity. At the higher transition speeds, $\partial C_m{}^s / \partial T_c{}^s$ is slightly positive and the speed stability tends to be neutral or unstable.

VARIATION OF WING-BODY NORMAL FORCE WITH VELOCITY ALONG THE Z-AXIS, $\frac{\partial N}{\partial w}$

From the definition of normal force in slipstream notation, the following partials may be written with respect to velocity w:

$$\frac{\partial N}{\partial w} = C_N^{\ s} A_F \frac{\partial q^s}{\partial w} + q^s A_F \frac{\partial C_N^{\ s}}{\partial w} \tag{71}$$

$$\frac{\partial q^s}{\partial w} = \frac{\partial \rho/2 V_T^{\ 2}}{\partial w} = \rho/2 2W = \rho W \tag{72}$$

$$\frac{\partial C_N^{\ s}}{\partial w} = C_L^{\ s} \frac{\partial \cos\alpha}{\partial w} + \cos\alpha \frac{\partial C_L^{\ s}}{\partial w} + C_D^{\ s} \frac{\partial \sin\alpha}{\partial w} + \sin\alpha \frac{\partial C_D^{\ s}}{\partial w} \tag{73}$$

Also, from Equation (73), the following relationships may be written:

$$\frac{\partial \cos\alpha}{\partial w} = -\sin\alpha \frac{\partial \alpha}{\partial w} = -\sin\alpha \times \frac{1}{U}$$

$$\frac{\partial \sin\alpha}{\partial w} = \cos\alpha \frac{\partial \alpha}{\partial w} = \cos\alpha \times \frac{1}{U}$$

$$\frac{\partial C_L^{\ s}}{\partial w} = \frac{\partial C_L^{\ s}}{\partial \alpha} \cdot \frac{\partial \alpha}{\partial w} = \frac{\partial C_L^{\ s}}{\partial \alpha} \times \frac{1}{U}$$

$$\frac{\partial C_D^{\ s}}{\partial w} = \frac{\partial C_D^{\ s}}{\partial \alpha} \frac{\partial \alpha}{\partial w} = \frac{\partial C_D^{\ s}}{\partial \alpha} \times \frac{1}{U}$$

Substituting these relationships into Equation (73),

$$\frac{\partial C_N^{\ s}}{\partial w} = \frac{1}{U} \left[\left(\frac{\partial C_L^{\ s}}{\partial \alpha} + C_D^{\ s} \right) \cos\alpha + \left(\frac{\partial C_D^{\ s}}{\partial \alpha} - C_L^{\ s} \right) \sin\alpha \right] \tag{74}$$

By making use of

$$W = V_T \sin\alpha$$

$$q^s = \frac{\rho/2 V_T^{\ 2}}{1 - T_c^{\ s}}$$

and $$\frac{V_T^2}{U} = \frac{V_T}{\cos\alpha}$$

Equation (71) may now be written as

$$\frac{\partial N}{\partial w} = (C_L^s \cos\alpha + C_D^s \sin\alpha) A_F \rho V_T \sin\alpha + \rho/2 \frac{V_T A_F}{\cos\alpha(1-T_c^s)} \left[\left(\frac{\partial C_L^s}{\partial \alpha} + C_D^s \right) \cos\alpha + \left(\frac{\partial C_D^s}{\partial \alpha} - C_L^s \right) \sin\alpha \right] \tag{75}$$

Combining terms and simplifying, assuming $\sin^2\alpha = 0$,

$$\frac{\partial N}{\partial w} = \rho A_F V_T \left\{ \left(\frac{\partial C_L^s}{\partial \alpha} + C_D^s + \frac{\partial C_D^s}{\partial \alpha} \frac{\sin\alpha}{\cos\alpha} \right) \frac{1}{2(1-T_c^s)} + \frac{C_L^s \sin\alpha\cos\alpha}{2(1-T_c^s)} \left[2(1-T_c^s) - \frac{1}{\cos^2\alpha} \right] \right\} \tag{76}$$

or

$$\frac{\partial N}{\partial w} = \frac{\rho A_F V_T}{2(1-T_c^s)} \left\{ \frac{\partial C_L^s}{\partial \alpha} + C_D^s + \sin\alpha \left[\left(\frac{\partial C_D^s}{\partial \alpha} \right) \frac{1}{\cos\alpha} + C_L^s \cos\alpha \left[2(1-T_c^s) - \frac{1}{\cos^2\alpha} \right] \right] \right\} \tag{77}$$

Since the drag coefficient and the terms containing $\sin\alpha$ are small for equilibrium flight conditions at small angles of attack, the normal force variation with velocity change along the Z-axis is primarily a function of the wing-body lift curve slope.

VARIATION OF WING-BODY LONGITUDINAL FORCE WITH VELOCITY ALONG THE Z-AXIS, $\frac{\partial X}{\partial w}$

Using the same procedure as for normal force, the following expression for longitudinal force is derived:

$$\frac{\partial X}{\partial w} = \frac{\rho A_F V_T}{2(1-T_c{}^s)} \left\{ C_L{}^s - \frac{\partial C_D{}^s}{\partial \alpha} + \sin\alpha \left[\frac{\partial C_L{}^s}{\partial \alpha} \frac{1}{\cos\alpha} + C_D{}^s \left[\frac{1}{\cos\alpha} - 2\cos\alpha \ (1-T_c{}^s) \right] \right] \right\} \tag{78}$$

If the product of $\sin\alpha$ and $C_D{}^s$, both of which are small, is neglected, the derivative may be simplified to the following form:

$$\frac{\partial X}{\partial w} = \frac{\rho A_F V_T}{2(1-T_c{}^s)} \left[C_L{}^s - \frac{\partial C_D{}^s}{\partial \alpha} + \frac{\partial C_L{}^s}{\partial \alpha} \tan\alpha \right] \tag{79}$$

VARIATION OF WING-BODY PITCHING MOMENT WITH VELOCITY ALONG THE Z-AXIS, $\frac{\partial M}{\partial w}$

From the definition of pitching moment in slipstream notation, the following partial with respect to w may be written:

$$\frac{\partial M}{\partial w} = C_m{}^s A_F D_F \frac{\partial q^s}{\partial w} + q^s A_F D_F \frac{\partial C_m{}^s}{\partial w} \tag{80}$$

where $\frac{\partial q^s}{\partial w} = \rho W = \rho V_T \sin\alpha$

$$\frac{\partial C_m{}^s}{\partial w} = \frac{\partial C_m{}^s}{\partial \alpha}\frac{\partial \alpha}{\partial w} = \frac{\partial C_m{}^s}{\partial \alpha}\frac{1}{U}$$

Eliminating q^s as before,

$$\frac{\partial M}{\partial w} = \rho V_T A_F D_F C_m{}^s \sin\alpha + \rho/2 \frac{V_T A_F D_F}{(1-T_c{}^s)\cos\alpha}\frac{\partial C_m{}^s}{\partial \alpha}$$

or

$$\frac{\partial M}{\partial w} = \rho V_T A_F D_F \left[C_m{}^s \sin\alpha + \frac{\frac{\partial C_m{}^s}{\partial \alpha}}{2\cos\alpha(1-T_c{}^s)}\right] \tag{81}$$

VARIATION OF WING-BODY NORMAL FORCE WITH PITCHING VELOCITY, $\frac{\partial N}{\partial q}$

The wing-body lift force moves from a point near the fan hub in the static condition to a point well forward of the c.g. in forward flight. Modulation of this force due to angle-of-attack changes induced by a pitching velocity about the c.g. produces a force change due to the pitch rate. In addition, due to the remote location of the lift vector with respect to the c.g., a damping moment is created by the lift vector due to pitch rate.

From Equation (57),

$$N = C_N^s q^s A_F$$

where $C_N^s = C_L^s \cos\alpha + C_D^s \sin\alpha$

Taking the partial derivative with respect to q,

$$\frac{\partial C_N^s}{\partial q} = C_L^s \frac{\partial \cos\alpha}{\partial q} + \cos\alpha \frac{\partial C_L^s}{\partial q} + C_D^s \frac{\partial \sin\alpha}{\partial q} + \sin\alpha \frac{\partial C_D^s}{\partial q} \qquad (82)$$

The induced angle of attack due to pitching velocity may be written as

$$-\Delta\alpha = \frac{qx}{U}$$

and

$$\frac{\partial\alpha}{\partial q} = \frac{-x}{U}$$

The partials of Equation (82) may now be developed as follows:

$$\frac{\partial \cos\alpha}{\partial q} = -\sin\alpha \frac{\partial \alpha}{\partial q} = \sin\alpha \frac{x}{U}$$

$$\frac{\partial C_L^s}{\partial q} = \frac{\partial C_L^s}{\partial \alpha} \frac{\partial\alpha}{\partial q} = \frac{-\partial C_L^s}{\partial \alpha} \frac{x}{U}$$

$$\frac{\partial \sin\alpha}{\partial q} = \frac{-x}{U}\cos\alpha$$

$$\frac{\partial C_D^{\,s}}{\partial q} = -\frac{\partial C_D^{\,s}}{\partial \alpha}\frac{x}{U}$$

Substitution in Equation (82) yields

$$\frac{\partial C_N^{\,s}}{\partial q} = \frac{-x}{U}\left[\left(C_D^{\,s} + \frac{\partial C_L^{\,s}}{\partial \alpha}\right)\cos\alpha + \left(\frac{\partial C_D^{\,s}}{\partial \alpha} - C_L^{\,s}\right)\sin\alpha\right]$$

or

$$\frac{\partial N}{\partial q} = -q^s A_F \frac{x}{U}\left[\left(C_D^{\,s} + \frac{\partial C_L^{\,s}}{\partial \alpha}\right)\cos\alpha + \left(\frac{\partial C_D^{\,s}}{\partial \alpha} - C_L^{\,s}\right)\sin\alpha\right] \qquad (83)$$

The distance $\bar{x}$ relative to the vertical plane of the fan hubs is proportional to the ratio of the pitching moment to lift, neglecting the small drag value at trim.

$$\bar{x} = \frac{C_m^{\,s}}{C_L^{\,s}} D_F$$

It can also be shown that this center of lift travel is a linear function of the fan momentum velocity ratio $\frac{V_o}{V_j}$.

$$\frac{\bar{x}}{D_F} = K\frac{V_o}{V_j}$$

With reference to the c.g., the length $\frac{x}{D}$ becomes

$$\frac{x}{D_F} = \frac{\left(x_{cg} - x_{WF}\right)}{D_F} + K\frac{V_o}{V_j}$$

or

$$\frac{x}{D_F} = \left(\frac{x_{cg} - x_{WF}}{D_F}\right) + K\sqrt{2\frac{\left(1-T_c^{\,s}\right)}{T_c^{\,s}}} \qquad (84)$$

Evaluated for typical trim conditions based on wind tunnel test data, K has the value of 1.50.

Simplifying Equation (83) as before, and assuming $\cos\alpha = 1.0$ and $\sin\alpha = 0$,

$$\frac{\partial N}{\partial q} = -\rho/2 \; V_T^2 \frac{A_F \; x}{(1-T_c^s)\; U} \left[\left(\frac{\partial C_L^s}{\partial \alpha} + C_D^s\right)\right]$$

or, replacing x by $\left(\frac{C_m^s}{C_L^s}\right) D_F$,

$$\frac{\partial N}{\partial q} = -\rho/2 \; V_T \frac{A_F D_F}{(1-T_c^s)} \; \frac{C_m^s}{C_L^s} \left(\frac{\partial C_L^s}{\partial \alpha} + C_D^s\right) \qquad (85)$$

VARIATION OF WING-BODY LONGITUDINAL FORCE WITH PITCHING VELOCITY, $\frac{\partial X}{\partial q}$

Using the same procedure developed for the normal force, the following expression is developed for the longitudinal force:

$$\frac{\partial X}{\partial q} = -\rho/2\, V_T \frac{A_F D_F}{(1-T_c{}^s)} \left(\frac{C_m{}^s}{C_L{}^s}\right)\left(C_L{}^s - \frac{\partial C_D{}^s}{\partial \alpha}\right) \tag{86}$$

VARIATION OF WING-BODY PITCHING MOMENT WITH PITCHING VELOCITY, $\frac{\partial M}{\partial q}$

The pitch damping contribution is determined by combining the normal and longitudinal force derivatives with the assumption that the longitudinal force acts in the horizontal plane of the fan hubs.

$$\frac{\partial M}{\partial q} = \frac{\partial N}{\partial q} x + \frac{\partial X}{\partial q} z$$

$$\frac{\partial M}{\partial q} = -\rho/2 V_T \frac{A_F D_F{}^2}{(1-T_c{}^s)} \left(\frac{C_m{}^s}{C_L{}^s}\right)\left[-\left(\frac{C_m{}^s}{C_L{}^s}\right)\left(\frac{\partial C_L{}^s}{\partial \alpha} + C_D{}^s\right) + \left(C_L{}^s - \frac{\partial C_D{}^s}{\partial \alpha}\right)\frac{z}{D_F}\right] \tag{87}$$

CONTRIBUTIONS OF THE NOSE FAN

The contributions of the nose fan, as determined from wind tunnel test data, may include interference effects due to the nose fan efflux affecting the flow about the wing or horizontal tail, but these effects are assumed to be negligible for small perturbations. The principal contributions to stability arise from momentum drag and damping in pitch. These and other derivations are considered in the following sections.

VARIATION OF NOSE FAN NORMAL FORCE WITH VELOCITY ALONG THE Z-AXIS, $\frac{\partial N}{\partial u}$

The normal force in terms of nose fan slipstream-based quantities is

$$N_{NF} = C_{N_{NF}}^{s} q_{NF}^{s} A_{NF} \tag{88}$$

and

$$\frac{\partial N_{NF}}{\partial u} = C_{N_{NF}}^{s} A_{NF} \frac{\partial q_{NF}^{s}}{\partial u} + q^{s} A_{NF} \frac{\partial C_{N_{NF}}^{s}}{\partial u} \tag{89}$$

where

$$\frac{\partial C_{N_{NF}}^{s}}{\partial u} = \frac{\partial C_{N_{NF}}^{s}}{\partial T_{c_{NF}}^{s}} \frac{\partial T_{c_{NF}}^{s}}{\partial u}$$

If use is made of Equations (61) and (62), Equation (89) may be reduced to

$$\frac{\partial N_{NF}}{\partial u} = \rho A_{NF} U \left[C_{N_{NF}}^{s} - \frac{\partial C_{N_{NF}}^{s}}{\partial T_{c_{NF}}^{s}} \left(T_{c_{NF}}^{s} \right) \right] \tag{90}$$

From Equation (88), and neglecting interference effects,

$$C_{N}{}^{s}{}_{NF} = \frac{N_{NF}}{q^{s}{}_{NF} A_{NF}} = \frac{N_{NF} T_{c}{}^{s}{}_{NF}}{\left(T_{o}/A\right)_{NF} A_{NF}} = \left(\frac{N}{T_{o}}\right)_{NF} T_{c}{}^{s}{}_{NF} \qquad (91)$$

where $\left(\frac{N}{T_{o}}\right)_{NF}$ is the nose fan door effectiveness parameter K_{NF}, and is constant for a given door position.

Also, from Equation (91),

$$\left(\frac{\partial C_{N}{}^{s}}{\partial T_{c}{}^{s}}\right)_{NF} = K_{NF}$$

or

$$\frac{\partial C_{N}{}^{s}{}_{NF}}{\partial T_{c}{}^{s}{}_{NF}} \left(T_{c}{}^{s}{}_{NF}\right) = K_{NF} T_{c}{}^{s}{}_{NF} \qquad (92)$$

Therefore, it is seen that Equations (91) and (92) are equivalent, and Equation (90) is equal to zero. Since the nose fan does not induce significant local lift forces due to velocity change, it is reasonable to expect that the derivative is small.

VARIATION OF NOSE FAN LONGITUDINAL FORCE AND MOMENT WITH VELOCITY ALONG THE X-AXIS, $\frac{\partial X}{\partial u}$, $\frac{\partial M}{\partial u}$

From the definition of longitudinal force, and using the same procedures as for the nose fan normal force, the following derivative is obtained:

$$\frac{\partial X}{\partial u} = \rho A_{NF} U \left[C_X^{\,s}{}_{NF} - \frac{\partial C_X^{\,s}}{\partial T_c^{\,s}} T_c^{\,s}{}_{NF} \right] \tag{93}$$

It can be shown that this expression is equivalent to the derivative obtained from simple momentum theory. From Ref. 14, the drag or longitudinal force coefficient in terms of thrust coefficient is

$$C_D^{\,s} = -C_X^{\,s} = \sqrt{2T_c^{\,s}(1-T_c^{\,s})} \tag{94}$$

from which

$$\frac{\partial C_X^{\,s}}{\partial T_c^{\,s}} = - \frac{(1-2T_c^{\,s})}{\left[2T_c^{\,s}(1-T_c^{\,s})\right]^{1/2}} \tag{95}$$

Multiplying both sides by $T_c^{\,s}$,

$$\frac{\partial C_X^{\,s}}{\partial T_c^{\,s}} T_c^{\,s} = \frac{-(1-2T_c^{\,s})T_c^{\,s}}{\left[2T_c^{\,s}(1-T_c^{\,s})\right]^{1/2}} \tag{96}$$

Combining Equations (94) and (96),

$$C_X^{\,s} - \frac{\partial C_X^{\,s}}{\partial T_c^{\,s}} T_c^{\,s} = - \frac{T_c^{\,s}}{\left[2T_c^{\,s}(1-T_c^{\,s})\right]^{1/2}} \tag{97}$$

From $$\rho/2\ U^2 = \frac{T/A(1-T_c{}^s)}{T_c{}^s}$$

$$U\rho = (2\rho)^{1/2}\left[T/A\ \frac{(1-T_c{}^s)}{T_c{}^s}\right]^{1/2} \tag{98}$$

Substituting Equations (97) and (98) into Equation (93),

$$\frac{\partial X}{\partial u} = A_{NF}\ (2\rho)^{1/2}\left[\frac{T/A\ (1-T_c{}^s)}{T_c{}^s}\right]^{1/2}\left[\frac{-T_c{}^\varepsilon}{\left[2T_c{}^s(1-T_c{}^s)\right]}\right]^{1/2} \tag{99}$$

which reduces to

$$\left(\frac{\partial X}{\partial u}\right)_{NF} = -\ (\rho A_{NF} T_{NF})^{1/2} \tag{100}$$

This expression, which gives momentum drag variation with velocity, may also be derived from simple momentum theory, which states that the momentum drag is equal to the product of the fan mass flow and the free stream velocity along the flight path.

The moment due to velocity for the nose fan is obtained from

$$\left(\frac{\partial M}{\partial u}\right)_{NF} = \left(\frac{\partial N}{\partial u}\right)_{NF} x_{NF} + \left(\frac{\partial X}{\partial u}\right)_{NF} z_{NF} \tag{101}$$

VARIATION OF NOSE FAN FORCES WITH VELOCITY ALONG THE Z-AXIS, $\frac{\partial N}{\partial w}$, $\frac{\partial M}{\partial w}$

Expressions for the derivatives with respect to velocity w may be derived which are identical to those developed for the wing-body contributions. However, insufficient wind tunnel data exist to evaluate these quantities.

The theoretical value of the nose fan force derivative with respect to either axial or nonaxial velocity is $(\rho A_{NF} T_{NF})^{1/2}$.

The normal force and pitching moment derivatives, respectively, may be written as

$$\frac{\partial N}{\partial w} = (\rho A_{NF} T_{NF})^{1/2} \tag{102}$$

$$\frac{\partial M}{\partial w} = (\rho A_{NF} T_{NF})^{1/2} x_{NF} \tag{103}$$

The variation of longitudinal force with vertical velocity is assumed to be zero.

VARIATION OF NOSE FAN FORCE AND MOMENT WITH PITCHING VELOCITY, $\frac{\partial N}{\partial q}, \frac{\partial M}{\partial q}$

From the discussion in the previous section of the force changes with respect to w,

$$N = \frac{\partial N}{\partial w} w$$

or

$$N = (\rho A_{NF} T_{NF})^{1/2} (-q x_{NF}) \tag{104}$$

Therefore,

$$\frac{\partial N}{\partial q} = -(\rho A_{NF} T_{NF})^{1/2} x_{NF} \tag{105}$$

and

$$\frac{\partial M}{\partial q} = \frac{\partial N}{\partial q} x_{NF} = -(\rho A_{NF} T_{NF})^{1/2} x_{NF}^2 \tag{106}$$

EFFECT OF CONSTANT POWER ON DERIVATIVES WITH RESPECT TO VELOCITY ALONG THE X-AXIS

In Equations (61) and (62) it was assumed that wing fan speed and, thus, fan disk loading were constant. If this restriction is removed and the fan speed is allowed to vary at constant power, the derivatives must be reevaluated. The primary derivatives affected are the variations of thrust coefficient and slipstream dynamic pressure with velocity, as both of these quantities include fan disk loading as a variable.

From the definition of power coefficient,

$$C_p{}^s = \frac{P_\rho{}^{1/2}}{(T/A)^{3/2} A} \tag{107}$$

Letting $C_p{}^s = \left(\frac{C_p{}^s}{C_p{}^s{}_c} \right) C_p{}^s{}_o$ and solving for the disk loading,

$$T/A = \left[\frac{P_\rho{}^{1/2}}{\left(C_p{}^s / C_p{}^s{}_o \right) C_p{}^s{}_o A} \right]^{2/3} \tag{108}$$

Letting $K = \frac{P_\rho{}^{1/2}}{C_p{}^s{}_o A}$ and $B = \left(\frac{C_p{}^s{}_o}{C_p{}^s} \right)$, the disk loading may be written as

$$T/A = \left[KB \right]^{2/3} \tag{109}$$

Substituting in the equation for thrust coefficient,

$$T_c^s = \frac{T/A}{T/A + q} = \frac{(KB)^{2/3}}{(KB)^{2/3} + q} = \left[1 + \frac{q}{(KB)^{2/3}}\right]^{-1} \tag{110}$$

Performing the differentiation with respect to u,

$$\frac{\partial T_c^s}{\partial u} = -\left[1 + \frac{q}{(KB)^{2/3}}\right]^{-2} \frac{\partial q/(KB)^{2/3}}{\partial u} \tag{111}$$

The partial derivative in this expression may be developed as follows:

$$\frac{\partial q/(KB)^{2/3}}{\partial u} = \frac{(KB)^{2/3}\frac{\partial q}{\partial u} - q\frac{\partial (KB)^{2/3}}{\partial u}}{\left[(KB)^{2/3}\right]^2} \tag{112}$$

where $$\frac{\partial (KB)^{2/3}}{\partial u} = 2/3(KB)^{-1/3}\frac{\partial (KB)}{\partial u}$$

and

$$\frac{\partial q}{\partial u} = \rho U \cong \rho V$$

Equation (111) may now be written as

$$\frac{\partial T_c^s}{\partial u} = \frac{-(KB)^{2/3}\rho V + q\left[2/3(KB)^{-1/3}\frac{\partial (KB)}{\partial u}\right]}{\left[(KB)^{2/3} + q\right]^2} \tag{113}$$

The following relationships are repeated for convenience:

$$T/A = (KB)^{2/3}$$

$$(T/A)^{1/2} = (KB)^{1/3}$$

$$q = \rho/2 V^2$$

Substitution in Equation (113) yields

$$\frac{\partial T_c^s}{\partial u} = \frac{-T/_A \rho V + \rho/_2 V^2 \left[2/3 \, (T/_A)^{-1/2} K \frac{\partial B}{\partial u}\right]}{\left[T/_A + \rho/_2 V^2\right]^2} \tag{114}$$

The second term of the numerator may be further reduced by use of

$$q^s = T/_A + \rho/_2 V^2$$

$$\frac{q}{q^s} = (1 - T_c^s)$$

$$q^s = \frac{T/_A}{T_c^s}$$

Therefore,

$$\frac{\rho/_2 V^2 \left[2/3 (T/_A)^{-1/2} K \frac{\partial B}{\partial u}\right]}{\left[T/_A + \rho/_2 V^2\right]^2} = \frac{2/3 (1 - T_c^s) \, T_c^s \, K \frac{\partial B}{\partial u}}{(T/_A)^{3/2}}$$

But $$\frac{K}{(T/_A)^{3/2}} = \frac{C_p^s}{C_{p_o}^s}$$

and $$\frac{\partial B}{\partial u} = \frac{\partial C_{p_o}^s / C_p^s}{\partial u}$$

Substitution back into Equation (114) gives the final expression for $\partial T_c^s / \partial u$,

$$\frac{\partial T_c^s}{\partial u} = - \frac{\rho V T_c^s}{q^s} + 2/3 (1 - T_c^s) \, T_c^s \, \frac{C_p^s}{C_{p_o}^s} \, \frac{\partial \left(C_{p_o}^s / C_p^s\right)}{\partial u} \tag{115}$$

The first term of this equation is the same as that derived for constant fan speed, and the second term accounts for fan speed change with constant power. This equation was evaluated for several trim speeds in the transition speed range, and the derivative for constant power was about 96 percent of the value of the derivative for constant fan speed. Therefore, the effect of constant power on this derivative is small and the simple form of the derivative may be used.

The other quantity affected by fan speed change is the slipstream dynamic pressure,

$$q^s = T/A + \rho/2 V^2$$

Substituting Equation (109) and differentiating with respect to u,

$$\frac{\partial q^s}{\partial u} = \frac{\partial (KB)^{2/3}}{\partial u} + \rho U \qquad (116)$$

The first term in Equation (112) was evaluated as

$$\frac{\partial (KB)^{2/3}}{\partial u} = 2/3 \, (T/A)^{-1/2} \, K \frac{\partial B}{\partial u}$$

From

$$\frac{K}{(T/A)^{3/2}} = \frac{C_p^s}{C_{p_o}^s},$$

$$\frac{K}{(T/A)^{1/2}} = \frac{C_p^s}{C_{p_o}^s} T/A$$

Equation (116) may now be written as

$$\frac{\partial q^s}{\partial u} = \rho U + 2/3 \frac{C_p^s}{C_{p_o}^s} \frac{\partial \left(C_{p_o}^s / C_p^s \right)}{\partial u} T/A \qquad (117)$$

Replacing T/A by $\frac{\rho/2 V^2 T_c^s}{1-T_c^s}$,

$$\frac{\partial q^s}{\partial u} = \rho U + 1/3 \frac{C_p^s}{C_{p_o}^s} \frac{\partial C_{p_o}^s / C_p^s}{\partial u} \rho V^2 \frac{T_c^s}{1-T_c^s}$$

$$\text{or} \quad \frac{\partial q^s}{\partial u} = \rho U \left[1 + \frac{U}{3 \cos^2 \alpha} \frac{T_c^s}{1-T_c^s} \frac{C_p^s}{C_{p_o}^s} \frac{\partial \left(C_{p_o}^s / C_p^s \right)}{\partial u} \right] \qquad (118)$$

Thus, for constant power, the magnitude of the partial of q^s with velocity is increased if the fan speed increases with velocity. The amount of the increase in the derivative was evaluated for several trim speeds and found to va from 80 percent at about 50 knots to 40 percent at 100 knots. The wing-body derivatives originally developed for constant RPM may now be rewritten to include the effects of constant power on q^s.

$$\frac{\partial N}{\partial u} = \rho U A_F \left\{ \left[\cos\alpha + \frac{U}{3\cos\alpha} \frac{T_c^s}{(1-T_c^s)} \frac{C_p^s}{C_{p_o}^s} \frac{\partial \left(C_{p_o}^s / C_p^s \right)}{\partial u} \right] C_L^s \right.$$

$$\left. - \left[\frac{\partial C_L^s}{\partial T_c^s} \cos\alpha + \frac{\partial C_D^s}{\partial T_c^s} \sin\alpha \right] T_c^s \right\} \tag{119}$$

$$\frac{\partial X}{\partial u} = \rho U A_F \left\{ \left[1 + \frac{U}{3\cos^2\alpha} \frac{T_c^s}{(1-T_c^s)} \frac{C_p^s}{C_{p_o}^s} \frac{\partial \left(C_{p_o}^s / C_p^s \right)}{\partial u} \right] (C_L^s \sin\alpha - C_D^s \cos\alpha) \right.$$

$$\left. + \frac{\partial C_D^s}{\partial T_c^s} T_c^s \cos\alpha - \sin\alpha \left[\frac{\partial C_L^s}{\partial T_c^s} T_c^s + \frac{C_L^s}{2(1-T_c^s)} \right] \right\} \tag{120}$$

$$\frac{\partial M}{\partial u} = \rho U A_F D_F \left\{ \left[1 + \frac{U}{3\cos^2\alpha} \frac{T_c^s}{(1-T_c^s)} \frac{C_p^s}{C_{p_o}^s} \frac{\partial \left(C_{p_o}^s / C_p^s \right)}{\partial u} \right] C_m^s \right.$$

$$\left. + \frac{\partial C_m^s}{\partial T_c^s} (-T_c^s) \right\} \tag{121}$$

LONGITUDINAL CONTROL DERIVATIVES

Longitudinal control contributions are derived from the elevator and nose fan reverser control doors. Although these controls are commonly related through the longitudinal control stick, the nose fan door gain varies with louver vector angle and, furthermore, the nose fan doors are actuated independently of stick position in response to stability augmentation system signals. Therefore, the control derivatives are evaluated separately in terms of elevator and nose fan door position.

ELEVATOR CONTROL DERIVATIVES

The elevator contribution may be determined by writing the equation for horizontal tail normal force and differentiating with respect to elevator angle.

$$\frac{\partial N_t}{\partial \delta_e} = \eta_t \; \rho/2 V_T^2 S_t \left[\frac{\partial C_{L_t}}{\partial \delta_e} \cos(\alpha_w - \epsilon) + \frac{\partial C_{D_t}}{\partial \delta_e} \sin(\alpha_w - \epsilon) \right] \qquad (122)$$

The drag term may be written as

$$\frac{\partial C_{D_t}}{\partial \delta_e} = \frac{\partial C_{D_t}}{\partial \alpha_t} \left(\frac{d\alpha}{d\delta} \right)$$

where

$$\frac{\partial C_{D_t}}{\partial \alpha_t} = 2K_i C_{L_t} \frac{\partial C_{L_t}}{\partial \alpha_t}$$

Therefore,

$$\frac{\partial C_{D_t}}{\partial \delta_e} = 2K_i C_{L_t} \frac{\partial C_{L_t}}{\partial \alpha_t} \left(\frac{d\alpha}{d\delta} \right) = 2K_i C_{L_t} \frac{\partial C_{L_t}}{\partial \delta_e}$$

and

$$\frac{\partial N_t}{\partial \delta_e} = \eta_t \, \rho/2 V_T^2 S_t \frac{\partial C_{L_t}}{\partial \delta_e} \left[\cos(\alpha_w - \epsilon) + 2K_i C_{L_t} \sin(\alpha_w - \epsilon) \right] \tag{123}$$

where $\partial C_{L_t} / \partial \delta_e$ is per radian

Similarly,

$$\frac{\partial X_t}{\partial \delta_e} = \rho/2 V_T^2 \eta_t S_t \frac{\partial C_{L_t}}{\partial \delta_e} \left[\sin(\alpha_w - \epsilon) - 2K_i C_{L_t} \cos(\alpha_w - \epsilon) \right] \tag{124}$$

and

$$\frac{\partial M_t}{\partial \delta_e} = -\rho/2 V_T^2 \eta_t S_t \ell_t \frac{\partial C_{L_t}}{\partial \delta_e} \left\{ \cos(\alpha_w - \epsilon) \left[1 + 2K_i C_{L_t} \frac{z_t}{\ell_t} \right] + \sin(\alpha_w - \epsilon) \left[2K_i C_{L_t} - \frac{z_t}{\ell_t} \right] \right\} \tag{125}$$

NOSE FAN THRUST REVERSER DOOR CONTROL DERIVATIVES

Nose fan door control characteristics developed from the wind tunnel tests of Reference 17 are shown in Figure 71, where the nose fan increments were determined from nose fan-on and nose fan-off data.

Dimensional derivatives may be developed from the nondimensional quantities of Figure 71 as follows:

$$\frac{\partial N}{\partial \delta_{pfd}} = \frac{\partial \Delta C_L^{\ s}}{\partial \delta_{pfd^o}} \; q^s A_F \times 57.3 = \frac{\partial \Delta C_L^{\ s}}{\partial \delta_{pfd^o}} \frac{T_{ooo}}{T_c^{\ s}} \times 57.3 \text{ per radian} \quad (126)$$

$$\frac{\partial X}{\partial \delta_{pfd}} = \frac{-\partial \Delta C_D^{\ s}}{\partial \delta_{pfd^o}} \frac{T_{ooo}}{T_c^{\ s}} \times 57.3 \text{ per radian} \quad (127)$$

$$\frac{\partial M}{\partial \delta_{pfd}} = \frac{\partial (N/T_o)}{\partial \delta_{pfd^o}} T_{NF} \; x_{NF} \; (57.3) + \frac{\partial X}{\partial \delta_{pfd}} z_{NF} \text{ per radian} \quad (128)$$

The nose fan thrust relative to the wing fan thrust may be determined from Figure 71 as

$$\frac{T_{NF}}{T_{ooo}} = .148 - .35 \; (1 - T_c^{\ s})$$

and the pitching moment derivative becomes

$$\frac{\partial M}{\partial \delta_{pfd}} = \frac{\partial (N/T_o)}{\partial \delta_{pfd^o}} x_{NF} \; T_{ooo} \left[.148 - .35 \; (1 - T_c^{\ s}) \right] 57.3 + \frac{\partial X}{\partial \delta_{pfd}} z_{NF} \quad (129)$$

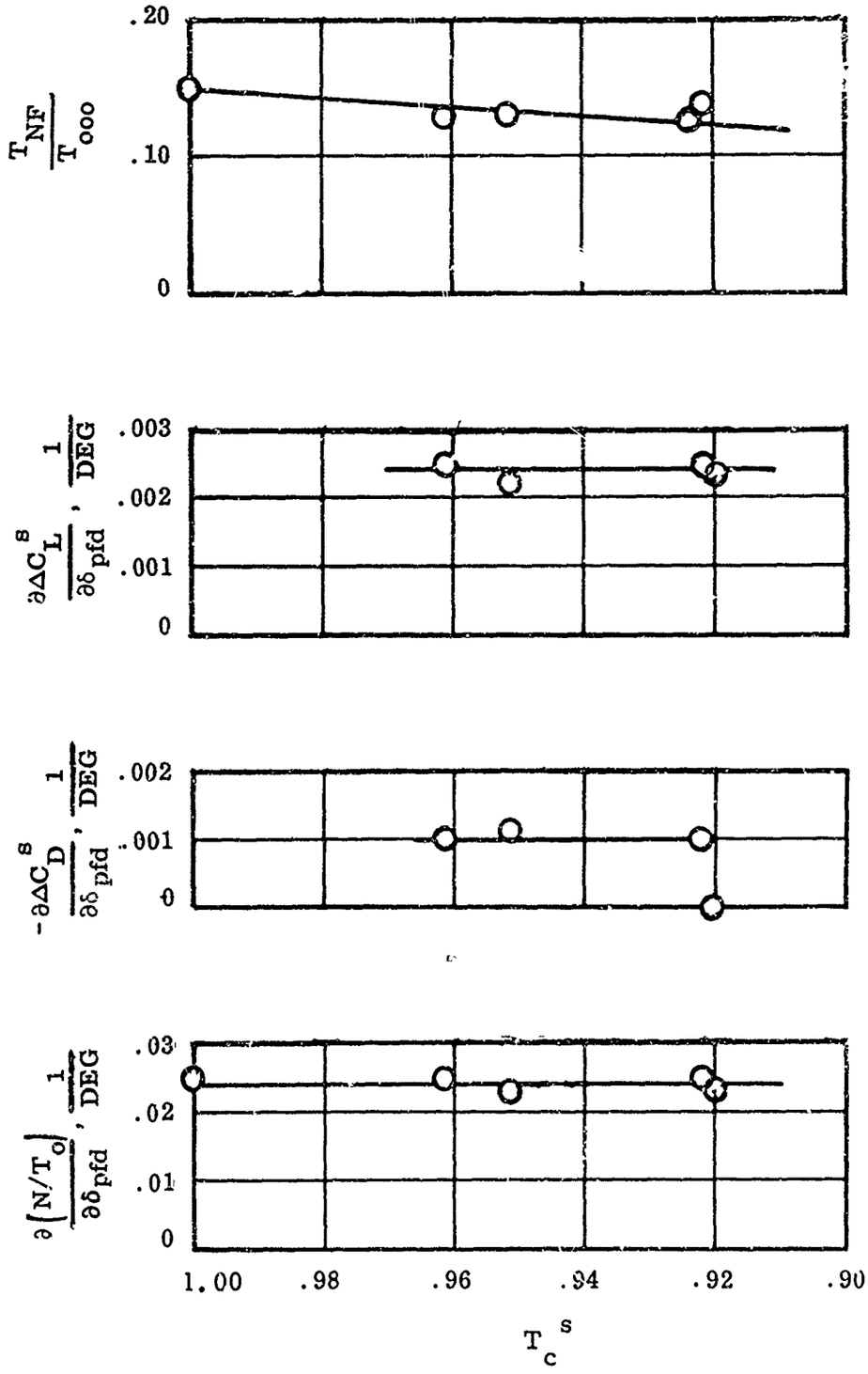

Figure 71. Nondimensional Nose Fan Control Derivatives.

HOVERING DERIVATIVES

The expressions for the stability derivatives in hovering or very low speed flight are derived from considerations of the wing and nose fan mass flow, as given by simple momentum theory and the induced forces due to the mass flow. Contributions due to the horizontal tail are neglected except for pitch damping and motion along the Z-axis.

DERIVATIVES WITH RESPECT TO VELOCITY ALONG THE X-AXIS

LONGITUDINAL FORCE, $\frac{\partial X}{\partial u}$

The momentum drag of the wing fans and nose fan is

$$X = \dot{m}_{WF} u + \dot{m}_{NF} u = (\dot{m}_{WF} + \dot{m}_{NF}) u \tag{130}$$

and the derivative with respect to velocity is

$$\frac{\partial X}{\partial u} = \dot{m}_{WF} + \dot{m}_{NF} \tag{131}$$

where $$\dot{m}_{WF} = (\rho A_F T_{ooo})^{1/2} = .049 (\sigma A_F T_{ooo})^{1/2} \tag{132}$$

and $$\dot{m}_{NF} = .049 (\sigma A_{NF} \bar{T}_{NF})^{1/2}$$

From Figure 71, the nose fan thrust in terms of wing fan thrust is

$$\left(\frac{T_{NF}}{T_{ooo}}\right)^{1/2} = (.148)^{1/2} = .386$$

Equation (131) may now be written as

$$\frac{\partial X}{\partial u} = .049 (\sigma A_F T_{ooo})^{1/2} + .049 (\sigma A_{NF})^{1/2} (.386) (T_{ooo})^{1/2}$$

$$= -.370 (\sigma T_{ooo})^{1/2} \tag{133}$$

VERTICAL FORCE, $\frac{\partial Z}{\partial u}$

The variation of normal force with change in forward velocity is derived from a method presented in Reference 18 based on two-dimensional jet flap theory. Since the method overestimates the lift at low speeds, it is modified by considering only the wing area immediately ahead of the fan as being affected by the fan inflow. From Reference 18, the two-dimensional lift coefficient is

$$C_{\ell_{2d}} = \frac{C_\ell}{\delta_j} \delta_j \left(\frac{S_1}{S_1 + S_2 + S_3} \right) + C_{\ell_3} \left(\frac{S_3}{S_1 + S_2 + S_3} \right) \qquad (134)$$

C_{ℓ_3}, which represents the loading on the area aft of the fan, is assumed to be equal to -1.0 according to the reference. Since this value is small compared to the first term at very low speeds, the equation is shortened by assuming that $S_3 = 0$ and incorporating an empirically determined correction factor K to account for the simplification.

$$C_{\ell_{2d}} = K \frac{C_\ell}{\delta_j} \delta_j \left(\frac{S_1}{S_1 + S_2} \right) \qquad (135)$$

where

$$\frac{C_\ell}{\delta_j} = 3 \sqrt{\frac{T}{q S_1}}$$

$$\delta_j = \frac{90^\circ}{57.3} = 1.57$$

S_1 = area ahead of fan, per semispan

S_2 = fan area, per fan

K = .75

The fan induced lift coefficient is

$$C_{L_i} = \frac{C_{\ell_{2d}}}{2\pi} \frac{\partial C_L}{\partial \delta_1} \tag{136}$$

where $\frac{\partial C_L}{\partial \delta_1}$ is assumed to be equal to unity.

Therefore,

$$C_{L_i} = \frac{.75 \times 3.0}{2\pi} \sqrt{\frac{T}{qS_1}} \times 1.57 \left(\frac{S_1}{S_1 + S_2} \right) \tag{137}$$

The induced lift is then calculated from

$$L = C_{L_i} qS_{ref}$$

$$= .562 \sqrt{\frac{T}{qS_1}} \left(\frac{S_1}{S_1 + S_2} \right) 2 (S_1 + S_2) q$$

$$= 1.125 \sqrt{TqS_1}$$

Expressing q as $\frac{\sigma \rho_o}{2} V^2$ and evaluating the lift for $S_1 = 13$ ft^2,

$$L = .141 \sqrt{\left(\frac{T_{ooo}}{2} \right) \sigma} \; V \tag{138}$$

and the derivative with respect to velocity becomes

$$\frac{\partial L}{\partial V} = - \frac{\partial Z}{\partial V} = .10 \, (\sigma T_{ooo})^{1/2} \tag{139}$$

It should be noted that this derivative becomes discontinuous at zero velocity because rearward flight would also produce a positive induced lift.

PITCHING MOMENT, $\frac{\partial M}{\partial u}$

Pitching moments due to translational velocity are created primarily due to the wing-fan center of lift transfer and secondarily due to the momentum drag terms.

The moment due to center of lift transfer is

$$M = L\,(\bar{x} - \Delta x_{cg}) \tag{140}$$

where $\bar{x} = \frac{d\bar{x}/D_F}{dV/V_j} \times V/V_j \times D_F = K\,V/V_j\,D_F$

and

$$L = \dot{m}V_j$$

Substituting these relationships into Equation (140),

$$M = \dot{m}V_j(K\,V/V_j\,D_F - \Delta x_{cg}) = \dot{m}KVD_F - \dot{m}V_j\Delta x_{cg}$$

and

$$\frac{\partial M}{\partial u} = \dot{m}KD_F = (\rho A_F T_{ooo})^{1/2} KD_F = .320(\sigma T_{ooo})^{1/2} KD_F \tag{141}$$

Based on test data for zero vector angle, K has the value of about 1.25 and the moment derivative is then

$$\frac{\partial M}{\partial u} = 2.08\,(\sigma T_{ooo})^{1/2} \tag{142}$$

The moment due to momentum drag is determined from the longitudinal force derivatives given by Equation (133).

$$\Delta\frac{\partial M}{\partial u} = \frac{\partial Z}{\partial u}\,z = -.370\,(\sigma T_{ooo})^{1/2} z \tag{143}$$

and when added to Equation (141),

$$\frac{\partial M}{\partial u} = (\sigma T_{ooo})^{1/2}\left[2.08 - .370z\right] \tag{144}$$

DERIVATIVES WITH RESPECT TO VELOCITY ALONG THE Z-AXIS

VERTICAL FORCE, $\frac{\partial Z}{\partial w}$

Motion along the Z-axis produces forces due to the fans and the aircraft vertical drag. The fan momentum term is

$$Z = -(\dot{m}_{WF} w + \dot{m}_{NF} w) \tag{145}$$

By inspection, this equation is identical to the momentum drag with respect to the Y-axis. Therefore, the vertical force derivative may be written as

$$\frac{\partial Z}{\partial w} = -.370 (\sigma T_{ooo})^{1/2} \tag{146}$$

The airframe vertical drag may be determined from data from Ref. 10.

$$D_V = C_{D_V} \rho/2 w^2 A_F$$

and

$$\frac{\partial Z}{\partial w} = -\rho A_F C_{D_V} w \tag{147}$$

where

$$C_{D_V} = 11.8$$

Combining Equations (146) and (147),

$$\frac{\partial Z}{\partial w} = -.370 (\sigma T_{ooo})^{1/2} - 1.19\sigma/w/ \tag{148}$$

Quantities dependent upon freestream dynamic pressure such as vertical drag introduce nonlinearities because they contain the independent variable. At zero velocity, these derivatives are zero and could be neglected for small perturbations; however, they are shown here in order to account for all the forces which contribute to the derivatives. These quantities may be further approximated in a linear form if the maximum value of the disturbance velocity is known.

$$\Delta\frac{\partial Z}{\partial w} = -1.19\frac{/w_{max}/\sigma}{2}$$

The absolute notation is used to preserve the proper sign convention.

PITCHING MOMENT, $\frac{\partial M}{\partial w}$

The pitching moment derivative is determined from the vertical force derivatives and the airframe pitching moment.

$$M = Z_{NF}(-x_{NF}) - Z_{WF}(x_{WF}) + C_m \rho/2 w^2 A_F D_F \tag{149}$$

Evaluated for a c.g. position at Station 240, the moment derivative is

$$\frac{\partial M}{\partial w} = .325 (\sigma T_{ooo})^{1/2} - 4.80 /w/\sigma \tag{150}$$

DERIVATIVES WITH RESPECT TO PITCHING VELOCITY

VERTICAL FORCE, $\frac{\partial Z}{\partial q}$, AND PITCHING MOMENT, $\frac{\partial M}{\partial q}$

The pitch rate derivatives are determined from the fan vertical force derivatives with respect to velocity w, where the velocity is induced by the pitch rate and from the force on the horizontal tail.

In general terms these derivatives may be written as

$$\frac{\partial Z}{\partial q} = .05(\sigma T_{ooo})^{1/2} x_{NF} - .319(\sigma T_{ooo})^{1/2} x_{WF} - C_{D_{V_t}} \rho_o \sigma S_t \ell_t^2 q \qquad (151)$$

$$\frac{\partial M}{\partial q} = -.05(\sigma T_{ooo})^{1/2} (x_{NF})^2 - .319(\sigma T_{ooo})^{1/2} (x_{WF})^2 - C_{D_{V_t}} \rho_o \sigma S_t \ell_t^3 q \qquad (152)$$

and evaluated for c.g. Station 240,

$$\frac{\partial Z}{\partial q} = .131(\sigma T_{ooo})^{1/2} - 61.5\dot{\theta}/\sigma \qquad (153)$$

$$\frac{\partial M}{\partial q} = -12.16\ (\sigma T_{ooo})^{1/2} - 1430\dot{\theta}/\sigma \qquad (154)$$

APPENDIX II

XV-5A LONGITUDINAL STABILITY DERIVATIVES

TABLE IX. SUMMARY OF STABILITY DERIVATIVES AT ZERO α - TRANSITION SPEED RANGE.

A. Horizontal Tail Terms

1. $$\frac{\partial Z_t}{\partial u} = -\frac{\partial N_t}{\partial u} = -\eta_t S_t \rho U \left[C_{L_t} \cos(\alpha_w - \epsilon) + C_{D_t} \sin(\alpha_w - \epsilon)\right]$$

2. $$\frac{\partial X_t}{\partial u} = \eta_t S_t \rho U \left[C_{L_t} \sin(\alpha_w - \epsilon) - C_{D_t} \cos(\alpha_w - \epsilon)\right]$$

3. $$\frac{\partial M_t}{\partial u} = -\ell_t \frac{\partial N_t}{\partial u} + z_t \frac{\partial X_t}{\partial u}$$

4. $$\frac{\partial Z_t}{\partial w} = -\frac{\partial N_t}{\partial w} = -\rho/2\, V_T \eta_t S_t \left(1 - \frac{d\epsilon}{d\alpha}\right) \left\{\left[\frac{\partial C_{L_t}}{\partial \alpha_t} + C_{D_t}\right] \cos(\alpha_w - \epsilon) + C_{L_t} \sin(\alpha_w - \epsilon) \left[2 K_1 \frac{\partial C_{L_t}}{\partial \alpha_t} - 1\right]\right\}$$

5. $$\frac{\partial X_t}{\partial w} = \rho/2\, V_T \eta_t S_t \left(1 - \frac{d\epsilon}{d\alpha}\right) \left\{C_{L_t} \left[1 - 2K_1 \frac{\partial C_{L_t}}{\partial \alpha_t}\right] \cos(\alpha_w - \epsilon) + \left[\frac{\partial C_{L_t}}{\partial \alpha_t} + C_{D_t}\right] \sin(\alpha_w - \epsilon)\right\}$$

6. $$\frac{\partial M_t}{\partial w} = -\ell_t \frac{\partial N_t}{\partial w} + z_t \frac{\partial X_t}{\partial w}$$

7. $$\frac{\partial Z_t}{\partial q} = -\frac{\partial N_t}{\partial q} = -\rho/2\, V_t \eta_t S_t \ell_t \frac{\partial C_{L_t}}{\partial \alpha_t} \left[\cos(\alpha_w - \epsilon) + 2K_1 C_{L_t} \sin(\alpha_w - \epsilon)\right]$$

8. $$\frac{\partial M_t}{\partial q} = -\ell_t \frac{\partial N_t}{\partial q}$$

TABLE IX. - Continued

9. $$\frac{\partial Z_t}{\partial \delta_e} = -\frac{\partial N_t}{\partial \delta_e} = -\eta_t \, \rho/2 \, V_T^2 \, S_t \frac{\partial C_{L_t}}{\partial \delta_e} \left[\cos(\alpha_w - \epsilon) + 2 K_i C_{L_t} \sin(\alpha_w - \epsilon)\right]$$

10. $$\frac{\partial X_t}{\partial \delta_e} = \rho/2 \, V_T^2 \, \eta_t \, S_t \frac{\partial C_{L_t}}{\partial \delta_e} \left[\sin(\alpha_w - \epsilon) - 2 K_i C_{L_t} \cos(\alpha_w - \epsilon)\right]$$

11. $$\frac{\partial M_t}{\partial \delta_e} = -\rho/2 \, V_T^2 \, \eta_t \, S_t \, \ell_t \frac{\partial C_{L_t}}{\partial \delta_e} \left\{\cos(\alpha_w - \epsilon) \left[1 + 2 K_i C_{L_t} \frac{z_t}{\ell_t}\right] + \sin(\alpha_w - \epsilon) \left[2 K_i C_{L_t} - \frac{z_t}{\ell_t}\right]\right\}$$

B. Wing-Body Terms

1. $$\frac{\partial Z}{\partial u} = -\frac{\partial N}{\partial u} = -\rho \, U \, A_F \left\{\left[1 + \frac{U}{3} \frac{T_c^s}{(1-T_c^s)} \left(\frac{C_p^s}{C_{p_o}^s}\right) \frac{\partial (C_{p_o}^s / C_p^s)}{\partial u}\right] C_L^s - \left[\frac{\partial C_L^s}{\partial T_c^s}\right] T_c^s\right\}$$

2. $$\frac{\partial X}{\partial u} = \rho \, U \, A_F \left\{\left[1 + \frac{U}{3} \frac{T_c^s}{(1-T_c^s)} \left(\frac{C_p^s}{C_{p_o}^s}\right) \frac{\partial (C_{p_o}^s / C_p^s)}{\partial u}\right] (-C_D^s) + \frac{\partial C_D^s}{\partial T_c^s} T_c^s\right\}$$

3. $$\frac{\partial M}{\partial u} = \rho \, U A_F D_F \left\{\left[1 + \frac{U}{3} \frac{T_c^s}{(1-T_c^s)} \left(\frac{C_p^s}{C_{p_o}^s}\right) \frac{\partial (C_{p_o}^s / C_p^s)}{\partial u}\right] C_m^s - \frac{\partial C_m^s}{\partial T_c^s} (T_c^s)\right\}$$

4. $$\frac{\partial Z}{\partial w} = -\frac{\partial N}{\partial w} = -\rho \frac{V_T A_F}{2(1-T_c^s)} \left\{\frac{\partial C_L^s}{\partial \alpha} + C_D^s\right\}$$

5. $$\frac{\partial X}{\partial w} = \rho \frac{V_T A_F}{2(1-T_c^s)} \left\{C_L^s - \frac{\partial C_D^s}{\partial \alpha}\right\}$$

6. $$\frac{\partial M}{\partial w} = \rho \frac{V_T A_F D_F}{2(1-T_c^s)} \left[\frac{\partial C_m^s}{\partial \alpha}\right]$$

TABLE IX. - Continued

7. $$\frac{\partial Z}{\partial q} = -\frac{\partial N}{\partial q} = +\rho \frac{V_T A_F D_F}{2(1-T_c^s)} \left(\frac{C_m^s}{C_L^s}\right)\left[\frac{\partial C_L^s}{\partial \alpha} + C_D^s\right]$$

8. $$\frac{\partial X}{\partial q} = -\rho/2 \frac{V_T A_F D_F}{(1-T_c^s)} \left(\frac{C_m^s}{C_L^s}\right)\left[C_L^s - \frac{\partial C_D^s}{\partial \alpha}\right]$$

9. $$\frac{\partial M}{\partial q} = -\rho/2 \frac{V_T A_F D_F^2}{(1-T_c^s)} \left(\frac{C_m^s}{C_L^s}\right)\left[\left(\frac{C_m^s}{C_L^s}\right)\left(\frac{\partial C_L^s}{\partial \alpha} + C_D^s\right) + \left(C_L^s - \frac{\partial C_D^s}{\partial \alpha}\right)\frac{z}{D_F}\right]$$

C. Nose Fan Terms

1. $$\frac{\partial Z}{\partial u} = -\frac{\partial N}{\partial u} = 0$$

2. $$\frac{\partial X}{\partial u} = -(\rho A_{NF} T_{NF})^{1/2}$$

3. $$\frac{\partial M}{\partial u} = \frac{\partial X}{\partial u} z_{NF} = -(\rho A_{NF} T_{NF})^{1/2} z_{NF}$$

4. $$\frac{\partial Z}{\partial w} = -\frac{\partial N}{\partial w} = -(\rho A_{NF} T_{NF})^{1/2}$$

5. $$\frac{\partial X}{\partial w} = 0$$

6. $$\frac{\partial M}{\partial w} = \frac{\partial N}{\partial w} x_{NF} = +(\rho A_{NF} T_{NF})^{1/2} x_{NF}$$

7. $$\frac{\partial Z}{\partial q} = -\frac{\partial N}{\partial q} = +(\rho A_{NF} T_{NF})^{1/2} x_{NF}$$

8. $$\frac{\partial M}{\partial q} = \frac{\partial N}{\partial q} x_{NF} = -(\rho A_{NF} T_{NF})^{1/2} x_{NF}^2$$

9. $$\frac{\partial Z}{\partial \delta_{pfd}} = -\frac{\partial N}{\partial \delta_{pfd}} = -\frac{\partial \Delta C_L^s}{\partial \delta_{pfd}^o} \frac{T_{000}}{T_c^s} \times 57.3$$

TABLE IX. - Continued

10. $$\frac{\partial X}{\partial \delta_{pfd}} = -\frac{\partial \Delta C_D{}^{s}}{\partial \delta_{pfd}{}^{o} T_c{}^{s}} \frac{T_{ooo}}{} \times 57.3$$

11. $$\frac{\partial M}{\partial \delta_{pfd}} = \frac{\partial (N/T_o)_{NF}}{\partial \delta_{pfd}{}^{o}} x_{NF} T_{ooo} \left[.148 - .35 (1-T_c{}^{s})\right] 57.3 + \frac{\partial X}{\partial \delta_{pfd}} z_{NF}$$

TABLE X. HOVERING STABILITY DERIVATIVES

$$\frac{\partial X}{\partial u} = -.370\,(\sigma T_{000})^{1/2}$$

$$\frac{\partial Z}{\partial u} = -.10\,(\sigma T_{000})^{1/2}$$

$$\frac{\partial M}{\partial u} = (\sigma T_{000})^{1/2}\,(2.08 - .370z)$$

$$\frac{\partial Z}{\partial w} = -.370\,(\sigma T_{000})^{1/2} - \frac{1.19/w_{max}/\sigma}{2}$$

$$\frac{\partial M}{\partial w} = .325\,(\sigma T_{000})^{1/2} - \frac{4.80/w_{max}/\sigma}{2}$$

$$\frac{\partial Z}{\partial q} = .131\,(\sigma T_{000})^{1/2} - 61.5\,\frac{/q_{max}/\sigma}{2}$$

$$\frac{\partial M}{\partial q} = -12.16\,(\sigma T_{000})^{1/2} - 1430\,\frac{/q_{max}/\sigma}{2}$$

TABLE XI, A. NUMERICAL VALUES OF THE STABILITY DERIVATIVES, $\sigma = 1.0000$

Derivative	Velocity (Kts)	Wing-Body	Tail	Nose Fan	Total Derivative*
$\frac{\partial X}{\partial u}$ $(\frac{\text{lb-sec}}{\text{ft}})$	0	-	-	-	-36.5
	16.6	-25.3	-0.4	-4.9	-30.7
	39.7	-41.2	-1.0	-4.9	-47.1
	57.4	-34.7	-1.5	-4.8	-41.1
	74.6	-41.5	-2.0	-4.8	-48.3
	90.0	-49.2	-1.4	-4.9	-55.5
$\frac{\partial Z}{\partial u}$ $(\frac{\text{lb-sec}}{\text{ft}})$	0		-	-	-9.9
	16.6	-10.0	-1.6	-	-11.6
	39.7	-19.1	-3.9	-	-23.0
	57.4	-42.0	-6.0	-	-48.0
	74.6	-56.3	-8.3	-	-64.6
	90.0	-59.3	-5.9	-	-65.2
$\frac{\partial M}{\partial u}$ (lb-sec)	0	-	-	-	168.8
	16.6	200.9	-29.7	-4.9	166.3
	39.7	147.2	-75.0	-4.9	67.3
	57.4	77.0	-115.1	-4.8	-42.9
	74.6	-15.7	-159.8	-4.8	-180.3
	90.0	-132.6	-114.6	-4.9	-252.1
$\frac{\partial X}{\partial w}$ $(\frac{\text{lb-sec}}{\text{ft}})$	0	-	-	-	-
	16.6	-	-	-	-
	39.7	27.9	-0.8	-	27.1
	57.4	33.0	-1.0	-	32.0
	74.6	25.5	-1.1	-	24.4
	90.0	22.8	-1.8	-	21.0
$\frac{\partial Z}{\partial w}$ $(\frac{\text{lb-sec}}{\text{ft}})$	0	-	-	-	-36.5
	16.6	-28.4	-2.7	-4.9	-36.0
	39.7	-75.6	-7.0	-4.9	-87.5
	57.4	-97.1	-10.6	-4.8	-112.5
	74.6	-121.0	-14.4	-4.8	-140.2
	90.0	-150.4	-17.5	-4.9	-172.8
$\frac{\partial M}{\partial w}$ (lb-sec)	0	-	-	-	32
	16.6	175	-5	75	195
	39.7	222	-141	74	155
	57.4	214	-217	73	70
	74.6	210	-295	72	-14
	90.0	215	-356	74	-67
$\frac{\partial X}{\partial q}$ $(\frac{\text{lb-sec}}{\text{rad}})$	0	-	-	-	-
	16.6	-2.9	-	-	-2.9
	39.7	-10.0	-	-	-10.0
	57.4	-38.3	-	-	-38.3
	74.6	-53.6	-	-	-53.6
	90.0	-57.8	-	-	-57.8

TABLE XI.A- Continued

Derivative	Velocity (Kts)	Wing-Body	Tail	Nose Fan	Total Derivative*
$\frac{\partial Z}{\partial q}$ ($\frac{\text{lb-sec}}{\text{rad}}$)	0	-	-	-	13
	16.6	-18	-99	75	-43
	39.7	24	-238	74	-139
	57.4	98	-345	73	-174
	74.6	199	-449	72	-177
	90.0	308	-547	74	-164
$\frac{\partial M}{\partial q}$ ($\frac{\text{lb-ft-sec}}{\text{rad}}$)	0	-	-	-	-1,201
	16.6	-14	-2,094	-1,125	-3,233
	39.7	-18	-5,019	-1,114	-6,151
	57.4	-136	-7,282	-1,102	-8,520
	74.6	-382	-9,481	-1,093	-10,955
	90.0	-690	-11,542	-1,123	-13,354

* At zero velocity, the total derivatives consist of the hovering derivatives only.

TABLE XI,B. NUMERICAL VALUES OF THE STABILITY DERIVATIVES, $\sigma = 0.9151$

Derivative	Velocity (Kts)	Wing-Body	Tail	Nose Fan	Total Derivative*
$\frac{\partial X}{\partial u}$ ($\frac{\text{lb-sec}}{\text{ft}}$)	0	-	-	-	-35.0
	17.3	-24.3	-0.4	-4.7	-29.4
	41.5	-39.7	-1.0	-4.7	-45.4
	60.0	-33.0	-1.5	-4.6	-39.1
	78.0	-39.8	-1.9	-4.6	-46.3
	94.1	-45.4	-1.3	-4.7	-51.4
$\frac{\partial Z}{\partial u}$ ($\frac{\text{lb-sec}}{\text{ft}}$)	0	-	-	-	-9.4
	17.3	-9.8	-1.5	-	-11.3
	41.5	-21.8	-3.8	-	-25.7
	60.0	-41.0	-5.8	-	-46.8
	78.0	-54.2	-7.9	-	-62.1
	94.1	-57.9	-5.7	-	-63.6
$\frac{\partial M}{\partial u}$ (lb-sec)	0	-	-	-	161.5
	17.3	192.7	-28.4	-4.7	159.6
	41.5	141.9	-71.8	-4.7	65.4
	60.0	73.4	-110.1	-4.6	-41.3
	78.0	-14.8	-152.8	-4.6	-172.2
	94.1	-126.0	-109.6	-4.7	-240.3
$\frac{\partial X}{\partial w}$ ($\frac{\text{lb-sec}}{\text{ft}}$)	0	-	-	-	-
	17.3	-	-	-	-
	41.5	26.6	-0.7	-	25.8
	60.0	30.3	-1.0	-	29.3
	78.0	24.3	-1.1	-	23.3
	94.1	21.7	-1.7	-	19.9
$\frac{\partial Z}{\partial w}$ ($\frac{\text{lb-sec}}{\text{ft}}$)	0	-	-	-	-35.0
	17.3	-27.2	-2.6	-4.7	-34.5
	41.5	-72.3	-6.7	-4.7	-83.7
	60.0	-92.9	-10.2	-4.6	-107.7
	78.0	-115.7	-13.8	-4.6	-134.1
	94.1	-143.9	-16.7	-4.7	-165.3
$\frac{\partial M}{\partial w}$ (lb-sec)	0	-	-	-	31
	17.3	176	-53	71	194
	41.5	213	-135	71	149
	60.0	205	-208	70	67
	78.0	201	-282	69	-12
	94.1	206	-340	71	-63
$\frac{\partial X}{\partial q}$ ($\frac{\text{lb-sec}}{\text{rad}}$)	0	-	-	-	-
	17.3	-2.8	-	-	-2.8
	41.5	-8.6	-	-	-8.6
	60.0	-30.4	-	-	-30.4
	78.0	-40.0	-	-	-40.0
	94.1	-44.5	-	-	-44.5

TABLE XI, B.-Continued

Derivative	Velocity (Kts)	Wing-Body	Tail	Nose Fan	Total Derivative*
$\frac{\partial Z}{\partial q}$ ($\frac{\text{lb-sec}}{\text{rad}}$)	0	-	-	-	12
	17.3	-17	-95	71	-41
	41.5	23	-227	71	-133
	60.0	93	-330	70	-167
	78.0	191	-429	69	-169
	94.1	295	-523	71	-157
$\frac{\partial M}{\partial q}$ ($\frac{\text{lb-ft-sec}}{\text{rad}}$)	0	-	-	-	-1,149
	17.3	-14	-2,003	-1,076	-3,093
	41.5	-16	-4,801	-1,066	-5,883
	60.0	-124	-6,966	-1,054	-8,144
	78.0	-355	-9,070	-1,046	-10,471
	94.1	-646	-11,041	-1,074	-12,761

* At zero velocity, the total derivatives consist of the hovering derivatives only.

TABLE XII. NUMERICAL VALUES OF THE CONTROL DERIVATIVES

Velocity σ = 1.00	Total Derivative* $\frac{\partial X}{\partial \delta_e}$	$\frac{\partial Z}{\partial \delta_e}$	$\frac{\partial M}{\partial \delta_e}$	Total Derivative** $\frac{\partial X}{\partial \delta_{pfd}}$	$\frac{\partial Z}{\partial \delta_{pfd}}$	$\frac{\partial M}{\partial \delta_{pfd}}$
(kts)	$\left(\frac{lb}{rad}\right)$	$\left(\frac{lb}{rad}\right)$	$\left(\frac{ft\text{-}lb}{rad}\right)$	$\left(\frac{lb}{rad}\right)$	$\left(\frac{lb}{rad}\right)$	$\left(\frac{ft\text{-}lb}{rad}\right)$
0	-	-	-	-	-1,339	29,930
16.6	-18	-61	-1,200	-569	-1,366	29,540
39.7	-102	-352	-6,600	-594	-1,424	28,910
57.4	-209	-740	-14,000	-627	-1,505	28,280
74.6	-348	-1,251	-23,700	-677	-1,625	27,710
90.0	-404	-1,837	-35,700	-768	-1,843	29,220

* The derivatives with respect to δ_e result from only the tail control derivatives.

** The derivatives with respect to δ_{pfd} result from only the nose fan control derivatives.

APPENDIX III
WIND TUNNEL WALL CORRECTIONS

INTRODUCTION

In support of the XV-5A Data Correlation Study, an investigation of available wind tunnel wall effect corrections and data testing limitations for VTOL vehicles was made. This investigation consisted of (1) a survey of the current state of the art[19, 20], including methods used for the collection of data utilized in the correlation study, and (2) an evaluation of the most promising correction technique applied to some of the data under study.

The fundamental techniques available consist of:

1. the conventional wing circulation infinite vortex image system representing the total lift [21],

2. the conventional wing circulation vortex image system representing only the wing lift with the lifting propulsion system airflow assumed not to have a wall effect contribution (CVAL 344),

3. a linear doublet stream tube image system representing highly downward deflected airflow caused by the propulsion system[7], and

4. a doublet stream tube image system with a stream tube curvature correction representing highly downward deflected airflow caused by the propulsion system[22].

There have been a number of investigations by NASA, References [23] to [29], which extensively cover wind tunnel data wall effect corrections. These studies indicate quite conclusively that the first two techniques mentioned above provide corrections of insufficient magnitude. The third method, modified by Heyson [32], provides a reasonable technique to correct the data to the free air condition. The fourth technique, which is an extension of the third, has two faults. It is a very cumbersome method requiring a computer program to apply corrections, and the results of applying the technique are inconclusive. The latter situation may very well be the fault of the data. Thus, it was decided to pursue Heyson's modified technique of wind tunnel wall effect corrections for application to the XV-5A Data Correlation Study.

WIND TUNNEL TESTING LIMITATIONS

There is an important factor which should be considered when using any wind tunnel data; that is, the low speed limit of applicability. Rae has indicated[13] that there is a flow breakdown region where the lifting propulsion system (fan or propeller) efflux will circulate laterally across the floor, up the sidewall, and then reenter the propulsion system inlet.

This breakdown region is indicated for some helicopter rotor-wind tunnel geometries. However, for the tunnel tests included in the subject Data Correlation Study, predicting this breakdown region is a considerable extrapolation of Rae's data and cannot be obtained with any accuracy. Even so, this breakdown region should be considered when analyzing data in the very low freestream velocity regime (near hover), since it is proven to exist. It is also indicated by Rae's investigation that tunnel fillets or curved sidewalls, such as those in the Ames wind tunnel, may aggravate this flow breakdown situation.

DISCUSSION OF HEYSON'S TECHNIQUE WITH RESPECT TO THE XV-5A CONFIGURATION

There is one significant point which should be kept in mind when considering the approach and assumptions of this technique; that is, even though the complexities can be severe and the assumptions or applications somewhat rough, the technique obtains the major portion of what is a fairly small correction.

Before discussing the technique used, a short explanation of wind tunnel wall effects is no doubt in order. One desires that wind tunnel data be obtained for the free air condition. However, the presence of the wind tunnel walls distorts the airflow around the model such that the model forces generated and/or the reference angle of attack is in error. For the usual lifting case, the tunnel walls distort the basic flow such that the vehicle is "flying" at a higher angle of attack than if it were in free air. Correction techniques apply a mathematical image system to represent the tunnel walls, and the magnitude of this effect is solved for comparison to the free air case.

Heyson's method of wall effect corrections[30] can be subdivided into two major portions: (1) a rigorous analytic portion which computes the induced wall effect interference factors, assuming a diminishingly small single propeller or fan induced stream tube with known physical properties, and (2) a simplified momentum portion[31] which enables one to define the physical properties required above to obtain the dimensional values of the induced velocities. These stream tube properties are determined from the measured values of lift and drag and the geometry of the model and tunnel.

The analytic portion solves for the wall effect interference factors (nondimensional parameters) in a general form as a function of wind tunnel geometry, a single model propulsive inlet and stream tube location in the cross section of the tunnel, and the inclination of this straight stream tube which lies in the longitudinal plane and continues to the tunnel floor. The solution is accomplished by employing the classical image system technique. Two assumptions are made which should be kept in mind when this method is employed:

1. The stream tube is represented by a string of point doublets which imply that the diameter of the stream tube is infinitely small in comparison to the wind tunnel test section. This is a good assumption for most tunnel tests where the model is kept reasonably small. This situation exists for the fans used in this study.

2. The model induced stream tube remains linear until it impinges upon the tunnel floor. A subsequent study and analysis by Heyson[32] indicate that the stream tube then rolls up and forms two vortices. He proposes a theoretical relationship between the angle of the stream tube and the line of the velocity. Thus, a correction for the stream tube inclination from the positive Z-axis (skew angle) is obtained. The flow is obviously very complex and nonlinear, and Heyson's arguments for the correction are reasonable. Thus, one would expect satisfactory results from the application of this technique. Close correlation is obtained upon comparing various corrected tunnel test data and near-free air data of the same model.

The second portion of Heyson's technique[31] is the standard momentum approach which uses the measured model lift, drag, geometry, and propulsive device configuration to determine the skew angle and the stream tube induced velocities. The implication of the propulsive device configuration is that one should know the stream tube contraction ratio from which the induced velocities at the inlet face (fan or propeller plane) can be computed. This contraction ratio is the stream tube cross-sectional area at the propulsive device ratioed to the wake cross-sectional area where the static pressure has returned to ambient. For the static case, this ratio is two for open propellers and unity for ducted fans. Since the basic application of this technique is the low-speed, highly deflected crossflow flight regime, the contraction ratio for the propeller does not vary significantly with forward speed, and the ducted fan variation is negligible. Thus, the technique and method are straightforward and reasonable for handling a small propeller or duct inside a wind tunnel. For the subject Data Correlation Study where ducted fans are involved, a constant contraction ratio value of unity can be used satisfactorily.

The XV-5A propulsive configuration is not quite as simple as the single duct discussed above, and additional considerations and corrections are required. Considerable data were obtained for the XV-5A aircraft and models for pitch fan off and horizontal tail off. Thus, the fundamental correction necessary for these data becomes the effect of two ducted fans laterally displaced in contrast to a single equivalent fan. Heyson includes this aspect in his report[7] and indicates methods to obtain the reduced induced upwash effects of two laterally displaced fans in terms of the "equivalent" single fan. A short study of lateral distribution of tunnel

wall induced upwash indicated that a reasonable average of induced upwash would be obtained by placing the mathematical point fan approximately at the outboard butt line of the real fans. These spanwise locations were found to be very close to the lateral nondimensional values of η tabulated by Heyson corresponding to 0.25 and 0.125 tunnel semiwidths for the full-scale and 1/6-scale model, respectively. Thus, these values were used. The values given above are the distances of the point fan of the two models from the longitudinal plane of symmetry in terms of tunnel semiwidth.

The correction for pitching moment for the tail-on configuration stems from the longitudinal variation of the induced upwash due to the tunnel wall. This longitudinal variation is greatly affected by the value of the skew angle. Since the flow nonlinearities are to a great extent related to this skew angle, it should be appreciated that the moment correction is subject to significantly larger errors than the lift or drag corrections. The procedure for determining the tail induced interference factors is identical to the wing lift and drag correction procedure, except that the induced upwash is determined at the tail location. When the aircraft characteristics are referenced to the wing, the correction in slipstream notation becomes

$$\Delta C_m{}^s = \frac{q_t}{q}\frac{S_t}{A_F}\frac{\ell_t}{D_F}\left(\frac{dC_L}{d\alpha}\right)_t (\Delta\alpha_t - \Delta\alpha_w)\,(1-T_c{}^s) \qquad (155)$$

(Ref. 33, p.11)

Again the lateral fan distribution correction should be made, but no lateral correction is given in Heyson's work for longitudinal stations other than the fan station. Thus, the longitudinal induced upwash at the tail is reduced by the same percentage as the induced upwash at the wing due to the lateral fan distribution effect. There is also the consideration of the effect upon the induced upwash due to the elevated position of the horizontal tail above the horizontal plane of the wing fans, and the additional complication that this distance is a function of angle of attack. No vertical displacement correction is given in Heyson's technique for longitudinal stations other than at the wing fan station. Therefore, an examination of the change of interference factors (wall induced upwash) was made at a point directed vertically from the fans a distance equal to the longitudinal distance between the fans and the horizontal tail. The results indicated that the variation of induced upwash is small for skew angles above 45 degrees in the full-scale Ames tests, and smaller yet for CVAL 344 tests. Therefore, this effect is ignored because it is small and because increases in angle of attack significantly reduce the distance, which tends to make the correction even smaller.

The additional aspect of correcting the data for the effect of the pitch fan and wing fans operating together should be considered. The lifting stream tube due to the pitch fan will be affected by the tunnel walls, causing an additional induced upwash on the wing. First, it is necessary to recall one of Heyson's basic assumptions that the stream tube formed by the fan efflux under consideration is deflected downward in the vertical

plane of symmetry. However, the lift control of the pitch fan is accomplished by two laterally placed deflector doors. Thus, the assumption is good near maximum lift of the pitch fan (trimmed low-speed flight regime), and is poorer as the doors are modulated to cancel the lift by deflecting the fan efflux laterally (trimmed high-speed flight regime). One should also keep in mind that this correction is involved with the longitudinal induced upwash distribution which is subject to greater errors. Also, the pitch fan lift is a maximum of 20 percent of the wing lift, thereby reducing the importance of this correction. In order to determine if this correction was of significant magnitude for the Ames tests, some estimates of the induced upwash on the wing due to the pitch fan-wing fan combination were compared to the induced upwash on the wing due to the wing fans alone. For the pitch fan high lift case (an effective skew angle of 45 degrees), it was found that the wing-induced upwash would be increased nearly 25 percent above that for the wing fan alone. This increase includes the correction for the effect of lateral displacement of the wing fans and variable lateral distribution of the induced upwash. The magnitude of this correction is indeed significant. There is the additional complication that the wind tunnel-measured pitch and wing fan thrust forces are not obtained separately, because only the total forces are obtained. If one assumes that the additional lift due to the pitch fan occurs at the wing fans and increases the wing fan area by the pitch fan area, and then computes the induced upwash again ratioed to the wing-fan-alone effect, the upwash is increased about 15 percent. Thus, this modified comparison of induced upwash of the equivalent wing fan to wing fan only (15 percent), divided by the proper comparison of pitch fan-wing fan effects to wing fan only (25 percent), gives the relative effect of the modified procedure to the more rigorous method. This error is indicated to be approximately 8 percent low. Thus, the attempt to define a rigorous correction for the pitch fan is not warranted, and a reasonable approximation is obtained by dividing the wing fan area by the pitch fan area.

The next consideration is a correction for the effect of operating the pitch fan when the model horizontal tail is on; that is, the induced upwash effect at the horizontal tail due to the pitch fan. This correction, which involves the longitudinal distribution of the induced upwash, was indicated previously to be of comparatively low accuracy due to the basic assumptions applied. Thus, with all the unknown subtleties concerning the pitch fan as indicated above, it is felt that any correction obtained would be academic.

APPLICATION OF HEYSON'S TECHNIQUE TO XV-5A DATA

The major portion of the wind tunnel data to be used for this Data Correlation Study was obtained in the GD/Convair 16-x-19-foot return section with the 1/6-scale model, and the Ames 40-x-80-foot section with the full-scale model and the XV-5A aircraft. The tunnel and model geometries and model placement dimensions were used to obtain the values of the parameters ζ, η, and γ for each tunnel. These parameters are required by Heyson's equations to compute the interference factors for the wing.

The vertical induced velocity w_o/w_h is needed for Heyson's method[7] in order to find the vertical and horizontal interference velocities due to the induced upwash. It is difficult, however, to obtain w_o/w_h with satisfactory accuracy from Heyson's Figure 6 for the range in values of D/L and V/w_h used in this study. Because of this, a portion of Heyson's figure is replotted in Figure 72 to a larger scale in order to obtain more accurate values of the induced velocity. The skew angle χ can then be found from Figure 73.

The Ames tunnel has semicircular sidewalls and does not match the rectangular cross section assumed in Heyson's analysis. It is felt that this discrepancy is not significant, since the parallel floor and ceiling extend laterally 5 feet beyond the wing. Also, the comparison of interference factors for a rectangular tunnel and a floor-only tunnel indicated a small change in induced value. Thus, the correction for sidewall curvature can be expected to be insignificant. An equivalent rectangular tunnel was determined using the test section height and area. The parametric values were then computed, and the three closest tabular values for tunnel width-to-height ratio were applied by use of the three-point Lagrangian interpolation formula. The lateral distribution correction for two fans was also applied, resulting in the summary of interference factors presented in Figures 74, 75, and 76. These figures, respectively, are used to find the wall corrections for the Ames tail-off, GD/Convair, and Ames tail-on data.

Preliminary calculations were conducted for both test series in order to determine the magnitude of the corrections involved. A sample calculation for the GD/Convair test series at high lift, 90-ft/sec tunnel speed, and zero louver stagger and vector angles was made. The correction to angle of attack was 0.45 degree. It is convenient to think in terms of an incremental angle-of-attack correction implying the magnitude of the correction to lift and drag coefficients. But one must keep in mind that the only true indication of the correction is the coefficient value versus angle of attack corrected and uncorrected at the same angle of attack. The corrections for the 1/6-scale coefficients were found to be less than 1 percent, which is well within the accuracy of the data. Thus, wind tunnel wall effects for the 1/6-scale data have been ignored. Similarly, some of the data for one of the Ames series tests were examined. The incremental induced angle of attack was 1.29 degrees. Lift and drag coefficients were then adjusted to the same angle of attack and found to be 4 percent different. This error was felt to be of sufficient magnitude that a representative group of Ames data should be corrected to determine if improved correlation is obtained.

$$V/_{w_h} = \left[\sqrt{\frac{1}{\left(\frac{w_o}{w_h}\right)^4} - 1} - \frac{D}{L} \right] \frac{w_o}{w_h}$$

Heyson, TR R-124

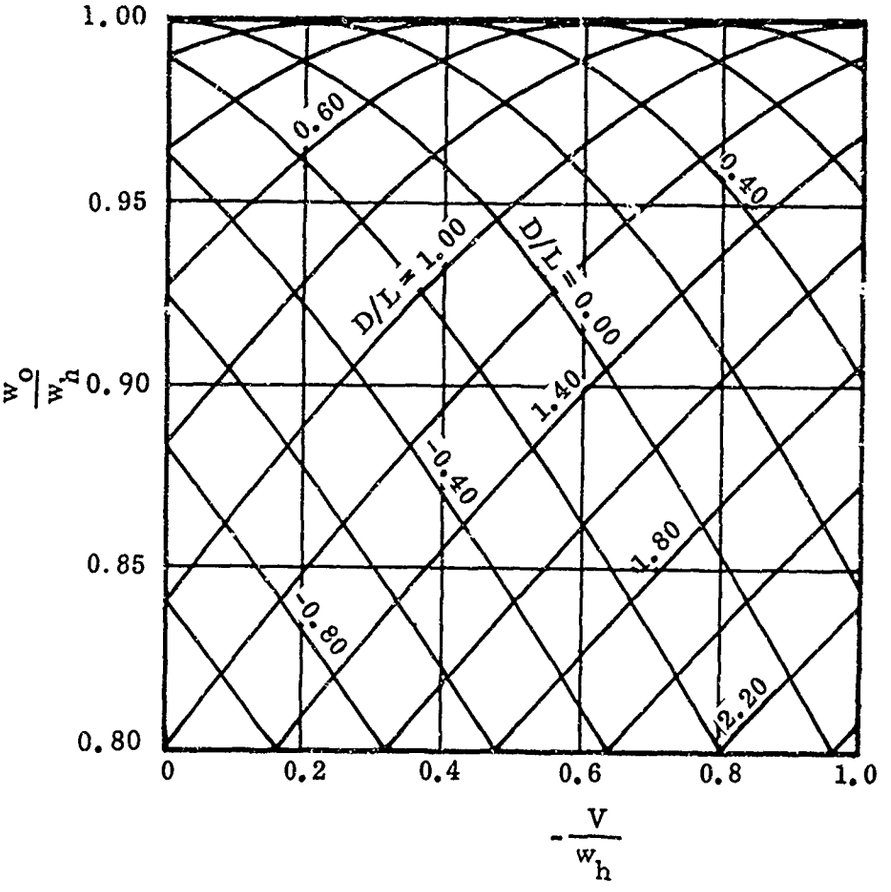

Figure 72. Values of the Vertical Induced Velocity for Various Values of D/L as a Function of Forward Velocity.

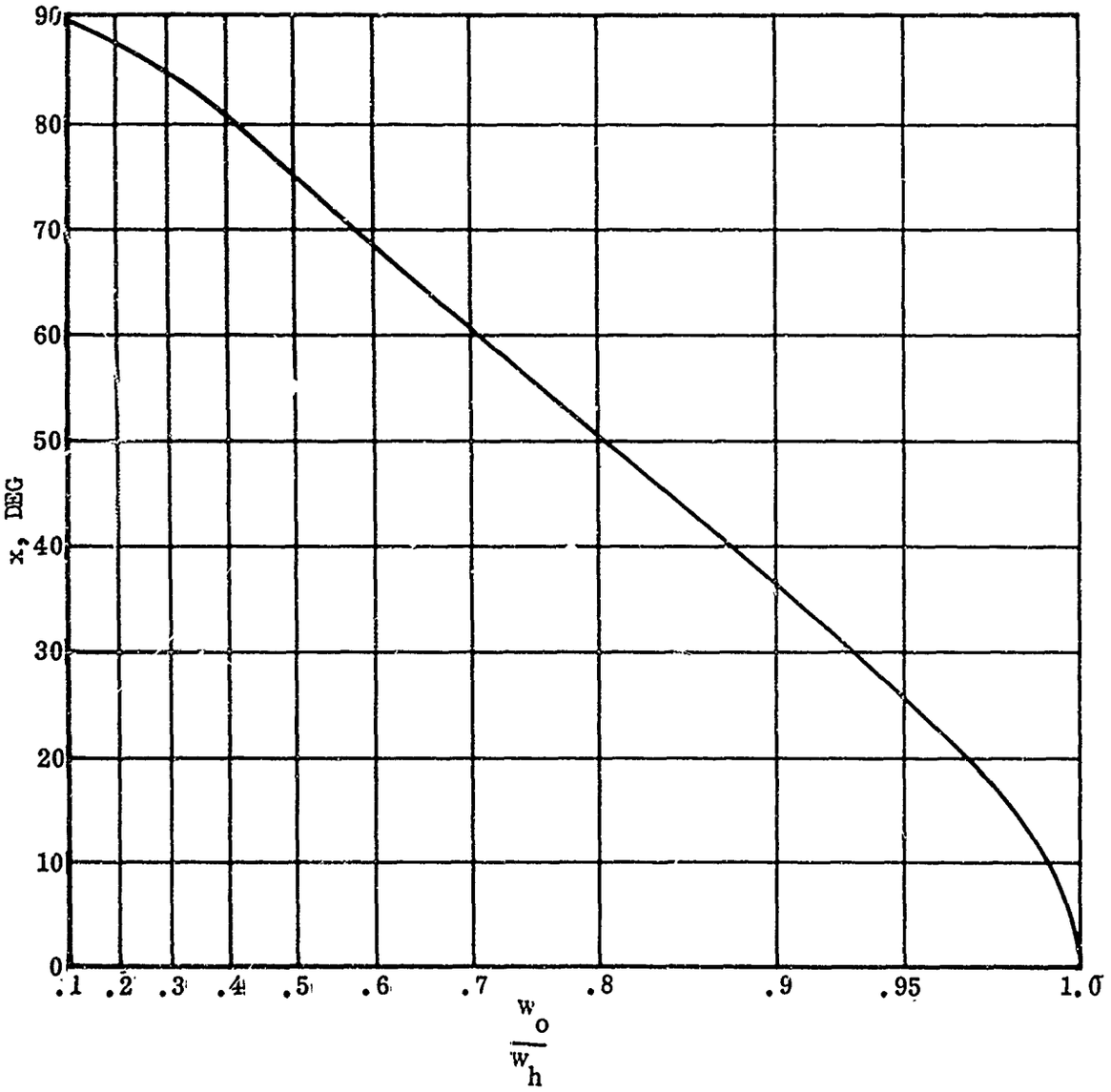

Figure 73. Skew and Wake Deflection Angle as Functions of w_o/w_h.

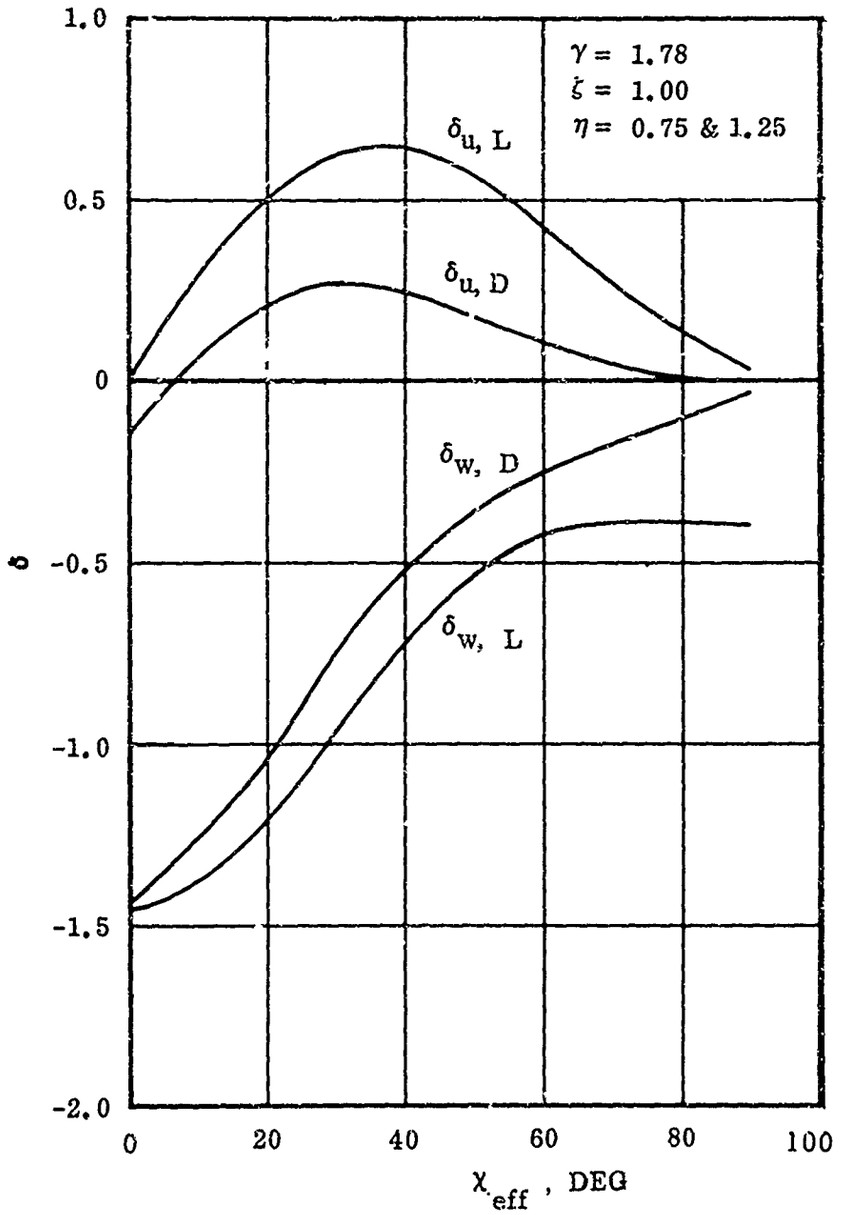

Figure 74. Wind Tunnel Interference Factors for Full-Scale Ames Test.

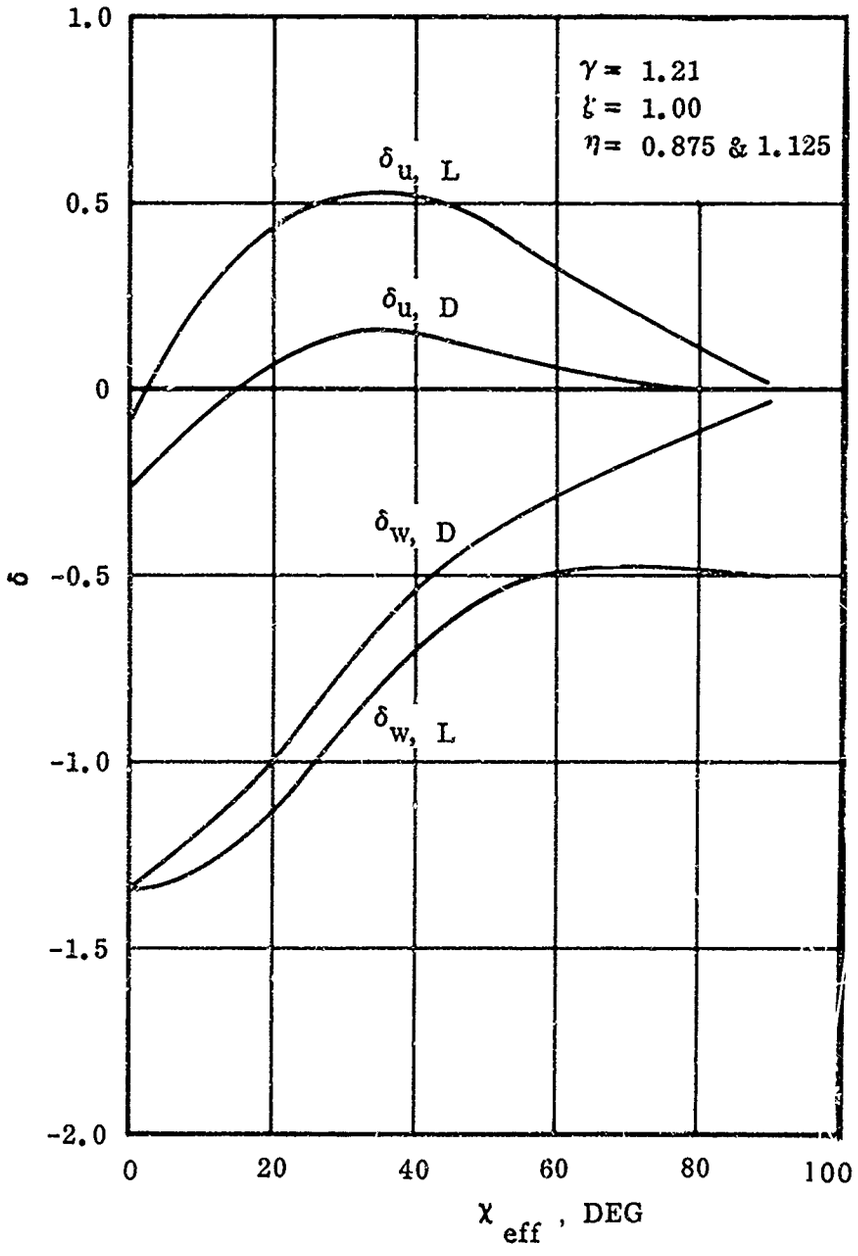

Figure 75. Wind Tunnel Interference Factors for CVAL 344 Test.

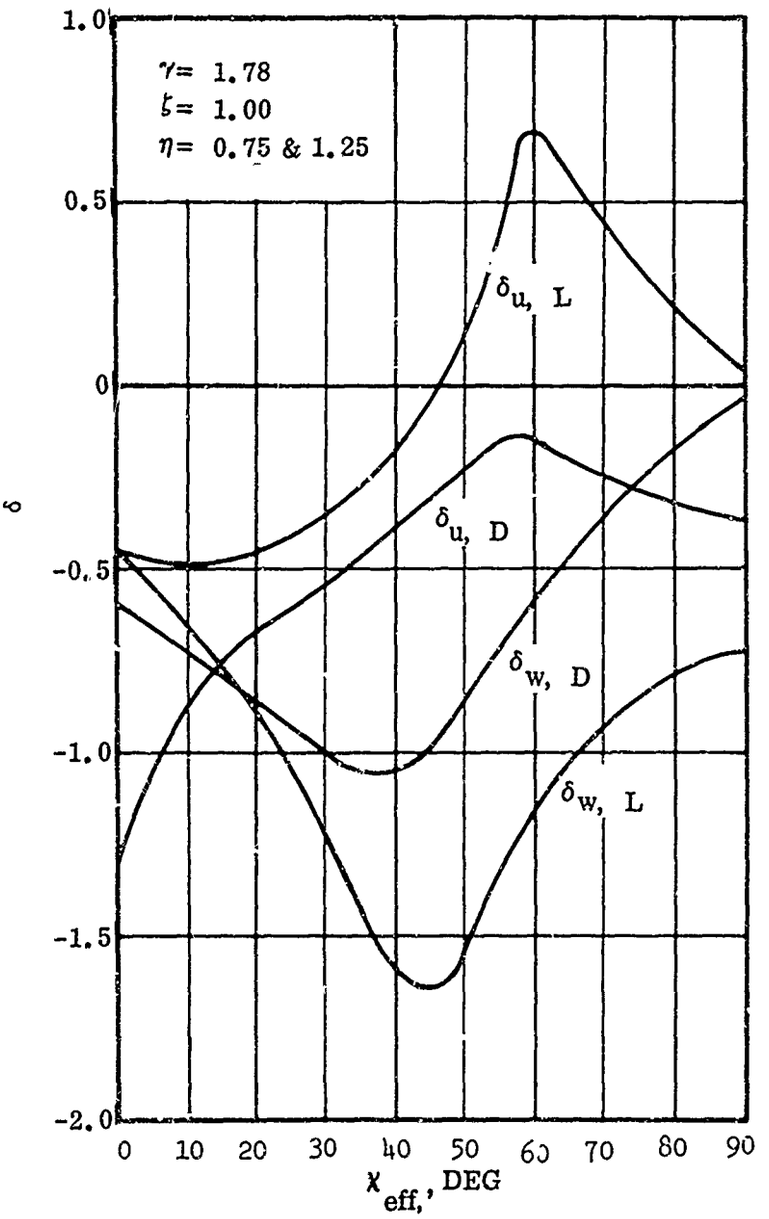

Figure 76. Wind Tunnel Interference Factors for Horizontal Tail - Full-Scale Ames Test.

CALCULATION PROCEDURE TO DETERMINE WIND TUNNEL WALL EFFECT CORRECTIONS

A detailed step-by-step wall correction procedure is presented by Heyson in Reference[7], and the procedure is repeated below with the proper geometric values and parameters used for the subject Data Correlation Study. The interference factors used below were obtained as discussed in the body of this appendix. The wall correction calculations utilize data taken from Ames Test 173 (run 12, point 20).

The following characteristics of the model and wind tunnel (closed) are assumed:

$\gamma = 1.78$ $\quad$ $n = 1.00$

$\zeta = 1.00$ $\quad$ $A_m = A_F = 42.6$ sq ft

$\eta = 0.75,\ 1.25$ $\quad$ $A_T = 2,856$ sq ft

The conditions and results of the test were:

$\alpha = 0°$ $\quad$ $q = 21.29$ lb/sq ft; and $V = 140.3$ ft/sec

$L = 7,320$ lb $\quad$ $T_c^s = 0.8546$

$D = 2,916$ lb $\quad$ $\rho = 0.002163$ slug/cu ft

$T_{ooo}/A = 125.10$ lb/sq ft

The wall effect calculations then proceed as follows (all equations are from Reference 7 unless otherwise noted):

$$D/L = 2,916/7,320 = 0.398$$

From Equation (35),

$$w_h = -\sqrt{L/n\rho A_m} = -\sqrt{7,320/(1.0)(0.002163)(42.6)} = -281.85 \text{ ft/sec}$$

$$V/w_h = 140.3/-281.85 = -0.498$$

From Figure 72 (which is plotted from Equation (36)),

$$w_o/w_h = 0.996$$

From Figure 73,

$$\chi = 7^\circ$$

From Reference 32, Equation (3),

$$\chi_{eff} = (\chi + 90^\circ)/2 = 48.5^\circ$$

$$V/w_o = (V/w_h)/(w_o/w_h) = (-0.498)/(0.996) = -0.500$$

Since $(-V/w_o) > D/L$, then χ is positive (directed rearward). From Figure 74, which was interpolated from References 34 and 35 for $\zeta = 1.0$ and $\eta = 0.75$ & 1.25,

$$\delta_{w,L} = -0.56 \qquad \delta_{u,L} = 0.58$$

$$\delta_{w,D} = -0.39 \qquad \delta_{u,D} = 0.19$$

From Equation (44),

$$M_w/M_T = (A_m/A_T)/(V/w_o) = (42.6/2,856)/(-0.500) = -0.030$$

From Equation (45),

$$M_u/M_T = (M_w/M_T)\ (D/L) = (-0.030)\ (0.398) = -0.012$$

From Equations (40) to (43),

$$\Delta w_L/V = \delta_{w,L}(M_w/M_T) = (-0.56)\ (-0.030) = 0.017$$

$$\Delta u_L/V = \delta_{u,L}(M_w/M_T) = (0.58)\ (-0.030) = -0.017$$

$$\Delta w_D/V = \delta_{w,D}(M_u/M_T) = (-0.39)\ (-0.012) = 0.005$$

$$\Delta u_D/V = \delta_{u,D}(M_u/M_T) = (0.19)\ (-0.012) = -0.002$$

From Equations (46) and (47),

$$\Delta w/V = (\Delta w_L/V) + (\Delta w_D/V) = 0.017 + 0.005 = 0.022$$

$$\Delta u/V = (\Delta u_L/V) + (\Delta u_D/V) = -0.017 - 0.002 = -0.019$$

From Equation (48b),

$$\Delta\alpha = \tan^{-1}\left[\frac{\Delta w/V}{1 + (\Delta u/V)}\right] = \tan^{-1}\left[0.022/(1-0.019)\right] = 1.29°$$

From Equation (48a),

$$\alpha_c = \Delta\alpha + \alpha = 1.29° + 0° = 1.29°$$

$$q_c/q = \left[1 + (\Delta u/V)\right]^2 + \left[\Delta w/V\right]^2 = \left[1-0.019\right]^2 + \left[0.022\right]^2 = 0.963$$

$$q_c = (q_c/q)q = (0.963)\ (21.29) = 20.50 \text{ lb/sq ft}$$

$$q^s_c = q_c + (T_{000}/A) = 20.50 + 125.10 = 145.60 \text{ lb/sq ft}$$

$$(T_c{}^s)_c = (T_{000}/A)/q^s_c = 125.10/145.60 = 0.8592$$

From Equations (50a, b),

$$L_c = L\cos\Delta\alpha - D\sin\Delta\alpha = (7,320)\ (0.9997) - (2,916)\ (0.0225)$$

$$= 7,252 \text{ lb}$$

$$D_c = L\sin\Delta\alpha + D\cos\Delta\alpha = (7,320)\ (0.0225) + (2,916)\ (0.9997)$$

$$= 3,080 \text{ lb}$$

$$(C_L{}^s)_c = L_c/q^s_c A_m = 7,252/(145.60)\ (42.6) = 1.169$$

$$(C_D{}^s)_c = D_c/q^s_c A_m = 3,080/(145.60)\ (42.6) = 0.497$$

Heyson presents some equations for correcting the pitching moment coefficient in one of his documents[33]. One of his equations (155) is in the body of this appendix, although it has been changed to slipstream notation. The slipstream pitching moment coefficient is not corrected for wall effects in this report; instead, it is plotted against the corrected angle of attack α_c.

Unclassified

Security Classification

DOCUMENT CONTROL DATA - R & D

(Security classification of title, body of abstract and indexing annotation must be entered when the overall report is classified)

1. ORIGINATING ACTIVITY (Corporate author) Ryan Aeronautical Company 2701 Harbor Drive San Diego, California	2a. REPORT SECURITY CLASSIFICATION Unclassified 2b. GROUP

3. REPORT TITLE

XV-5A Aerodynamic-Propulsion Data Correlation and Characteristics Development Based on Wind Tunnel Characteristics

4. DESCRIPTIVE NOTES (Type of report and inclusive dates)

Final Report

5. AUTHOR(S) (First name, middle initial, last name)

William C. Parks
Robert L. Swingle
William A. Swope

6. REPORT DATE July 1968	7a. TOTAL NO. OF PAGES 244	7b. NO. OF REFS 37
8a. CONTRACT OR GRANT NO. DA 44-177-AMC-456(T) b. PROJECT NO. Task 1F125901A14233 c. d.	9a. ORIGINATOR'S REPORT NUMBER(S) USAAVLABS Technical Report 67-75 9b. OTHER REPORT NO(S) (Any other numbers that may be assigned this report) 29467-1	

10. DISTRIBUTION STATEMENT

This document has been approved for public release and sale; its distribution is unlimited.

11. SUPPLEMENTARY NOTES	12. SPONSORING MILITARY ACTIVITY US Army Aviation Materiel Laboratories Fort Eustis, Virginia

13. ABSTRACT

This report presents the results of efforts to correlate data for the XV-5A V/STOL aircraft configuration, including small-scale and full-scale wind tunnel investigations and wind tunnel and thrust stand tests of the actual aircraft. The majority of the data correlation work was performed utilizing results from the Ryan 1/6-scale and NASA full-scale model tests which had been conducted during the period of aircraft development. Correlation was limited primarily to wing-body characteristics. Corrections for configuration differences were developed, and the effects of dynamic dissimilarity of the fan systems were evaluated in the data comparison effort. Wind tunnel wall corrections were applied to the full-scale data.

DD FORM 1 NOV 68 1473 REPLACES DD FORM 1473, 1 JAN 64, WHICH IS OBSOLETE FOR ARMY USE.

Unclassified

Security Classification

Unclassified
Security Classification

14. KEY WORDS	LINK A		LINK B		LINK C	
	ROLE	WT	ROLE	WT	ROLE	WT
Wind tunnel Data correlation Lift fans						

Unclassified
Security Classification

7174-68